

NOAA Technical Memorandum ERL NSSL-80

THE UNION CITY, OKLAHOMA TORNADO
OF 24 MAY 1973

Property of
NWC Library
University of Oklahoma

Rodger A. Brown, Editor

Contributors:

Gary L. Achtemeier	Joseph H. Golden
Ronnie L. Alberty	Herbert G. Hughes
Edward A. Brandes	Leslie R. Lemon
Rodger A. Brown	Daniel Purcell
Donald W. Burgess	Dale Sirmans
Robert P. Davies-Jones	William L. Taylor
Ralph J. Donaldson, Jr.	Charles L. Vlcek
W. David Zittel	

National Severe Storms Laboratory
Norman, Oklahoma
December 1976

UNITED STATES
DEPARTMENT OF COMMERCE
Juanita M. Kreps, Secretary

NATIONAL OCEANIC AND
ATMOSPHERIC ADMINISTRATION
Robert M. White, Administrator

Environmental Research
Laboratories
Wilmot N. Hess, Director



NOTICE

The Environmental Research Laboratories do not approve, recommend, or endorse any proprietary product or proprietary material mentioned in this publication. No reference shall be made to the Environmental Research Laboratories or to this publication furnished by the Environmental Research Laboratories in any advertising or sales promotion which would indicate or imply that the Environmental Research Laboratories approve, recommend, or endorse any proprietary product or proprietary material mentioned herein, or which has as its purpose an intent to cause directly or indirectly the advertised product to be used or purchased because of this Environmental Research Laboratories publication.

DEDICATED

to the memory,
to the work of

NEIL B. WARD
(1914 - 1972)

*who was ahead of his time in
understanding mesocyclones and tornadoes*

and

ROBERT J. KETCHUM
(1922 - 1975)

*whose dedicated thoroughness in all
aspects of rawinsonde quality control have
resulted in extremely high quality upper air data*

PREFACE

On 24 May 1973, the National Severe Storms Laboratory (NSSL) collected a unique data set on the Union City, Oklahoma tornadic storm. This data set is unparalleled in several ways: for the first time a team of meteorologists sought out and photographed the life history of a tornado; for the first time Doppler radar measurements were made in a storm producing a major tornado; all the Laboratory's sensors, as well as those of visiting scientists, covered the storm.

After the uniqueness of this situation became apparent, Dr. Edwin Kessler, NSSL Director, commissioned an in-depth study of the tornado and its parent storm. Dr. Stanley Barnes, then head of the Severe Storms Morphology and Dynamics Project, helped to get the study underway. This Technical Memorandum reports the results.

Individual research results have been grouped into three main categories: macroscale, mesoscale and tornado scale. Abstracts are written so that a reader can scan the entire report, sense the gist of the findings and then read pertinent chapters.

This study represents the involvement and cooperative efforts of the entire Laboratory: meteorology research supervised by Dr. Ron Alberty; administrative and graphic arts support supervised by Jack Andrews; engineering and electronic technician support supervised by Dr. Richard Doviak; computer data processing supervised by Kathryn Gray; and operation and maintenance of the Laboratory's meteorological sensors supervised by Ken Wilk. Members of these groups joined forces under the leadership of 1973 Spring Program Coordinator J. T. Lee to make the Laboratory's data collection program a success.

Within NSSL a special group of individuals--the electronic and meteorological technicians--deserve recognition for their competence and resourcefulness. The high-quality data available for this study bear testimony to their dedication.

The physical appearance of this Technical Memorandum is due to the conscientious efforts of several individuals. Connie Hall, Evelyn Horwitz and Joy Walton typed preliminary drafts of various chapters. The task of typing later drafts, as well as setting up the entire report in its final "camera-ready" form, was handled admirably by Debbie Killian. Jennifer Farris skillfully drafted the figures. Charles Clark did a fine job preparing the photographic prints.

As coordinator and editor, I appreciate the time and effort devoted by the authors of each chapter. This treatise is a tribute to these scientists who represent the Air Force Geophysics Laboratory, Illinois State Water Survey, National Severe Storms Laboratory, Naval Electronics Laboratory Center, and the Wave Propagation Laboratory.

My colleagues, Don Burgess and Les Lemon, were very helpful during the several years of report preparation. In addition to being major contributors they critically reviewed preliminary drafts of most chapters.

Drs. Ron Alberty and Edwin Kessler reviewed the entire manuscript; their comments significantly improved the text. The suggestions and comments of other NSSL staff members have been most appreciated. Helen J. Ardrey's editorial seasoning added a special savor.

Rodger A. Brown
December 1976

N. B. Several chapters are to be published in the Monthly Weather Review and the Journal of Geophysical Research. Before referencing chapters from this volume, please consult those journals.

ACKNOWLEDGMENTS

Evolving research at the National Severe Storms Laboratory has been significantly enhanced through encouragement by many organizations outside the Environmental Research Laboratories. Contributions have taken various forms ranging from equipment loans and cooperative support to contracts that provide funds to expand our program. Major contributors include:

- Agricultural Research Service
- Atomic Energy Commission
- Department of the Air Force
- Department of the Army
- Energy Research and Development Administration
- Environmental Data Service
- Federal Aviation Administration
- National Aeronautics and Space Administration
- National Environmental Satellite Service
- National Research Council
- National Severe Storms Forecast Center
- National Weather Service
- NOAA Corps
- Nuclear Regulatory Commission

Many other individuals, organizations, and Universities have contributed to the Laboratory in less tangible, but muchly appreciated, ways. To all these, we offer a sincere "thank you".

TABLE OF CONTENTS

	<u>Page</u>
Dedication	iii
Preface	v
Acknowledgments	vii
<u>Part I: Prologue</u>	
1. FLASHBACK: 24 MAY 1973 Rodger A. Brown	3
<u>Part II: Meteorological Setting</u>	
2. GENERAL SYNOPTIC SITUATION Charles L. Vicek	11
3. SUBSYNOPTIC-SCALE METEOROLOGICAL FEATURES AND ASSOCIATED CONVECTIVE ACTIVITY ON 24 MAY 1973 Edward A. Brandes	19
4. TALL TOWER MEASUREMENTS PRECEDING THE UNION CITY TORNADIC STORM W. David Zittel	27
<u>Part III: Parent Storm</u>	
5. UNION CITY STORM HISTORY Donald W. Burgess and Leslie R. Lemon	35
6. SEVERE STORM SPLITTING AND LEFT-MOVING STORM STRUCTURE Donald W. Burgess, Leslie R. Lemon and Gary L. Achtemeier	53
7. OBSERVATIONS OF THE UNION CITY TORNADIC STORM BY PLAN SHEAR INDICATOR Ralph J. Donaldson, Jr.	67
8. TORNADIC STORM AIRFLOW AND MORPHOLOGY DERIVED FROM SINGLE DOPPLER RADAR MEASUREMENTS Leslie R. Lemon and Donald W. Burgess	85

	<u>Page</u>
9. ELECTROMAGNETIC SIGNATURE OF THE UNION CITY TORNADIC STORM AT THREE MEGAHERTZ William L. Taylor	107
10. DIRECTIONAL MEASUREMENTS OF VERY LOW FREQUENCY (VLF) SFERICS IN THE UNION CITY TORNADIC STORM Rodger A. Brown and Herbert G. Hughes	113

Part IV: The Tornado

11. HISTORY OF THE UNION CITY TORNADO Daniel Purcell	123
12. COMPARISON OF UNION CITY TORNADO LIFE CYCLE WITH FLORIDA KEYS WATERSPOUT LIFE CYCLE Joseph H. Golden	135
13. INTERPRETATION OF SURFACE MARKS AND DEBRIS PATTERNS FROM THE UNION CITY TORNADO Robert P. Davies-Jones, Donald W. Burgess, Leslie R. Lemon and Daniel Purcell	141
14. AIRFLOW CHARACTERISTICS AROUND THE UNION CITY TORNADO Joseph H. Golden and Daniel Purcell	157
15. EVOLUTION OF THE DOPPLER RADAR TORNADIC VORTEX SIGNATURE IN THE UNION CITY STORM Rodger A. Brown and Leslie R. Lemon	167

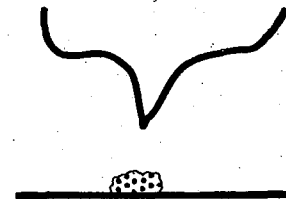
Part V: Epilogue

16. UNION CITY TORNADO AND BEYOND Ronnie L. Alberty and Rodger A. Brown	179
--	-----

Appendices

A. TORNADO INTERCEPT STRATEGY AND MORPHOLOGICAL OBSERVATIONS Joseph H. Golden	185
B. HOURLY SURFACE WEATHER MAPS AND ANALYZED FIELDS OF METEOROLOGICAL VARIABLES: 24 MAY 1973 Edward A. Brandes	191

	<u>Page</u>
C. RAWINSONDE OBSERVATIONS ON 24 MAY 1973 Edward A. Brandes	205
D. NSSL DOPPLER AND WSR-57 RADAR CHARACTERISTICS Dale Sirmans	209
E. SINGLE DOPPLER RADAR DATA ACQUISITION AND ANALYSIS Rodger A. Brown	215
F. TORNADIC STORM EVOLUTION: VORTEX VALVE HYPOTHESIS Leslie R. Lemon	229
Other Papers Pertaining to the Union City Tornadic Storm	235



PART I: PROLOGUE

1. FLASHBACK: 24 MAY 1973

Chapter 1

FLASHBACK: 24 MAY 1973

Rodger A. Brown

*National Severe Storms Laboratory
Norman, Oklahoma 73069*

On 24 May 1973, NSSL meteorologists and visiting scientists were prepared--as on any other day during the Laboratory's Spring data collection program--to document fully tornadic storms developing in central Oklahoma. Preparation and perseverance paid off. The appearance of an isolated radar echo, ahead of a cold front, focused attention on the storm that would produce the devastating Union City tornado. This chapter provides an overview of Laboratory activities during the storm's lifetime.

At 1545 CST on 24 May 1973, the darkened National Severe Storms Laboratory (NSSL) radar room was a typical beehive of activity. The surveillance meteorologist carefully monitored storm development on the WSR-57 radar console; the Federal Aviation Administration (FAA) aircraft controller, NSSL aircraft coordinator and his assistant were gathered around a nearby repeater scope; the radar technician was keeping an eye on a balky radar data tape recorder. A visiting scientist was monitoring Doppler velocity shear regions on the Plan Shear Indicator scope. Meanwhile, the tornado intercept coordinator had just hung up the phone and was leaving the room to check on the latest teletype reports when the phone rang again. An excited member of the NSSL tornado intercept team reported that a large tornado was touching down to his northwest. That team was positioned 5 km south of a small farming community in Canadian County with an unfamiliar name, Union City. A quick check revealed that Union City was 47 km west-northwest of NSSL.

Excitement in the radar room intensified as more details were relayed via radio telephone from the field location. "Funnel is half-mile wide at cloud base." "Tornado is less than a mile away." (In reality, the funnel was about half the estimated size but six times farther away than originally thought.) In the meantime, the forecaster hurried into the radar room with a teletype report that the tornado was visible to the west of the National Weather Service Office in Oklahoma City.

As word quickly spread throughout the Laboratory, a number of staff members crowded onto the observation platform atop the building. The tornado was visible in the distance adjacent to a dark rain shaft. With time, the tornado became obscured by rain. The storm's anvil, with many mammatus formations, extended over the Laboratory and was stretching far to the east and southeast.

1. *Flashback: 24 May 1973*

Twenty-four hours earlier, the NSSL Spring Program forecaster had seen nothing to indicate a chance of severe weather on the next day. However, by morning of the 24th, conditions looked more portentous (Chapter 2). An advancing weak cold front was entering northwestern Oklahoma and moist unstable air was streaming northward into the state. At midlevels in the atmosphere, a minor short wave soon would be overtaking the cold front (Chapter 3). The rawinsonde coordinator alerted the NSSL, Fort Sill and Tinker Air Force Base personnel that special rawinsonde releases (Appendix C) might be requested during the afternoon.

By noon, conditions were becoming even more favorable for severe storm activity. Monitoring of a remote display from the NSSL-instrumented tower north of Oklahoma City indicated that the moisture content of northward-flowing air had been increasing steadily during the past 12 hours (Chapter 4). Radar echoes along the front in southeastern Kansas were extending southwestward to the Oklahoma border. At 1300, the National Severe Storms Forecast Center issued a Tornado Watch covering most of southwestern, central and northeastern Oklahoma for the afternoon and early evening.

During this time, the tornado intercept team was making final plans. Cameras already were packed in the intercept vehicle and at 1300 the team headed toward the cold front in western Oklahoma. A Popular Science writer, who was spending the week at the Laboratory exploring its various research activities, accompanied the intercept team (Gannon, 1973).

Radar echoes were appearing by 1400 in north central and southwestern Oklahoma along the advancing cold front (Appendix B). Based on this development, the aircraft coordinator notified the crews of the Colorado State University F-101 and U.S. Air Force F-100 aircraft based at Tinker Air Force Base to be prepared for take-off at 1500.

In the nearby Doppler radar building, the Doppler radar meteorologist, engineer and technician were making final preparations for data collection. At about 1415 the Doppler radar began scanning the largest echo within range along the developing line--located just south of the Kansas border in north central Oklahoma. A few minutes later word was received from the radar room via "hot line" telephone that there was a teletype report of a funnel sighting with that storm.

The surveillance meteorologist in the radar room, while monitoring storm development and computing echo movement, was keeping an eye on small intermittent echoes that were popping up just ahead of the line. By 1420 it was clear that a significant isolated echo was growing well ahead (50 to 60 km) of the line. Since echoes developing in such a location occasionally become tornadic, the Doppler meteorologist was informed of the new echo. It was decided that the Doppler radar should continue to collect data in the previous funnel-producing (perhaps tornado-producing) storm for a while longer.

Between 1415 and 1420, the tornado intercept team passed within a few kilometers of the cumulus congestus cluster that was producing the isolated radar echo; darkened cloud bases with little or no precipitation were observed. They continued west until 1425 when they stopped to photograph new cloud development ahead. After stopping, they called NSSL and learned of the

isolated echo's existence. From their vantage point they could see that now the storm had a rapidly developing cirrus anvil. The intercept team faced a crucial decision: Should they turn north toward a major echo along the front? Turn southwest toward another major echo along the front? Or turn around and overtake the now distant isolated storm? After much debate, they decided to pursue the isolated storm. They not only had to catch the storm but also had to maneuver to get southeast of it where tornado photography would be better. Due to limited mobility, it would take an hour to get into position (Appendix A).

By this time Doppler radar data collection on the severe storm to the north had ceased; at 1446 sampling of the new storm began. The only real-time Doppler velocity display was the Plan Shear Indicator (PSI) display that the Air Force Cambridge Research Laboratories had brought to NSSL for the 1973 Spring Program (Chapter 7). The first PSI scan through the storm showed appreciable flow disturbances at 1453. Five minutes later, the first clear evidence of a vortex (5 km diameter) appeared at heights of 5 to 8 km.

As aircraft take-off time approached, the aircraft coordinator called off the mission for the day. It had been agreed that when a tornado was likely to develop, the Doppler radar would sample the tornadic storm. Thus, the radar would not be available to record Doppler velocity spectra in nontornadic storms where the aircraft would have been making comparative turbulence measurements.

The storm--like so many in the past--taunted the research meteorologist by skirting along the northern edge of the surface β -scale mesonet network (Chapter 5). Primary purposes of the mesonet network are to establish surface characteristics associated with tornadic storms: convergence, vorticity, gust front evolution, mesoscale low pressure areas, thermodynamic air characteristics, etc.

Seeing thunderstorms approaching, a visiting scientist from the Naval Electronics Laboratory Center turned on his directional sferics detection equipment at 1450. As one of three widely separated sites to study radio propagation of sferics caused by lightning discharges, this equipment in Norman documented the azimuths of sferics activity during the remainder of the storm's lifetime (Chapter 10). At the Oklahoma City National Weather Service Office, 27 km northwest, all sferics activity within 70 km was recorded continuously with a higher-frequency nondirectional detector built by the Wave Propagation Laboratory (Chapter 9).

As the tornado intercept team slowly overtook the storm from the west, they were able to document its visual evolution. Soon after 1500, they noticed that the storm had extensive north-south dimensions. Although then not recognizing it, they were watching a storm that was about to split (Chapters 5, 6 and 8). Alas, the team did not witness the split because they were moving southeastward to get around the storm's southern edge. Instead, they watched the development of a slowly rotating lowered cloud base southwest of the storm's primary precipitation area.

1. *Flashback: 24 May 1973*

By 1515, there was distinct Doppler velocity evidence that a tornado-scale vortex was present at midlevels near the storm's southwest edge (Chapters 7 and 15). At the same time, the NSSL intercept team was observing funnel-like protrusions extending beneath the more rapidly rotating lowered cloud base.

Also watching and photographing the storm were two teams of University of Oklahoma (OU) meteorology students (Moller *et al.*, 1974). One team, approaching the storm from the southeast, got into position 12 km southeast of Union City just before the funnel first appeared. The second team had headed toward the cold front, but--based on a phone call to NSSL--had turned around and now was rushing southeast to catch the storm.

With time, what now is known as the Doppler tornadic vortex signature descended to the ground and, concurrently, a funnel appeared below cloud base (Chapter 15). From 1538 to 1548, while the funnel descended and retracted several times as it moved eastward, a dust cloud continuously was evident on the ground. The NSSL intercept team, racing eastward during this development stage, arrived at their final photography site--9 km southeast of the tornado--just before the visual funnel made continuous contact with the ground (Chapter 11).

By the time the tornado reached Union City, it had left in its wake a 10-km long damage swath through open farmland. Of the six farmsteads affected, five had damage limited primarily to outbuildings and trees. However, on the sixth farm--2 km west of Union City--the house was destroyed completely (Chapter 13). Post-analysis of photographs taken by the intercept team about the same time would reveal tangential velocities over 80 m s^{-1} in the debris cloud (Chapter 14).

As the tornado entered the northwest outskirts of Union City at 1556, it started to shrink in size, move more toward the southeast and gain forward speed. In Union City, about 20 houses were totally destroyed and an equal number received major damage. All mobile homes (18) within the tornado's path were demolished. The town's grain elevator was toppled and several churches and businesses were heavily damaged. Miraculously, no one was killed. The populace was alerted both by seeing the approaching tornado as well as by timely National Weather Service warnings.

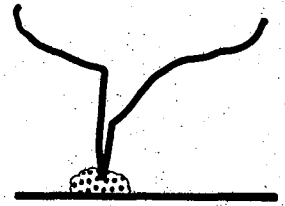
From the north, the second OU student team entered Union City just as the tornado was leaving the southeast part of town. The team had been forced to drive through heavy rain and increasingly large hail to get to the storm's south side. Setting up cameras in the damage path, the students photographed the receding tornado (Moller *et al.*, 1974).

The damage path extended another 6 km southeast of Union City. Although the tornado was shrinking and becoming more tilted, it remained destructive with photogrammetric wind speeds of at least 65 m s^{-1} (Chapter 14). It passed over two more farmsteads southeast of town and both received heavy damage; the second farmhouse completely disappeared leaving a clean concrete slab. When the fragmented serpentine tornado funnel dissipated at 1604, it was 4 km east of the NSSL tornado intercept team.

Before sunset, an NSSL-chartered aircraft surveyed and documented the damage path. Later that night, NSSL meteorologists and OU meteorology students exchanged experiences and outlined procedures for conducting damage surveys and eyewitness interviews starting early the next morning. The days and weeks to follow would be occupied by the arduous tasks of organizing and interpreting data that should lead toward a better understanding of tornadic storms.

REFERENCES

- Gannon, R., 1973: Tornado! How science tracks down the dread twister. Popular Science, September, 64-66, 122-125.
- Moller, A., C. Doswell, J. McGinley, S. Tegtmeier and R. Zipser, 1974: Field observations of the Union City tornado in Oklahoma. Weatherwise, 27, 68-77.



PART II: METEOROLOGICAL SETTING

2. GENERAL SYNOPTIC SITUATION
3. SUBSYNOPTIC-SCALE METEOROLOGICAL FEATURES AND ASSOCIATED CONVECTIVE ACTIVITY ON 24 MAY 1973
4. TALL TOWER MEASUREMENTS PRECEDING THE UNION CITY TORNADIC STORM

Chapter 2
GENERAL SYNOPTIC SITUATION

Charles L. Vlcek¹

*National Severe Storms Laboratory
Norman, Oklahoma 73069*

The synoptic-scale situation leading to the occurrence of severe weather on 24 May 1973 is investigated. Severe weather events in the central Plains were concentrated along an advancing cold front and those in the southern Plains formed along an axis of moist air. The Union City tornado occurred in the region where the front intersected the moisture axis.

2.1 Synoptic Analysis at 0600 CST

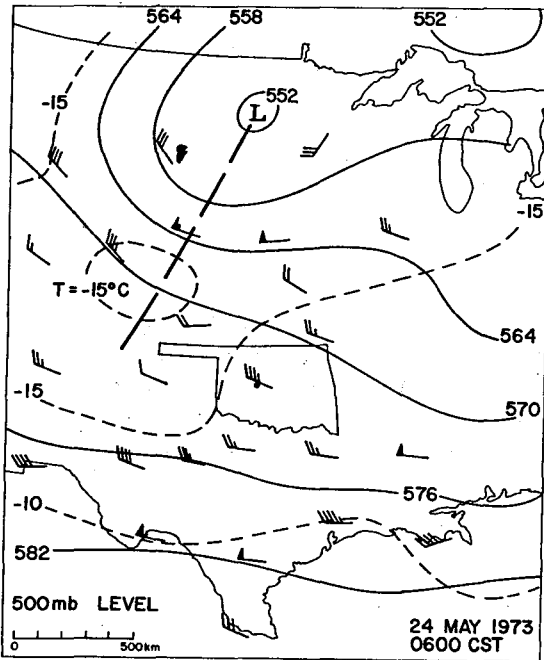
The sequence of events leading to the Union City tornado began on 23 May 1973 when a 500 mb low north of Lake Superior elongated west-southwestward and a new center formed at the junction of North Dakota, South Dakota and Minnesota. A weak, but well-defined, short wave associated with the new low began to sweep southeastward from the northern High Plains. The principal features of the 500 mb chart at 0600 CST on 24 May (Fig. 2.1a) are (1) moderate jets in southern Nebraska and southern Texas and (2) a thermal trough coincident with the approaching short wave which indicates the beginning of cold air advection over Oklahoma. The pocket of warm air over eastern Colorado, actually quite weak (maximum temperature -14°C), probably is due to mountain-induced subsidence and may be ignored since it did not persist. A region of weak diffluence and velocity divergence was present over the Oklahoma and Texas Panhandles. However, there was little or no change in local vorticity in or near that area throughout the day.

Analysis of the 700 mb field at 0600 (Fig. 2.1b) revealed a sharp short-wave ridge over extreme western Oklahoma with its following trough almost directly underneath the 500 mb trough. Warm air advection occurred in Oklahoma at the time with the temperature at 9°C over Amarillo, 8°C over Dodge City, and 7°C over Oklahoma City. Cold advection took place behind and along the trough. There were no definite regions of maximum winds or dry intrusions. Instead the air was rather uniformly dry with dew-point depressions of 13°C or more south of the Kansas-Nebraska border.

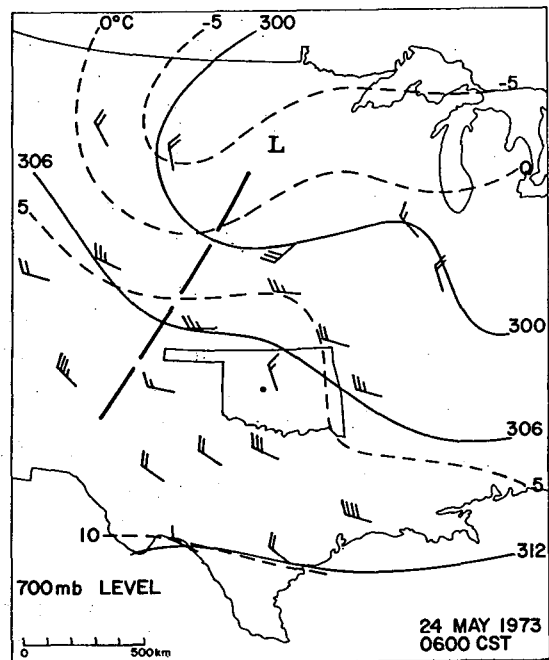
¹Present affiliation: National Meteorological Center, National Weather Service, Washington, D.C. 20233.

2. Synoptic-Scale Environment

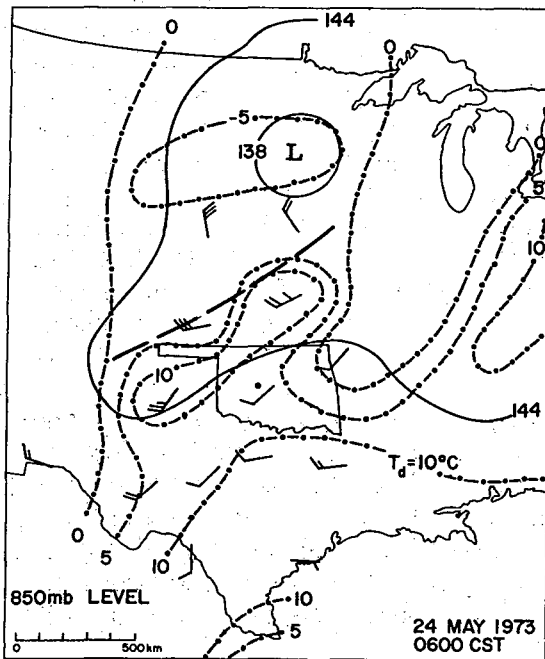
a)



b)



c)



d)

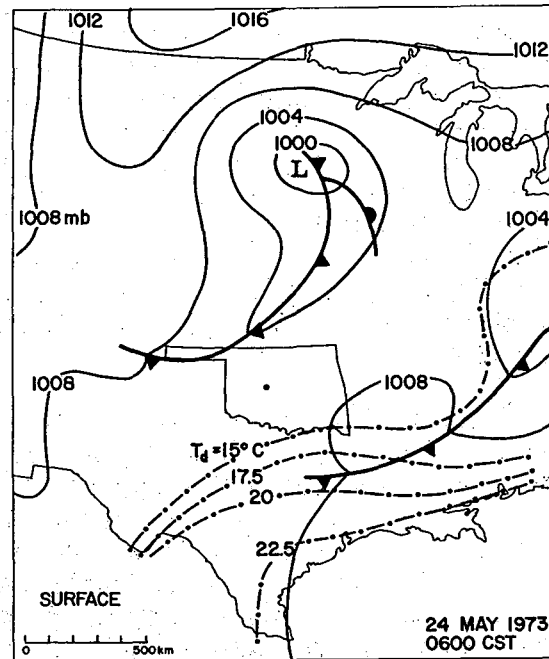


Fig. 2.1 Meteorological parameters analyzed at a) 500 mb, b) 700 mb, c) 850 mb and d) surface, 0600 CST, 24 May 1973. Solid lines, height above sea level (decameters) or sea-level pressure (millibar); thin dashed lines, temperature; dash-dot lines, dew-point temperature; wind barb, 5 m s⁻¹, flag, 25 m s⁻¹. Pressure trough indicated by heavy dashed line. Union City location denoted by dot in west-central Oklahoma.

Moist air was present at the 850 mb level-(Fig. 2.1c). The region with greatest moisture extended from the Texas Gulf coast northwestward into the Texas panhandle, western Oklahoma and eastern Kansas. Meanwhile a thermal ridge lay over eastern New Mexico and southwestern Texas, while a thermal trough extended from the Dakotas to southeastern Colorado. A branch of the thermal ridge, coinciding with the moist air over the Texas Panhandle, northwestern Oklahoma and central Kansas, lay parallel to and just ahead of the height trough. This particular configuration greatly enhances the prospects for severe activity in the form of a squall line along the front by combining maximum instability with maximum low-level convergence.

At 0600 on 24 May, moisture at the surface (Fig. 2.1d) was still mostly confined to Texas and the Gulf coast as low-level return had not yet become organized. At 1800 on 23 May, the surface front northwest of Oklahoma was poorly defined but frontogenesis continued through the night and by the next morning the front was well marked with clearly defined support at all levels up to 500 mb. Strength and definition of the trough continued to increase at all levels as the day progressed.

Over central Oklahoma the strongest tropospheric winds were about 40 m s^{-1} from the west-northwest occurring at the tropopause near the 200 mb pressure level (12 km). These winds were at the northern edge of a broad band of slightly stronger winds at tropopause height which were centered over Texas and Oklahoma.

A composite view of some of the pertinent synoptic features at 0600 (Fig. 2.2) reveals that--although severe weather was not imminent for Oklahoma and the Texas Panhandle--there was strong likelihood that severe weather would occur if the front and upper troughs invaded the region occupied by the moist 850 mb air. The moist air in the Texas panhandle coincided with a small region of greatest temperature difference between 850 and 500 mb levels, as well as a moderate amount of wind shear between these two levels. This area was the scene of some early convective development shortly after noon.

Since the low-level moisture had just begun to return in Oklahoma, local soundings made at 0600 were not representative of the severe weather potential for Oklahoma that day, but there was little doubt that unstable air was on its way for a rendezvous with the front and upper troughs over Oklahoma. Abilene, in west-central Texas, recorded a Lifted Index of -8 and a Lifted Index of -5 was forecast for Oklahoma City by the

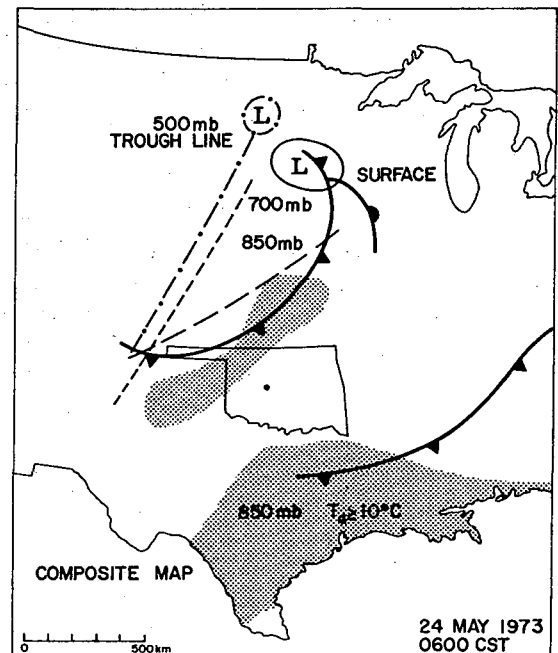


Fig. 2.2 Composite map key parameters presented in Fig. 2.1.

2. *Synoptic-Scale Environment*

National Severe Storms Forecast Center (NSSF), later verified by soundings taken at NSSL.

The sequence of events through 0600 on 24 May gave enough indication of potential severe weather to permit NSSL to prepare for data collection; meanwhile NSSF put out a Convective Outlook indicating the possibility of a few severe thunderstorms in the eastern two-thirds of Oklahoma, later amended to include all of Oklahoma except the Panhandle.

2.2 DEVELOPMENT OF SEVERE WEATHER POTENTIAL

As the day progressed the likelihood of severe weather increased. Although the next available upper level charts show the condition of the atmosphere at 1800, two hours after the occurrence of the Union City tornado, the intervening sequence of events can be inferred by interpolation between these and the charts shown in Fig. 2.1. The surface front and associated upper level troughs continued to advance into Oklahoma. The approach of the 500 mb trough was marked by slight (1°C) cooling over Oklahoma City between 0600 and 1800 CST, a time when diurnal warming would be expected.

Cooling at 700 mb was also slight, with a 1°C drop during the day over Amarillo and Oklahoma City. The strong cold advection occurring over western South Dakota and western Nebraska at 0600 had not reached Oklahoma during the day. However, the short-wave ridge which had been over central Oklahoma at 0600 moved east and winds were backing from northwest to southwest with the approach of the next trough.

Winds over Oklahoma were backing a few degrees at the 850 mb level, drawing in moisture over Oklahoma City and raising the Total Totals Index from 48 at 0600 to 53 at 1800. Significant low-level convergence at 1800 was indicated along the 850 mb trough and attendant surface front by winds which were southerly ahead, northwesterly behind, and southwesterly along the trough.

The surface front which had been south of the Red River moved back into southwestern Oklahoma, then gradually dissipated. Moist air flowed into southwestern Oklahoma where dew-point temperature exceeded 20°C . Dew-points were generally in the upper teens elsewhere in Oklahoma except in the northeast where drier air was slow to evacuate. Meanwhile solar heating raised the temperatures ahead of the front to 25°C or greater.

2.3 SYNOPTIC FEATURES AT 1400 CST

By 1400, just before the NSSL surveillance radar detected first echo of the Union City storm, linearly-interpolated positions of significant synoptic-scale features were stacked almost vertically over northwestern Oklahoma (Fig. 2.3). The superposition of these features would mean that the regions of maximum horizontal wind shear at each level and maximum low-level moisture would overlap, with considerable vertical wind shear and low-level convergence

also present. The timing of trough line passages at various levels through special rawinsondes sites operated by NSSL is discussed by Brandes (Chapter 3).

Evolution of key severe storm parameters during the day indicated that environmental thermodynamics provided the primary influence on severe storm development (Table 2.1). The Lifted and Total Totals Indices at 1400 indicated strong potential instability near the developing storm.

Despite the absence of certain ingredients for producing severe thunderstorms (Table 2.1), those that were present were potent enough. The NSSF forecasters issued Tornado Watch #267 at 1300, valid from 1330 to 1930. The area covered was along and 110 km either side of a line from 35 km southwest of Altus, Oklahoma, to 35 km northwest of Joplin, Missouri; this area included most of southwestern, central and northeastern Oklahoma. Scattered severe thunderstorms (upgraded from "few severe" in the Convective Outlook) were expected as the result of an anticipated southwestward extension of the heavy activity that had already formed in northeast Kansas and west central Missouri. The squall line did build southwestward as forecast and resulted in severe weather in northwest and north central Oklahoma, while the activity which had erupted in the southern Texas Panhandle moved eastward into southwest Oklahoma resulting in some severe weather occurrences there.

The composite map (Fig. 2.3) shows all severe weather events reported by Storm Data (NOAA, 1973) during the afternoon and early evening. As expected, the severe activity was concentrated along the advancing cold front, as well as in Texas near the axis of low-level moisture where a surface intrusion of dry air led to late afternoon severe weather occurrences.

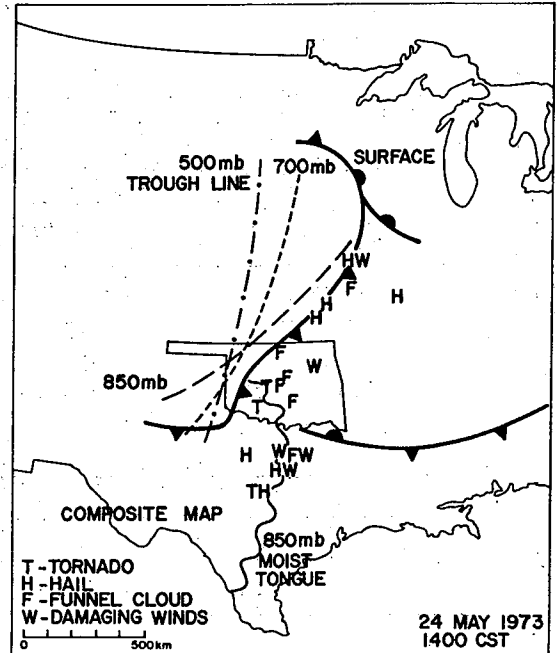


Fig. 2.3 Composite map key parameters interpolated to 1400 CST on 24 May 1973. Shown are the locations of severe weather events during the afternoon and early evening.

2.4 SUMMARY

Severe activity surrounding the tornadic Union City storm resulted from the meteorological sequence:

- (1) A west-southwestward elongation developed from a 500 mb low pressure area just north of the Great Lakes, and a new center formed at the western end of this elongation over the Dakotas and Minnesota.

2. Synoptic-Scale Environment

TABLE 2.1 Strength of Key Severe Storm Parameters (after Miller, 1972) Over Central Oklahoma on 24 May 1973. Strength Categories are Weak (W), Moderate (M), or Strong (S). Parameters at 1400 CST Obtained From Composite Sounding and Interpolated Constant-Pressure Maps.

RANK	PARAMETER		0600 CST	1400 CST	1800 CST
1	500 mb Vorticity		No Positive Vort. Advection (W)	No Positive Vort. Advection (W)	No Positive Vort. Advection (W)
2	Stability	Lifted Index	+2 (W)	-7.6 (S)	-4.9 (M)
		Total Totals	48 (W)	60 (S)	53 (M)
3	Middle Level	Jet	9 m s ⁻¹ (W)	16 m s ⁻¹ (W)	17 m s ⁻¹ (W)
		Shear	3x10 ⁻⁵ s ⁻¹ (W)*	3x10 ⁻⁵ s ⁻¹ (W)*	3x10 ⁻⁵ s ⁻¹ (W)*
4	Upper	Jet	39 m s ⁻¹ (M)	42 m s ⁻¹ (M)	32 m s ⁻¹ (M)
		Shear	5.5x10 ⁻⁵ s ⁻¹ (M)*	6x10 ⁻⁵ s ⁻¹ (M)*	6x10 ⁻⁵ s ⁻¹ (M)*
5	Low-Level Jet		6 m s ⁻¹ (W)	12 m s ⁻¹ (W-M)	10 m s ⁻¹ (W)
6	Low-Level Moisture (Mean Mixing Ratio)		7 g kg ⁻¹ (W)	11.3 g kg ⁻¹ (M)	14 g kg ⁻¹ (S)
7	850 mb Max. Temp. Field		West of Moist Ridge (S)	West of Moist Ridge (S)	West of Moist Ridge (S)
8	700 mb Dry Air Intrusion		Dry Air Present (S)	Dry Air Present (S)	Dry Air Present (S)
9	Surface 12-h Pressure Falls		1 mb (M)	1 mb (M)	2 mb (M)
10	500 mb Height Change		20 m (W)	20 m (W)	20 m (W)
11	Wet-Bulb 0°C Height AGL		1.83 km (M)	2.75 km (M)	3.35 km (M)
12	Surface Pressure		1007 mb (M)	1003 mb (S)	1005 mb (M-S)
13	Surface Dew-Point Temperature		11.5°C (W)	17.6°C (M-S)	21.0°C (S)

*Shear over 165 km distance

Charles L. Vlcek

- (2) A short-wave trough formed at all levels, including frontogenesis at the surface, and rotated about the low.
- (3) As the trough and front approached Oklahoma, low-level winds ahead of the front backed to a more southerly or southeasterly direction, increasing the convergence along the front and drawing moist unstable air around an old front which lay parallel to the Red River in northern Texas. The western end of the old front backed into southwest Oklahoma under the influence of the approaching short wave, concentrating low-level moisture into that region.
- (4) Initial activity broke out in two regions particularly favorable for such development. The first region, in northeastern Kansas, was one of maximum dynamic lifting, where high-level divergence coincided with the intersection of the tip of the moist tongue with the surface front, near the low-level jet. The second region, in the southern Texas Panhandle, was one of maximum instability triggered by the arrival of the cold front and upper troughs as well as by solar heating at the surface.
- (5) The initial severe weather activity in Oklahoma resulted from the squall line in northeastern Kansas building southwestward along the front into northwestern Oklahoma and the activity in the Texas Panhandle advecting into southwestern Oklahoma.
- (6) Juxtaposition of the surface front, upper troughs and low-level moist tongue in western Oklahoma at 1400 CST led to concentrated dynamic forces in central Oklahoma later that afternoon.

2.5 REFERENCES

- Brandes, E. A., 1976: Subsynoptic-scale meteorological features and associated convective activity on 24 May 1973. Chapter 3, The Union City, Oklahoma Tornado of 24 May 1973, R. A. Brown, Editor. NOAA Tech. Memo. ERL NSSL-80, Norman, Nat. Severe Storms Lab., 19-25.
- Miller, R. C., 1972: Notes on analysis and severe-storm forecasting procedures of the Air Force Global Weather Central. Air Weather Service, Technical Report 200 (Revised), 188 pp.
- NOAA, 1973: Storm Data, Asheville, Environmental Data Service, 15 (5).

Chapter 3

SUBSYNOPTIC-SCALE METEOROLOGICAL FEATURES AND ASSOCIATED CONVECTIVE ACTIVITY ON 24 MAY 1973

Edward A. Brandes

*National Severe Storms Laboratory
Norman, Oklahoma 73069*

The Union City tornadic storm developed approximately 55 km ahead of a slow-moving cold front. Environmental conditions were characterized by deep surface moisture and large vertical wind shear. The storm apparently was triggered by a minor upper air trough that moved out ahead of the cold front.

3.1 Introduction

In this Chapter we examine subsynoptic-scale meteorological conditions associated with the convection of 24 May 1973 and describe the environment in which the Union City tornadic storm developed. For our investigation we utilize hourly products (1300-1700 CST) from a subsynoptic objective analysis routine (Barnes, 1973). The output includes streamlines, divergence, vorticity, wet-bulb potential temperature, and moisture convergence fields in addition to the more familiar wind speed, pressure, temperature, and dew-point temperature fields. Reports from National Weather Service and military stations have been supplemented with observations from the National Severe Storms Laboratory (NSSL) α mesonet network (average combined station spacing 80 km). A complete collection of all hourly maps and all analyzed fields is given in Appendix B. Observations from the NSSL β mesonet network (average station spacing 15 km), a three-station rawinsonde network, and the NSSL weather radars also were used.

3.2 SURFACE METEOROLOGICAL FEATURES

At 1300 (all times CST) a weak cold front stretched across northwestern Oklahoma. Strong thunderstorm activity along the front in eastern Kansas tapered to small but intensifying showers in north central Oklahoma. In northwest Texas, an area of moderate thundershowers was located ahead (south) of the cold front, in a region of westerly winds which converged further east with southeasterly winds. The attendant cloud pattern as viewed from the Defense Meteorological Satellite at 1252 is shown in Fig. 3.1. The wind streamline pattern (see Brandes, Appendix B) reveals a confluent wave-like wind feature with its crest in the southwestern corner of Oklahoma; surface observations indicate convective activity was just beginning in this area.

3. *Subsynoptic-Scale Features*

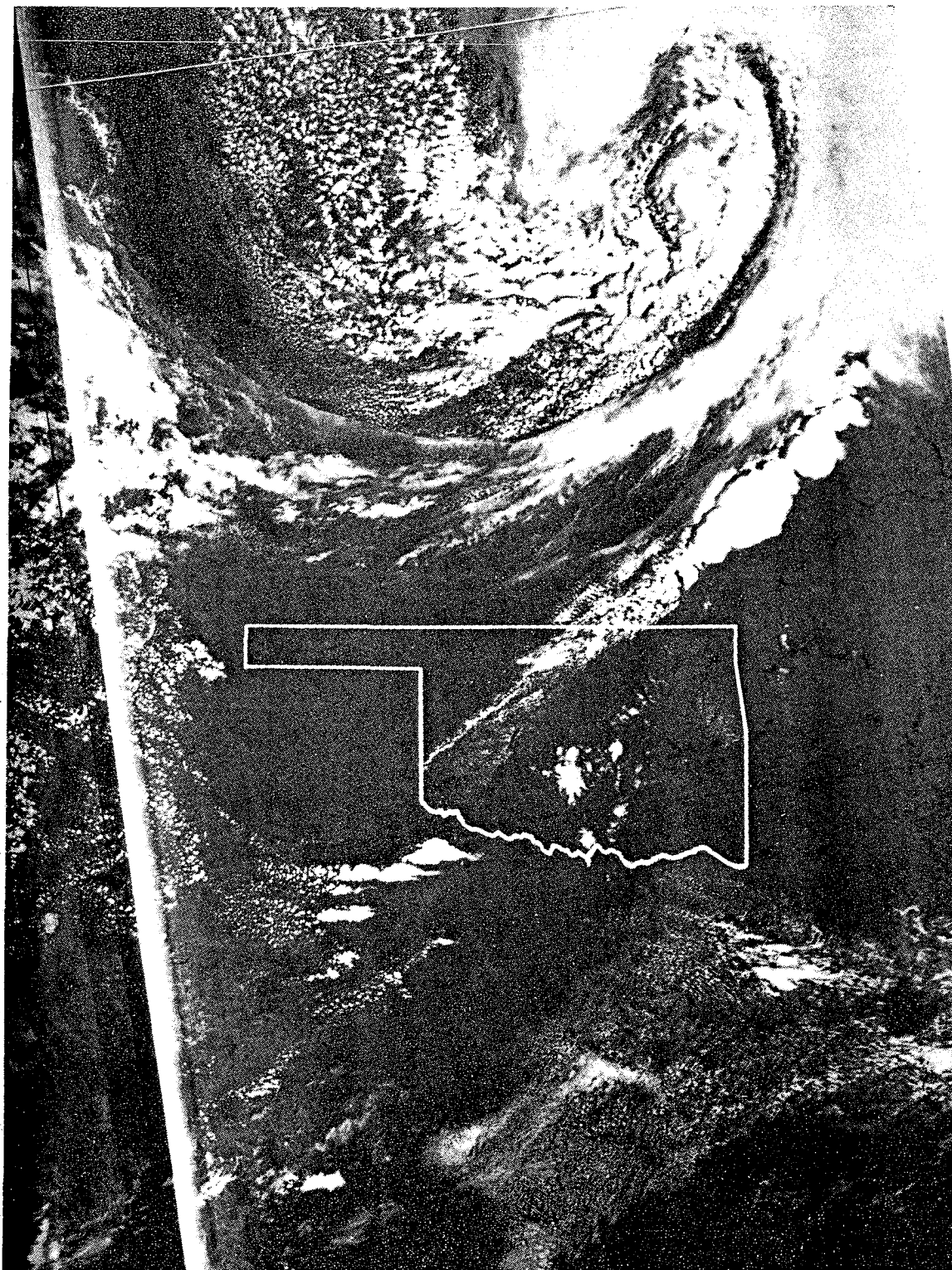


Fig. 3.1 Defense Meteorological Satellite cloud photograph at 1252 CST, 24 May 1973.

The surface pressure pattern consists of a trough extending from a low pressure center in southeastern Kansas southwestward to a second center south of the Texas Panhandle. Nearly uniform temperatures, in the upper 20's°C, were observed over Oklahoma except behind the front. Maximum dew-point temperatures ($>18^{\circ}\text{C}$) were in a band along and just ahead of the front--coincident with the broad band of cumulus clouds evident in Fig. 3.1. The presence of dry air, both at the surface and aloft, suppressed convection along the front in the Texas Panhandle. A dry line *per se* was not readily apparent in the data, due--in part--to missing dew-point temperatures at Plainview and Lubbock, Texas.

Except in western Texas, thunderstorms were near the axis of maximum wind convergence located slightly to the west of the high moisture axis. Compared with other severe weather days, convergence, vorticity and moisture convergence were not particularly strong.

After 1300, thunderstorm activity increased. Nearly all radar echoes remained within the moisture convergent area and in general were oriented along the maximum moisture convergence axis. The largest and most intense thunderstorms were near moisture convergence maxima. A surface low pressure center was located in the vicinity of the wave crest between 1400 and 1700. However, a closed cyclonic circulation was evident only at 1600 and 1700.

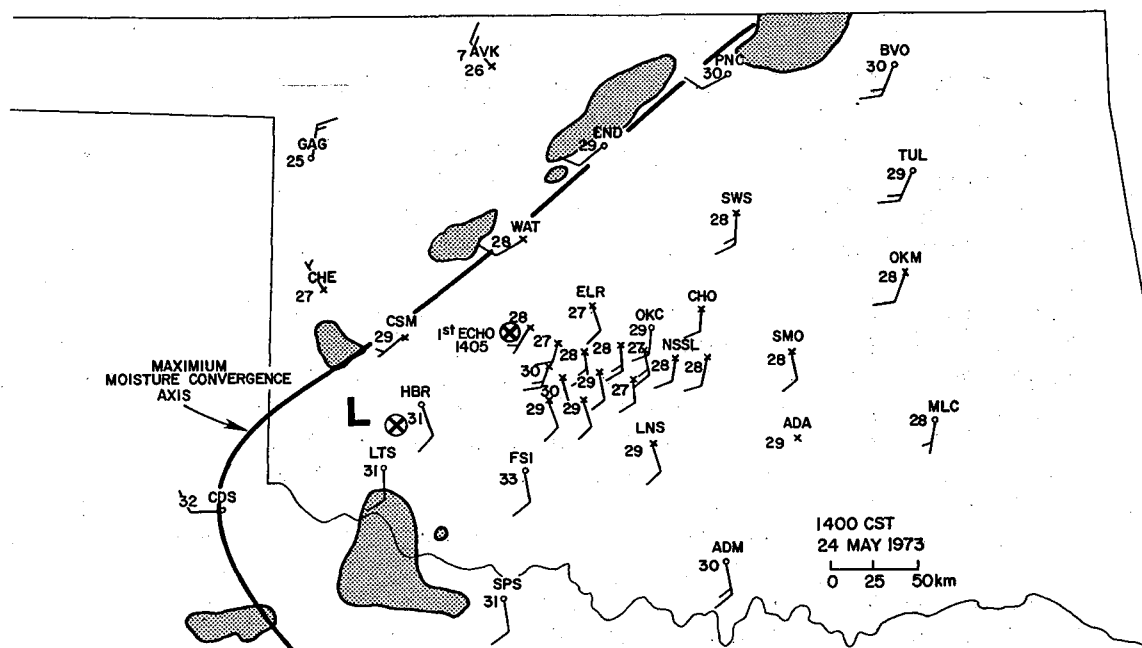


Fig. 3.2 Surface conditions at 1400 CST, 24 May 1973 using observations from National Weather Service stations (o) and NSSL α and β mesonet stations (x). L denotes center of low pressure area. Temperature ($^{\circ}\text{C}$) is plotted next to station location. Long wind barb is 5 m s^{-1} . Stippled areas are 0° elevation radar echo outlines from NSSL WSR-57 surveillance radar. Position of first radar echo (1405 CST) of Union City storm is indicated.

3. *Subsynoptic-Scale Features*

The Union City storm "first echo" was observed at 1405 approximately 55 km ahead of the cold front (see Fig. 3.2). NSSL field observers noted that the echo was associated with the largest cloud tower in a north-south line of developing cumuli within the general cloud band ahead of the cold front (see Golden, Appendix A). Further east and west, except in the frontal zone, clouds had considerably less vertical development. Showers which formed between the Union City storm and the front remained small scale and dissipated as the storm grew rapidly between 1400 and 1500. New cell growth to the north and south eventually extended to the cold front and to the activity in Texas.

As convection coverage and intensity increased, temperature and computed meteorological fields dependent upon wind observations (i.e., vorticity, divergence, etc.) became increasingly dominated by smaller scale features. By 1700, southerly winds began to return at sites west of the thunderstorms indicating storms in eastern Oklahoma were detached from the front.

Still later, precipitation coverage and intensity slowly began to decrease. The wind pattern revealed two distinct convergent areas--one along the cold front and another in southeastern Oklahoma. The "noise level" remained high in the computer products (especially in the vorticity and convergence fields) while extrema decreased. Moisture convergence was considerably weaker and was primarily located at the leading edge of the thundershower line.

3.3 ENVIRONMENT OF THE UNION CITY TORNADIC STORM

The Union City storm formed within a region of light southwesterly winds and surface temperatures of approximately 28°C. Slightly greater wind speeds (6 to 8 m s⁻¹) from the southeast were located to the east (Fig. 3.2). On the subsynoptic scale winds were convergent and vorticity was slightly negative.

In anticipation of severe weather, rawinsondes were released from Fort Sill (FSI) and Tinker Air Force Base (TIK) at 1400 (see Appendix C for illustrated soundings). The FSI sounding, northeast of the Texas activity and within the prefrontal band of southwesterly winds where the storm formed, revealed a Lifted Index of -7 and a low-level moist layer extending to nearly 850 mb (1.06 km AGL). The TIK release, east of all showers, revealed the moisture layer to be below 900 mb (0.56 km). The Lifted Index for this sounding (TIK) was -2, a decrease from +2 at 0600. Except near the ground, low level winds were parallel to the front throughout the moist layer while at greater heights they veered rapidly to the west. Environmental stability and wind shear characteristics given by Marwitz (1972) for several documented supercell storms are reproduced in Table 3.1. Computed parameters for the TIK sounding (Union City tornadic storm) are included for comparison.

An interesting feature of the NSSL sounding released at 1532 is the appearance of a 1°C low-level inversion near 870 mb (0.85 km). Beebe (1963) has shown that low-level temperature inversions in the vicinity of severe storms are lifted by the approaching storm. It may be that some inversions owe their existence to large severe storms. Mass continuity considerations require strong updrafts to have subsidence in surrounding regions. Fankhauser

TABLE 3.1 *Thermodynamic Stability and Wind Shear Parameters for Certain Well-Documented Supercell Storms (after Marwitz, 1972).*

CASE STUDY	Thermal buoyancy at 500 mb using parcel method (°C)	Veering in subcloud layer (deg)	Mean wind in subcloud layer (deg/m s ⁻¹)	Mean wind surface to 10 km (deg/m s ⁻¹)	Storm motion (deg/m s ⁻¹)	Shear in cloud layer (10 ⁻³ s ⁻¹)
Browning and Donaldson	+4	50	180/17	260/27	255/10	2.5
Browning	+8	80	190/13	255/25	270/10	4.0
Haglund	+5	60	200/13	265/25	280/14	2.5
Marwitz and Berry	+9	90	190/10	250/17	285/14	4.5
Grover Storm	+5	60	160/11	250/15	320/9	4.0
Union City Storm (TIK 1400)	+8	60	227/9	268/19	283/10	3.7

(1971) has found that moisture requirements for large thunderstorms are met by drawing moisture from an area approximately three times that swept out by the storm. Convective activity, except in proximity to the main updraft, would be suppressed due to a reduction in low-level moisture content in surrounding regions. Furthermore, the temperature inversion would restrict the region of low-level energy release--a self-preserving characteristic of large severe storms.

3.4 POSSIBLE TRIGGERING MECHANISMS

The TIK and FSI soundings indicated a 31°C surface temperature would be required to initiate convective overturning. Inspection of standard level wind data (Table 3.2) shows that northwesterly wind directions early in the day (700 and 500 mb) backed to the southwest at 1532 and later returned to the northwest. The extent to which severe storm blocking influenced the 1532 sounding is not known but is thought to be less than the total directional change over the period shown. The pattern suggests the passage of a minor upper air trough that likely acted to trigger the Union City storm. During the afternoon, this upper air feature, which may also have been responsible for the early activity in Texas, overran both the front and the moist tongue to the east. Thus, after 1700, activity decreased along the front due to lack of upper air support and decreased further east due to reduced convergence of moist surface air.

3.5 SUMMARY AND CONCLUSION

The Union City storm environment has been described with the aid of hourly objective surface analysis products and periodic rawinsonde measurements. Storm formation was approximately 55 km ahead of a developing line of frontal thunderstorms. Presence of large vertical wind shear, abundant low

3. Subsynoptic-Scale Features

TABLE 3.2 *Trend in Wind Direction at Standard Levels.*

TIK	and	NSSL		FSI
850 mb				
0600		230/4 m s ⁻¹		1400 206/9 m s ⁻¹
1400		241/11		1600 222/13
1532		212/14		1715 231/12
1715		244/7		
1818		226/8		
700 mb				
0600		340/8		1400 255/13
1400		248/12		1600 263/17
1532		239/16		1715 295/18
1715		283/15		
1818		295/15		
500 mb				
0600		295/16		1400 278/16
1400		285/18		1600 MISSING
1532		265/18		1715 277/20
1715		268/15		
1818		283/19		

level moisture, and a front are typical of severe storm environs. The isolated severe storm ahead of the squall line most probably was triggered by the passage of an upper-level trough.

3.6 ACKNOWLEDGMENTS

The author appreciates the many contributions of Guy Lappie, Lester Showell and Gerald Wardius who set up and maintained the NSSL α and β mesonet-works.

3.7 REFERENCES

- Barnes, S. L., 1973: Mesoscale objective map analysis using weighted time series observations. NOAA Tech. Memo. ERL NSSL-78, Norman, National Severe Storms Laboratory, 60 pp. (Available from National Technical Information Service, Springfield, Virginia 22151, No. COM-73-10781.)
- Beebe, R. G., 1963: Tornado proximity soundings. Proceedings, Third Conf. on Severe Local Storms, Boston, Amer. Meteor. Soc., 6 pp.
- Brandes, E. A., 1976: Hourly surface weather maps and analyzed fields of meteorological variables: 24 May 1973. Appendix B, The Union City, Oklahoma Tornado of 24 May 1973, R. A. Brown, Editor. NOAA Tech. Memo. ERL NSSL-80, Norman, Nat. Severe Storms Lab., 191-203.
- Fankhauser, J. C., 1971: Thunderstorm-environment interaction determined from aircraft and radar observations. Mon. Wea. Rev., 99, 171-192.
- Golden, J. H., 1976: Tornado intercept strategy and morphological observations. Appendix A, The Union City, Oklahoma Tornado of 24 May 1973, R. A. Brown, Editor. NOAA Tech. Memo. ERL NSSL-80, Norman, Nat. Severe Storms Lab., 185-189.
- Marwitz, J. D., 1972: The structure and motion of severe hailstorms. Part I: Supercell storms. J. Appl. Meteor., 11, 166-179.

Chapter 4

TALL TOWER MEASUREMENTS PRECEDING THE UNION CITY TORNADIC STORM

W. David Zittel

*National Severe Storms Laboratory
Norman, Oklahoma 73069*

Data from a 481 m meteorologically-instrumented TV tower in north Oklahoma City are analyzed for the 24-hour period prior to a tornadic storm during the afternoon of 24 May 1973. Differential advection during the night enhanced a radiational low-level inversion that restricted convective mixing the following morning. Also, a shallow moist layer permitted strong surface radiational heating. In the late morning, a deeper moisture layer was advected into the area.

4.1 Introduction

Since 1966, the National Severe Storms Laboratory (NSSL) has collected data from a 481 m tall meteorologically instrumented TV transmitting tower owned by WKY Television Systems¹. The tower is located 37 km north of NSSL in gently rolling terrain. Downtown Oklahoma City is 10 km southwest while its suburbs extend to within 4 km of the site. Sanders and Weber (1970) provide details of the local terrain.

On 24 May 1973, the Union City tornado occurred approximately 45 to 55 km west-southwest of the tower facility. Being east of the developing tornadic storm, tower measurements reflect general characteristics of the lowest 0.5 km of the environment in which the storm formed. Round-the-clock monitoring of the atmosphere has made it possible to deduce the sequence of events which favored convective activity on this day.

4.2 TOWER INSTRUMENTATION

For the 1973 spring season, meteorological instruments were located at 89, 266 and 444 m above the ground. Wind speed and direction were sensed with aerovanes, while vertical velocity was sensed with Gill vanes. Dry- and wet-bulb temperatures were measured using aspirated shielded linearized thermistors; wet-bulb temperature measurement was achieved by attaching a muslin wick over a thermistor and placing the other end in a water reservoir. Pressure

¹Now KTVY.

4. Tall Tower Measurements

units were mounted at 89 and 444 m and a pyranometer and raingage were located at the surface. Some signal conditioning was performed at the tower site. Data were converted from analog to digital form and then telemetered to NSSL in Norman for recording on magnetic tape. Carter (1970) and Goff and Zittel (1974) give more information about instrumentation and calibration procedures.

4.3 MEAN DIURNAL PATTERNS FOR mT AIR

During the 1973 spring season, 37 days of digital data were collected at a 10 sec sampling rate. From these data, mean hourly values were computed and then the values were averaged by hour to determine an overall diurnal pattern for the approximately 20 days when a southerly wind was present. Data were stratified in this manner to provide a homogeneous sample of maritime tropical (mT) air originating over the Gulf of Mexico. The smaller diurnal temperature change and lapse rate variation revealed in the stratified data are consistent with that reported by Goff and Hudson (1972) for mT air. The mean moisture values for all hours averaged together at 89, 266, and 444 m are 11.2, 10.7, and 10.2 g kg⁻¹, respectively. The resultant wind follows the expected diurnal pattern of veering during the night and backing during the day (Crawford and Hudson, 1973).

4.4 CONDITIONS ON 23-24 MAY 1973

During the evening of 23 May and the morning of 24 May, tower-layer temperatures exhibited several interesting features--the two most prominent being the warming at 444 m after 2300 CST on the 23rd and the strong heating at 89 m which occurred the morning of the 24th (Fig. 4.1). The 89 m temperature rise was nearly 10°C while the diurnal temperature variation for other days with a southerly wind component was only about 7°C.

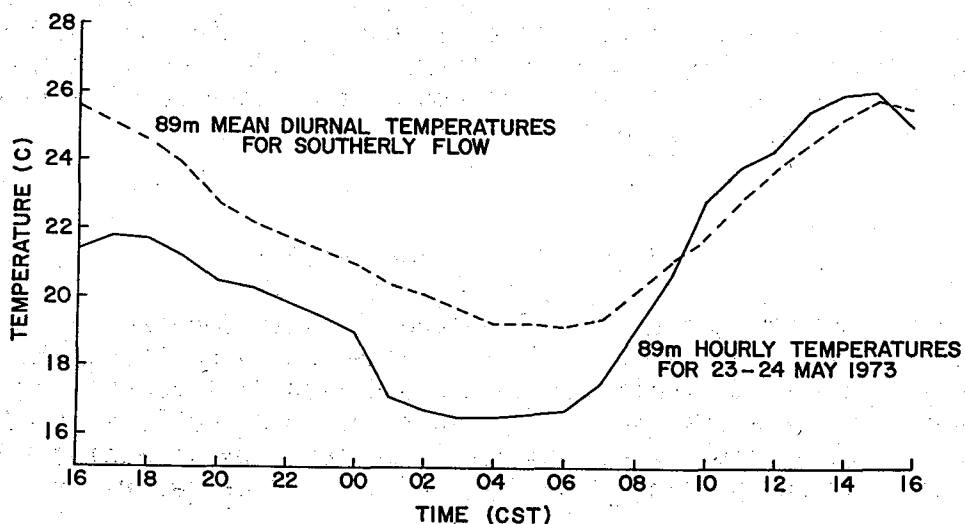


Fig. 4.1 Comparison of diurnal pattern of averaged temperature data at 89 m for southerly wind days (dashed line) to mean hourly temperatures (solid lines) at 89 m for 23-24 May 1973.

Excessive low-level heating was favored by the presence of an inversion in the tower layer (Fulks, 1951). The inversion acted as a cap, restricting convection to a shallow surface layer and thus, preventing dilution of the surface layer (Fleagle and Businger, 1963; Lee, 1973). Inversions are formed by three processes: (a) radiational cooling, (b) differential advection, and (c) subsidence (Watson, 1971). The first two contributed directly to the formation of the inversion through the tower layer. A subsidence inversion, while not directly observable by the tower, was indicated in the 24 May, 0600 Tinker AFB (OKC) sounding at a height of 1750 m above the ground.

On the evening of the 23rd, the temperature fell at 89 m (Fig. 4.1) due to surface radiational cooling, while after 2300, the temperature started to rise at 444 m (Fig. 4.2). Warm air advection which likely accounted for the warming at 444 m, was also indicated on the 0600 850 mb map. Between 0500 and 0800 the lowest tower layer warmed quickly destroying the surface inversion (Fig. 4.2). Between 0800 and 1100 both the lower and mid levels warmed several degrees while the top warmed only slightly. After 1100 the entire tower layer warmed rapidly, the inversion through the tower having lifted and weakened. As late as 1530 CST, a Norman sounding still indicated a 1°C cap at about 850 m height (see Brandes, Appendix C).

Differential advection, while not strong on 23-24 May, played a crucial role in establishing favorable severe storm conditions. During the night and most of the morning winds veered both with time and height shifting to south-westerly flow (Fig. 4.3). Air arriving at 444 m after midnight was considerably drier than that at 89 m; the difference became especially pronounced between 0500 and 1000 (Fig. 4.4). The drier air permitted long-wave radiation loss and surface cooling during the night as well as strong surface heating in the morning (Fig. 4.1). After 1100, tower layer winds began to back with time and height. As a result, the mixing ratio increased during the early afternoon reflecting moist air advection. Maximum hourly mixing ratio values for the day--12.2 g kg⁻¹ and 12.0 g kg⁻¹ at 89 and 444 m respectively--occurred at 1600. Also affected by the moisture return was the rate of temperature rise with time. The slope was much steeper between 0600 and 1000 CST than between 1000 and 1500 CST.

The events, in chronological order, were differential advection during the early morning hours of 24 May which produced a capping inversion. After sunrise, with moisture restricted to the ground layer, strong surface radiational heating occurred. By late

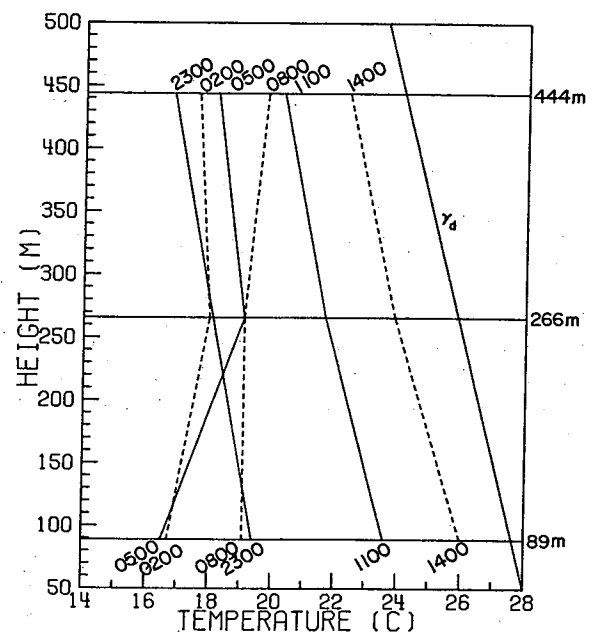


Fig. 4.2 Tower temperature profiles at three hour intervals from 2300, 23 May 1973 to 1400, 24 May 1973.

4. Tall Tower Measurements

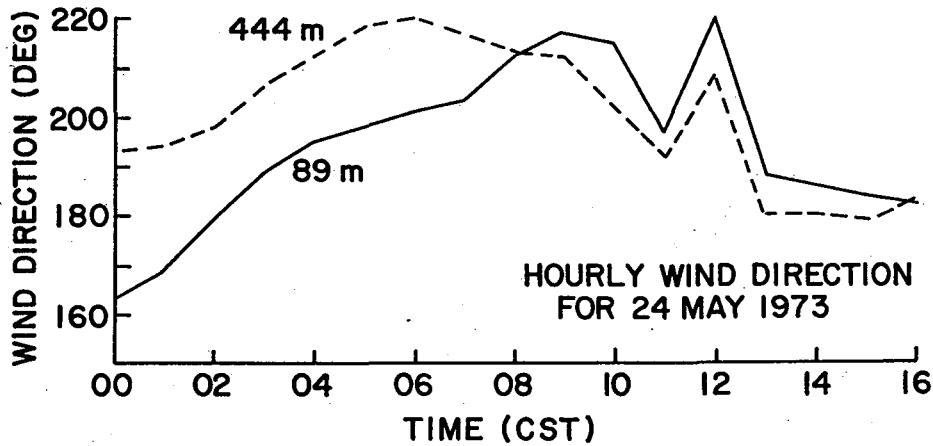


Fig. 4.3 Variation of wind direction with time for 24 May 1973 at 89 m (solid line) and 444 m (dashed line).

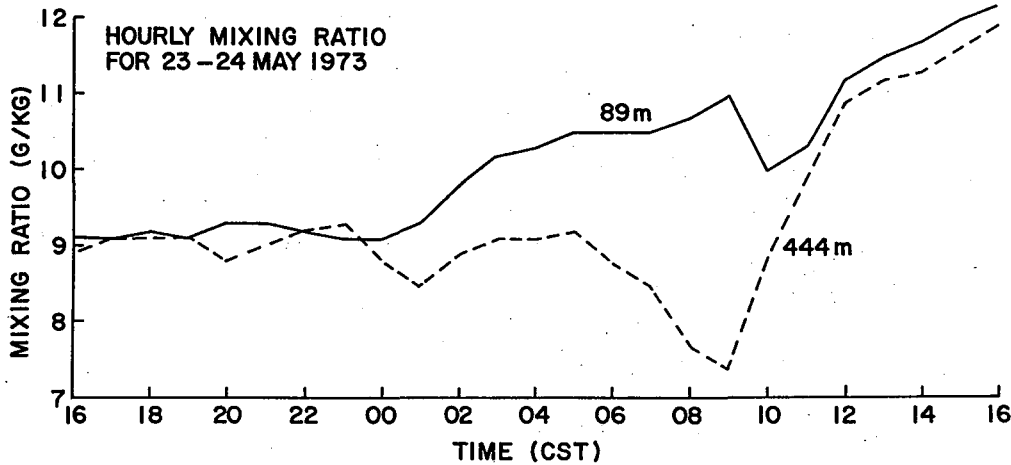


Fig. 4.4 Mean hourly mixing ratio computed for 89 m (solid line) and 444 m (dashed line) for 23-24 May 1973.

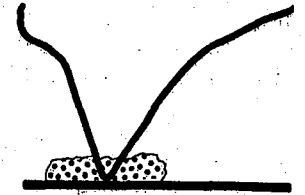
morning, a deeper moist layer was advected into the area. These events--along with other atmospheric conditions discussed by Vlcek (Chapter 2) and Brandes (Chapter 3)--provided a favorable environment for the development of the Union City storm.

4.5 ACKNOWLEDGMENTS

The author wishes to acknowledge the assistance of Leonard Johnson in the installation, calibration and maintenance of the tower system.

4.6 REFERENCES

- Brandes, E. A., 1976a: Subsynoptic-scale meteorological features and associated convective activity on 24 May 1973. Chapter 3, The Union City, Oklahoma Tornado of 24 May 1973, R. A. Brown, Editor. NOAA Tech. Memo. ERL NSSL-80, Norman, Nat. Severe Storms Lab., 19-25.
- _____, 1976b: Rawinsonde observations on 24 May 1973. Appendix C, The Union City, Oklahoma Tornado of 24 May 1973, R. A. Brown, Editor. NOAA Tech. Memo. ERL NSSL-80, Norman, Nat. Severe Storms Lab., 205-207.
- Carter, J. K., 1970: The meteorologically instrumented WKY-TV tower facility. NOAA Tech. Memo. ERL TM-NSSL-50, Norman, Nat. Severe Storms Lab., 18 pp.
- Crawford, K. C., and H. R. Hudson, 1973: The diurnal wind variation in the lowest 1500 ft in central Oklahoma: June 1966-May 1967. J. Appl. Meteor., 12, 127-132.
- Fleagle, R. G., and J. A. Businger, 1963: An Introduction to Atmospheric Physics. Intern. Geophys. Ser., Vol. 5, New York, Academic Press, 346 pp.
- Fulks, J. R., 1951: The instability line. Compendium of Meteorology, Boston Amer. Meteor. Soc., 647-652.
- Goff, R. C., and H. R. Hudson, 1972: The thermal structure of the lowest half kilometer in central Oklahoma: December 9, 1966-May 31, 1967. NOAA Tech. Memo. ERL NSSL-58, Norman, Nat. Severe Storms Lab., 53 pp.
- _____, and W. D. Zittel, 1974: The NSSL/WKY tower data collection program: April-July, 1972. NOAA Tech. Memo. ERL NSSL-68, Norman, Nat. Severe Storms Lab., 45 pp.
- Lee, R., 1973: The "greenhouse" effect. J. Appl. Meteor., 12, 556-557.
- Sanders, L. D., and A. H. Weber, 1970: Evaluation of roughness lengths at the NSSL/WKY meteorological tower. ESSA Tech. Memo. ERL TM-NSSL-47, Norman, Nat. Severe Storms Lab., 24 pp.
- Vlcek, C. L., 1976: General synoptic situation. Chapter 2, The Union City, Oklahoma Tornado of 24 May 1973, R. A. Brown, Editor. NOAA Tech. Memo. ERL NSSL-80, Norman, Nat. Severe Storms Lab., 11-17.
- Watson, G. F., 1971: A diagnostic study of the kinematic and physical processes maintaining a strong low level subsidence inversion over land. Dept. Meteor., Florida State Univ., Report No. 71-3, 149 pp.



PART III: PARENT STORM

5. UNION CITY STORM HISTORY
6. SEVERE STORM SPLITTING AND LEFT-MOVING STORM STRUCTURE
7. OBSERVATIONS OF THE UNION CITY TORNADIC STORM BY PLAN SHEAR INDICATOR
8. TORNADIC STORM AIRFLOW AND MORPHOLOGY DERIVED FROM SINGLE DOPPLER RADAR MEASUREMENTS
9. ELECTROMAGNETIC SIGNATURE OF THE UNION CITY TORNADIC STORM AT THREE MEGAHERTZ
10. DIRECTIONAL MEASUREMENTS OF VERY LOW FREQUENCY (VLF) SPHERICS IN THE UNION CITY TORNADIC STORM

Chapter 5

UNION CITY STORM HISTORY

Donald W. Burgess and Leslie R. Lemon¹

*National Severe Storms Laboratory
Norman, Oklahoma 73069*

High resolution NSSL radar recorded the reflectivity life history of the Union City tornadic storm. The developing storm is categorized as multicellular, but evolves into the classical supercell structure (sloping overhang, vault and hook echo). During the supercell phase, a complex of nearby cells develops but the Union City storm retains its dominance over all other convection. While the tornado is on the ground, the supercell undergoes collapse. The tornado's final stages occur in an echo whose intensity is weakening and whose character appears benign.

5.1 Introduction

Historically, the interpretation of radar echoes has played a leading role in research aimed at understanding thunderstorm structure and evolution. It was a radar study of two storms (Wokingham and Geary) which led Browning and Donaldson (1963) to the conclusion that the severe local storm maintained a distinctive structure. Similarities in echo characteristics for severe storms pointed to classification systems and life cycles based on radar echo appearance. Notable severe storm classifications, proposed by Browning (1968), Marwitz (1972) and Chisholm (1973), include the categories of squall line, multicell, supercell, and severely sheared storms.

Radar echoes also have been used as the leading tool in storm severity determinations for warning purposes. Tornado warnings are issued partly from observations of pendant or hook type echoes (Donaldson, 1965).

The location of the Union City tornadic supercell storm provided a unique opportunity for the National Severe Storms Laboratory (NSSL) radars to record its reflectivity life history. Using reflectivity data, we examine the storm's multicellular origin, its development into a dominant single cell (supercell) and subsequent evolution into a storm complex composed of several cells. The character of the supercell weak echo region (WER) is emphasized.

¹Present affiliation: National Severe Storms Forecast Center, Techniques Development Unit, Federal Building, Kansas City, Missouri 64106.

5. Union City Storm History

A portion of storm development was over the NSSL mesonetwork of surface recording sites, permitting echo character to be compared with surface parameters. In addition, reports from NSSL storm intercept teams were blended with surface data to provide more information.

All radar reflectivity, surface and storm intercept data were utilized to prescribe storm life cycle. The conventional radar data, comparable with that available to facilities with warning responsibility, are tested for its value in providing accurate tornado warnings to the public.

5.2 DATA SOURCES

Reflectivity data were available from the NSSL WSR-57 surveillance radar (beamwidth 2.2°) and Doppler radar (beamwidth 0.8°). See Sirmans (Appendix D) for complete radar parameters. Multiple pulse integration in spatial volumes by both radars provide very accurate intensity estimates (Sirmans and Doviak, 1973). The data collection mode for both radars consisted of antenna tilt sequences. The WSR-57 sequence interval was 5 minutes and the Doppler sequence interval was approximately 10 minutes. Only the WSR-57 tilt sequences included scans through the altitude of storm echo top.

The storm echo was first detectable by the WSR-57 radar at 1405 CST, but Doppler reflectivity data collection did not begin until 1445. Therefore, early echo development was traced through the use of the WSR-57 and later echo evolution was studied by analyzing the higher resolution Doppler data. Unfortunately, a Doppler radar malfunction caused receiver saturation at relatively low power return levels after 1503. As a consequence, absolute values of intensities much above 45 dBZ at storm ranges were not determined and the highest intensity contoured from the Doppler data after 1503 is 45 dBZ. Doppler radar data were objectively analyzed using the method described by Brown (Appendix E).

5.3 FIRST ECHO DEVELOPMENT

Union City storm first echo formed just northwest of the NSSL mesonetwork and several kilometers west of a wind-shift line separating regions of southeasterly and southwesterly winds (Brandes, Chapter 3). Intensification of the first precipitation core or cell (labelled 1' in Fig. 5.1) was depicted at 0° elevation angle as continuous growth. However, at higher elevation angles, exemplified by 4° elevation, Cell 1' grew rapidly until 1430 and then weakened. A second 4° elevation cell (labelled 1) developed just behind 1' at 1430 and immediately experienced explosive growth. Apparently, precipitation from the two cells aloft merged at low levels giving rise to the single cell appearance at 0° elevation. Cell 1 became dominant by 1440 and served as the parent for future development while Cell 1' gradually weakened and lost its identity.

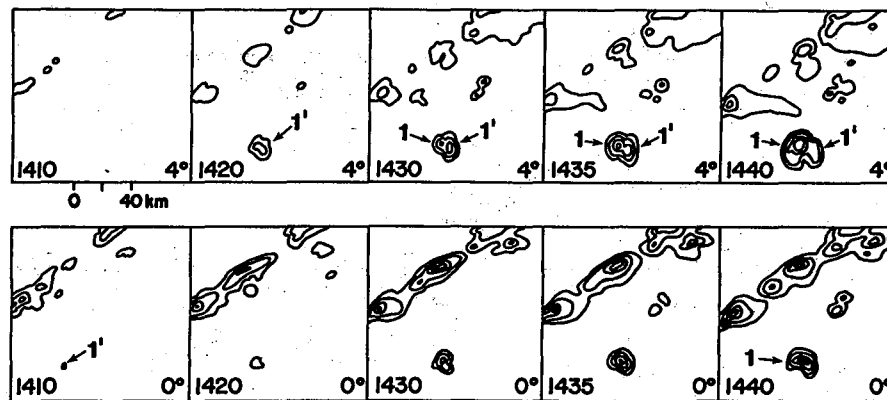


Fig. 5.1 WSR-57 radar echoes at given times and elevation angles for developing Union City storm. Contours are in 10 dBZ intervals beginning at 10 dBZ.

First echo height has been correlated with later storm severity. Storms with great first echo height are quite often severe (Browning and Atlas, 1965). The great height is attributed to strong updrafts which carry cloud particles to high levels before they grow to radar detectable sizes. Cell 1' first-echo midheight was 4.0 km, a level common for showers that fail to develop into severe storms. Cell 1 first-echo midheight was considerably higher--8.2 km--indicating the existence of much stronger updraft and high potential for severe storm development.

Low-level echo motion for Cell 1 from 1410 to 1510 was from 260° at 8 m s^{-1} . This motion is slower and somewhat to the left of the pressure-weighted mean wind (cloud base to tropopause), determined to be 274° at 19.6 m s^{-1} (Fig. 5.2). A portion of the deviation from the mean wind may be explained by the development of Cell 1 aloft to the left rear of the existing cell (1') and both their contributions to the low-level echo.

5.4 STORM EVOLUTION

At 1446 the Doppler radar began a series of tilt sequences through the Union City storm which continued until the storm moved within the radar ground clutter after 1600. Tilt sequence time periods, maximum elevation angles per tilt and selected reference times are in Table 5.1. These radar data are summarized (Fig. 5.3) by displaying together the objectively analyzed low-level reflectivity fields and regions where mid-levels echo between 4 and 7 km above the ground extended outward beyond low-level echo. These mid-level overhang regions are used to detect new echoes, measure approximate echo size aloft and indicate possible updrafts. It is realized that all overhang does not indicate updraft, but consistent observation of overhang along echo flanks (not in the anvil outflow direction) is believed to reflect rising air within the storm's weak echo region or WER (Marwitz, 1972; Chisholm, 1973). Intense

5. Union City Storm History

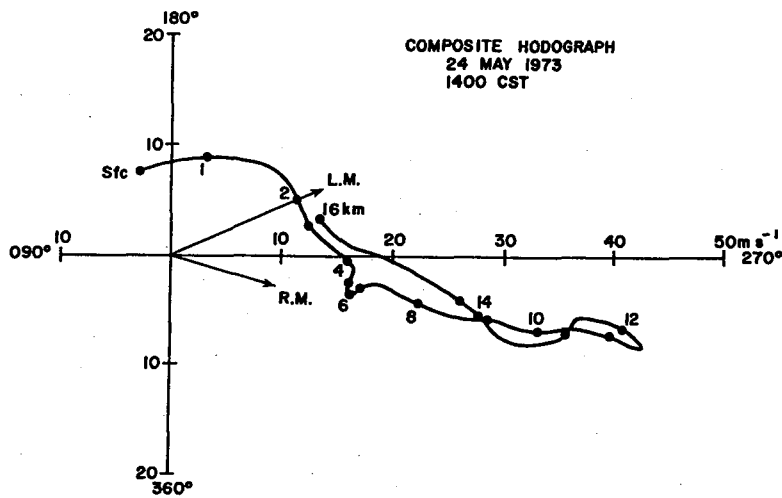


Fig. 5.2 Hodograph of winds at 1400 composited from simultaneous rawinsonde releases 90 km south and 90 km east of the developing Union City storm. Speed and direction of right-moving (R.M.) and left-moving (L.M.) portions after split are indicated.

updraft centers are often indicated by weak echo completely bounded by strong echo (Browning, 1965a). Bounded weak echo regions (BWER) appear hatched in Fig. 5.3; see Fig. 5.7 for enlarged presentation

TABLE 5.1 NSSL Doppler Radar Tilt Sequences through the Union City Tornadoic Storm on 24 May 1973.

Number	Time Period (CST)	Max. Elev. Angle	Reference Time
1	1446 - 1453	(Intermittent) 5.9°	1446
2	1503 - 1510	10.0°	1503
3	1515 - 1519	4.9°	1515
4	1527 - 1532	5.9°	1528
5	1535 - 1540	9.8°	1536
6	1544 - 1550	11.9°	1545
7	1556 - 1601	11.9°	1556
8	1604 - 1609	11.9°	1604

Surface mesonet network parameters of pressure, temperature, dew-point temperature and three minute average wind, were obtained at one minute intervals from chart records. These data are plotted at selected times; time-to-space converted data were used to determine surface discontinuity positions (Fig. 5.3). In addition, accurately timed observations from NSSL intercept teams are plotted to further illuminate the surface wind field along the storm's right flank.

Early Doppler reflectivity data at 1446 (Fig. 5.3a) portray a small, west-east elongated, low-level echo (Cell 1 from Fig. 5.1) with large overhang areas on both left and right storm flanks (storm is moving generally toward the east). Embedded within the right flank overhang is a developing BWER labelled as A. The large overhang and developing BWER serve as an indication of updraft intensification and transformation into a severe, supercell storm.

The storm at 1446 has overtaken the wind-shift line between southeasterly and southwesterly winds (broad dashed line in Fig 5.3a). It may be seen that the region of southwesterly wind is characterized by high moisture values, generally higher, in fact, than the region of southeasterly winds. Note that the developing BWER A is apparently situated above the wind-shift line but data are sparse and preclude knowledge of exact line placement and possible extension to the north of the storm. The wind discontinuity preceded the storm in time and should not be thought of as a storm related gust front. A storm gust front is not inferred from the available data until 1528.

Rapid storm intensification occurs (Fig. 5.3b) as evidenced by increases in echo size, maximum reflectivity and BWER strength. Overhangs along the storm's left and right flanks persist, permitting inference of organized updrafts along both storm flanks.

A north-south elongation and turn to the right of Cell 1 coincided with separate mid- and high-level reflectivity core development above the left and right flank WER's (Fig. 5.3c); only one reflectivity core had been detected earlier. The multiple cores mark a developing split of the parent cell (1) into two separate thunderstorms. One cell (labeled 1L) moves left of the mean wind and the other (1R) moves to the right. The splitting process and airflow within cells 1L and 1R are discussed by Burgess *et al.* (Chapter 6) and Lemon and Burgess (Chapter 8). It will suffice here to indicate that the WER's located on both left and right storm flanks are associated with the observed storm split.

The wind-shift line and storm migrated eastward in a manner permitting the line to remain beneath the right flank WER. Confluence along the wind-shift line is depicted at all analysis times and strong convergence is inferred at 1515 from the appearance of a new weak echo center, BWER B. Its development is accompanied by a simultaneous dissipation of BWER A, so that by 1528 (Fig. 5.3d) BWER B is taken as the right flank updraft center.

A slight concavity in low-level echo contours is noted along the storm's right flank at 1515. This concavity grows and results in pendant echo formation (Fig. 5.3d)--a change consistent with cyclonic circulation along the storm's right flank. The cyclonic perturbation continues to expand at low levels and may be called a hook echo by 1536 (Fig. 5.3e) and 1545 (Fig. 5.3f) although it is poorly developed.

5. Union City Storm History

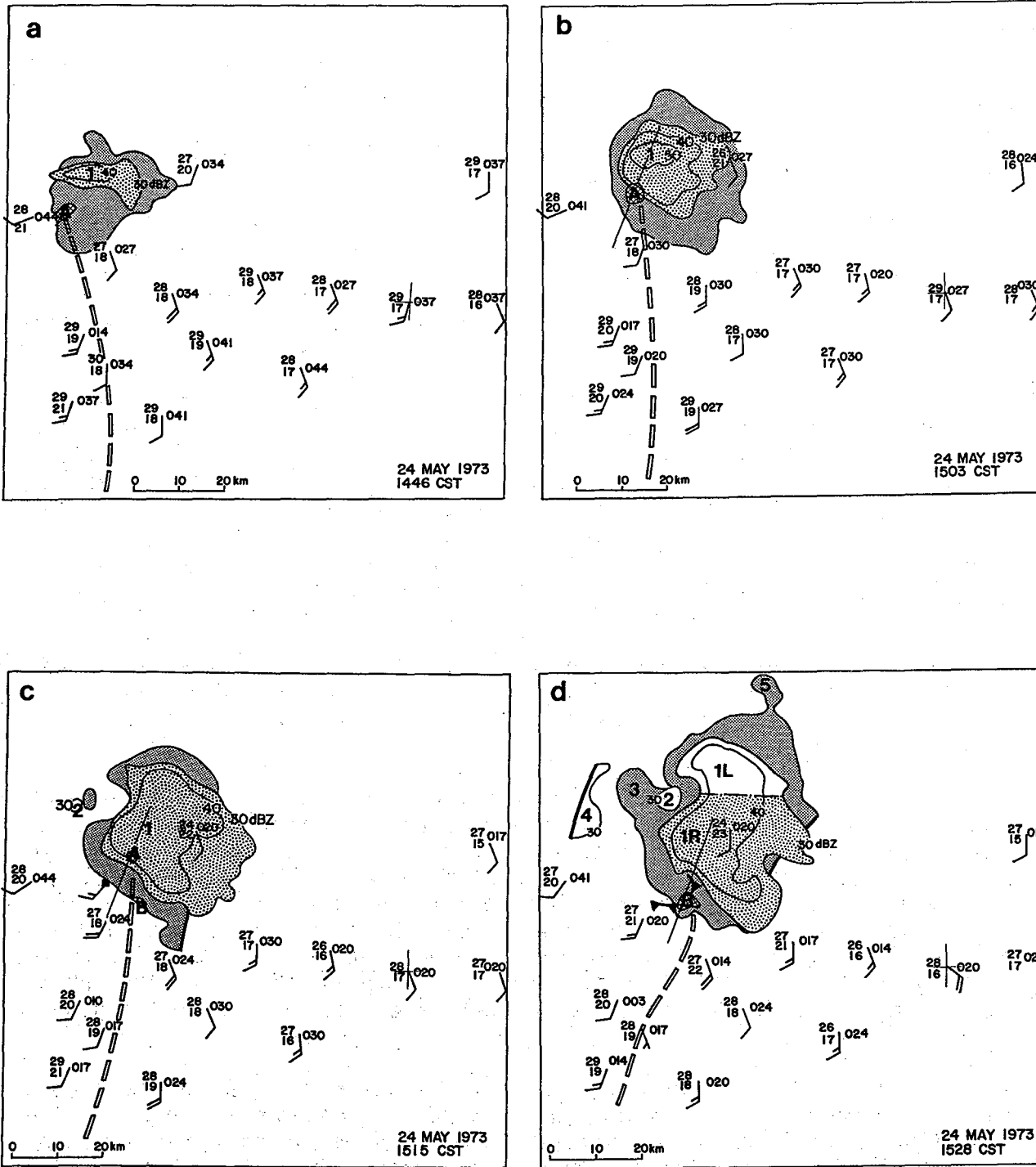
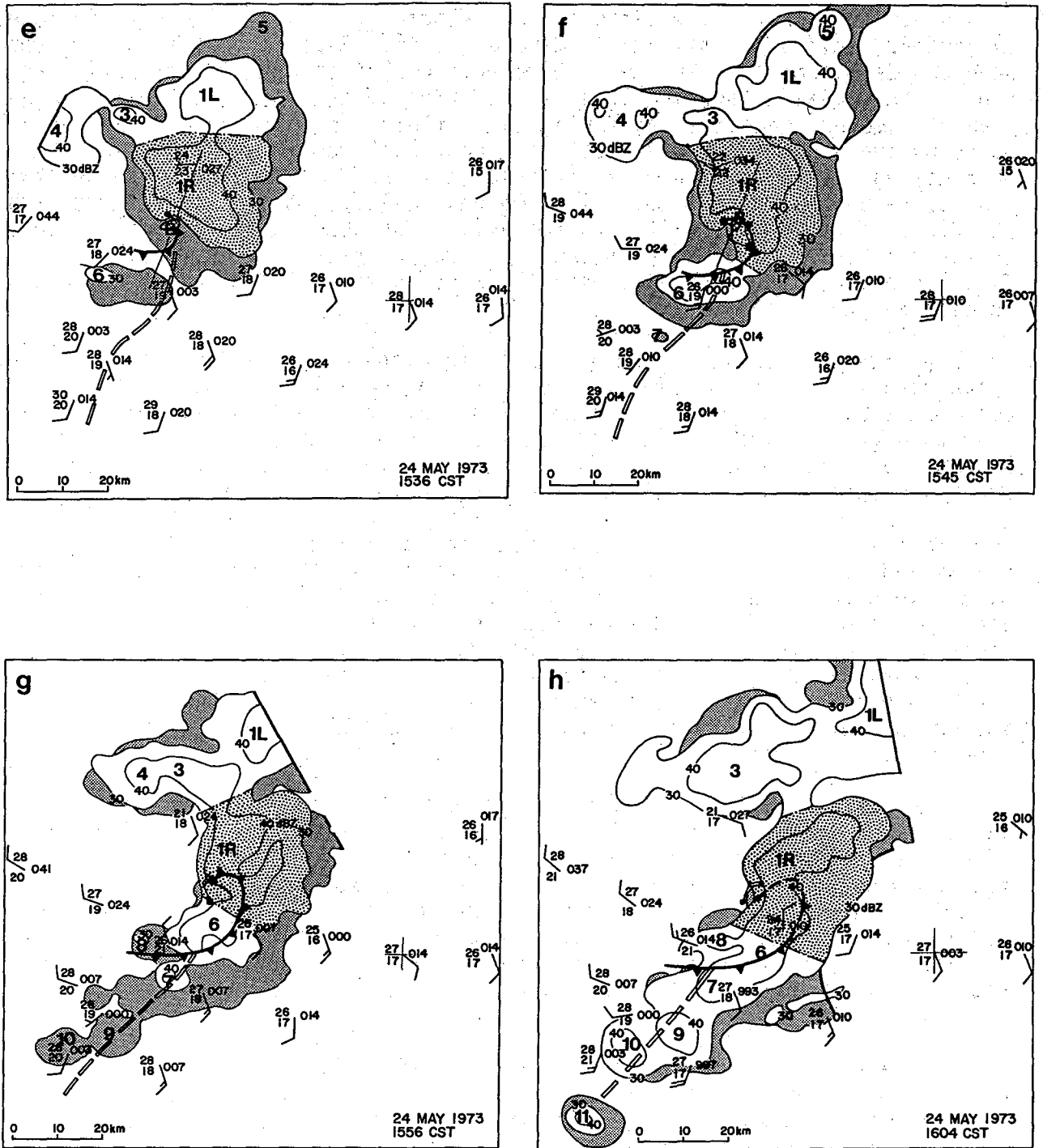


Fig. 5.3 Objectively analyzed Doppler reflectivity data and surface meso-network data. Union City storm echo is stippled. Reflectivity contours are for 0 km height; shading indicates echo overhang aloft from 4 km to 7 km height. Areas labeled A and B denote bounded weak echo regions. Long dash-dot line is arbitrary boundary between Union City storm and other convection with cells identified by numbers. Double line is edge of radar data collection.



(Fig. 5.3 continued)
 Temperature and dew-point temperature are in $^{\circ}\text{C}$; pressure is to nearest 0.1 mb, with leading 10 or 9 omitted; long and short wind barbs are 5 and 2.5 m s^{-1} , respectively. Long dashed line marks position of windshift line; cold front symbols indicate gust front. Intercept team observations marked with dark square, tornado position by the circle at northern end of gust front. Straight lines (b through f) show orientations for Fig. 5.4 cross-sections.

5. Union City Storm History

A new cell, 2, is identified to the storm's rear at 1515 and is followed by another, Cell 3, identified 13 minutes later. Expansion of the rear overhang and development of new cells give evidence of strong updrafts existing behind the splitting storm. This is confirmed by the observation of a large area of cumulus congestus overtaking and building into the storm from the rear--noted by the storm intercept team from their 1515 camera stop location (Golden, Appendix A). Cell 4, a part of the original squall line, overtakes the storm rear flank beginning at 1536. Also two new cells, 5 and 6, are observed near the WER's of Cells 1L and 1R, respectively. The appearance of these two new cells is taken as discrete propagation along the storm flanks. Cell 6 is first seen in a confluent area near the wind-shift line and just ahead of the developing gust front.

By 1536, the split of the original storm and the addition of several new cells result in a storm complex. However, one cell (1R) continues to dominate all others by virtue of its size and organization. Cell 1R, stippled in Fig. 5.3d through h, evidences its high degree of organization, i.e., supercell status, by maintaining the largest horizontal echo area and maximum echo top, and by possessing a large WER with bounded center and accompanying hook echo.

Most supercell storms produce a surface gust front along their right flanks and Cell 1R is no exception. Unfortunately, the sparsity of surface sites along the right flank precludes accurate positioning. The gust front locations shown in Fig. 5.3 were obtained from storm intercept wind observations and to a greater extent, by tracing, via photographs, the development of a low-level cloud line believed to describe the gust front position at 1545 (for example, see Golden, Chapter 12, Fig. 12.1). As inferred, the gust front formed on the right rear cell flank just before 1528 and accelerated rapidly toward the right forward flank.

The Union City tornado funnel first appeared within the hook echo of Cell 1R near 1536 (dot at north end of gust front) and produced damage beginning at 1538. As can be seen from Fig. 5.3e, the gust front rotates around the tornado position from south at 1536 to east at 1545. A rapid intensification of Cell 6 is noted as the gust front passes beneath it at 1545. The juxtaposition of the gust front and Cell 6 combine to explain, in part, the weakening and collapse of storm 1R. It can be seen (Fig. 5.3f) how the updraft region of 1R is cut off from the low-level southerly inflow source that existed earlier.

The wind-shift line becomes stationary after 1545 to the south of Cell 6 and vigorous convection occurs along its boundary. Cells 7, 8, 9, 10 and 11 form in rapid succession so that by 1604 the storm complex has transformed into a short northeast-southwest oriented line, stretching from Cell 5 on the northeast to Cell 11 on the southwest. Cell 1R is greatly reduced in intensity and loses its supercell status, becoming just another moderate cell within the line at 1604. Heavy rain, hail, high winds and funnel clouds were reported from Cells 3 and 6 through 11 after 1604.

Echo motion for all observed cells is tabulated in Table 5.2. Cell 1R moves farthest to the right of the mean wind of any cell although other well documented storms have deviated much further to the right (Marwitz, 1972; reproduced by Brandes, Chapter 3, Table 3.1).

All cells move slower than the mean wind with the most rapidly moving cells being 1L and those along the wind-shift line south of Cell 1R.

TABLE 5.2 *Motion of Echoes in Vicinity of Union City Storm (1R) on 24 May 1973. Deviation Directions and Speeds are Relative to Mean Environmental Winds from Cloud Base to Tropopause.*

Cell	Direction	Speed	Time Period	Dev. Dir.	Dev. Speed
1	260°	8 m s ⁻¹	1410-1510	14° left	-12 m s ⁻¹
1R	286°	10 m s ⁻¹	1515-1604	12° right	-10 m s ⁻¹
1L	246°	15 m s ⁻¹	1515-1604	28° left	-5 m s ⁻¹
2	N.A.	N.A.	N.A.	N.A.	N.A.
3	264°	9 m s ⁻¹	1528-1604	10° left	-11 m s ⁻¹
4	275°	12 m s ⁻¹	1500-1556	1° right	-8 m s ⁻¹
5	268°	15 m s ⁻¹	1528-1545	6° left	-5 m s ⁻¹
6	278°	14 m s ⁻¹	1535-1604	4° right	-6 m s ⁻¹
7	270°	15 m s ⁻¹	1545-1604	4° left	-5 m s ⁻¹
8	268°	16 m s ⁻¹	1556-1604	6° left	-4 m s ⁻¹
9	267°	18 m s ⁻¹	1556-1604	7° left	-2 m s ⁻¹
10	267°	16 m s ⁻¹	1556-1604	7° left	-4 m s ⁻¹
11	N.A.	N.A.	N.A.	N.A.	N.A.

5.5 WEAK ECHO REGION WITHIN CELL 1-1R

The previous section described the evolution of all cells making up the storm complex. Mention was made of the large weak echo region (WER) along the right flank of Cell 1 before echo split and 1R after the split. This section examines the right flank WER in greater detail through the use of vertical cross-sections of Doppler reflectivity data oriented perpendicular to cell motion. These cross-sections are used to make inferences about updraft distribution.

A vertical section through the right flank of Cell 1 at 1503 is oriented as shown by the solid line in Fig. 5.3b. The orientations for all cross-sections are shown at the appropriate times by solid lines in Fig. 5.3. The 1503 section (Fig. 5.4a) shows the full extent of BWER A as it penetrates to the great height of 14 km. The BWER is believed to represent an unusually intense updraft center. Almost all of the BWER tilt is contained within the plane of the cross-section and is toward the north-northeast with increasing

5. Union City Storm History

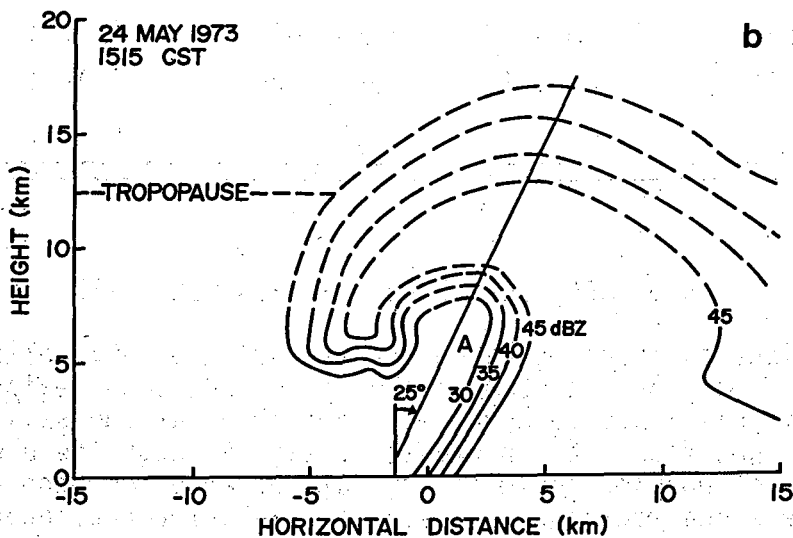
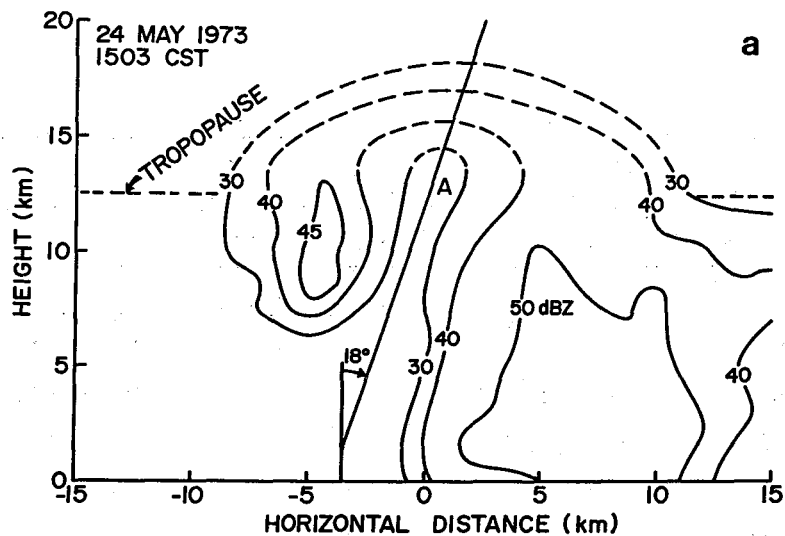
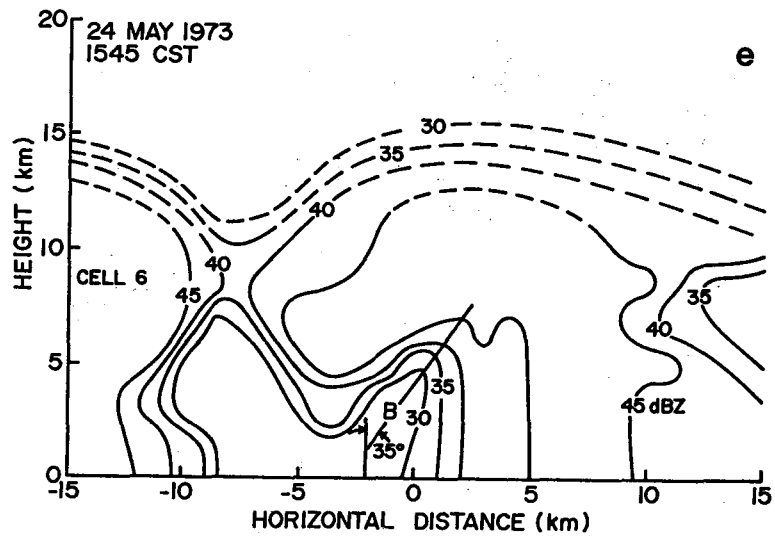
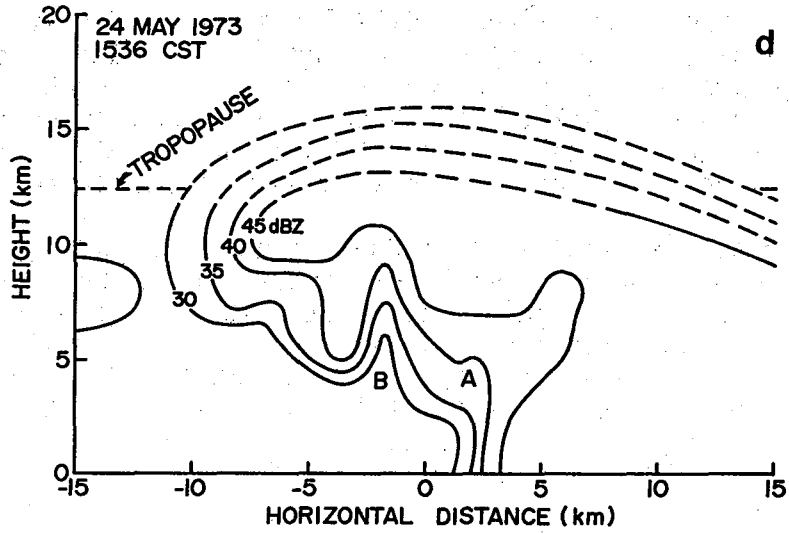
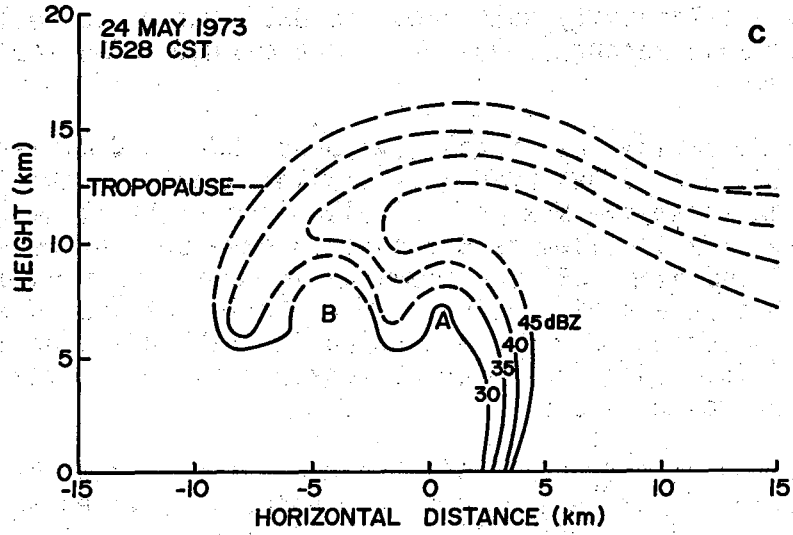


Fig. 5.4 Vertical cross-sections of radar reflectivity factor normal to storm motion as measured with Doppler radar. Cross-sections have orientations as shown in Fig. 5.3. Horizontal distances are relative to arbitrary cross-section center. Dashed contours were inferred from WSR-57 data.



5. Union City Storm History

height. A high-reflectivity dome caps the BWER and rises well above the estimated tropopause height (behavior of the maximum echo top is treated in the next section).

Seemingly as rapidly as it has developed, BWER A diminishes in vertical extent. At 1515 (Fig. 5.4b) BWER A is smaller and is in the process of dissipating. An extensive WER remains along the right flank (Fig. 5.3c) and within it a new BWER labelled as B begins to develop (not detected in Fig. 5.4b). The WER and even BWER are known to propagate continuously (Marwitz, 1972) but in this case a discontinuous propagation of the BWER apparently occurs. The developing BWER B and dissipating BWER A are depicted in the 1528 cross-section (Fig. 5.4c) with bounded center B extending the right flank echo overhang further to the south.

It is curious that BWER A would become so strong and then begin dissipating so quickly. Past researchers have noted long-lived BWER's and related their longevity to tilts which allow precipitation to fall outside the rising air. Also, those updraft centers ventilated aloft by strong winds--that carry precipitation away from the updraft summit before mass overloading can occur--are believed to have longer lives. BWER A dissipated despite its favorable tilt and existence in a field of strong winds at its summit level. The larger dome of capping precipitation apparent at 1515 is responsible for updraft water loading (Kessler, 1969), but probably not enough to destroy the intense updraft. A possible explanation for the observed updraft core dissipation based on Doppler derived airflow is discussed by Lemon (Appendix F).

Along with the development of bounded center B, a channel of weak echo is formed between centers A and B with horizontal extent shown by the hatched areas in Fig. 5.5. Cross-sections taken at 1515, 1528 and 1536 (Figs. 5.4b, c and d) are along the weak echo channel. The WER features of BWER A, BWER B and connection channel are used to infer that before 1515 the updraft is concentrated into one intense center (A), but after 1515 the updraft covers a larger area with center B never approaching the size or vertical extent of center A.

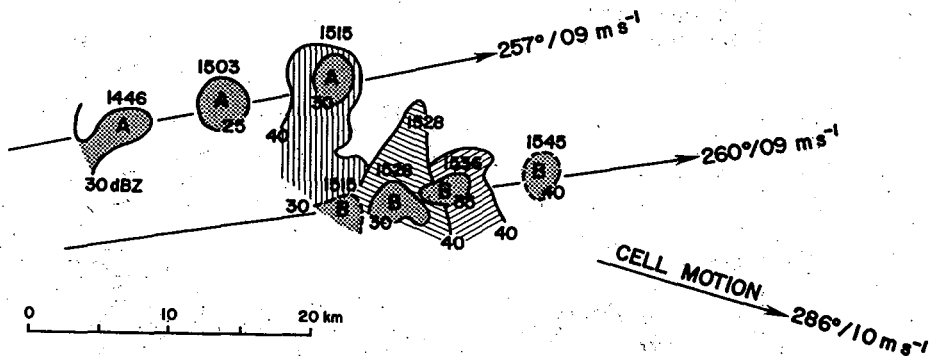


Fig. 5.5 Motion of bounded weak echo regions A and B. Solid contours are for 6 km height, dashed for 5 km. Hatching denotes weak reflectivity channel at 1515, 1528 and 1536.

BWER B grows until 1536 when it too begins to dissipate. Note that it is nearly vertical before 1545 (Fig. 5.4) and its limited lifetime may be caused by precipitation falling back through the rising air. During the dissipation of BWER B (Fig. 5.4e) the updraft core does not propagate further south and the supercell weakens. A contributing cause for the failure of updraft propagation is the nonbuoyant air found beneath the updraft as a result of the gust front movement and development of Cell 6. By 1545, BWER B and the entire right flank overhang are collapsing. Cross-sections at 1556 and 1604 (not shown) do not reveal a WER for Cell 1R.

The movement of BWER's A and B (shown in Fig. 5.5) is to the left of cell motion and, also, left of the pressure-weighted mean wind for the height interval involved (cloud base to 7 km wind-- 269° at 15 m s^{-1}). The observed deviate motion is most likely produced by updraft mixing of momentum from different levels or internal storm circulation steering. In any event, it may be seen that discontinuous propagation of the intense updraft center (BWER) was necessary to maintain its position on the cell's right flank.

5.6 STORM LIFE CYCLE

The Union City storm is best summarized by viewing its maximum radar echo tops (Fig. 5.6). As previously mentioned, the developing storm was composed of two cells (multicell) until one cell became dominant and assumed supercell characteristics (persistent sloping overhang (WER), BWER and hook echo). The supercell stage began near the time of first Doppler data collection (1445) and, with time, the maximum echo top grew until it exceeded the tropopause height by 5 km.

During the one hour supercell stage, the parent storm split into two deviate-moving thunderstorms and new convection appeared around the storm flanks. This resulted in the formation of a cell complex. However, during this period, the supercell (right-moving portion) retained its characteristics and dominance over the surrounding cells. Also, a gust front appeared on the supercell right rear and accelerated toward the right front flank.

Historically, quasisteadiness has characterized the supercell's radar appearance (Browning, 1965b); however, important changes were detected in the Union City supercell. Echo split and new cell development on multiple storm flanks provided for a continually changing radar echo. Only the right flank overhang (WER) approached a quasisteady nature (Fig. 5.7). Evolution was seen even within the overhang as differential movement between the BWER and the overall cell caused the BWER to discontinuously propagate to retain its position relative to the inflow.

Near 1536, the supercell structure began to collapse. This was evidenced by loss of the BWER, rapid storm top decrease and descent of the overhang to the surface. The 1545 and 1556 portions of Fig. 5.7 depict the loss of overhang and masking of the hook echo. The observed collapse is inferred to occur for two reasons. The first is attributed to the vortex valve effect (Lemon, Appendix F). The second, perhaps interrelated, is due to gust front movement and new convection which deprive the updraft of its supply of moist unstable

5. Union City Storm History

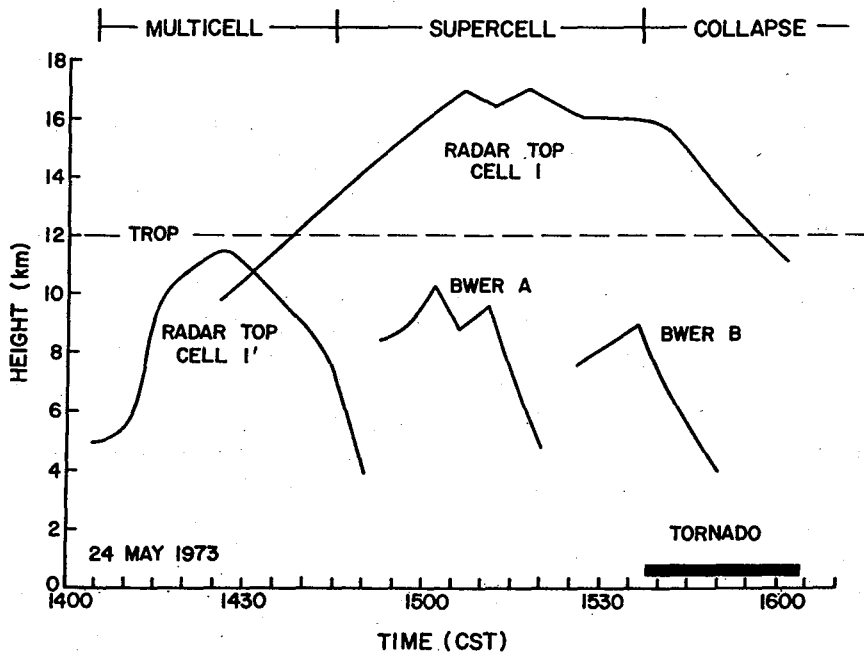


Fig. 5.6 WSR-57 radar echo and bounded weak echo region (BWER) tops versus time. Storm classification is shown at top. Dark bar indicates time period of tornado. Note that maximum echo intensities and BWER tops are different from those obtained with the higher resolution Doppler data (see Fig. 5.4).

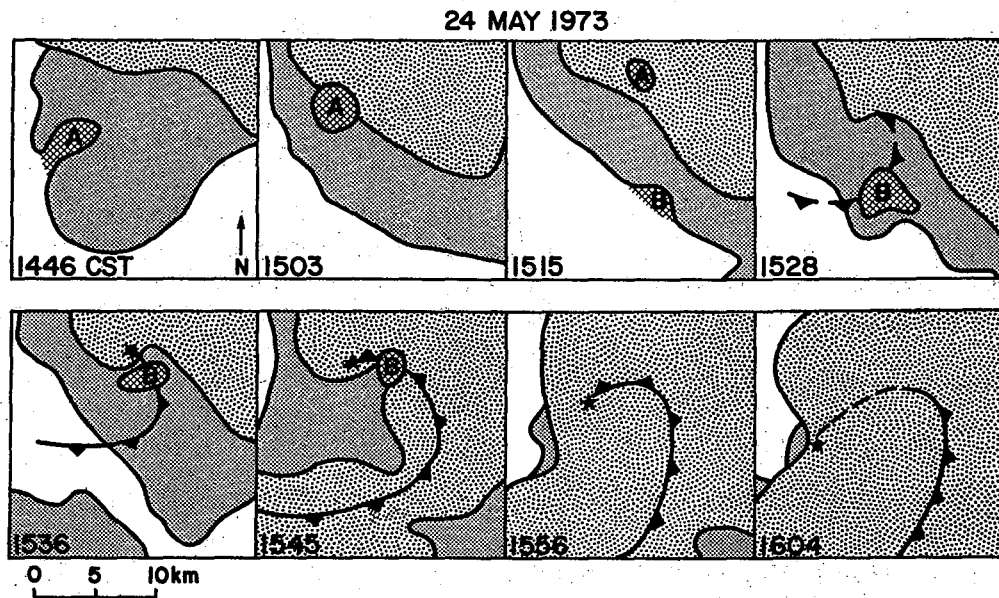


Fig. 5.7 Supercell right flank changes with time (extracted from Fig. 5.3). Star represents surface tornado location.

air. Total cell dissipation was averted by new updraft along the front quadrant (see Fig. 5.3h overhang) as the laterally aligned cells formed a short squall line.

With the above life cycle in mind, it is interesting to compare changes in the radar echo structure with tornado occurrence. Fig. 5.6 shows that the tornado formed during the supercell stage but continued well into the supercell collapse. Tornadoes occurring during supercell collapse have been previously documented (e.g., Burgess, 1974) and may be common for many storms.

The tornado was initially located within the hook echo (Fig. 5.7) but after collapse began, the descending overhang placed the tornado well within the radar echo. During the tornado's later stages, no indication of its presence could be found from the radar reflectivity data. However, this is not the case with Doppler velocity data that provided a continuous tornado signature (see Donaldson, Chapter 7; Brown and Lemon, Chapter 15). A conclusion from this study must be that, if reflectivity fields are the only data source, initial supercell collapse should not be inferred as an "all clear" with respect to tornado or damage producing potential within a storm but rather should be considered as a period of very high potential.

5.7 ACKNOWLEDGMENTS

We are indebted to Dale Sirmans for designing the Norman Doppler radar and for masterminding modifications of the WSR-57 surveillance radar. Glen Anderson has done a fine job updating and maintaining the Norman Doppler radar. Walter Watts and Jesse Jennings have skillfully modified and maintained the WSR-57 radar. On 24 May 1973, Rodger Brown assisted with Doppler radar data collection and J. T. Dooley and Kenneth Wilk assisted with WSR-57 data collection. Tully Davis, under the supervision of Edward Helm, had the tedious task of digitizing the mesonetwork data. This work was partially supported by the Federal Aviation Administration under Interagency Agreement FA72 WAI-265.

5.8 REFERENCES

- Brandes, E. A., 1976: Subsynoptic-scale meteorological features and associated convective activity on 24 May 1973. Chapter 3, The Union City, Oklahoma Tornado of 24 May 1973, R. A. Brown, Editor. NOAA Tech. Memo. ERL NSSL-80, Norman, Nat. Severe Storms Lab., 19-25.
- Brown, R. A., 1976: Single Doppler radar data acquisition and analysis. Appendix E, The Union City, Oklahoma Tornado of 24 May 1973, R. A. Brown, Editor. NOAA Tech. Memo. ERL NSSL-80, Norman, Nat. Severe Storms Lab., 215-228.
- _____ and L. R. Lemon, 1976: Evolution of the Doppler radar tornadic vortex signature in the Union City storm. Chapter 15, The Union City, Oklahoma Tornado of 24 May 1973, R. A. Brown, Editor. NOAA Tech. Memo. ERL NSSL-80, Norman, Nat. Severe Storms Lab., 167-175.

5. *Union City Storm History*

- Browning, K. A., 1965a: Some inferences about the updraft within a severe local storm. J. Atmos. Sci., 22, 669-677.
- _____, 1965b: The evolution of tornadic storms. J. Atmos. Sci., 22, 664-668.
- _____, 1968: The organization of severe local storms. Weather, 23, 429-434.
- _____ and D. Atlas, 1965: The initial development of a severe storm as observed by radar. Chapter 11, A Family Outbreak of Severe Local Storms - A Comprehensive Study of the Storms in Oklahoma on 26 May 1963. Part I, K. A. Browning, Editor. Air Force Cambridge Res. Lab., Special Reports, No. 32, 197-236.
- _____ and R. J. Donaldson, Jr., 1963: Airflow and structure of a tornadic storm. J. Atmos. Sci., 20, 533-545.
- Burgess, D. W., 1974: Study of a severe rightmoving thunderstorm utilizing new single Doppler radar evidence. Master's Thesis, Dept. of Meteor., Univ. of Oklahoma, 77 pp.
- _____, L. R. Lemon and G. L. Achtemeier, 1976: Severe storm splitting and left-moving storm structure. Chapter 6, The Union City, Oklahoma Tornado of 24 May 1973, R. A. Brown, Editor. NOAA Tech. Memo. ERL NSSL-80, Norman, Nat. Severe Storms Lab., 53-66.
- Chisholm, A. J., 1973: Alberta hailstorms, Part I: Radar case studies and airflow models. Meteor. Monograph, 14 (36), Boston, Amer. Meteor. Soc., 1-36.
- Donaldson, R. J., Jr., 1965: Methods for identifying severe thunderstorms by radar: A guide and bibliography. Bull. Amer. Meteor. Soc., 46, 174-193.
- _____, 1976: Observations of the Union City tornadic storm by plan shear indicator. Chapter 7, The Union City, Oklahoma Tornado of 24 May 1973, R. A. Brown, Editor. NOAA Tech. Memo. ERL NSSL-80, Norman, Nat. Severe Storms Lab., 67-83.
- Golden, J. H., 1976a: Comparison of Union City tornado life cycle with Florida Keys waterspout life cycle. Chapter 12, The Union City, Oklahoma Tornado of 24 May 1973, R. A. Brown, Editor. NOAA Tech. Memo. ERL NSSL-80, Norman, Nat. Severe Storms Lab., 135-140.
- _____, 1976b: Tornado intercept strategy and morphological observations. Appendix A, The Union City, Oklahoma Tornado of 24 May 1973, R. A. Brown, Editor. NOAA Tech. Memo. ERL NSSL-80, Norman, Nat. Severe Storms Lab., 185-189.
- Kessler, E., 1969: On the distribution and continuity of water substance in atmospheric circulation. Meteor. Monogr., 10 (32), 84 pp.

- Lemon, L. R., 1976: Tornadic storm evolution: Vortex valve hypothesis. Appendix F, The Union City, Oklahoma Tornado of 24 May 1973, R. A. Brown, Editor. NOAA Tech. Memo. ERL NSSL-80, Norman, Nat. Severe Storms Lab., 229-234.
- _____ and D. W. Burgess, 1976: Tornadic storm airflow and morphology derived from single Doppler radar measurements. Chapter 8, The Union City, Oklahoma Tornado of 24 May 1973, R. A. Brown, Editor. NOAA Tech. Memo. ERL NSSL-80, Norman, Nat. Severe Storms Lab., 85-106.
- Marwitz, J. D., 1972: The structure and motion of severe hailstorms. Parts I, II, and III. J. Appl. Meteor., 11, 166-201.
- Sirmans, D., 1976: NSSL Doppler and WSR-57 radar characteristics. Appendix D, The Union City, Oklahoma Tornado of 24 May 1973, R. A. Brown, Editor. NOAA Tech. Memo. ERL NSSL-80, Norman, Nat. Severe Storms Lab., 209-213.
- _____ and R. J. Doviak, 1973: Meteorological radar signal intensity estimation. NOAA Tech. Memo. ERL NSSL-64, Norman, Nat. Severe Storms Lab., 80 pp.

Chapter 6

SEVERE STORM SPLITTING AND LEFT-MOVING STORM STRUCTURE

Donald W. Burgess, Leslie R. Lemon¹

*National Severe Storms Laboratory
Norman, Oklahoma 73069*

and

Gary L. Achtemeier²

*Illinois State Water Survey
Urbana, Illinois 61801*

The initial Union City storm split into two separate echoes-- one moving left and the other moving to the right of the mean wind. Storm evolution was identical to that observed in other well documented splitting cases. Factors that promoted the split remain unknown because the splitting process occurred outside the range of all NSSL sensors except the WSR-57 surveillance radar.

However, single Doppler radar data were used to infer the structure and airflow within the left-moving echo after the split. The airflow pattern, similar to that proposed previously, includes updraft on the left storm flank and downdraft on the rear flank. Mid-level airflow is dominated by anticyclonic rotation of the updraft and obstacle flow around the updraft. High-level divergence is observed above the updraft. Propagation and forces produced by updraft rotation are hypothesized to yield the deviate left storm motion.

6.1 Introduction

Why thunderstorms split when they come under the influence of one or more disruptive factors is not yet well understood. Occasionally storms may develop in close proximity and briefly appear as splitting storms. However, these storms show little if any change in propagation characteristics or intensity. In other instances, the split seems to be from a single echo. In these cases, the postsplit character of the storm differs so markedly from the presplit conditions that extensive dynamic reorganization within the storm is implied.

¹Present affiliation: National Severe Storms Forecast Center, Techniques Development Unit, Federal Building, Kansas City, Missouri 64106.

²Research initiated while at the National Severe Storms Laboratory as a Post-Doctoral Associate of the National Research Council.

6. *Left-Moving Storm*

One of the earliest references to these 'dynamic splitting storms' was by Hitschfeld (1960) who found adjacent storms moving on paths that diverged at angles as large as 50 degrees. More recent splitting storm occurrences are tabulated in Table 6.1. One result of these studies is the knowledge that storms which travel to the right of the mean wind (RM storms) move slowly and are accompanied by hail, high wind and tornado reports. The left of the mean wind (LM) storms move much more rapidly and are accompanied by hail and high winds, but usually not tornadoes.

This chapter documents the character of storm split as viewed by radar and presents the LM storm airflow derived from Doppler radar. Where needed, features of RM storm character and airflow are drawn from Burgess and Lemon (Chapter 5), Donaldson (Chapter 7) and Lemon and Burgess (Chapter 8). The LM storm structure is compared with existing storm models and theories on deviate storm motion are discussed.

6.2 DATA SOURCES

NSSL's 10-cm WSR-57 radar recorded a nearly complete history of the 24 May 1973 splitting storm. Reflectivities in tilt sequence format were available from first detection at 1405 CST until dissipation of the postsplit echoes. Higher resolution reflectivity and velocity component data from the NSSL Doppler radar (see Sirmans, Appendix D for radar characteristics) were gathered during four tilt sequences through the LM storm. Those tilt sequences began at 1515, 1528, 1536 and 1545. The digital Doppler data were corrected, objectively analyzed (see Brown, Appendix E) relative to LM storm motion and displayed in constant altitude planes. Ancillary data are available from the NSSL surface mesonet network (south and east of the LM storm) and special rawinsonde releases (southwest and east of the LM storm).

6.3 CHARACTER OF THE STORM SPLIT

Although splitting thunderstorms observed to date have occurred under varying synoptic conditions, they are found to share a number of general characteristics. Regardless of size or presplit direction of motion, splitting appears to develop similarly. Achtemeier (1969b) has proposed a four stage sequence of changes observed on radar that remarkably resembles biological mitosis as seen with a microscope. These stages are:

- (1) **The Formation Stage:** A thunderstorm develops and propagates generally eastward or northeastward not necessarily in the direction of the mean wind. A pronounced reflectivity gradient appears along the storm's rear flank.
- (2) **The Elongation Stage:** The thunderstorm elongates to an elliptical shape with the major axis of the ellipse generally perpendicular to the direction of storm motion. During this stage, splitting of the intense reflectivity core is observed. The broadness of the radar beam makes it difficult to determine whether a single cumulus tower

TABLE 6.1 Summary of Postsplit Storms Giving Approximate Lifetimes, Accompanying Severe Weather (Hail - H, Damaging Wind - W, Tornado or Funnel Aloft - T), Deviations from the Mean Wind and Average Speeds.

DATE	STORM	APPROX. LIFETIME (Hours)	SEVERE WEATHER	MAX. DEV. (deg) FROM MEAN WIND	AVERAGE SPEED (m s ⁻¹)	SOURCE
7/27/56	1a	>2	--	8L	15	Hitschfeld (1960)
	1b	>2	--	43R	13	
	1a'	>1	--	29L	17	
	1a''	>1	--	8R	14	
4/3/64	R _c	4	H, W, T	20R	10	Fujita, Grandoso (1968); Charba, Sasaki (1971)
	R _a	>5	H, T	20R	10	
	L	>5	H, W	37L	15	
4/23/64		>4	H, W, T	40L	20	Hammond (1967)
5/27/65	R	>3	H, T	35R	10	Harrold (1966)
	L	>2	H, T	35L	15	
8/25/65	C3	>3	H, W	32R	10	Achtemeier (1969a)
	C8	--	H	25R	13	
	C9, 11	3	H	17L	18	
	C17	1	H	21R	15	
	C18	1	H	15L	23	
	E1	>3	H, W, T	15R	8	
	E2	2	H	48L	17	
	E4	--	H, T	12R	13	
	E5	--	H	40L	20	
	k1	2	H	5L	23	
8/26/65	S1	>3	H, T	16R	19	Achtemeier (1969a)
	S2	2	H	29L	26	
4/16/67	B	>5	H, T	45R	14	Haglund (1969)
	A	>2	H	15L	17	
4/19/72	L	>3	H	22L	29	Brown, Burgess, Crawford (1973)
	R	>3	H, T	25R	13	
6/27/72	L1	>2	H, W, T	47L	16	Achtemeier (unpublished)
	R1	2		25R	10	
	L2	>2	H	35L	16	
	R2	>2		22R	11	
5/24/73	L	2	H	28L	15	
	R	2	H, T	12R	10	
Total No. of Storms		Average Deviation From Mean Wind			Average Speed (m s ⁻¹)	
RM 16		24R			12	
LM 16		28L			19	

6. Left-Moving Storm

divides or two towers develop in close proximity. The 'split cores' grow apart and reflectivity gradients intensify along the left and right storm flanks.

- (3) The Splitting Stage: The central portion of the echo rapidly diminishes in size and intensity. This dissipation leaves two separate thunderstorm cells.
- (4) The Deviate Stage: To a viewer looking along the direction of motion, the left member veers sharply to the left of the mean wind and increases in speed. Conversely, the right member veers to the right of the mean wind and decreases in speed. Because of the deviate motion, a considerable horizontal distance develops between the two echoes.

These four stages are well illustrated (Fig. 6.1) by views of the Union City storm radar echo at low levels. Higher level data (not shown) indicate the splitting process begins aloft about five minutes before it is apparent at low levels. The formation stage begins with first echo at 1405 and continues until 1500. A new convective tower emerges about 1430 and rapid storm intensification begins. The echo remains a single entity as it changes from a small and east-west oriented cell (1444) to a larger and more rounded cell (1459).

The elongation stage occurs between 1500 and 1525 as the storm core expands in a direction perpendicular to storm motion and separates into two cores. It is during this period that extensive overhang develops on the storm's left flank (see Burgess and Lemon, Chapter 5--Fig. 5.2 b and c) and organized updraft may be identified. Another updraft has been present on the right storm flank since before 1446.

A rapid decrease in reflectivity between the two cores occurs from 1525 to 1535, denoting the splitting stage. Two distinct and separate cells are visible. After 1535, new convection takes place on all storm flanks and masks the echo separation in the deviate stage. The two cores (L and R) are 50 km apart at 1600 but are beginning to dissipate. Deviate echo motions are computed to be from 246° (28° left of mean winds) at 15 m s^{-1} for the LM echo and from 286° (12° right of mean winds) at 10 m s^{-1} for the RM echo.

The factor or combination of factors that promote storm split cannot be identified from this study. The area of the split is outside the NSSL surface mesonet network and the split's first two stages occur before Doppler velocity coverage of the storm began.

However, the evolution of the storm updraft is judged most important to the splitting process and a limited amount of information is available on updraft changes. The major updraft of the presplit storm develops on the right flank by 1446 (Burgess and Lemon, Chapter 5) and the same intense updraft continues on the RM storm right flank after the split. Storm split does not seem to greatly influence this updraft.

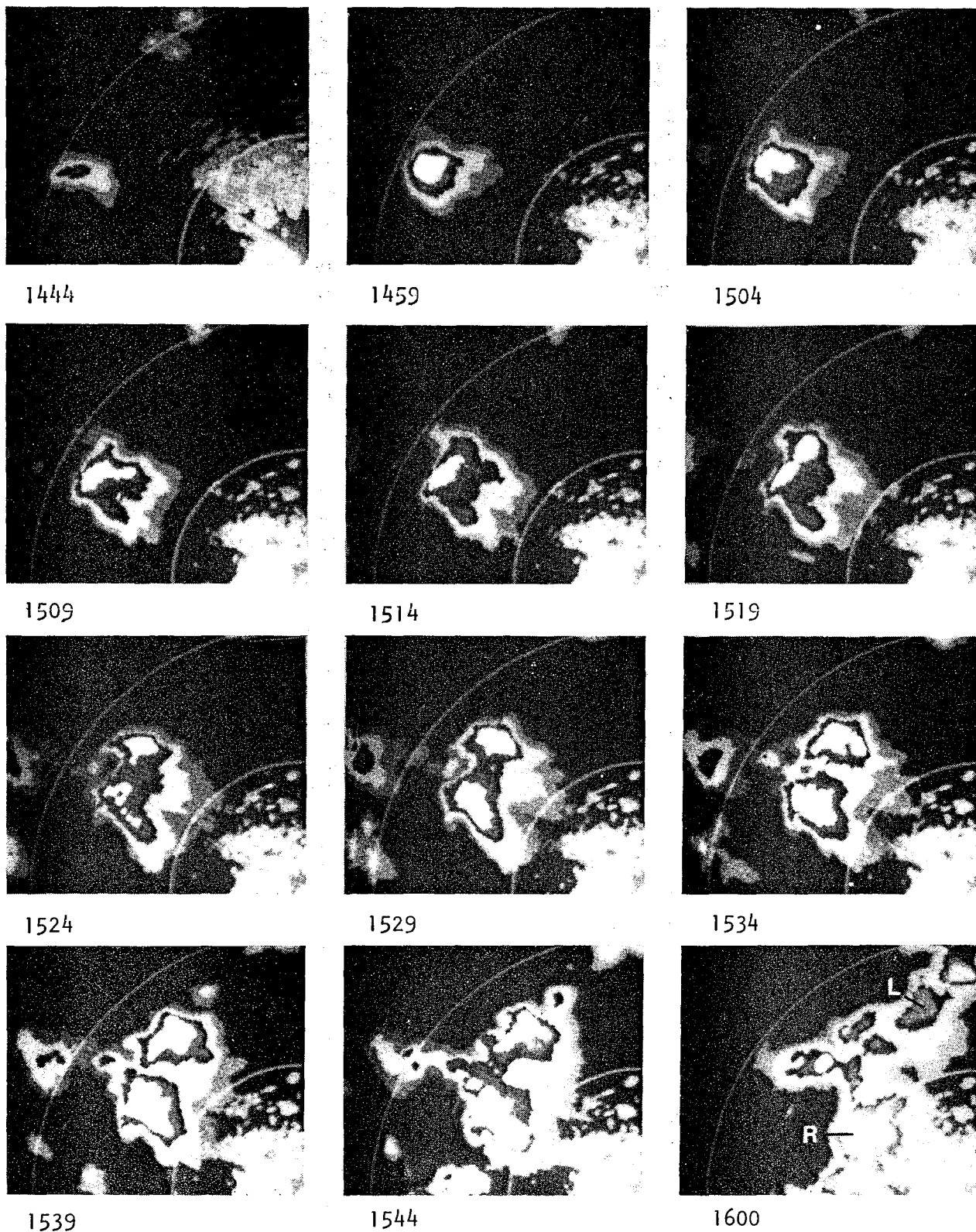


Fig. 6.1 WSR-57 radar echoes at 0° elevation for Union City storm split. Contour intervals are 21-30 dBZ (dim), 31-40 (bright), 41-45 (black), 46-49 (dim), 50-57 (bright) and >58 dBZ (black). At 1600, L and R identify left-moving and right-moving echoes. Right side and bottom of photographs are due north and west, respectively, of the Norman radar.

6. *Left-Moving Storm*

Secondary updrafts are inferred to exist along the rear and left storm flanks of the presplit echo for two reasons. First, the NSSL and University of Oklahoma tornado intercept teams, west of the developing storm, reported a continuous north-south line of towering and building cumulus flowing into the storm's rear. Second, a small finger of weak echo is consistently visible (Fig. 6.1--1459 to 1509) on the storm's left flank during the formation stage. The location and persistence of this small echo indicates the possibility of a separate weak updraft, but a strong updraft is precluded because of the lack of any significant overhang or weak echo region (WER) aloft.

Shortly after 1500, during the elongation stage, a significant WER does develop on the left storm flank and the primary LM updraft is identified. The updraft source cannot be established. It could be the result of actual splitting of the right flank updraft, intensification of the previously inferred rear or left flank updrafts, or the development of an entirely new updraft. In any event, the updraft becomes intense and is the parent for the LM storm.

The split is completed when the two intense updrafts (left flank and right flank) move in different directions and their accompanying radar echoes separate. Explanations for the differential movement are treated in a later section. However, the mechanisms that promoted the formation and rapid intensification of the left flank updraft remain unknown.

6.4 LEFT-MOVING STORM AIRFLOW

A single Doppler radar measures a precipitation particle's radial velocity component but is unable to measure the particle's velocity component normal to the radar beam. This inability greatly limits the application of the data unless the unknown wind component may in some way be deduced.

For the study presented in this chapter, an interpretive technique described by Lemon and Burgess (Chapter 8) was used to estimate the unknown wind component and, thereby, derive horizontal streamlines (see Fig. 8.3, 1515 CST at 5 km height). Briefly, the technique utilizes 12 restrictive, interpretive assumptions which perturb the upwind ambient flow in a manner that doesn't violate the radial velocity component distribution while accounting for radial velocity signatures. The upwind ambient flow is prescribed from a composite hodograph relative to the LM storm (Fig. 6.2). The hodograph was obtained by averaging simultaneous rawinsonde releases 90 km east and 90 km south of the developing storm.

The resulting streamline fields (Fig. 6.3) are subjective and nonunique solutions to the within-storm flow. However, they do deserve careful consideration because of their correlation with past observations and the continuity maintained between different analysis times.

6.4.1 Low-Level Flow (0 km)

Streamline analyses in lowest storm levels, typified by the 0 km display (data are interpolated downward from 200-300 meters above ground), indicate

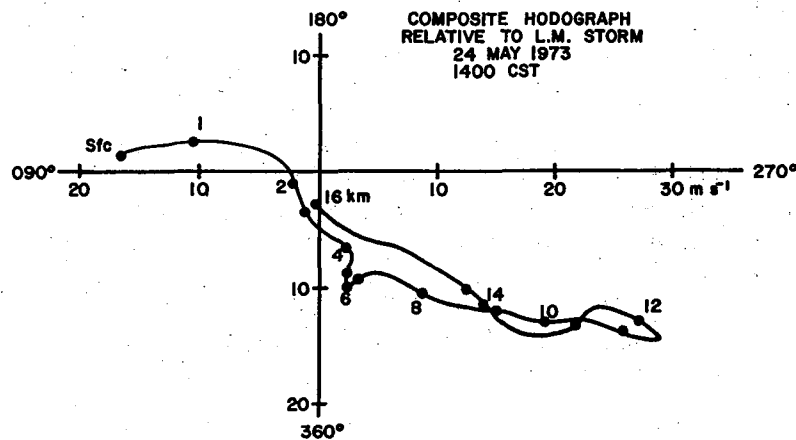


Fig. 6.2 Left-moving storm relative hodograph of winds at 1400 CST composited from simultaneous rawinsonde releases 90 km south and 90 km east of the developing Union City storm.

that storm relative easterly winds apparently pass through the echo nearly unaffected. However, a diffluence region is located in the left rear echo portion at all times except 1545. Detailed analyses of LM storm mesoscale surface data by Fujita and Grandoso (1968) and Charba and Sasaki (1971) have depicted similar divergent areas on left rear storm flanks. The diffluence location suggests its association with the thunderstorm downdraft, but this cannot be verified.

A second low-level flow feature is a wind-shift line and confluence area detected on the left front storm flank at 1515. Similarity to past studies, e.g., Charba and Sasaki (1971), Fujita and Grandoso (1968), and Hammond (1967), permits interpretation of the shift line as the LM storm gust front and extension of the shift line outside the echo at 1528, 1536 and 1545. The streamline outside the echo indicates the probable source for updraft air lifted up over the gust front.

6.4.2 Mid-Level Flow (5 to 6 km)

The dominant feature at mid-levels is the blocking of ambient upwind flow on the left front storm flank in an area of anticyclonic vorticity. The blocking and vorticity occur in the echo overhang previously identified as the result of storm updraft. These features are vertically above the low-level gust front location at 1515; apparently the same relationship exists at other times. Downwind from the updraft momentum block a turbulent wake region is indicated. Ambient flow entering the storm at mid-levels is dry (see Brandes, Appendix C) and would be evaporatively cooled by encountering large liquid water concentrations at the periphery of the blocking updraft. Therefore, the downdraft source is thought to be on the flanks of the block with subsidence continuing into the downwind wake.

6. Left-Moving Storm

Fig. 6.3 Storm-relative streamlines for low, mid and (where available) high levels within storm. Reflectivity contour levels are 30, 40 and 45 dBZ; areas greater than 45 dBZ have dark stippling. Relative environmental wind is indicated at each height. Long wind barb equals 5 m s^{-1} . Cold front symbols mark inferred gust front location and dashed streamline indicates probable path of inflow air. Double line indicates data edge and long dash-dot line is arbitrary left-moving storm boundary.

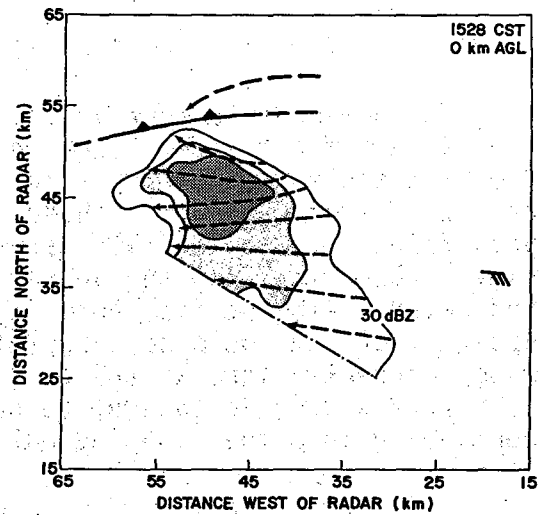
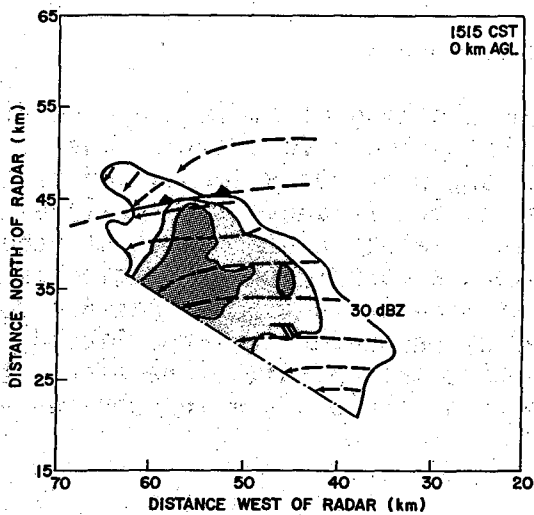
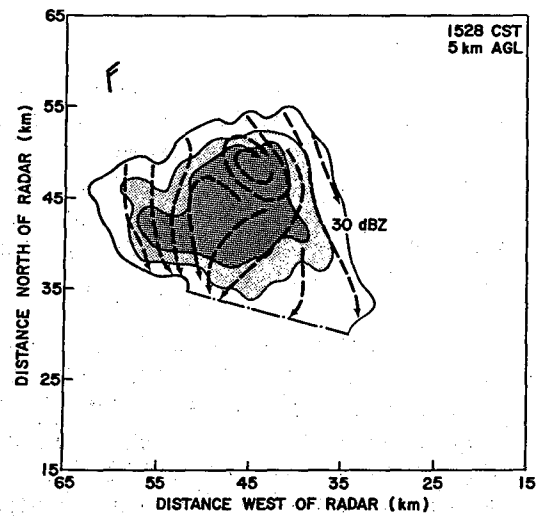
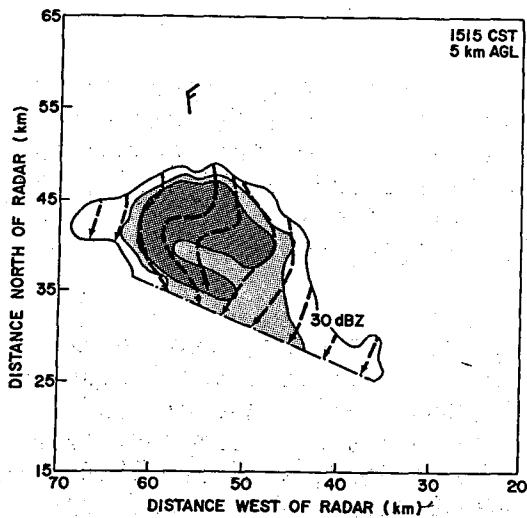
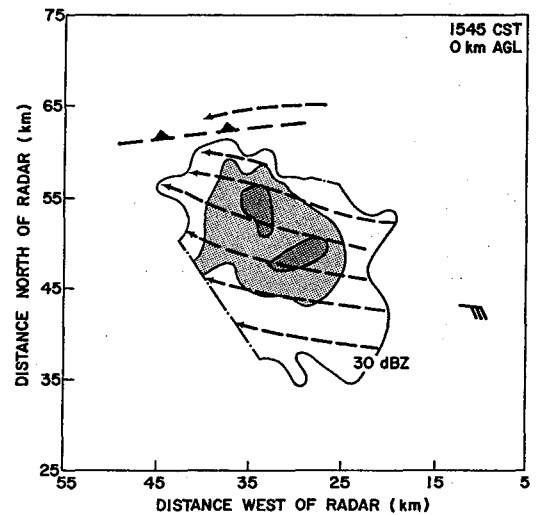
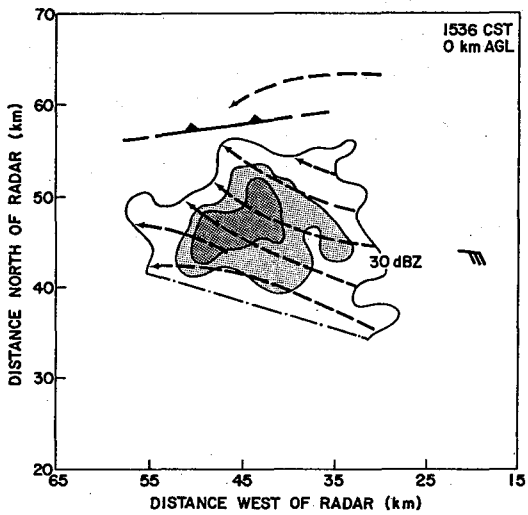
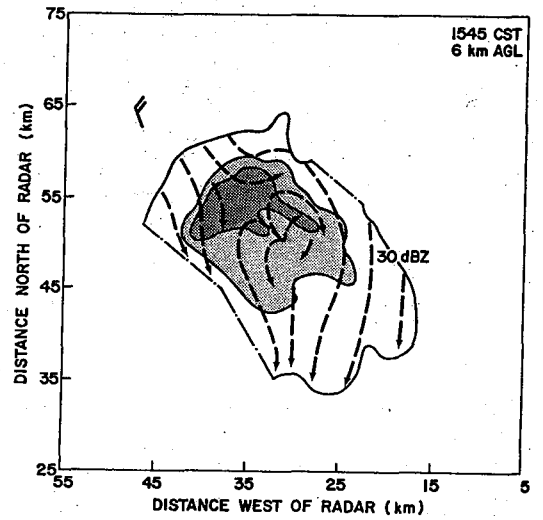
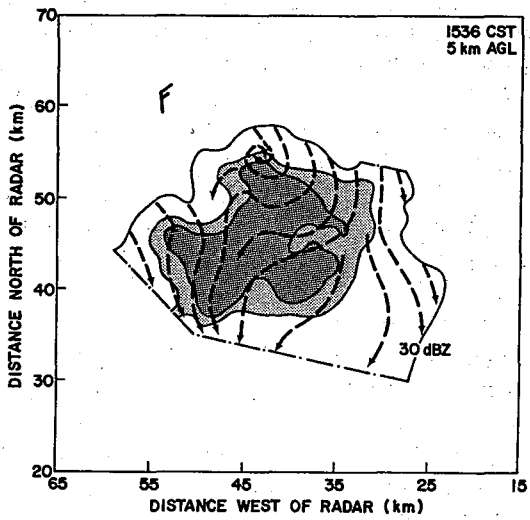
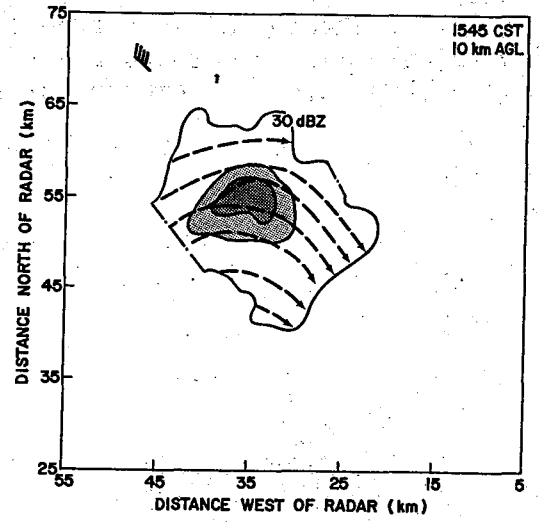
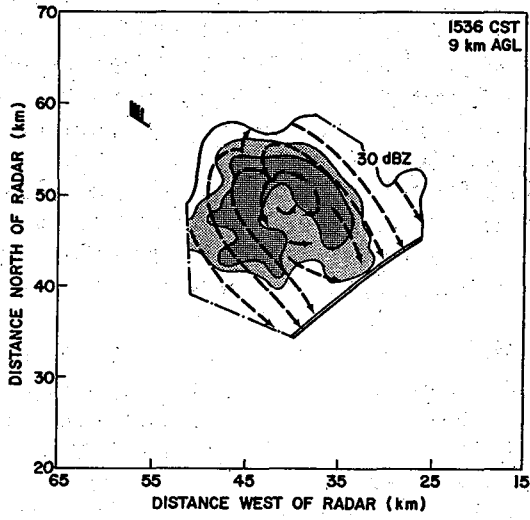


Fig. 6.3 (continued).



6. Left-Moving Storm

The anticyclonic vorticity becomes organized in such a manner after 1515 that it satisfies criteria (proposed by Donaldson, 1970 and listed by Lemon and Burgess, Chapter 8) to establish it as a closed circulation situated about a vertical axis--a mesoscale anticyclone. The single Doppler anticyclone signature (Fig. 6.4) is composed of a couplet with adjacent closed contours of

flow away from and toward the radar. At the center of the couplet is a region of strong shear with flow contours oriented radially. This signature is analogous to that seen for the right flank cyclonic vortex.

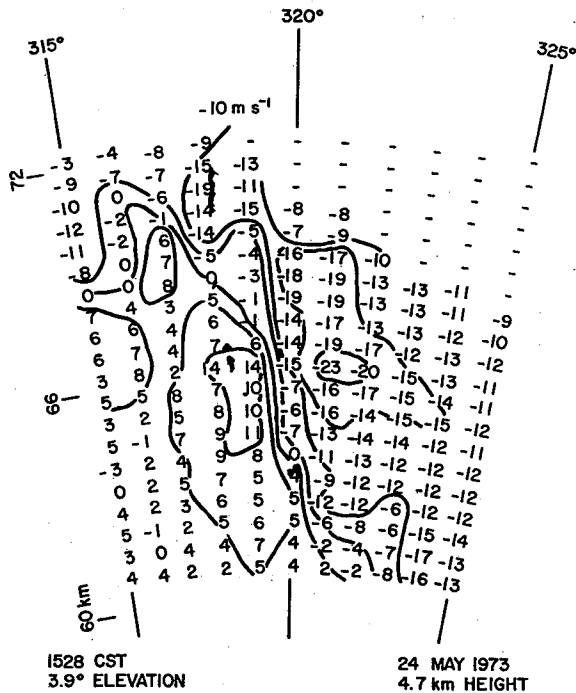


Fig. 6.4 Field of single Doppler mean velocities for a portion of Union City LM storm. Velocities are relative to storm motion and negative values are flow toward radar. Azimuths and ranges from radar are included.

The anticyclone has a lifetime greater than 17 minutes and extends from a base at 3 km to at least 7 km height (Fig. 6.5). Data collected below 3 km reveal small amounts of anticyclonic shear but no indication of a closed circulation. Mid-level core circulation (defined by Lemon and Burgess, Chapter 8) is 3 to 4 km in diameter with a peak rotational velocity of 15 m s^{-1} . The vorticity source for the anticyclonic rotation cannot be identified from available data. However, it may be important that the anticyclone is above the confluence region associated with the gust front.

The concept of a mid-level momentum block agrees with the severe left-moving storm models advanced by Hammond (1967) and Browning (1968). They propose a mirror image of the well-known right-moving storm model introduced by Browning and Ludlum (1962). The updraft of the proposed LM storm model is inclined over the surface cold air outflow and fed by low-level warm air approaching the storm front quadrant. The low-level downdraft is located within the precipitation area and is fed by potentially cold mid-level air approaching the left front storm quadrant.

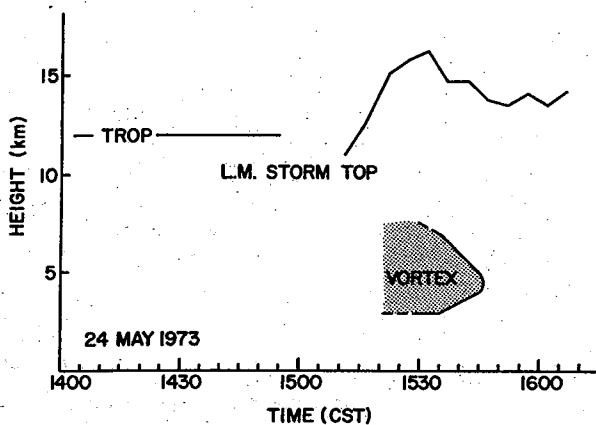


Fig. 6.5 WSR-57 radar echo tops and anticyclonic vortex extent versus time for left-moving storm. Storm tops after 1615 are from merged echoes.

Several authors, including Fujita and Grandoso (1968) and Charba and Sasaki (1971), have inferred weak anticyclonic rotation for the LM storm echo as a whole. A recent storm model developed by Raymond (1976) predicts significant anticyclonic vorticity in left-moving storm updrafts. These Doppler data, however, are the first measurements to show an anticyclone confined to a diameter smaller than the storm and coincident with the updraft.

6.4.3 High-Level Flow (9 to 10 km)

Flow information at high levels is limited to the last two data collection times (1536 and 1545). In general, it would appear we are viewing the updraft summit with divergence centered on the precipitation core. At 1536, ambient flow encounters the divergent momentum block with obstacle flow and a wake region. Upstream flow exists in the face of ambient 20 m s^{-1} relative winds indicating strong divergence.

High-level flow at 1545 is significantly different from that at 1536. Upstream flow is absent and the amount of diffluence indicated is greatly reduced. The direction of the ambient winds entering the storm has apparently shifted from northwesterly to westerly. Reasons for the wind shift are unknown but it may be related to the blocking influence of new convection developing west of the LM storm.

6.5 LM STORM EVOLUTION

The first Doppler observations (1515) occur during the early stages of the LM storm development but well after the splitting process began. The storm updraft has been in existence for at least 15 minutes and a downdraft apparently has reached the surface producing an outflow boundary or gust front. The storm updraft is intensifying as evidenced by the rapidly ascending storm top (Fig. 6.5). Anticyclonic shear is noted in the updraft area and rotation is developing.

By 1528, the LM storm reaches maximum maturity with a large echo core area and a storm top that penetrates the estimated tropopause height by 5 km. An anticyclone of at least 4 km depth has formed and is at the center of a momentum block to ambient airflow. The mature stage persists beyond 1536. Very little change in storm character or airflow is noted between 1528 and 1536. Hail, up to 2.5 cm diameter, was reported during the mature stage.

Pronounced weakening of reflectivities and the dissipation of storm characteristics are beginning by 1545. Confluence on the gust front is inferred to be lessening and the WER (overhang), that has persisted for 45 min, is almost entirely gone. At mid-levels, updraft rotation is being replaced by divergence. In turn, the divergence, which had existed at high levels earlier, is no longer identified. New convection competing for available low-level flow is occurring on several storm flanks (see Fig. 6.1), particularly near the updraft region, and is a possible cause of storm dissipation. The original LM echo is difficult to identify by 1600 and completely lost by 1630.

6. *Left-Moving Storm*

6.6 THEORIES ON LEFT DEVIATE MOTION

Several explanations for the anomalous translation speeds and directions observed for postsplit LM storms have been suggested. Fujita and Grandoso (1968) studied the severe 3 April 1964 splitting storm that yielded 60° divergent echo motions. They concluded that deflecting forces generated by storm rotation acted to produce observed motions. Rotation was considered to exist throughout the horizontal cloud diameter. Good agreement was found between observed echo deviations and those derived from a numerical simulation model when rotation rates were just a few meters per second.

Charba and Sasaki (1971) also studied the 3 April 1964 storms. Their detailed analysis of cell tracks within the LM storm provided evidence for anticyclonic circulation of the entire storm. However, they recognized that rotation alone could not account for observed motions (in opposition to Fujita and Grandoso). Therefore, Charba and Sasaki concluded that a second factor must be at work. A qualitative model revealed that propagation is an additional influence. The model suggests that rotation enhances propagation on the left flank and it is a vector combination of the two that produces observed deviate motion.

Raymond (1975) has developed a linear model of moist convective instability which predicts LM and RM storm propagation velocity. His calculations suggest that such storms take the form of convectively forced internal gravity waves. Excellent agreement has been achieved between predicted propagation values and observed deviate storm motion. Unfortunately, the model does not include the possible effects of environmental rotation. Vorticity aloft is produced by the tilting term of the vorticity equation acting in a sheared environment. The model constrains LM storm updrafts to be anticyclonic and RM storm updrafts to be cyclonic.

New evidence from the present study reveals the anticyclonic rotation to be confined to a smaller diameter, but possessing faster rotation rates than previously hypothesized. Additionally, strong evidence for left flank propagation exists based on inferred gust front and updraft location.

However, nothing is found to invalidate the qualitative model of Charba and Sasaki. Rotation-generated forces alone can explain some but not all, of the deviate storm motion. It would appear likely that a vector combination of rotation influence and propagation are responsible for the observed deviate motion of the LM storm.

6.7 SUMMARY

The splitting of one thunderstorm into two deviate moving halves was observed by 10-cm surveillance radar. The character of the radar echoes during the split agrees well with past studies. Just after the split began, a WER was identified on the left storm flank and the development of strong updraft was inferred. Unfortunately a lack of additional data sources prohibit knowledge of the mechanisms that promoted the split and the development of an intense left flank updraft. We hope future Doppler radar data collected during the initial phases of storm splitting will shed light on this important phenomenon.

The airflow of the left moving storm was specified from analysis of single Doppler radar data. The airflow pattern is similar to that proposed previously. The LM storm model, a mirror image of the well-known RM storm, includes a low-level gust front and substantial blocking flow at mid-levels.

Anticyclonic rotation of the LM storm updraft was discovered at storm mid-levels. The anticyclone's position, small circulation diameter and moderate rotational velocity are probably the most significant new knowledge of LM storms contributed by this study. Rotation and propagation toward the left flank likely work together to produce observed storm motion to the left of mean winds.

6.8 ACKNOWLEDGMENTS

We appreciate the hard work of Dr. Richard Doviak, Dale Sirmans and Glen Anderson in making the Norman Doppler radar an effective and flexible research tool. This work was partially supported by the Federal Aviation Administration under Interagency Agreement FA72 WAI-265.

6.9 REFERENCES

- Achtemeier, G. L., 1969a: Some observations of splitting thunderstorms over Iowa on August 25-26, 1965. Report No. 69-4, Florida State Univ., Tallahassee, 17 pp.
- _____, 1969b: On the correlation between severe weather and the trajectories of deviate storms over the Midwest on August 25, 1965. Report No. 69-5, Florida State Univ., Tallahassee, 21 pp.
- Brandes, E. A., 1976: Rawinsonde observations on 24 May 1973. Appendix C, The Union City, Oklahoma Tornado of 24 May 1973, R. A. Brown, Editor. NOAA Tech. Memo. ERL NSSL-80, Norman, Nat. Severe Storms Lab., 205-207.
- Brown, R. A., 1976: Single Doppler radar data acquisition and analysis. Appendix E, The Union City, Oklahoma Tornado of 24 May 1973, R. A. Brown, Editor. NOAA Tech. Memo. ERL NSSL-80, Norman, Nat. Severe Storms Lab., 215-228.
- _____, D. W. Burgess and K. C. Crawford, 1973: Twin tornado cyclones within a severe thunderstorm: Single Doppler radar observations. Weatherwise, 26, 63-71.
- Browning, K. A., 1968: The organization of severe local storms. Weather, 23, 429-434.
- _____, and F. H. Ludlum, 1962: Airflow in convective storms. Quart. J. R. Meteor. Soc., 88, 117-135.

6. Left-Moving Storm

- Burgess, D. W., and L. R. Lemon, 1976: Union City storm history. Chapter 5, The Union City, Oklahoma Tornado of 24 May 1973, R. A. Brown, Editor. NOAA Tech. Memo. ERL NSSL-80, Norman, Nat. Severe Storms Lab., 35-51.
- Charba, J., and Y. Sasaki, 1971: Structure and movement of the severe thunderstorms of 3 April 1964 as revealed from radar and surface meso-network data analysis. J. Meteor. Soc. of Japan, 49, 191-214.
- Donaldson, R. J., Jr., 1970: Vortex signature recognition by a Doppler radar. J. Appl. Meteor., 9, 661-670.
- _____, 1976: Observations of the Union City tornadic storm by plan shear indicator. Chapter 7, The Union City, Oklahoma Tornado of 24 May 1973, R. A. Brown, Editor. NOAA Tech. Memo. ERL NSSL-80, Norman, Nat. Severe Storms Lab., 67-83.
- Fujita, T., and H. Grandoso, 1968: Split of thunderstorm into anticyclonic and cyclonic storms and their motion as determined from numerical model experiments. J. Atmos. Sci., 25, 416-439.
- Haglund, G., 1969: A study of a severe local storm of 16 April 1967. ESSA Tech. Memo. ERLTM-NSSL 44, Norman, Nat. Severe Storms Lab., 54 pp.
- Hammond, G., 1967: Study of a left moving thunderstorm of 23 April 1964. ESSA Tech. Memo. IERTM-NSSL 31, Norman, Nat. Severe Storms Lab., 75 pp.
- Harrold, T., 1966: A note on the development and movement of storms over Oklahoma on May 27, 1965. ESSA Tech. Memo. IERTM-NSSL 29, Norman, Nat. Severe Storms Lab., 1-8.
- Hitschfeld, W., 1960: The motion and erosion of convective storms in severe vertical wind shear. J. Meteor., 17, 270-282.
- Lemon, L. R., and D. W. Burgess, 1976: Tornadic storm airflow and morphology derived from single Doppler radar measurements. Chapter 8, The Union City, Oklahoma Tornado of 24 May 1973, R. A. Brown, Editor. NOAA Tech. Memo. ERL NSSL-80, Norman, Nat. Severe Storms Lab., 85-106.
- Raymond, D. J., 1975: A model for predicting the movement of continuously propagating convective storms. J. Atmos. Sci., 32, 1308-1317.
- _____, 1976: Wave-CISK and convective mesosystems. J. Atmos. Sci., 33, 2392-2398.
- Sirmans, D., 1976: NSSL Doppler and WSR-57 radar characteristics. Appendix D, The Union City, Oklahoma Tornado of 24 May 1973, R. A. Brown, Editor. NOAA Tech. Memo. ERL NSSL-80, Norman, Nat. Severe Storms Lab., 209-213.

Chapter 7

OBSERVATIONS OF THE UNION CITY TORNADIC STORM BY PLAN SHEAR INDICATOR

Ralph J. Donaldson, Jr.

*Air Force Cambridge Research Laboratories¹
Bedford, Massachusetts 01731*

The storm that spawned the devastating Union City, Oklahoma tornado of 24 May 1973 was observed by Doppler radar, with velocities recorded at various times by Plan Shear Indicator (PSI). The PSI is an analog technique for display of velocity gradients that was developed at AFCRL and had been mated temporarily to the 10-cm Norman Doppler radar operated by the National Severe Storms Laboratory (NSSL). The first PSI picture showed intense shear at 8 to 9 km altitude in the Union City storm, 45 minutes before the earliest tornado damage. About 40 minutes before the tornado struck the ground, a vortex pattern with cyclonic rotation was recognizable at 5 to 8 km, but the wind field in the storm below 4 km was quite uniform. The base of the flow disturbance as well as the vortex descended and intensified during this early period prior to the appearance of the tornado. The vortex was tilted toward the left of the storm direction of travel, at an angle of about 30° from vertical. Vortex diameter was as large as 5 km when initially detected but decreased to less than 1 km at the surface when the tornado was in progress. Measured maximum tangential speeds of the vortex were generally 10 to 25 m s⁻¹, with the higher values measured just before and during the period of surface damage. Shears as large as 0.1 s⁻¹ were measured in the vortex. While the tornado was in progress the vortex was a highly organized, intense singularity in an otherwise smooth wind field near the ground; but in the upper third of the storm, at heights of 10 to 14 km, the disturbance was greatly enlarged and rather disorganized in space and unstable in time. These observations suggest a within-cloud tornado structure which extends up into the lower half of the storm as an organized vortex circulation, but somewhere in the upper half of the storm the disturbed region expands and degenerates into a disorganized but energetically boiling caldron.

7.1 DESCRIPTION OF THE PLAN SHEAR INDICATOR DISPLAY

The Plan Shear Indicator, or PSI, is a display scheme for portraying, in plan view, the location and magnitude of Doppler velocity gradients. It has been discussed in detail by Armstrong and Donaldson (1969), and its main features have been summarized briefly by Battan (1973). A brief description is provided here for the benefit of readers who are not familiar with its operation.

¹Now the Air Force Geophysics Laboratory.

7. Observations by Plan Shear Indicator

The PSI display resembles the picture obtained on the familiar PPI scope of an ordinary incoherent radar, except that the PSI pattern is not solid but is broken up into a series of concentric arcs. Fig. 7.1 is the PSI display photographed during the development of a severe thunderstorm in Massachusetts. Ground targets are indicated by the arcs at the bottom left corner (radar location) and by the tiny scattered segments of arcs at greater distances in several directions.

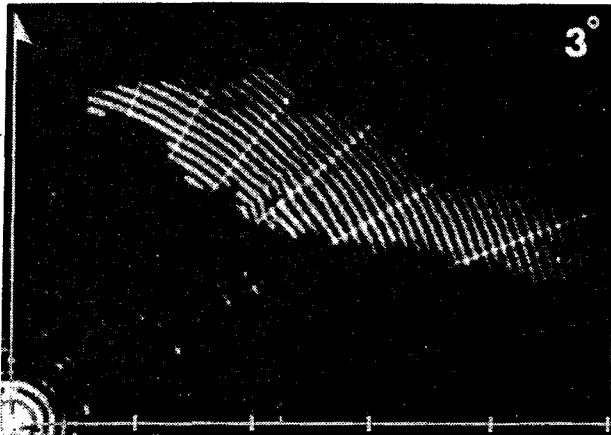


Fig. 7.1 PSI photograph of the Marblehead, Mass. storm of 9 August 1968, taken at 3° elevation angle at 1426 EST. Radar is located at lower left corner of picture, north is toward the top, and tick marks toward the east indicate range in 10-km increments. Storm moved toward the ESE. From Donaldson (1970).

The key to the PSI display is a sharing of range and velocity information on the same radial coordinate. As the radar antenna rotates, the location of any precipitation echo is marked by a series of concentric arcs which represent consecutive adjacent range gates, each having a width of 855 m. The distance of each arc from the center of the display is the sum of a large term which corresponds to range, plus a small term, no greater than the range gate width, which represents velocity. The maximum range of the PSI circuitry developed by AFCRL is 164 km. After successful mating to the 10-cm NSSL Doppler radar, the PSI is capable of displaying a velocity interval of 48.3 m s^{-1} unambiguously, utilizing the space between consecutive arcs.

A smooth, evenly spaced pattern of arcs, as portrayed most clearly in the eastern end of the echo in Fig. 7.1, indicates a homogeneous wind field, with no appreciable shear or velocity gradients. A disturbed wind pattern, on the other hand, is easily recognized by the irregular appearance of its PSI arcs. A good example is provided by the central part of the echo in Fig. 7.1, where disturbances are especially pronounced in the vicinity of the echo hole. Wrinkles in the arcs and/or variability in their spacing indicate intense shear or local gradients in the observed wind component.

Within-storm wind field disturbances are conveniently characterized by measurement of the maximum value of the slope of any arc with respect to its tangent circle. Arc slope is proportional to tangential shear of radial velocity, that is, the gradient of the radial velocity in a direction normal to this velocity vector. Minimum discernible tangential shears are of the order of 10^{-2} s^{-1} .

The PSI is particularly useful for display and measurement of regions of high shear occurring within a scale of a kilometer, because it is not limited by grid conformity and hence always utilizes the full azimuthal resolution of

the radar beam. Consequently, the PSI is well adapted for following tornado-scale motions. On the other hand, it has the disadvantage of insensitivity to small gradients of velocity, so it is especially difficult to determine, from a PSI display, the dimensions (and sometimes, indeed, the existence) of a broad, low-shear maximum or minimum in velocity. Therefore, large mesocyclones with shears considerably below 10^{-2} s^{-1} may be missed or their size recorded inaccurately by PSI.

Recognition of a vortex by Doppler radar is a significant aid in understanding how a tornado develops and for providing adequate warning. The tangential shear of radial velocity determines one of the two vorticity terms for a vortex with axis normal to a radial from the Doppler, as is the case for a vortex oriented more or less vertically, viewed by a radar with small antenna elevation angles. Fig. 7.2 shows, in plan view, the wind field of a typical vortex and the corresponding PSI pattern. Unfortunately, a single Doppler radar is sensitive only to components of velocity directed parallel to its beam and there is no certainty that the PSI pattern in the vicinity of the echo hole in Fig. 7.1 represents a vortex rather than a deformation in the wind field. Undisputed vortex identification is possible only by the use of at least two Doppler radars viewing the feature from different aspects.

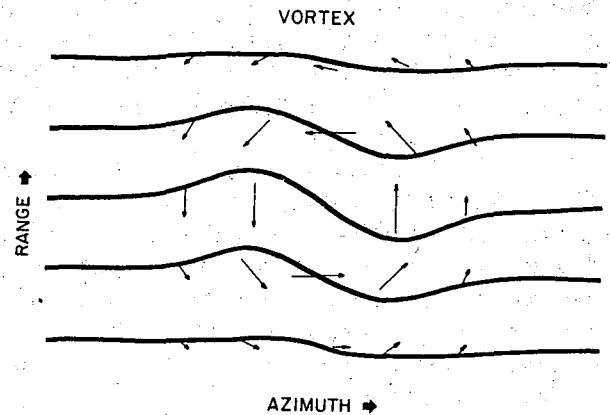


Fig. 7.2 Schematic PSI pattern for a cyclonic vortex. Arrows represent wind vectors and thick lines indicate how the PSI arcs would appear when radar is viewing such a wind field. From Armstrong and Donaldson (1969).

Nevertheless, a reasonable inference of vortex existence may be drawn from the appearance of a vortex signature (as provided by nature in Fig. 7.1 and portrayed schematically in Fig. 7.2) and a set of qualifying conditions. The conditions for credibility of vortex recognition, using data from a single Doppler radar, have been discussed at length by Donaldson (1970). In brief, these conditions require the vortex signature to extend vertically through a depth greater than its diameter, and to persist for a greater time than required for half a revolution. The necessary time duration is π divided by the tangential shear. For example, for a shear of 10^{-2} s^{-1} , the minimum persistence time is slightly more than five minutes.

7.2 DEVELOPMENT OF FLOW DISTURBANCES DETECTED BY PSI

The first PSI observation of the Union City storm, taken at 1453 CST, revealed appreciable flow disturbances at 8 to 9 km altitudes a full 45 min prior to initial tornado damage. The largest tangential shear at this time

7. Observations by Plan Shear Indicator

was $3 \times 10^{-2} \text{ s}^{-1}$, with a velocity increment of 30 m s^{-1} across the shear zone. Velocities, however, did not seem to be organized into a pattern suggestive of a vortex.

Following the first picture, four elevation sequences were photographed while the antenna was raised in one-degree increments. Then several miscellaneous PSI photographs were taken at a very high elevation angle while the tornado was inflicting its initial damage, followed by a sequence of nearly-zero elevation pictures while the tornado was in and just beyond the central part of Union City. (PSI observations had to be alternated with another data collection mode because the two modes were incompatible.)

All photographs were sector scans, some with azimuthal width as narrow as 40° . By this means the Union City storm could be covered quickly, an important consideration because of rapidly developing storm characteristics and the large number of elevation angles encompassed by the storm depth. The time-height coverage of the Union City storm represented by the useful PSI photographs is depicted in Fig. 7.3. Some time gaps are filled by other Doppler modes. Storm top, indicated by echo heights measured on the NSSL WSR-57 radar, ascended from a linearly interpolated 15 km at the beginning of PSI observations, to a measured value of 17 km at 1515.

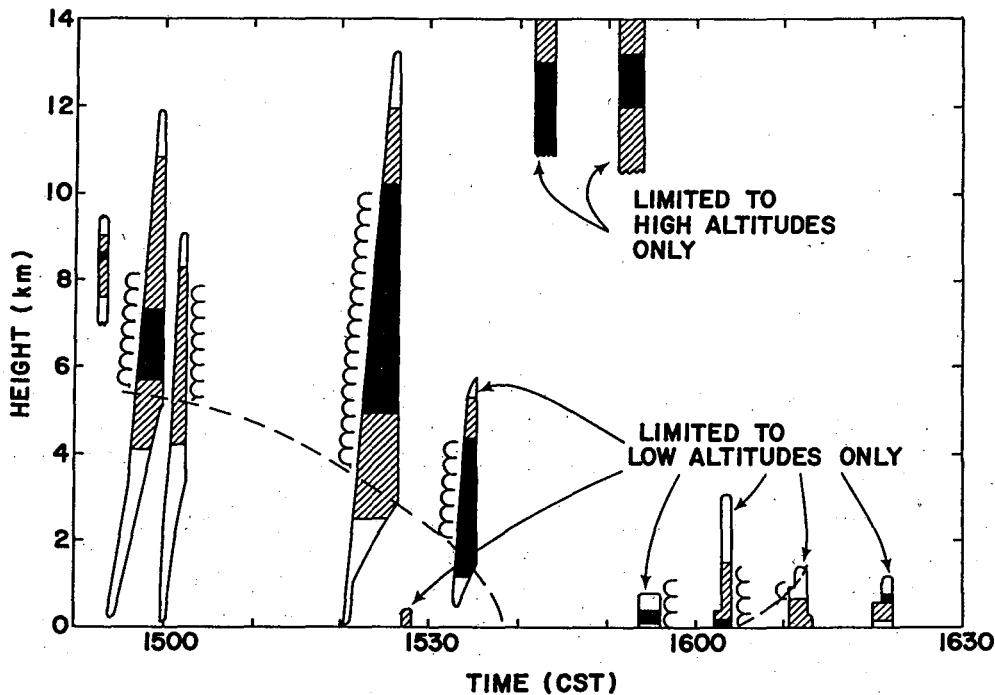


Fig. 7.3 Time-height coverage by PSI of the Union City storm. Hatched areas show where maximum tangential shear exceeded 10^{-2} s^{-1} , and solid black areas where it exceeded three times this value. Spirals adjacent to the areas indicate observation of a vortex pattern. Dashed curves indicate base of vortex. All heights are above the Norman Doppler radar.

Tangential shear with a magnitude of at least $2 \times 10^{-2} \text{ s}^{-1}$ was observed somewhere in the Union City storm during every elevation sequence (1453 to 1640). Measurable shear was observed throughout storm depth except in its early stages, when little or no shear was detected near the surface. Table 7.1 indicates the minimum height of two shear values during the pre-tornado period, and shows the rapid descent of disturbed flow toward the ground.

TABLE 7.1 *Base Height (km) of Tangential Shear Values in the Union City Storm Measured by PSI.*

Time (CST)	Shear Magnitude	
	$\geq 10^{-2} \text{ s}^{-1}$	$\geq 2 \times 10^{-2} \text{ s}^{-1}$
1454-59	4.2	5.6
1500-02	4.2	5.7
1521-26	2.5	5.0
1527	0.2	0.2

It is interesting to compare these observations with a study, using Doppler PSI, of 22 thunderstorm days in Massachusetts (Donaldson, 1971). Storms with a relatively smooth wind field, characterized by maximum tangential shears of 10^{-2} s^{-1} or less, never produced large hail or inflicted wind damage at the ground. In other words, low shears measured by the PSI display faithfully indicated nonsevere storms. Tangential shear magnitudes of at least $2 \times 10^{-2} \text{ s}^{-1}$ were observed somewhere within the echo volume of 94% of severe storms. Wind field disturbances of this magnitude or larger occurred aloft far more frequently and more extensively than severe weather at the ground. The Union City storm thus is consistent with Massachusetts storms.

Another similarity between the Union City tornadic storm and several well-observed severe storms in Massachusetts is the initial appearance of large shears at middle altitudes. During the first half hour of observations the wind field at lower levels in the Union City storm was quite unruffled, as indicated by smooth PSI arcs (Fig. 7.4). In Massachusetts, the appearance of high shears aloft and their gradual descent toward the ground have preceded destructive surface winds by nearly an hour in two severe storms. Again, the Union City storm is in essential agreement, displaying tangential shear in excess of $3 \times 10^{-2} \text{ s}^{-1}$ at an altitude of 8.5 km at the first PSI observations, 45 minutes before the earliest tornado damage at 1538. Quantitatively, however, the Union City storm was much larger and more vicious than anything we have observed in Massachusetts. Not only was the Union City tornado far more devastating than the most severe Doppler-observed Massachusetts storm, but its wind field was more disturbed, and the disturbance extended to higher altitudes.

7. Observations by Plan Shear Indicator

(a)

(b)

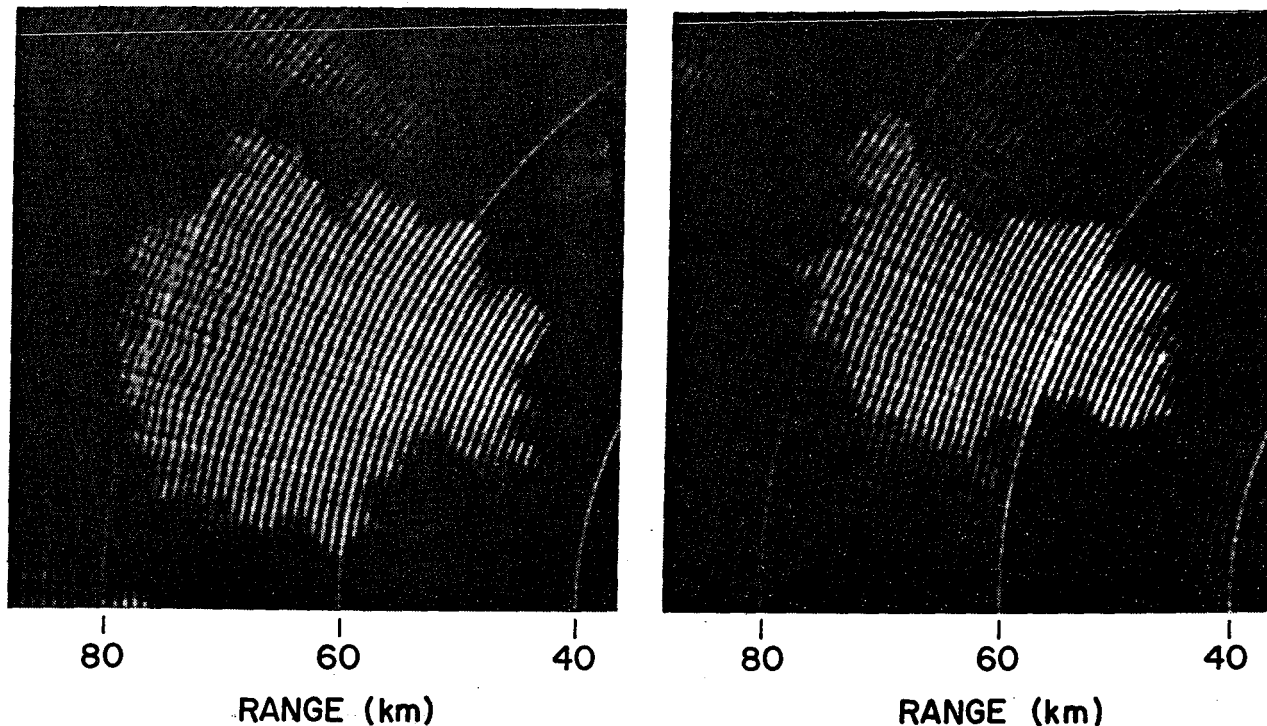


Fig. 7.4 Earliest PSI photographs of the Union City storm. Range markers in Figs. 7.4 through 7.8 are at 20 km intervals and base of each figure is due west of the radar. (a) 1453 CST, elevation 5.9° showing disturbed flow, indicated by wiggles in the arcs, at an altitude of 8 to 9 km. (b) 1456 CST, elevation 1.9° showing relatively homogeneous flow, indicated by smooth PSI arcs, at an altitude of 1.8 to 3.2 km.

7.3 THE UNION CITY TORNADO VORTEX

The most exciting event during the PSI observations was the appearance, intensification, and descent of a recognizable vortex pattern. Although, on some pictures there were several PSI arc wiggles which resembled the model vortex depicted in Fig. 7.2, rather stringent requirements were imposed during the analysis for a pattern to qualify as a probable vortex. First of all, the pattern must display a definite maximum in Doppler velocity adjacent to a minimum. Next, it must appear as such a singularity that it can, without confusion, be traced into adjacent heights and successive times. Finally, it must satisfy the vortex credibility standards of persistence in time and extension in height discussed earlier. This selection process may have eliminated many minor or ephemeral vortices, but there is high confidence that any velocity pattern which passes the tests is in fact a vortex circulation.

7.3.1 Quality of Vortex Measurements

Table 7.2 presents the history of the Union City tornado vortex as portrayed by PSI. Bracketed entries in the table indicate another possible vortex pattern but it is uncertain whether and how it is connected with the Union City vortex. Time was read from a dial clock which appeared on the film. A + or - after the time indicates that the average time during the picture was clearly greater or less than the tabulated minute by 10 to 30 seconds. Where two elevation angles occur together (at times 1502 and 1526) there was a double exposure on the film owing to camera malfunction. Azimuth angles with a ~ in front have an unknown inaccuracy which probably exceeds the half-power radar beamwidth of 0.8° . There are three main sources of this error: double exposures, off-centering of the sector scans, and the tendency of echoes to shift a degree or two in apparent azimuth with reversal in direction of the sector scan.

The range of a PSI arc, which cannot be determined with an accuracy greater than the range gate width of 855 meters, was specified as the beginning of each range gate. To better evaluate the instantaneous vortex tilt, a correction was made for storm motion during the time required for each elevation sequence. Range was corrected by assuming a 10 m s^{-1} motion toward the radar and referring all ranges in the sequence to the earliest time of the sequence. This correction was an excellent one between 1522 and 1555 CST, when the vortex positions indicate a motion from about 290° , almost directly toward the radar, at a speed of 10 m s^{-1} .

Height was computed from the product of uncorrected range and sine of the elevation angle, plus a small increment for earth curvature. The maximum tangential shear, $\partial v / r \partial \beta$, (β is azimuth angle) was given by the peak slope of a PSI arc, according to the formula $5.65 \times 10^{-2} \tan \delta \text{ s}^{-1}$, where δ is the angle of a sloping arc toward the radar from its tangent circle. This formula is easily derived by noting that the distance between normal arc spacing on the PSI display is 855 meters, which also corresponds to the maximum unambiguous velocity interval of 48.3 m s^{-1} . The total velocity increment, Δv , was estimated by eye to the nearest 5 m s^{-1} . Vortex diameter is an estimate of the distance between maximum and minimum velocities. Velocity extrema are generally flat and therefore difficult to locate accurately, so a spread of values is tabulated, indicating smallest, most likely, and largest possible estimates. Note that the average shear across a vortex, $\Delta v / \text{diameter}$, is always somewhat less than the maximum shear values recorded in Table 7.2, which are limited only by the resolution capacity of the radar and PSI circuitry.

7.3.2 Vortex Features

The first clear evidence of a vortex appeared in the height range of 5.4 to 8.0 km at 1457-58 CST. At this time the vortex was broad (involving several adjacent PSI arcs), had only moderate shear, and was accompanied by a fairly large echo hole or bounded weak echo region (see Table 7.3) centered at

7. Observations by Plan Shear Indicator

TABLE 7.2 Development of the Union City Tornado Vortex

Time (CST)	Elevation Angle	Azimuth Angle	Range (km)	Height (km)	Maximum Tangential Shear ($10^{-2} s^{-1}$)	Δv ($m s^{-1}$)	Diameter (km)	Remarks
1457+	3.8°	285.5°	75.7	5.4	+1	15	1.8-2.4-3.0	Bottom
1458-	4.9°	286°	75.5	6.7	+1	25	3.5-4.8-5.7	
1458+	5.9°	-286°	75.3	8.0	+1	15	2.0-2.7-3.4	Top of primary vortex.
[1459-	6.9°	-284°	74.6	9.2	+2	20	1.0-1.2-1.4]	Secondary vortex.
1501+	3.9°	-286°	73.1	5.3	+2	30	1.5-2.0-2.5	Bottom; in weak echo.
1502	4.9° +5.9°	-287°	73.1	6.5 +7.8	+1	25	2.5-3.0-3.5	No info on top.
1522	2.9°	-290.5°	67.8	3.7	+1	25	2.5-2.9-3.2	Bottom.
1523	3.9°	-291°	68.0	4.8	+3	25	0.9-1.3-2.5	
1523	4.9°	-291°	68.2	6.0	+5	40	1.0-1.4-1.7	High quality observation.
1524	5.9°	291.5°	67.7	7.1	+6	35	0.6-0.9-1.3	High quality observation.
1525-	7.0°	291.5°	67.5	8.2	+3	30	1.0-1.3-1.6	High quality observation.
1526	8.0° +9.0°	-293°	66.7	9.1 +10.2	+2	30	1.7-2.3-2.8	No info on top.
[1525-	7.0°	287°	67.0	8.2	+2	25	1.3-1.4-1.6]	Bottom of secondary vortex.
[1526	8.0° +9.0°	-288°	65.9	9.0 +10.1	+5	40	0.8-1.1-1.4]	No info in top.
1534	1.9°	-291°	59.6	2.2	+7	50	1.1-1.4-2.2	No info on bottom.
1535-	2.9°	-291.5°	59.6	3.3	+4	45	1.4-2.1-2.8	All three in this series are high quality observations.
1535	3.9°	292°	59.4	4.2	+4	45	1.3-2.3-3.2	No info on top.
1554	0.2°	-292°	48.5	0.3	+10	>50	0.7-1.0-1.2	No info on top for this or next two listings.
1555-	0.2°	-292°	48.1	0.3	+10	45	0.5-0.7-1.1	High quality observation.
1555+	0.2°	-291.5°	47.7	0.3	+3	20	0.7-0.9-1.0	
1602+	-0.1°	-289°	43.0	0.1	+4	20	0.5-0.8-1.0	High quality observation.
1603+	1.8°	-290°	42.8	1.4	+2	20	1.0-1.4-1.7	No info on top.
1611+	0.8°	-281.5°	38.5	0.6	+1	10	~1	Bottom; no info on top.

TABLE 7.3 Bounded Weak Echo Region (BWER) Related to Union City Vortex.

Time (CST)	Elevation Angle	Center Azimuth	Center Range (km)	Center Height (km)	BWER Extent
1457+	3.8°	286°	75.7	5.4	3.5 km in range by 2 km in azimuth
1458-	4.9°	286.5°	75.5	6.7	2.5 km in range by 1.5 km in azimuth
1458+	5.9°	~286.8°	~76.1	8.1	2.5 km in range by ~1 km in azimuth

NOTE: Center location difficult to pin down on 5.9° picture because BWER is long and thin. At all three elevation angles the maximum shear is definitely along south side of BWER.					

1502	4.9° +5.9°	~287°	73.1	6.5 +7.8°	1 km diameter

NOTE: At both of these elevation sequences, the BWER at lower elevation angles becomes unbounded and open toward the south.					

about the same range but nearly a kilometer north of the vortex (Fig. 7.5). Similar characteristics existed in the Marblehead, Mass. severe storm of August 9, 1968 (Donaldson, 1970). Below 5.4 km the weak echo region was unbounded, opening toward the south. There were extremely weak arcs, detected by the sensitive integrating capability of the PSI, that were free of wiggles. Therefore, we are confident that the vortex base was at 5.4 km when first detected.

During the next elevation sequence, 1501-02 CST, vortex base was detected at a height of 5.3 km in weak echo a few kilometers southwest of a right-angle indentation in the strong echo. Four minutes previously at the same height, this region had been an echo hole surrounded by strong echo. The southern part of the strong-echo ring had disappeared by 1501. PSI arcs in the weak echo were a bit sketchy so it was difficult to specify shear accurately; it could have been larger than indicated. This sequence terminated at an elevation of 5.9°, so there was no information on the top of the vortex.

The vortex intensified during a 20-minute hiatus in PSI observations. By 1521 CST a classical reflectivity hook had developed at low levels on the southwest side of the Union City storm, and the PSI showed a disturbance in the hook down to a height of 1.3 km. However, a vortex could not be validated clearly by the PSI at this height, because the velocity profile on either side of the disturbed region was so flat that neither minimum nor maximum velocity was discernible. At a height of 2.5 km the case for existence of a vortex is

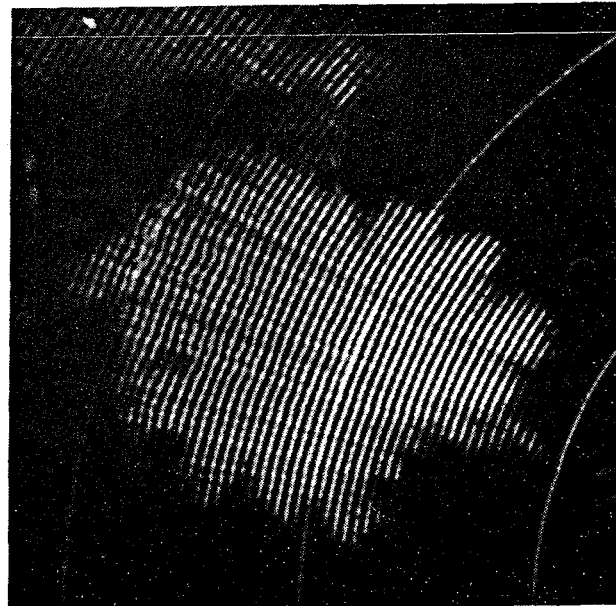
7. Observations by Plan Shear Indicator

stronger because a small velocity maximum, indicating flow toward the west, appeared between the hook and the main body of echo. However, the PSI was unable to detect an adjacent velocity minimum, or eastward flow, which would have suggested a vortex pattern. The requisite couplet of velocity extrema did appear on the 2.9° photograph, so a vortex base height of 3.7 km is indicated by PSI. Fig. 7.6 shows how the vortex appeared on the PSI display during this sequence at a height of 6 km, where it was most intense.

An interesting complexity of the elevation sequence of 1522-26 is the appearance of velocity structures above 8 km which are very suggestive of a secondary vortex several kilometers south of the Union City vortex. These are bracketed in Table 7.2 to indicate doubt about their validity. The only suggestion of persistence of this hypothesized secondary vortex is a possible connection with the bracketed entity which appeared nearly a half hour earlier at 1459.



80 60 40
RANGE (km)



80 60 40
RANGE (km)

Fig. 7.5 An early PSI view of the Union City vortex, centered along the southern edge of the echo hole. Time is 1458 CST, elevation is 4.9° , and echo hole and vortex are at a range of 74 km (6.7 km height).

Fig. 7.6 The Union City vortex is intensifying. In this PSI photograph, taken at 1523 at 4.9° elevation, the vortex is at a range of 67 km, corresponding to a height of 6 km, and is located a short distance north of the weak echo nearly enclosed by the hook.

A 0° elevation photograph taken at 1527 showed that moderate shear of 10^{-2} s^{-1} had reached the ground by this time, but it was not yet a vortex. By 1534-35, the vortex had intensified remarkably. Tornado damage started only 3 to 4 minutes later. Fig. 7.7 shows the wild PSI pattern typical of all three elevations. With increase in height from 2.2 to 4.2 km, the area of heavy involvement with the vortex circulation roughly doubled, going from three to four arcs in range with a corresponding azimuthal increase from 1.4 to 2.3 km in diameter. Furthermore, the vortex for the first time became highly asymmetrical; the main anomaly was a strong westerly flow (toward the radar) on the south side of the vortex.

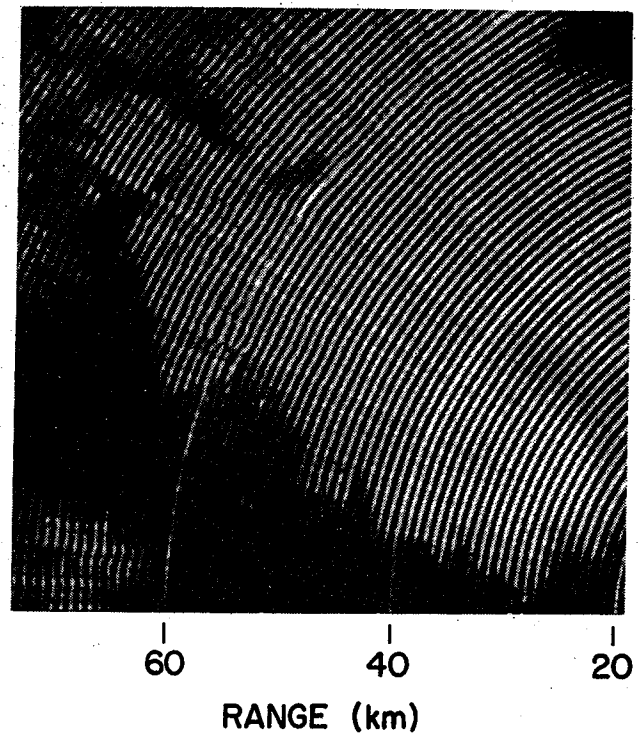


Fig. 7.7 Extremely intense vortex at a height of 3.3 km, elevation 2.9° at 1535 CST, just three minutes prior to the earliest tornado damage. The large vortex straddles the 60 km range marker.

Between 1542 and 1553 several high-altitude PSI photographs were taken. No vortex could be identified on any of these pictures, but they did show, mostly above 10 km, an elliptical region roughly 10 to 15 km in horizontal extent centered somewhat northeast of the extrapolated surface vortex, with many extreme flow disturbances. Shears as high as $7 \times 10^{-2} \text{ s}^{-1}$ were measured, with Δv in excess of 50 m s^{-1} in several places. Also, successive pictures at the same elevation, separated in time by less than a minute, showed remarkable changes in velocity pattern. One gets the impression of a vast, wildly boiling caldron above the smaller and more organized vortex down below. Apparently the Union City tornado funnel extended its violence right up towards cloud top, but exhibited progressively disorganized circulation as it expanded with increasing height.

Three of the most fascinating PSI photographs were taken successively between 1554 and 1555, with the elevation angle fixed at 0.2° (Fig. 7.8). They show the tornado circulation roughly between ground and cloud base. In all three pictures the highly disturbed region is small, only 1 to 1.5 km in diameter, with very little disturbance anywhere else on the photograph except for a slight and narrow "broadcasting" of the disturbance several kilometers toward the southeast of the tornado. The time between first and last picture in this series is 75 seconds. In this time the vortex traversed one range gate, as nearly as we can measure, so the vortex is now traveling at a ground speed of about 11 m s^{-1} and is beginning to accelerate. Also, as nearly as we can tell it is beginning to turn slightly toward its right during the last two pictures.

7. Observations by Plan Shear Indicator

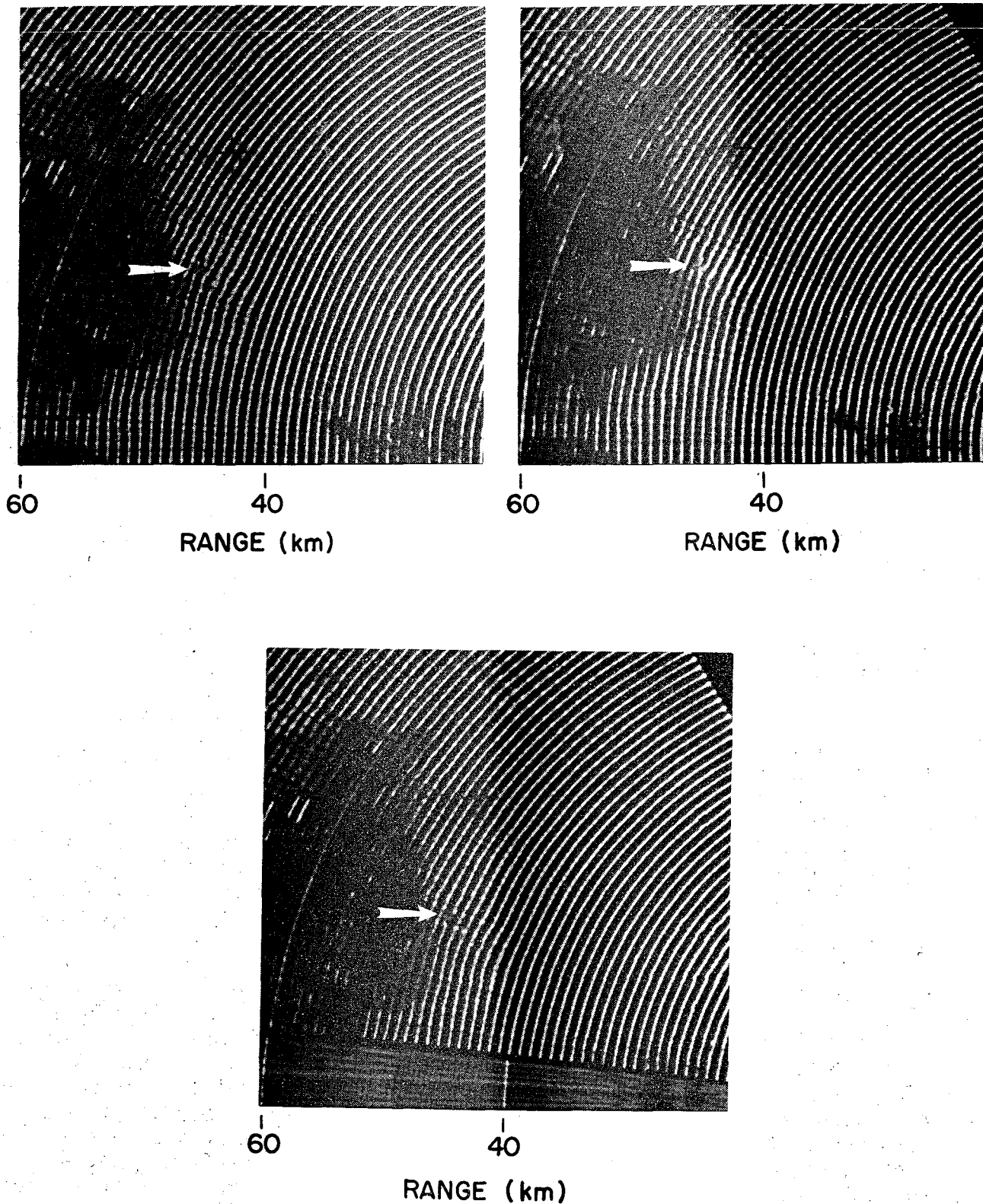


Fig. 7.8 PSI photographs taken consecutively during 1554-55 CST of the Union City tornado on the ground. All have elevation of 0.2° , so radar beam is viewing tornado funnel and associated debris.

Velocities measured below cloud base likely are not those of the funnel cloud, because the radar is not sensitive enough to detect backscattered power from a condensation cloud. Near the damage path, tracers of air motion probably consist of wet debris and organic material (e.g. leaves) torn loose and picked up by the tornado, as well as scattered raindrops observed in the vicinity. Such tracers probably underestimate winds in the funnel, but the shears are still impressive. In the first picture at 1554, Δv exceeds the maximum unambiguous velocity of 48 m s^{-1} , since the PSI arc is split for a short azimuthal segment. The shear is difficult, if not impossible to measure under these circumstances. It was roughly estimated to be about 0.1 s^{-1} .

The second picture reveals a Δv of about 45 m s^{-1} ; great care was taken to accurately determine the maximum tangential shear. The result is indisputable: the maximum shear is 0.1 s^{-1} . This implies that the resolving power of the radar can reveal detail in a sharp velocity structure only 0.7 of the half-power beamwidth.

The third picture shows a sudden and marked decrease in vortex intensity, both in shear and in Δv . Not surprisingly, this decrease occurred within one minute of the observation of a rapid shrinking in the size of the condensation funnel (Purcell, Chapter 11). In all three pictures the probable vortex width is less than a kilometer and there is a notable asymmetry, with the main flow disturbance moving toward the west.

A later PSI view of the vortex at 1602-03, when the funnel was rope-like but still inflicting heavy damage, shows the vortex turning markedly toward its right. Only two pictures were taken during this sequence. We know only that the top of the vortex extended up to 1.4 km and was fairly symmetrical.

The final PSI evidence of the vortex, at 1611, was barely distinguishable from several other minor disturbances in the wind field at 0.8° elevation. It was found by extrapolation from the previous vortex position. The vortex was definitely absent (i.e., PSI arcs were smooth) on the previous picture taken at an elevation of 0.4° and on the succeeding one at -0.1° . Therefore, its minimum base height just before extinction was at least 0.6 km, the height of the radar beam axis, and probably was higher in consideration of the lack of any vortex signature in the radar echo only half a beamwidth below 0.8° . Incidentally, this final radar observation of the vortex is consistent with visual observation, that is, a small turbulent area in the cloud base was noted after the funnel had disappeared and the damage had ceased.

A plan view of all Union City vortex locations identified by PSI is presented in Fig. 7.9. Table 7.4 shows the vertical dimensions of the vortex. Its base descended gradually at first, and then pounced. For example, from 1501 to 1522 its descent rate was only 1.3 m s^{-1} ; from 1522 to 1534 it descended at a rate of at least 2 m s^{-1} ; and considering it hit the ground at 1538 with the initial damage, the descent rate averaged over 1522 to 1538 was nearly 3.9 m s^{-1} .

7. Observations by Plan Shear Indicator

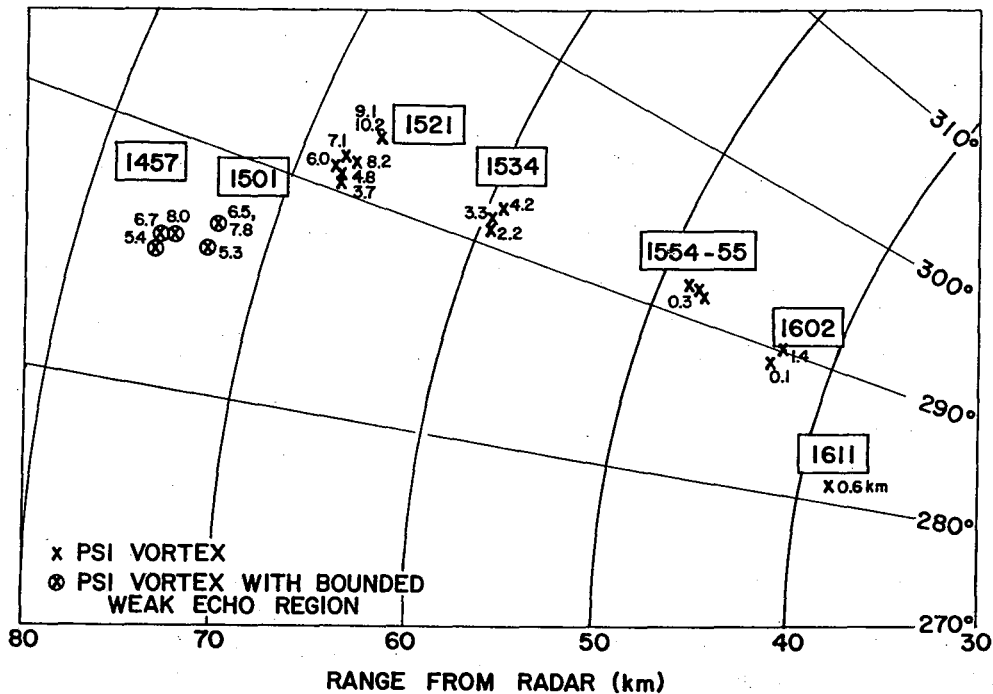


Fig. 7.9 Plan view of Union City vortex positions located by PSI. X denotes vortex position corrected for storm motion to time of elevation sequence, which is boxed in. Circles around X's show bounded weak echo regions attendant with vortices. Heights in km are printed alongside each vortex location.

TABLE 7.4 Altitude Limits of the Union City Vortex

BASE OF IDENTIFIABLE VORTEX		TOP OF IDENTIFIABLE VORTEX	
Time (CST)	Height (km)	Time (CST)	Height (km)
1457	5.4	1458	8.0
1501	5.3	1502	7.8 or above
1522	3.7	1526	9.1 or above
1534	2.2 or below	1535	4.2 or above
1554-55)	on the	1603	1.4 or above
1602)	ground		
1611	0.6		

7.4 VORTEX TILT

Measurements of vortex tilt were attempted where possible. In all instances except one these observations contained small but unknown azimuth errors. The measurement at 1534-35, however, is regarded as especially accurate because the azimuth errors at the lower and upper heights of the vortex segment were of the same polarity and approximately the same magnitude.

Results of the tilt measurements are listed in Table 7.5. "Left" and "front" refer to the direction of tilt, with increasing height, as seen by an observer at the vortex facing in the direction of translation. The compass direction of tilt is the projection on the ground of the tilted vortex axis, going from lower to higher height.

TABLE 7.5 *Tilt of the Union City Vortex*

Time (CST)	Measured Vortex Height Interval (km)	Azimuth Tilt (km)	Range Tilt (km)	Angle with Vertical	Compass Direction of Tilt
1457-58	5.4-6.7	left 0.7	front 0.2	28°	032°
1457-58+	5.4-8.0	left 0.7	front 0.4	17°	046°
1524-25	7.1-8.2	left <0.3	front 0.2	<18°	>055°
*1534-35	2.2-4.2	left 1.0	front 0.2	28°	032°
1602-03	0.1-1.4	left 0.8	front 0.2	30°	034°

*High Quality Measurement

Several interesting features are revealed by the tilt data. For example, the prime axis of tilt is invariably normal to the direction of travel, and to its left, rather than along it. The greatest tilt occurred toward the end of the vortex existence, when the tornado was in the rope stage. Finally, the two measurements with significantly lesser tilts involved the two greatest upper height limits. The vortex apparently became more vertical at higher altitudes.

7.5 CONCLUDING REMARKS

Progress of the Union City tornado vortex, using the PSI display, was observed for a period of 74 minutes. Although data are intermittent, we have traced vortex development from its early appearance as a large, weak circulation located 5 to 8 km aloft, through its descent, contraction and remarkable intensification while the tornado funnel touched down and inflicted severe

7. Observations by Plan Shear Indicator

damage, until it finally disappeared into the cloud base as a small and weak disturbance. PSI measurements complement digital Doppler time-series data acquired at alternate times and presented elsewhere in this volume. Each method has advantages that compensate in large measure for the disadvantages of the other technique. The most important feature of the PSI display is its capability for accurate measurement of large values of shear and their easy recognition in real time.

The Union City tornado, should it prove to be typical of such storms, furnishes a basis for significant improvements in tornado warning systems. A vortex was first detected by Doppler radar 41 minutes before initial damage. The means are available to recognize a potentially threatening mesoscale cyclone aloft and monitor its development and descent in order to provide an accurate and reliable short-term warning of destructive winds. Future research should address why some vortices never descend to the ground and a consideration of conditions that affect the descent, intensification and stability of vortices that evolve into dangerous tornadoes.

7.6 ACKNOWLEDGMENTS

The study of Oklahoma thunderstorms by PSI would not have been possible without the active encouragement and inspired cooperation of Ed Kessler, Director of NSSL, and his staff. Special thanks are due Dale Sirmans of NSSL, who accomplished the difficult job of mating the PSI circuitry with the Norman Doppler radar and kept the hybrid in good working order. I am also grateful to Bill Smith of AFCRL who assisted Dale and his technicians in the installation, testing, and adjustment of the PSI at Norman, and Dick Doviak of NSSL who capably supervised Doppler radar operations and improvements. Valuable conversations with Ken Hardy and Mike Kraus of AFCRL contributed to the analysis. But most of all, I am happy to have this opportunity to acknowledge the enthusiastic and effective cooperation of Rodger Brown, Don Burgess, and Les Lemon of NSSL. They played a vital part in the PSI observations of the Union City tornado and contributed much to my analysis through their perceptive remarks and questions and keen, friendly interest. I am well pleased to have served as their colleague. Finally, I wish to thank June Queijo of AFCRL for typing the original draft of this manuscript.

7.7 REFERENCES

- Armstrong, G. M., and R. J. Donaldson, Jr., 1969: Plan shear indicator for real-time Doppler radar identification of hazardous storm winds. J. Appl. Meteor., 8, 376-383.
- Battan, L. J., 1973: Radar Observation of the Atmosphere. Chicago, Univ. of Chicago Press. See pp. 157-160.
- Donaldson, R. J., Jr., 1970: Vortex signature recognition by a Doppler radar. J. Appl. Meteor., 9, 661-670.

Ralph J. Donaldson, Jr.

_____, 1971: Doppler radar identification of damaging convective storms by plan shear indicator. Preprints, Seventh Conf. on Severe Local Storms, Boston, Amer. Meteor. Soc., 71-74.

Purcell, D., 1976: History of the Union City tornado. Chapter 11, The Union City, Oklahoma Tornado of 24 May 1973, R. A. Brown, Editor. NOAA Tech. Memo. ERL NSSL-80, Norman, Nat. Severe Storms Lab., 123-133.

Chapter 8

TORNADIC STORM AIRFLOW AND MORPHOLOGY DERIVED FROM SINGLE DOPPLER RADAR MEASUREMENTS

Leslie R. Lemon¹ and Donald W. Burgess

*National Severe Storms Laboratory
Norman, Oklahoma 73069*

Single Doppler velocity data reveal a tornadic thunderstorm dominated by a core cyclonic circulation, 2 to 6 km in diameter, extending to at least 9 km above ground. Deduced in-storm relative flow fields are characterized by apparent flow through the precipitation echo at low levels and by divergence at high levels. Considerable similarity is noted between mid-level flow structure around the core circulation and that observed around a solid rotating cylinder embedded in classical potential flow. Core circulation tangential velocities increase with time while diameter decreases. Contemporaneously, collapse of storm top and extensive echo overhang suggest updraft weakening.

8.1 Introduction

Doppler radar measures both the reflectivity distribution and also radial precipitation particle velocity. The radial velocity component changes with azimuth; this inability to measure motion normal to the radar beam limits the application of single Doppler radar to investigate the convective storm. Some limitations are overcome by using interpretive techniques and restrictive assumptions about the velocity field character.

Pulsed Doppler radar investigations of convective storms were originally limited by vertical pointing antennas. Probert-Jones and Harper (1961) were the first to show that vertical air motion in showers could be obtained. Battan (1964) and Battan and Theiss (1966) mapped the vertical air patterns in air mass thunderstorms by extending the technique of Probert-Jones and Harper. With the Air Force Cambridge Research Laboratories' Doppler radar in a VAD (Velocity-Azimuth-Display) mode at intermediate elevation angles, Donaldson (1970b) determined wind direction and speed in a thunderstorm anvil. When sufficient echo encircles the radar, the VAD technique can provide estimates of the horizontal wind as well as particle fall speeds.

¹Present affiliation: National Severe Storms Forecast Center, Techniques Development Unit, Kansas City, Missouri 64106.

8. Tornado Storm Airflow and Morphology

During the late 1960's and 1970's, attention has turned toward the study of horizontal motions in convective storms using data at low elevation angles. Easterbrook (1967) deduced wavelike perturbations (wavelength about 4 km) in the horizontal wind field of a convective echo. Donaldson (1967, 1971) and Donaldson *et al.* (1969), using the single Doppler Plan Shear Indicator (PSI), identified localized regions of strong tangential shear (i.e., normal to the beam) up to $4 \times 10^{-2} \text{ s}^{-1}$ and possible cyclonic vortices within severe thunderstorms. With the NSSL Doppler, Brown *et al.* (1971), Burgess and Brown (1973) and Sirmans *et al.* (1974) obtained quasi-horizontal data within tornadic thunderstorms containing cyclonic circulations (vortices) averaging about 5 km in diameter above funnel cloud or surface tornado locations.

During the afternoon of 24 May 1973 the NSSL Doppler radar obtained the most extensive (at the time) single Doppler data set in a tornadic storm. Digital velocity measurements began 23 minutes before tornado touchdown and continued until after tornado dissipation. The purpose of this paper is to derive a within-storm flow structure, determine its relationship to storm evolution and examine the relationship between the tornadic vortex signature--directly related to the tornado (see Brown and Lemon, Chapter 15)--and the larger cyclonic circulation revealed by Doppler measurements.

8.2 DATA AND ANALYSIS ASSUMPTIONS

The primary data source used here is the Doppler radar; its characteristics are listed by Sirmans in Appendix D. These data were edited and, using a three-dimensional weighting function, objectively processed and displayed for analysis (see Brown, Appendix E).

Recognizing limitations of single Doppler radar, Donaldson (1970a) introduced a somewhat objective method for defining a flow pattern which has an identifiable Doppler velocity signature--namely, that of a Rankine combined vortex. The vortex (which tornadoes and mesocyclones most closely resemble) is characterized by essentially two flow regimes. The first regime is the vortex core ($r \leq R$), where R is the radius of maximum tangential velocity. The core, in solid rotation (most easily identified in single Doppler radar data by the radially separated velocity peaks of opposite polarity, Fig. 8.1), has an idealized velocity distribution:

$$\frac{V}{r} = C_1, \quad \text{where } C_1 = \frac{V_{\max}}{R} \quad (8.1)$$

and V is the tangential velocity. Outside the core, the flow regime is that of a potential vortex

$$V \cdot r = C_2, \quad \text{where } C_2 = V_{\max} \cdot R \quad (8.2)$$

and is very difficult to detect by single Doppler radar. In this study we have chosen to combine Donaldson's vortex criteria and a number of assumptions to deduce internal storm flow structure (streamline patterns) from measured Doppler radial velocities (Section 8.3). The four primary vortex identification criteria established by Donaldson (1970a) are:

1. There is significant tangential shear of radial velocity in a quasi-horizontal plane with the sum of the angular diameter and elevation angle of observation being less than 30° .
2. Tangential shear persists for at least half the period required for one vortex revolution.
3. Shear pattern vertical extent exceeds its horizontal diameter.
4. Qualitative shear pattern is invariant during a viewing angle change approaching or exceeding 45° .

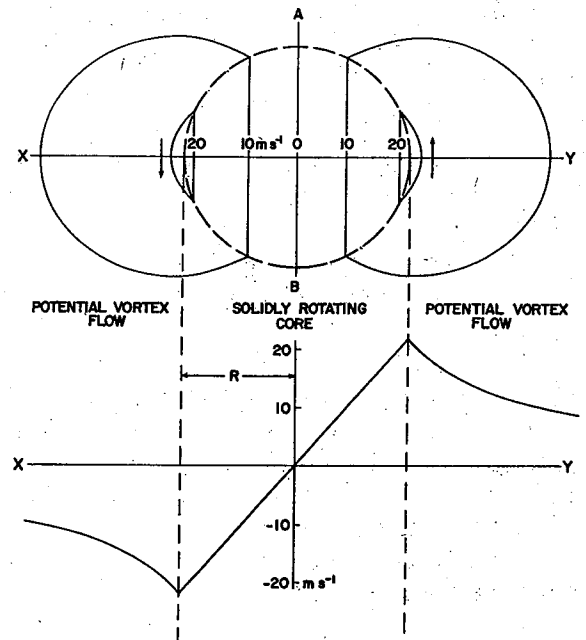


Fig. 8.1 Single Doppler horizontal signature of a stationary Rankine combined vortex (upper) and velocity profile along axis xy (lower).

A cyclonic shear signature in the 24 May data satisfies the first three criteria and identifies a solidly rotating vortex core. The flow pattern in the shear signature portion of the field is thus defined (providing the assumptions listed below also apply). The remainder of the streamline pattern is determined through the use of the following assumptions:

5. Precipitation particles, regardless of size, flow with the horizontal wind.
6. Vertical components contributing to the measured radial velocities are negligible.
7. The flow field is characterized by stationarity (i.e., all time derivatives are zero) during each radar tilt sequence.
8. Changes in radial velocity component indicate flow curvature rather than radial changes of wind speed (except in the upper level divergence region above the updraft).
9. Zero Doppler velocities represent winds normal to the beam.

8. *Tornadoic Storm Airflow and Morphology*

10. As a first approximation, regions of maximum radial velocities represent flow directly toward or away from the radar.
11. Free stream relative (to the moving storm) flow is modified within the storm by convective processes to obtain perturbed flow field, i.e., streamlines originate with incoming relative ambient wind.
12. Streamline solutions requiring minimum flow accelerations are used where possible.

Assumptions 5 through 7 have been commonly used in single Doppler radar storm investigations. Assumptions 8 and 11 were first used by Lhermitte (1969) and subsequently by Brown *et al.* (1971) who also used 9 and 10 with success. The circumstance that storm motion, relative environmental wind and storm inflow generally are parallel to radar radials aids considerably in use of this technique to analyze data for the Union City storm. However, it must be emphasized that the resulting storm-relative streamline fields presented here represent one nonunique solution to the true within storm flow.

8.3 SINGLE DOPPLER DERIVED THUNDERSTORM FLOW STRUCTURE

Digital Doppler velocity data were collected from 1515 through 1608 CST. Relative (to storm) velocity and streamline fields in horizontal cross-sections are analyzed at about 10 minute intervals for the surface (data collected 0.1-0.2 km above ground level (AGL) and extrapolated downward to 0 km), mid levels (5 km) and upper levels (highest data collection level).

To begin building the streamline pattern for a given level, an ambient relative wind was established using either surface mesonet or rawinsonde data. A mean environmental hodograph (Fig. 8.2) was obtained using two rawinsondes at the time of first storm echo (1405), one 90 km south and the other 9 km east of the storm. Streamline solutions were subjectively determined from the relative radial velocity fields. An example of streamline construction from the Doppler velocity fields using the earlier stated assumptions is shown in Fig. 8.3 at 5 km.

Perhaps the most significant aspects of the Doppler velocity (and therefore streamline) fields at low and mid levels (Figs. 8.3 through 8.8) is the stationarity or persistence of larger scale features (wavelengths generally \times 5 km). The flow field persistence is surprising in light of substantial reflectivity structure changes during the same period. The stationarity assumption was invoked only during each tilt sequence (3 to 4 minutes). Outside of those restricted periods, any large-scale velocity field changes would be apparent from the analyses.

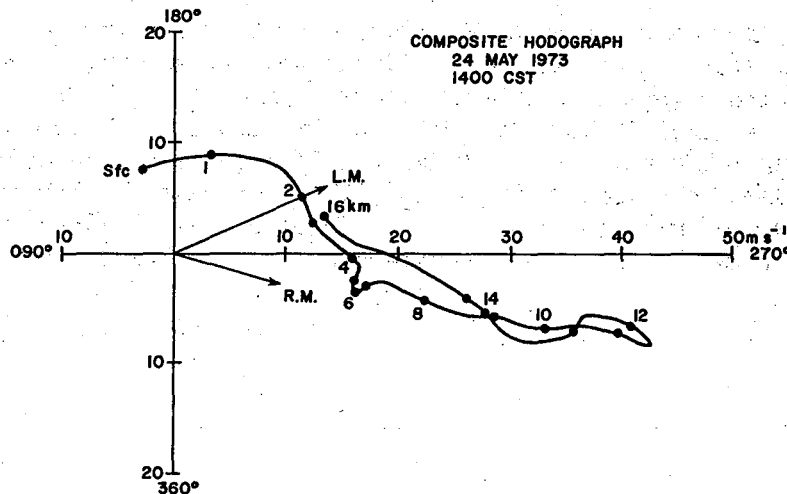


Fig. 8.2 Hodograph of winds at 1400 CST on 24 May 1973 composited from simultaneous rawinsonde releases 90 km south and 90 km east of the developing Union City storm. Speed and direction of right-moving (R.M.) and left-moving (L.M.) portions after split are indicated (see Burgess *et al.*, Chapter 6).

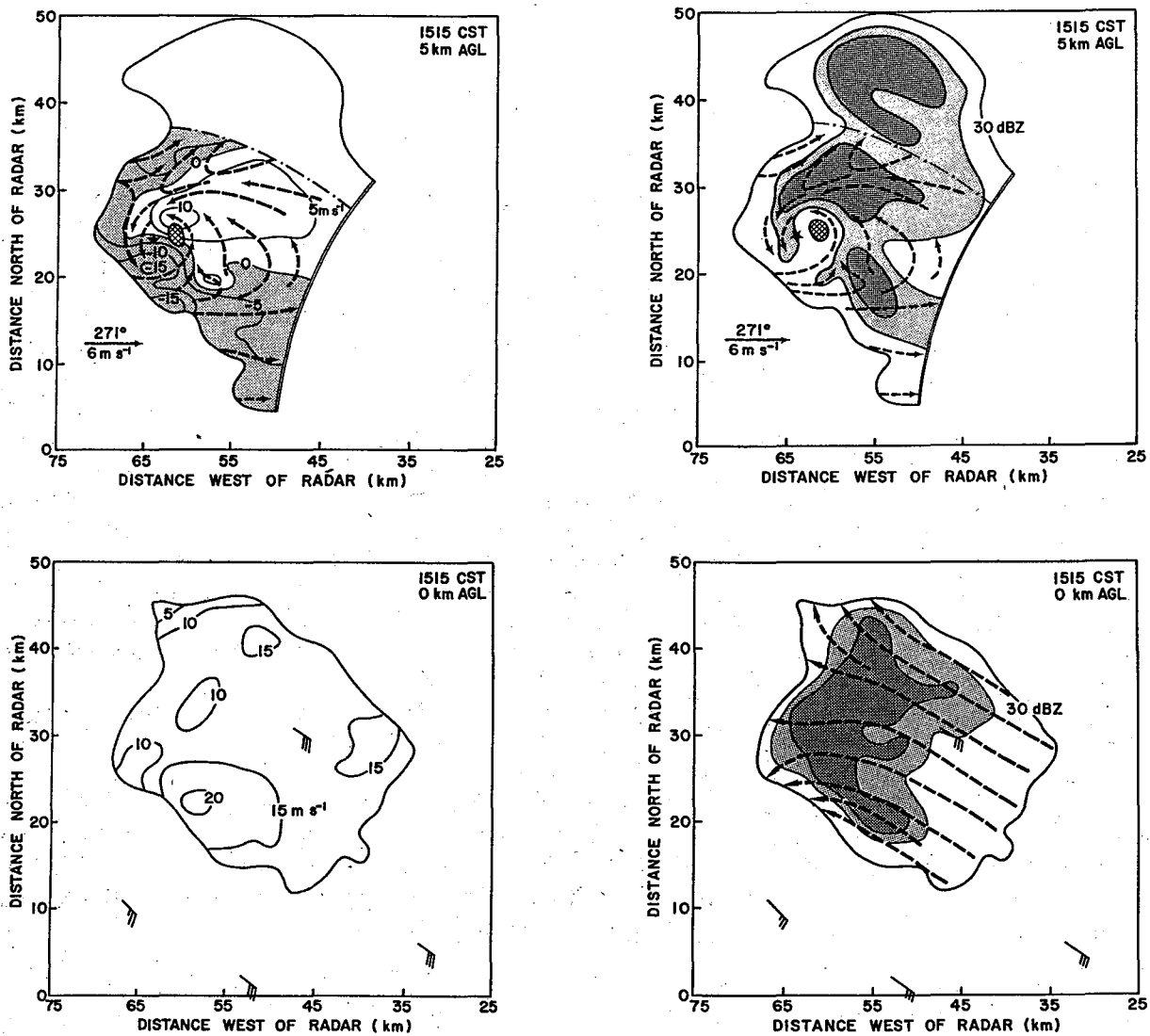
8.3.1 Surface Flow (0 km)

Streamline analysis in the lowest storm levels, typified by the 0 km display, indicates that storm-relative southeast flow ($110^\circ - 140^\circ$) apparently passed through the echo nearly unaffected, consistent with Brown *et al.* (1971) findings. Only small amounts of cyclonic curvature are apparent in the right rear echo quadrant (echo quadrant is defined relative to echo motion). Surface observations at 1515 indicated convergence and strong updraft without significant cloud base circulation in this region (Golden, Appendix A). The gradual core circulation emergence from 1515 to 1545 (Figs. 8.3 through 8.6) is due to descent and advection of precipitation into the feature with the collapse of the echo overhang (see Burgess and Lemon, Chapter 5) and the bounded weak echo region--BWER (Chisholm, 1970; Chisholm and Renick, 1972). At 1556 (Fig. 8.7), the circulation is located at the echo rear edge and by 1604 (Fig. 8.8) appears to be outside the low level echo. During this period (1545 to 1604) the eastward circulation movement was only half that of the storm (5.3 m s^{-1} versus 11.4 m s^{-1}), and caused the relative westward displacement. After 1545 the storm became front feeding (forward flank updraft). Thus, through propagation, the storm was able to persist beyond 1630--well after all radar indications of the supercell updraft along the rear flank had disappeared.

A second flow characteristic conserved during the analysis is a diffluence region in the central rear portion of the echo. The region is most noticeable at 1536 and 1545 located 7 to 9 km north of the core circulation. Diffluence location suggests its association with the thunderstorm downdraft, however, this cannot be verified due to inadequate surface data.

8. Tornadoic Storm Airflow and Morphology

Fig. 8.3 Objectively determined storm-relative radial Doppler velocity isotachs (left side), derived streamlines and reflectivity (right side) for surface, 5 km and highest complete data at 1515 CST. Reflectivity contour levels are 30, 40 and 45 dBZ; areas greater than 45 dBZ have dark stippling. Hatching is the BWER and star indicates TVS location. Relative environmental wind is in lower left except for 0 km AGL which shows relative winds at surface sites. Long wind barb equals 5 m s^{-1} . Double line indicates data edge and long dash dot line is arbitrary right-moving storm boundary.



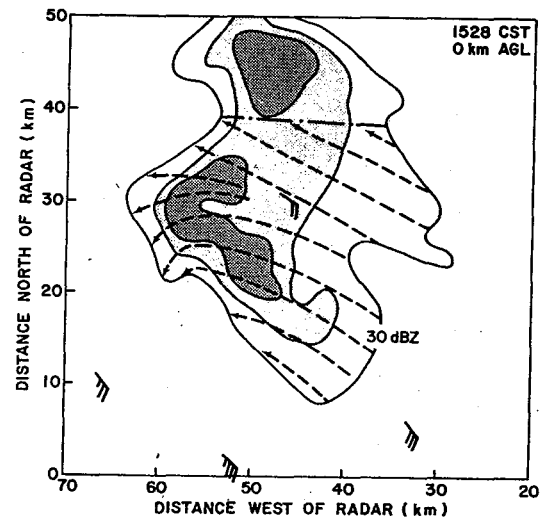
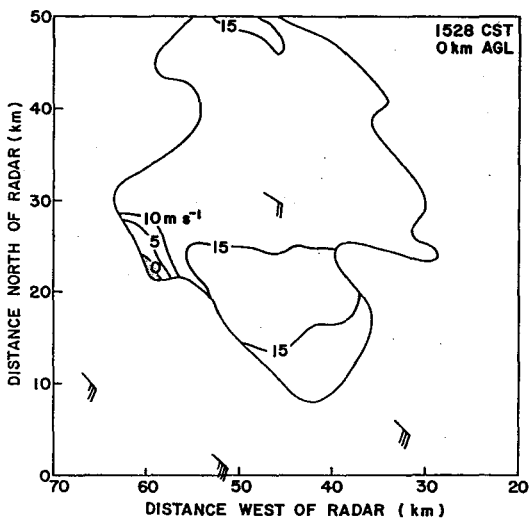
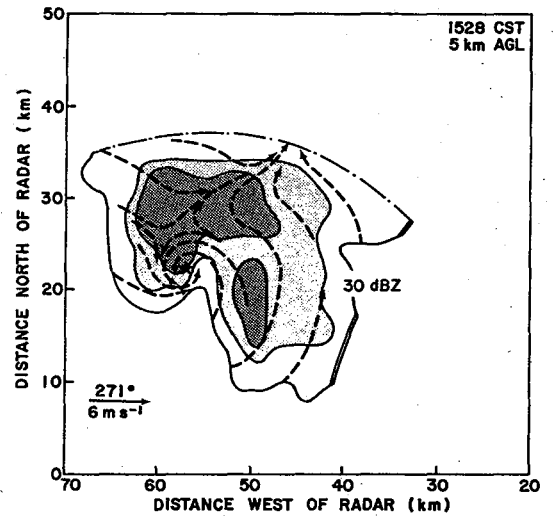
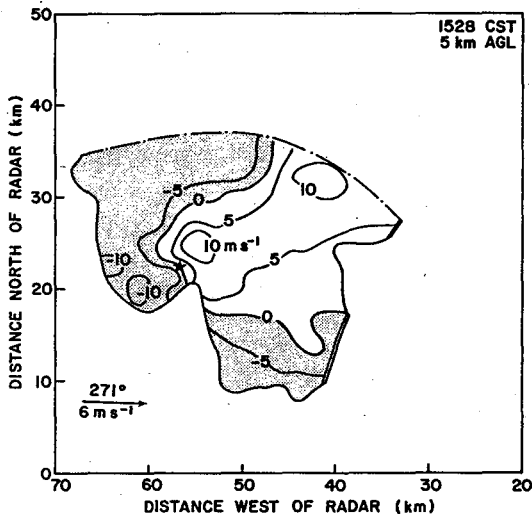
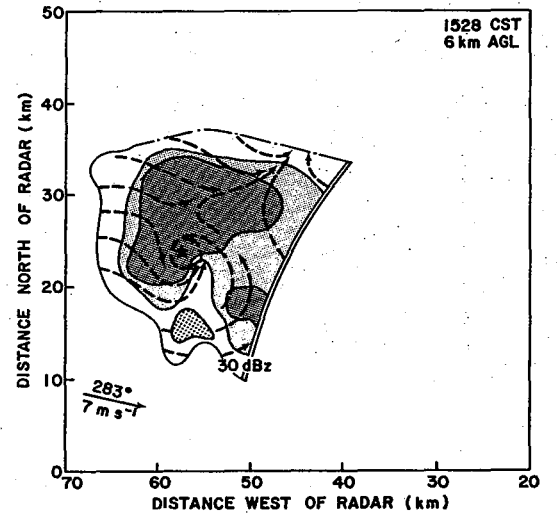
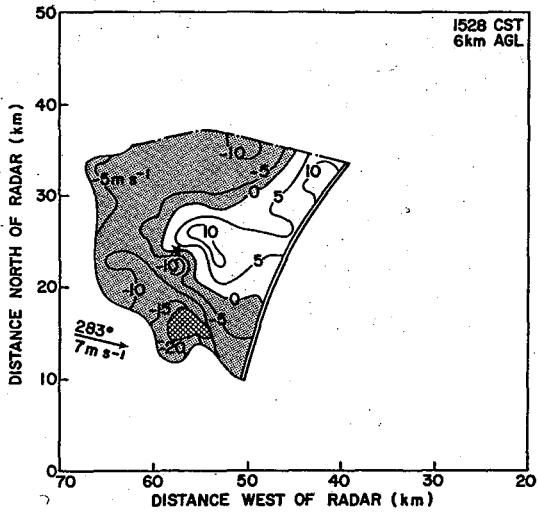


Fig. 8.4 Same as Fig. 8.3, except for 1528 CST.

8. Tornadoic Storm Airflow and Morphology

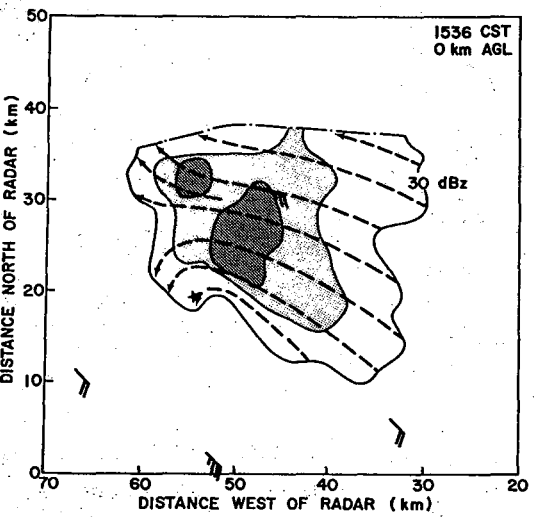
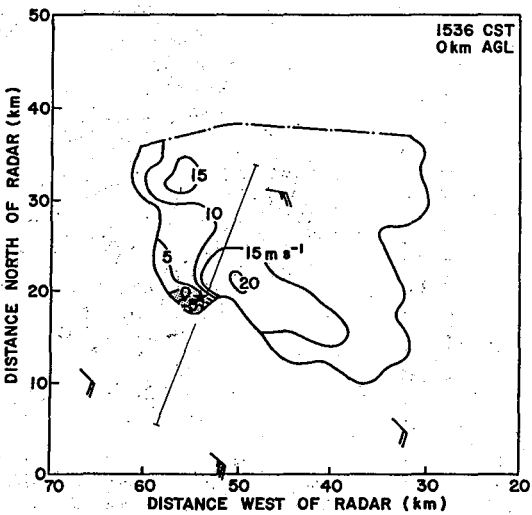
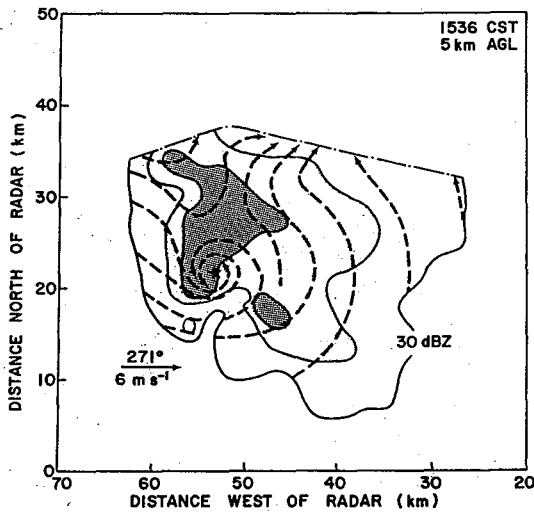
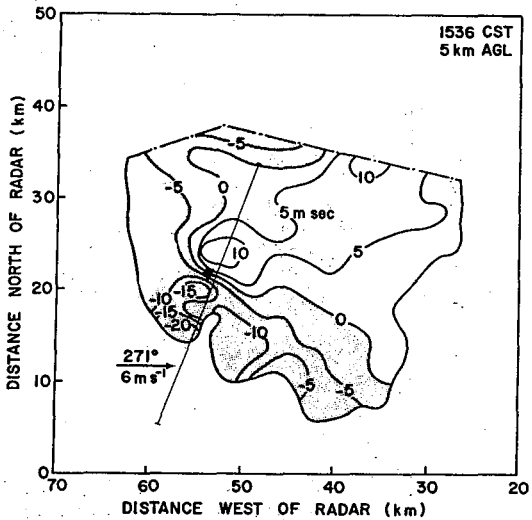
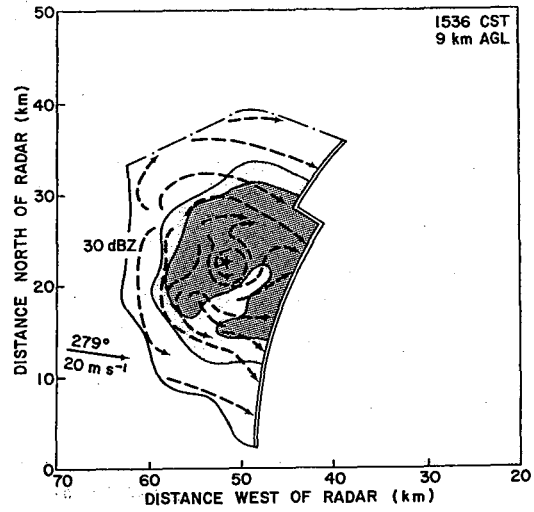
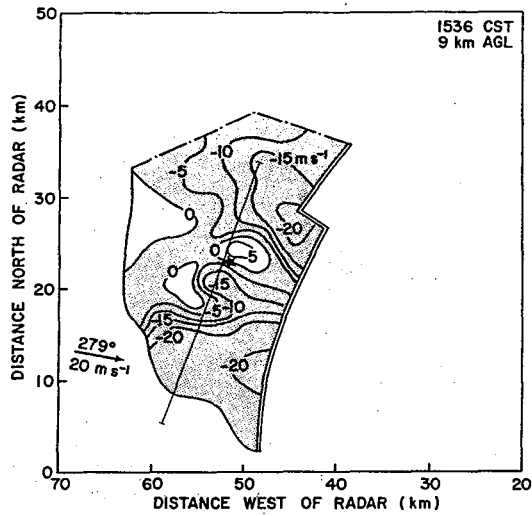


Fig. 8.5 Same as Fig. 8.3, except for 1536 CST.

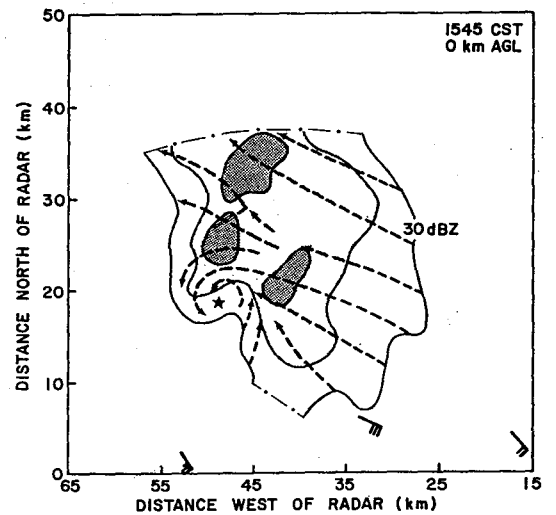
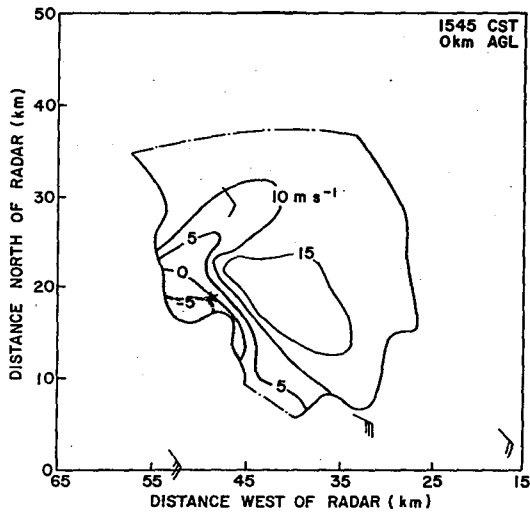
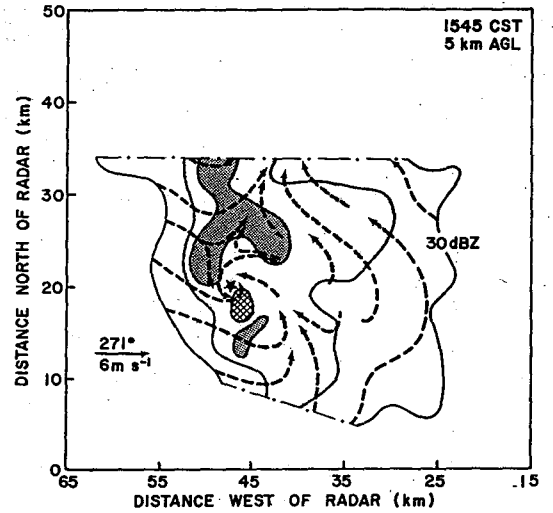
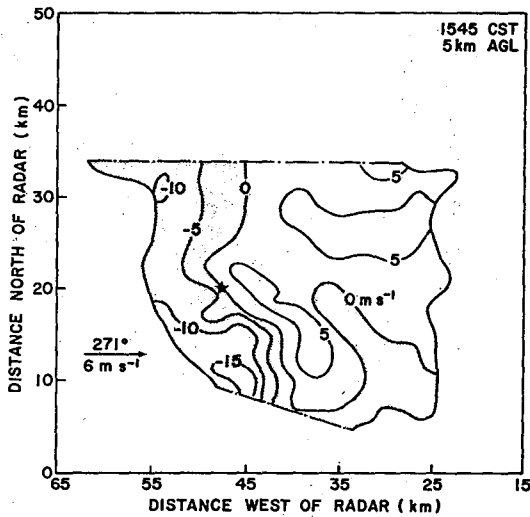
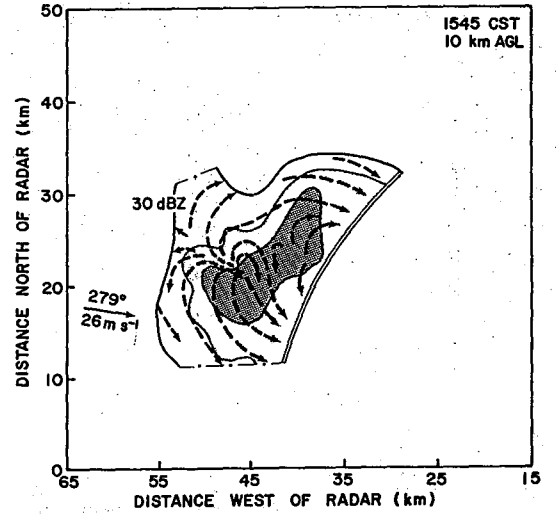
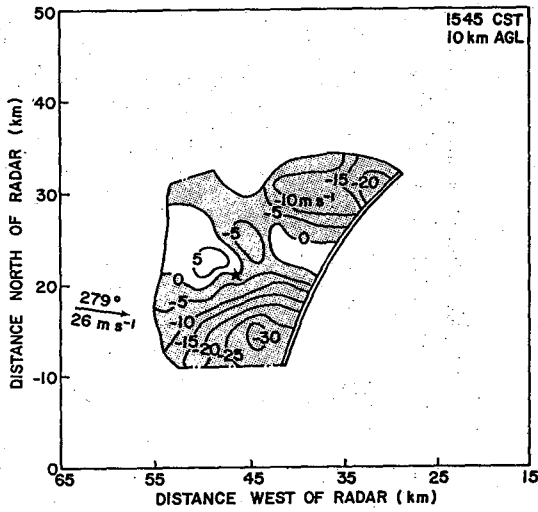


Fig. 8.6 Same as Fig. 8.3, except for 1545 CST.

8. Tornadoic Storm Airflow and Morphology

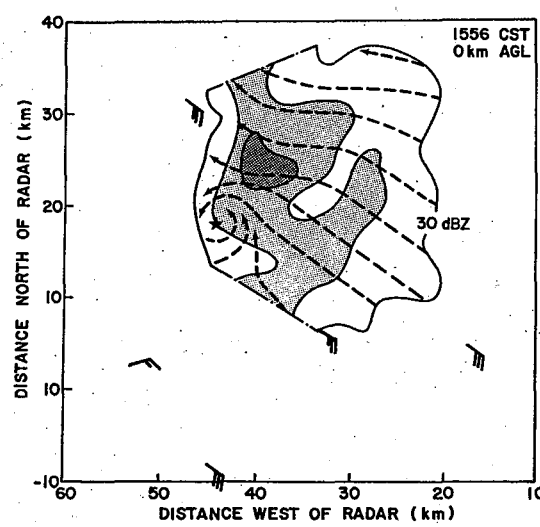
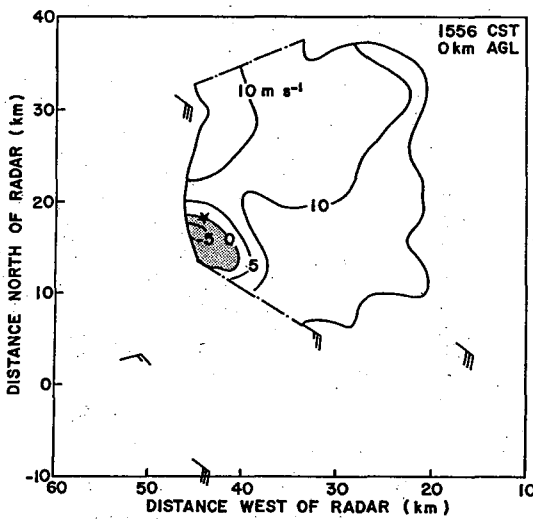
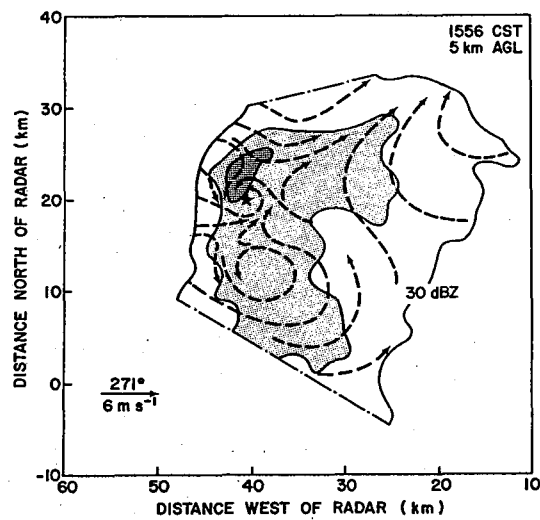
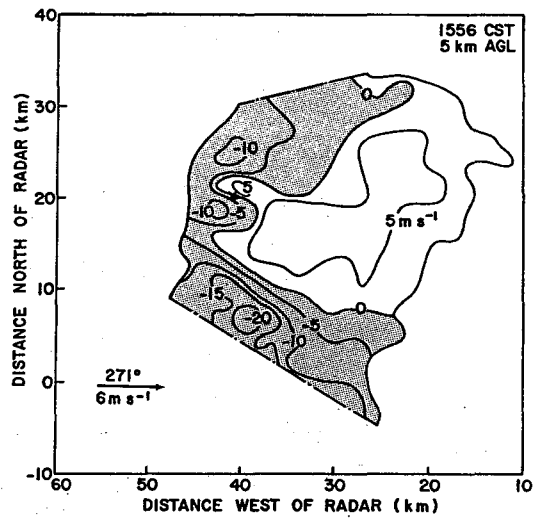
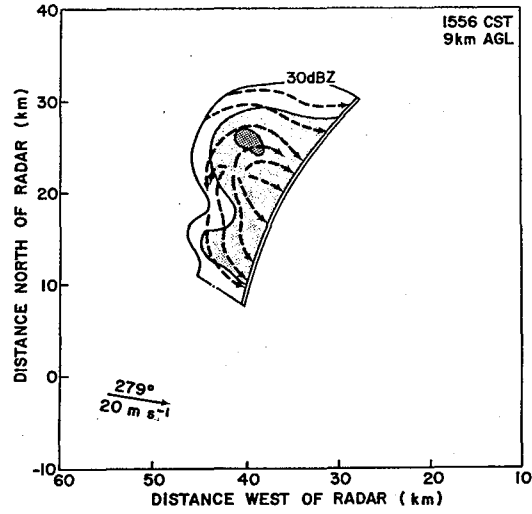
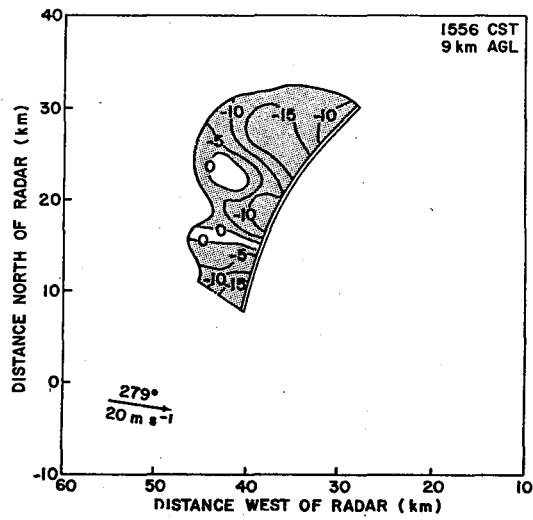


Fig. 8.7 Same as Fig. 8.3, except for 1556 CST.

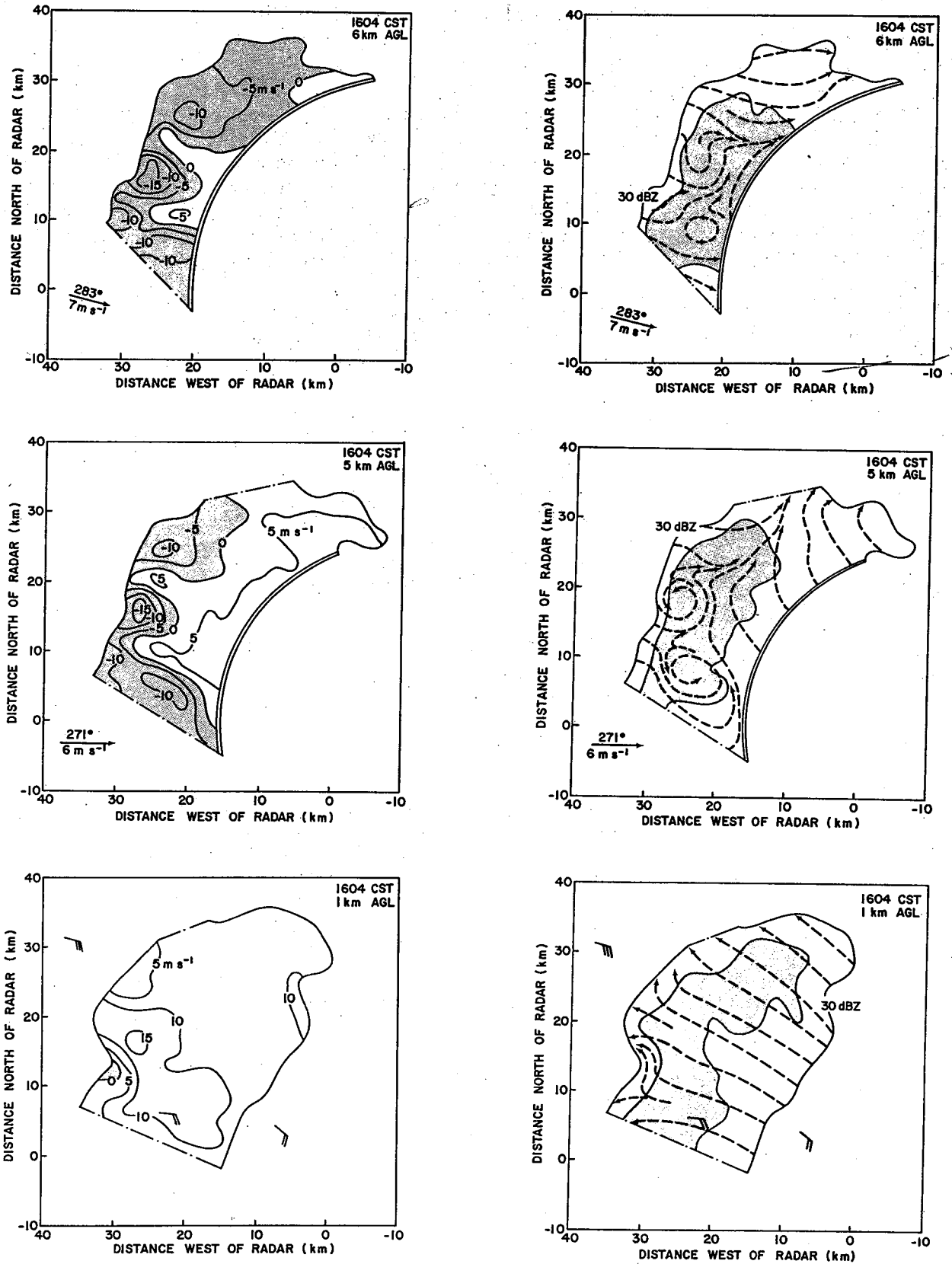


Fig. 8.8 Same as Fig. 8.3, except for 1604 CST.

8. Tornadoic Storm Airflow and Morphology

8.3.2 Mid-Level Flow (5 km Above Ground)

Major flow field characteristics in mid levels are also conserved. The feature which dominates the flow throughout the analysis is the core circulation centered on the BWER at 1515. Circulation diameter, considered in much greater detail in Section 8.4, decreases from 1515 to 1545 and increases thereafter. By 1528 the collapsing weak echo region (BWER A in Fig. 8.9 and detectable only as a weaker reflectivity channel east of the circulation) has become separated from the circulation. Throughout the rest of the analysis period, the circulation is embedded in high reflectivity. This type of separation has been documented in another tornadoic storm by Burgess and Brown (1973) and Burgess (1974). Between 1528 and 1545 the circulation is centered northwest of BWER B while both are moving on closing paths (Fig. 8.9). At 1545 BWER B is rapidly collapsing and has completely disappeared by 1556.

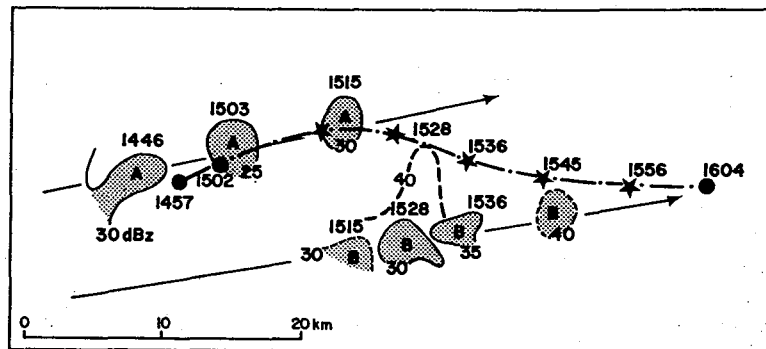


Fig. 8.9 Paths of bounded weak echo regions (arrows) as well as mesocyclone (dot) and tornadoic vortex signature (star). Solid contours are from 6 km height; dashed, 5 km.

Browning (1964), Chisholm (1970), Marwitz and Berry (1971) and others have presented theoretical as well as observational data supporting the contention that the BWER (also called echo weak or echo free vault) is created and sustained by organized intense updraft. Doppler velocity data in this case also lends supportive evidence. BWER A is coincident with the core circulation and probably coincident with the updraft (based on visual observations of lowered cloud base and rapidly ascending cloud fragments beneath the circulation). Strongest evidence for an updraft with BWER B occurs during the 1536 tilt sequence (corresponding to initial BWER collapse stages). At 6 km (not shown), the first height at which BWER B is bounded, weak divergence is centered on the BWER. At 9 km, in higher reflectivity above the BWER, a divergence signature exists (Fig. 8.5, Doppler velocity analysis, 55 km west, 18 km north); upwind flow (away) is nearly 5 m s^{-1} and downwind flow (toward the radar) exceeds 15 m s^{-1} .

Related to, but in the lee of, the circulation at mid levels is a large "back flow" region; winds with strong easterly components as opposed to ambient westerly winds. The back flow sustained throughout the analysis gives rise to a confluence line or dilatation axis that extends northeast from the circulation. The curved "back flow" resembles flow in a rotating cylinder wake. Similarly the confluence axis resembles flow merger occurring in the rotating cylinder wake in classical fluid mechanics (Schlichting, 1960).

Prandtl and Tietjens (1934) filmed experiments to investigate flow structure around solid rotating cylinders embedded in free stream flow. The ratio of the cylinder's peripheral (tangential) velocity V_t to the ambient free stream velocity v was varied as in Eq. (8.3).

$$V_t/v = C \quad \text{where } 0 < C < \infty \quad (8.3)$$

Figure 8.10 shows the streamline patterns around a rotating cylinder for $C = 3$ and $C = 4$. Ratio between core circulation tangential velocities (before objective analysis smoothing) and the relative ambient wind speed at 5 km from 1515 to 1535 varied between 3 and 4. The resemblance of the experimental patterns including back flow (especially when $C = 4$, Fig. 8.10) and the confluence axis orientation and structure are impressively similar to the actual data derived streamline patterns (see especially 1528, Fig. 8.4).

A shear region is centered on the zero Doppler velocity contour south-east of the core circulation. Following the analysis assumptions, this region is interpreted as curving flow. Beginning about 1528, the shear region strengthens and between 1545 and 1556 transforms into a second closed cyclonic circulation. Lee vortex formation in association with blocking, rotating thunderstorm updrafts has been found by Lemon (1976a). Those vortices, also occurring in severe or tornadic thunderstorms, were confined primarily to mid levels (4 to 8 km) as is the second cyclonic vortex in this case. Fluid theory predicts the development of a cyclonic vortex when the rotational speed of a blocking cyclonically rotating cylinder slows (Prandtl and Tietjens, 1934). This theory may account for the second cyclonic vortex because core circulation tangential velocities decreased about 10 m s^{-1} or 40% just before it developed. By 1604 the elongated second vortex (6 km diameter) no longer is in the parent circulation lee. This vortex, like those studied by Lemon (1976a), is believed to be passive and no severe weather was associated with the circulation.

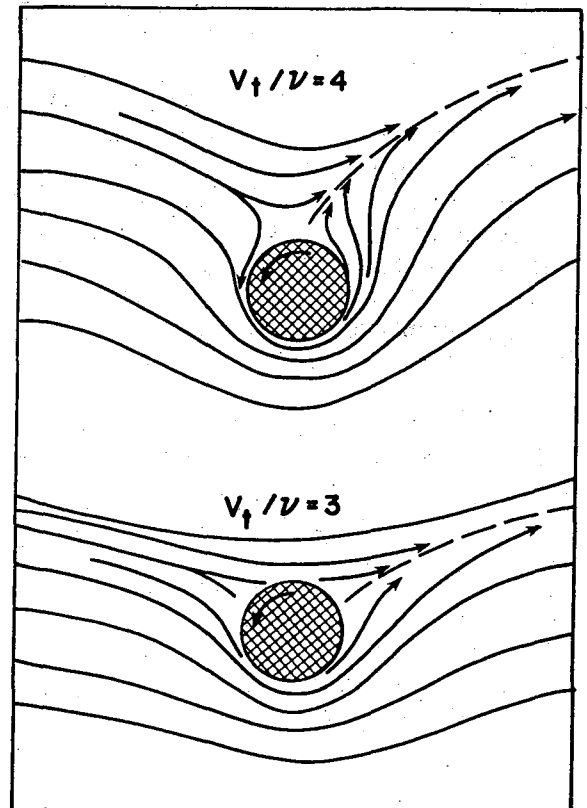


Fig. 8.10 Schematic of streamlines produced in laboratory experiment involving a solid rotating cylinder (peripheral velocity V_t) embedded in free stream flow (with velocity v). Resulting confluence axis in the cylinder wake is indicated by a dashed line. After Prandtl and Tietjens (1934).

8. *Tornadic Storm Airflow and Morphology*

As occurred at the surface, the core circulation after 1545 slowly propagates toward the echo back edge. Unlike lower levels, the circulation in mid levels stays within the echo through 1604. However, examination of 1614 data indicates the parent circulation is no longer detectable--having either dissipated or emerged from the echo rear flank.

8.3.3 Upper-Level Flow (9 to 10 km Above Ground)

Adequate Doppler radar data were obtained at 9 to 10 km levels only during three tilt sequences--1536, 1545, and 1556. The 9 km level at 1536 (storm top approximately 16 km) is influenced as at lower levels, by the core circulation (Fig. 8.5). The large "back flow" region evident at 5 km has been replaced at 9 km with flow essentially parallel to relative ambient winds. Back flow absence may be explained by the lee side wake being occupied by air diverging from within the core circulation updraft. Ambient flow blocking is still occurring, however, and is identified by two velocity maxima either side of the circulation. This type flow-around-an-obstacle signature in single Doppler data has been discussed by Brown and Crawford (1972).

Two diffluent or divergent zones can be deduced from the velocity and streamline pattern at 1536 and 9 km. The first (as described in Section 8.3.2) in association with BWER B lies just southwest of the circulation and is most easily identified by a velocity region slightly greater than zero. The second divergent region lies to the circulation northwest and is again characterized by small positive upwind velocities. Most impressive however, is that the weak upstream flow exists in the face of ambient 20 m s^{-1} relative winds. Nonhydrostatic pressure excess forces are obviously active here at a height of over half the storm depth.

One kilometer higher and only 10 minutes later at 1545 (Fig. 8.6) no core circulation is present (nor was present at any level at 1545); storm top at this time was approximately 15 km. Only the small intense cyclonic shear--the tornadic vortex signature (TVS)--is present, embedded at the divergence center. The vortex and divergence coincidence suggests that, despite BWER collapse, the major supercell updraft (although weakening) is still associated with the core circulation and tornadic vortex. Divergence is the dominate feature at this level and includes flow upwind in excess of 5 m s^{-1} into ambient 26 m s^{-1} flow. The divergence acts as a block to the ambient winds and produces the flow-around-an-obstacle signature referred to previously. Storm-relative velocities of 20 to 30 m s^{-1} are present in the blocking signature maxima.

While the core circulation does exist at lower heights, neither it, nor the TVS, is present in the 9 km data by 1556 (Fig. 8.7); storm top is approximately 12 km. Instead, divergence dominates the field. The core circulation upper detectable limit has decreased considerably. Areal echo coverage also has decreased considerably since the 9 km scan at 1536, consistent with lowering divergence level and storm top. During this collapse the intense tornado is still on the ground, remaining there until 1604 and inflicting considerable damage.

At 1604 no high-level data were acquired; the highest complete data were obtained at 6 km. There the circulation breaks down into an open wave or trough-like flow.

8.3.4 Flow Structure Summary

Low-level relative winds apparently flowed through the precipitation echo with limited disruptions of a core circulation and diffluence (possible down-draft) region. The core circulation, weakening and expanding, exited the rear echo flank during later analysis stages (moving more slowly than the precipitation area).

Mid-level flow exhibited features similar to laboratory experiments with solid rotating cylinders embedded in free stream flow. These features include a wake region in the core circulation lee, "boundary layer" separation and eventual formation of a wake cyclonic vortex. Core circulation and BWER A were found to be coincident as consistent with theory; however, BWER A subsequently collapsed and separated from the circulation, leaving the circulation and associated updraft wholly contained within high reflectivity echo. Evidence indicates that BWER A and B were associated with updrafts for at least a portion of their existence.

High-level flow (9-10 km) was dominated by divergence that blocked ambient flow. The core circulation initially extended to high levels but dissipated from the top downward.

8.4 CORE CIRCULATION RELATIONSHIP TO TVS AND STORM EVOLUTION

Core circulation relationship to overall storm flow structure has been included in some detail in previous sections. The present section treats the core circulation's relationship to a small high shear region--the TVS--and the relationship of both to storm metamorphosis.

A closed cyclonic circulation of thunderstorm updraft size has been labeled "mesocyclone". Fujita (1965) in his study of the Fargo, North Dakota storm and other tornadic storms labels a large rotating thunderstorm cloud mass a "tornado cyclone" when a tornado is associated with the mesocyclone. Here "core circulation" describes the mesocyclone (or tornado cyclone) core as detected in single Doppler radar data; in this case, the core diameter varied from 2 to 6 km. Core diameter--having a unique single Doppler velocity signature--is specified by the distance (along xy in Fig. 8.1) between the two opposing velocity peaks at the edge of the vortex's solid rotation core.

Temporal changes of core circulation diameter have been mentioned previously and are illustrated in Fig. 8.11 along with diameter changes in the vertical. The internal TVS location is also shown. This is the first time that such detailed data concerning the core circulation has been obtained and affords the opportunity to examine how core circulation changes relate to tornado production and storm morphology.

Diameter determined for the core circulation in Fig. 8.11 can be measured with confidence only in the direction normal to the radar beam. Axial symmetry is assumed. Diameter in general decreased from 1515 until 1545 when the larger vortex core signature was no longer discernible, leaving only the tornado vortex signature. The larger potential vortex region outside the TVS

8. Tornadoic Storm Airflow and Morphology

was evident, however. After 1545, a larger core circulation was once again detectable and continued to increase in size.

Peak core circulation tangential velocities were examined at 3 and 6 km and are presented as a function of time in Fig. 8.12. Diameter change as a function of time is also presented. Velocity trend is generally inversely proportional to the circulation radius. During the 1545 data collection, maximum tangential velocities and minimum circulation diameter were recorded; these extreme tangential velocity and diameter values represent the TVS and therefore are under and over estimates, respectively, for the tornado (see Brown and Lemon, Chapter 15). The 1545 collection period was also near the time of the largest visible tornado size.

Circulation, Γ , can be expressed by Eq. (8.4)

$$\Gamma = 2\pi r \bar{V}_t, \quad (8.4)$$

where r and \bar{V}_t are radius and mean peak tangential velocity, respectively. Using this expression, circulation values for the core vortex range from 0.7 to $3.7 \times 10^5 \text{ m}^2 \text{ s}^{-1}$, consistent with Fujita's (1965) findings for the tornado cyclone.

Internal relationships between the core circulation flow structure and the TVS early in the observation period (see Fig. 8.11) could not be conclusively identified from the data. Two possibilities exist and are shown in Fig. 8.13. The tornado could act as the displaced (relative to velocity maxima) circulation center. The second possibility is that the closed tornadoic circulation is embedded within the closed parent circulation. Available data tend to support the former possibility.

Throughout its observed vertical depth the TVS was displaced west (to the rear flank) of the core circulation center at 1515. The TVS migrated to the circulation center with time, first at low levels, then at progressively higher levels. During the migration process, TVS intensity and core circulation tangential velocities increased (Fig. 8.12). Contemporaneously the TVS (and tornado) lowered to the surface while the core circulation decreased in size. This progression of events suggests concentration (and conservation) of angular momentum on a small scale, perhaps that of the tornado.

During the TVS arrival at the surface and rapid decrease in core circulation size, the storm BWER and rear flank storm top also collapsed (Fig. 8.14). After 1545, the level at which the core circulation (and TVS) broke down and was replaced by divergence lowered considerably. Tornado occurrence at the time of storm top and WER collapse has been documented elsewhere by Burgess (1974). Fujita (1973) proposed an updraft water loading and twisting downdraft hypothesis to explain storm top collapse and tornado production. A "vortex valve" hypothesis has been proposed by Lemon (Appendix G) as a possible explanation for storm top collapse.

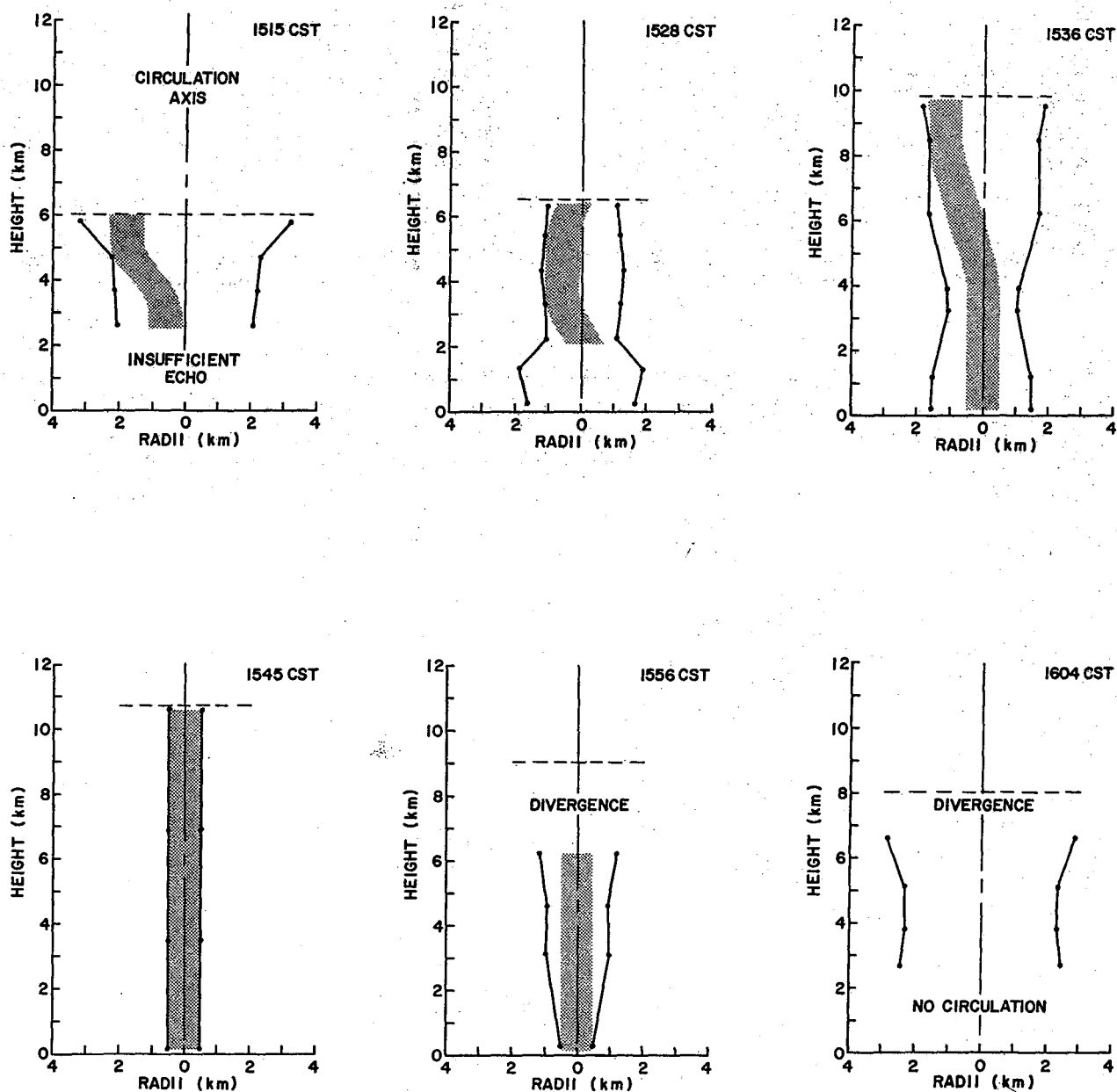


Fig. 8.11 Position of TVS (stippled) relative to center of tilted core circulation. Dark dots indicate measured circulation radii. Dashed line identifies Doppler data collection upper limit in the circulation region. Tornado was on the ground from 1538 to 1604.

8. Tornadoic Storm Airflow and Morphology

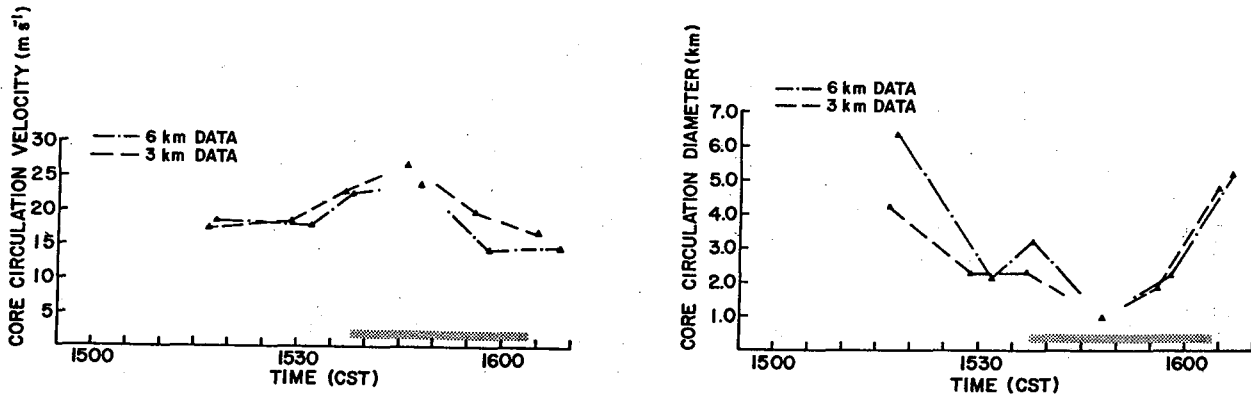


Fig. 8.12 Core circulation tangential velocity and diameter at two heights above ground as a function of time. Velocity and diameter values obtained at about 1547 are from the TVS gates and are therefore considerable under and over estimates, respectively. Tornado duration on the ground indicated by stippled bar.

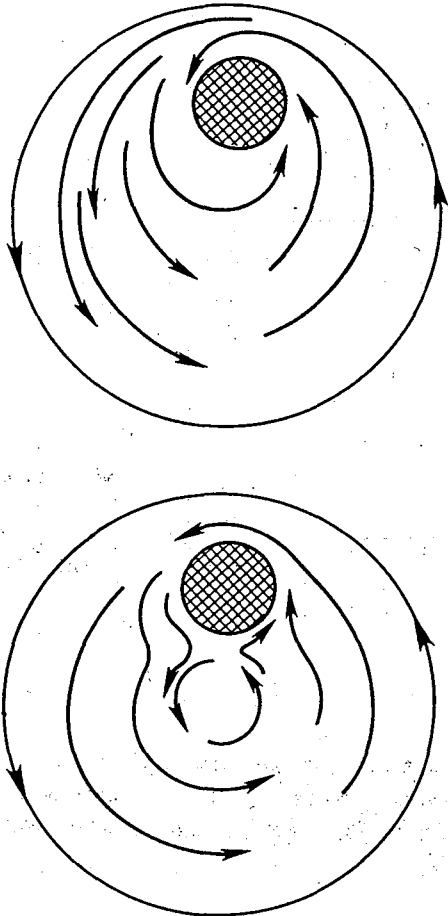


Fig. 8.13 Possible relationship of the TVS (stippled) to the internal core circulation flow structure at 1515 CST.

8.5 SUMMARY

Objectively analyzed single Doppler velocity data reveal a severe thunderstorm dominated by a Rankine combined cyclonic vortex with a 2 to 6 km core diameter. At low levels outside the vortex circulation, relative flow is mostly southeast through the storm with some diffluence in the central rear flank. Considerable similarity is noted between the derived mid-level flow structure around the core circulation and that around a solid rotating cylinder embedded in potential flow. Dominant flow at high levels underwent a transition from circulation to divergence as the storm top descended.

Core circulation diameter decreased as tangential velocities increased. Minimum diameter and maximum velocities were reached at the time of largest visible tornado size. The tornadic vortex signature (related directly to the tornado vortex) descended with time as its relative position migrated to the circulation center. Tangential velocities lessened as the visible tornado decreased in size. Core circulation increased in diameter and the discernable circulation's upper limit lowered markedly as the tornado dissipated.

In summary, the following steps were observed in the Union City storm evolution:

1. The storm updraft increases rapidly and develops an overhang and bounded weak echo region (BWER).
2. BWER and core circulation coincide at mid levels where both are detectable. Separation of radar detected echo mass into left and right moving thunderstorms begins.
3. The tornadic vortex signature (TVS) is first detected in mid levels.
4. Swirl in the core circulation increases as circulation diameter decreases. BWER and circulation separate as BWER begins collapse.
5. Echo overhang and storm top begin collapse.
6. Tornado and TVS reach the surface.
7. Upper limit of circulation lowers and is replaced by divergence.

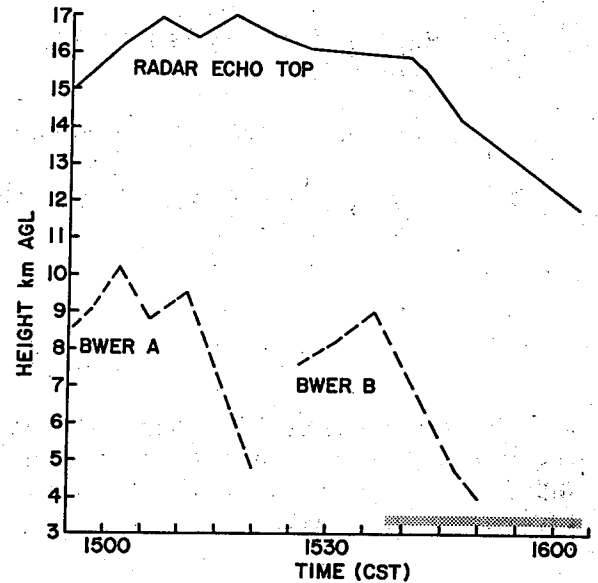


Fig. 8.14 Graph of Union City storm top and maximum height of bounded weak echo regions A and B as a function of time. Tornado duration on the ground indicated by stippled bar.

8. *Tornadoic Storm Airflow and Morphology*

8. Reorganization begins with new updraft development on the forward storm flank.
9. Supercell updraft, tornado and TVS dissipate.
10. Newly organized moderate thunderstorm persists without supercell characteristics.

8.6 ACKNOWLEDGMENTS

We appreciate the fine work of Dale Sirmans and Glen Anderson in making the Doppler radar an effective and flexible research tool. This work was supported partially by the Federal Aviation Administration under Interagency Agreement FA72 WAI-265.

8.7 REFERENCES

- Battan, L. J., 1964: Some observations of vertical velocities and precipitation sizes in a thunderstorm. J. Appl. Meteor., 3, 415-420.
- _____ and J. B. Theiss, 1966: Observations of vertical motions and particle sizes in a thunderstorm. J. Atmos. Sci., 27, 293-298.
- Brown, R. A., 1976: Single Doppler radar data acquisition and analysis. Appendix E, The Union City, Oklahoma Tornado of 24 May 1973, R. A. Brown, Editor. NOAA Tech. Memo. ERL NSSL-80, Norman, Nat. Severe Storms Lab., 215-228.
- _____ and K. C. Crawford, 1972: Doppler radar evidence of severe storm high-reflectivity cores acting as obstacles to airflow. Preprints Fifteenth Radar Meteor. Conf., Boston, Amer. Meteor. Soc., 16-21.
- _____ and L. R. Lemon, 1976: Evolution of the Doppler radar tornadic vortex signature in the Union City storm. Chapter 15, The Union City, Oklahoma Tornado of 24 May 1973, R. A. Brown, Editor. NOAA Tech. Memo. ERL NSSL-80, Norman, Nat. Severe Storms Lab., 167-175.
- _____, W. C. Bumgarner, K. C. Crawford, and D. Sirmans, 1971: Preliminary Doppler velocity measurements in a developing radar hook echo. Bull. Amer. Meteor. Soc., 52, 1186-1188.
- Browning, K. A., 1964: Airflow and precipitation trajectories within severe local storms which travel to the right of the winds. J. Atmos. Sci., 4, 634-639.
- Burgess, D. W., 1974: Study of a right-moving thunderstorm utilizing new single Doppler radar evidence. Masters Thesis, Dept. of Meteorology Univ. of Okla., 77 pp.

8. *Tornadoic Storm Airflow and Morphology*

- Golden, J. H., 1976: Tornado intercept strategy and morphological observations. Appendix A, The Union City, Oklahoma Tornado of 24 May 1973, R. A. Brown, Editor. NOAA Tech. Memo. ERL NSSL-80, Norman, Nat. Severe Storms Lab., 185-189.
- Lemon, L. R., 1976a: Wake vortex structure and aerodynamic origin in severe thunderstorms. J. Atmos. Sci., 33, 678-685.
- _____, 1976b: Tornadoic storm evolution: Vortex valve hypothesis. Appendix F, The Union City, Oklahoma Tornado of 24 May 1973, R. A. Brown, Editor. NOAA Tech. Memo. ERL NSSL-80, Norman, Nat. Severe Storms Lab., 229-234.
- Lhermitte, R. M., 1969: Doppler radar observation of a convective storm. Preprints, Sixth Conf. on Severe Local Storms, Boston, Amer. Meteor. Soc., 139-145.
- Marwitz, J. D., and E. X Berry, 1971: The airflow within the weak echo region of an Alberta hailstorm. J. Appl. Meteor., 10, 487-492.
- Prandtl, L., and O. G. Tietjens, 1934: Applied Hydro- and Aeromechanics. New York, Dover Publications, Inc., 306 pp.
- Probert-Jones, J. R., and Harper, W. G., 1961: Vertical air motion in showers as revealed by Doppler radar. Proc. Ninth Wea. Radar Conference, Boston, Amer. Meteor. Soc., 225-232.
- Schlichting, H., 1960: Boundary Layer Theory. New York, McGraw-Hill Book Company, Inc., 647 pp.
- Sirmans, D., 1976: NSSL Doppler and WSR-57 radar characteristics. Appendix D, The Union City, Oklahoma Tornado of 24 May 1973, R. A. Brown, Editor. NOAA Tech. Memo. ERL NSSL-80, Norman, Nat. Severe Storms Lab., 209-213.
- _____, R. J. Doviak, D. Burgess and L. Lemon, 1974: Real time Doppler isotach and reflectivity signature of a tornado cyclone. Bull. Amer. Meteor. Soc., 55, 1126-1127.

Chapter 9

ELECTROMAGNETIC SIGNATURE OF THE UNION CITY TORNADIC STORM AT THREE MEGAHERTZ

William L. Taylor

*Wave Propagation Laboratory
Boulder, Colorado 80302*

The Union City tornadic storm produced a 3 MHz electromagnetic signature. The burst rate observed on a detector located at Will Rogers World Airport exceeded 20 bursts per minute almost 10 minutes before tornado touchdown and continued for 20 minutes after tornado decay.

9.1 Introduction

The development of an electromagnetic technique possibly suitable for tornadic storm detection was undertaken several years ago in the Wave Propagation Laboratory. Initial observations were made by Taylor (1971, 1972) during the 1969-1971 tornado seasons in cooperation with the National Severe Storms Laboratory. This earlier work consisted of searching for an electromagnetic signature associated with tornadic conditions by observing the radiation from lightning discharge processes in the frequency band from 10 kHz to 137 MHz.

Taylor (1973a, 1973b, 1974) concluded from the previous work that:

- (1) The observed level of sferic activity, i.e., emissions from lightning discharges, corresponded closely with thunderstorm severity as indicated by reported tornadoes, funnel clouds, damaging winds or hail.
- (2) Severe storms that produced tornadoes were generally associated with greatly enhanced sferic activity, with many bursts of high sferic rates. Nevertheless, relatively few storms with high burst rates produce tornadoes.
- (3) The enhancement in burst rates was easily recognized only at frequencies above about 1 MHz.
- (4) Sferic bursts originated in the parent storm rather than in the tornado vortex.

Some of these conclusions agree with the work of Jones (1965), Lind et al. (1972), Scouten et al. (1972), Silberg (1965) and Stanford et al. (1971).

9. 3 MHz Sferics Measurements

9.2 INSTRUMENTATION

For the 1972 tornado season, an instrument was developed to measure the sferic activity of thunderstorms as indicated by the sferics "burst rate" which is simply the number of clusters or groups of large-amplitude sferics occurring in a one-minute period. The signals applied to a single-stage tuned-radio-frequency circuit with a center frequency near 3 MHz and a bandwidth of 10 percent were supplied by a one-meter-long vertical monopole antenna. Amplitude threshold levels of the detector were adjusted to 5 V/m and 2 V/m, and correspond to nominal sferic amplitudes expected at ranges of 30 and 70 km, respectively. A burst was counted in each threshold circuit when the amplitude of a received signal was greater than the threshold level and the sferic rate exceeded 500 per sec for a period longer than 0.1 sec. Burst rates were obtained from integrator circuits and presented to a multichannel event recorder to show when the burst rate exceeded 3, 10, 20 and 30 per min. The data available consisted of 8 channels of burst rate information and one channel of time marks from a local clock.

9.3 OBSERVATIONS AND RESULTS

A total of 15 tornadic storm detectors were installed within or near "tornado alley" during the 1972 and 1973 tornado seasons. The results of evaluating this tornado-detection technique have been presented previously by Taylor (1973a). One detector in the network was located at the Oklahoma City National Weather Service Office at Will Rogers World Airport. The response of this detector during the time of the Union City tornado on 24 May 1973 is presented in Fig. 9.1. The tornado was on the ground from 1538 to 1604 CST.

Figure 9.1 shows that sferics exceeding an amplitude threshold of 2 V/m produced burst rates faster than 3 per min between 1510 and 1652. (At no time during the 24 hr either preceding or following this period was the minimum detector response burst rate of 3 per min exceeded.) Beginning about 1520 the burst rate increased rather rapidly and exceeded 30 bursts per min at 1533. A burst rate greater than 20 per min--frequently measured in tornadic storms (Taylor, 1973a)--was attained about 9 min before the tornado touched down. The burst rate remained above this 20 per min "warning level" until 1625, more than 20 min after the tornado dissipated.

The increase in burst rates prior to the tornado was approximately that of an exponential rise. Differences between the observed and the actual burst rate produced during the increasing phase of this tornado activity should be very small, in the time domain of interest here, since the charging time constant of the burst rate integrators was of the order of 10 sec. But this was not the situation for the decay period because the discharge time constant of the burst rate integrators was about three minutes and in addition there was a relay hysteresis of about 20 percent of the burst rate. Consequently, the actual burst rate undoubtedly decreased somewhat more rapidly than is shown in Fig. 9.1.

9. 3 MHz Sferics Measurements

Very little activity was observed on the 5 V/m threshold level as shown in Fig. 9.1. The burst rate exceeded 3 per min between about 1537 and 1622. Only for a brief 2 min period around 1606 was the burst rate faster than 10 per min.

9.4 DISCUSSION

Typically, a rapid rise in burst rate is observed prior to tornadic conditions and a burst rate exceeding 20 per min generally is observed about 15 min before tornado touchdown. Usually the burst rate decays much slower than it rises. Often other severe storm activity in an area tends to mask burst rate enhancement accompanying a tornadic storm by increasing the background burst rate level. In these respects, the Union City tornadic storm was typical. Although, during the Union City storm period, numerous funnel clouds were reported in the Oklahoma City area, there is no evidence they were associated with any enhanced electrical activity.

Initial touchdown point of this tornado was about 40 km due west of our detector. The storm moved toward the east-southeast through Union City and dissipated at a range of about 28 km. Figure 9.2 indicates the distance to low-level radar reflectivity cores (≥ 45 dBZ) of the closest echoes. The ranges of the Doppler radar tornadic vortex signature aloft and the tornado damage track also are shown. After the tornado dissipated at 1604, there was no longer a Doppler tornadic vortex signature in the storm (Brown and Lemon, Chapter 15.)

Figure 9.1 shows clearly that the sources of the bursts were within 70 km range but farther than 30 km since (1) the burst rate for the 0 to 30 km threshold level was less than 3 per min until after the tornado had formed and (2) the 0 to 70 km threshold level indicated a burst rate exceeding 30 per min. As the storm moved closer to the detector, the burst rate of the 0 to 30 km channel tended to increase until, just after 1600, a burst rate between 10 and 20 per min was attained. However, from this storm, burst rate activity probably began to decrease around 1600; there were insufficient sources of electrical activity within the 30 km range to produce a burst rate more frequent than 20 per min. As new storms--developing south of the decaying Union City storm--moved close to the detector, the burst rate continued to decrease, indicating that the enhanced electrical activity diminished rather rapidly after the tornado and its parent storm had dissipated.

9.5 ACKNOWLEDGMENTS

I thank Harold Burdick and Joe Howard for much of the construction, installation and maintenance of the tornadic storm detectors. I especially thank Mr. Raymond C. Crooks, MIC, and the staff of the Oklahoma City National Weather Service Forecast Office for their cooperation and assistance in this experimental effort to develop tornado detection techniques.

9.6 REFERENCES

- Brown, R. A., and L. R. Lemon, 1976: Evolution of the Doppler radar tornadic vortex signature in the Union City storm. Chapter 15, The Union City, Oklahoma Tornado of 24 May 1973, R. A. Brown, Editor. NOAA Tech. Memo. ERL NSSL-80, Norman, Nat. Severe Storms Lab., 167-175.
- Jones, H. L., 1965: The tornadic pulse generator. Weatherwise, 18, 78-80.
- Lind, M.A., J. S. Hartman, G. S. Takle and J. L. Stanford, 1972: Radio noise studies of several severe weather events in Iowa in 1971. J. Atmos. Sci., 29, 1220-1223.
- Scouten, D. C., D. T. Stephenson and W. G. Biggs, 1972: A spheric rate azimuth-profile of the 1955 Blackwell, Oklahoma tornado. J. Atmos. Sci., 29, 929-936.
- Silberg, P. A., 1965: Passive electrical measurements from three Oklahoma tornadoes. Proc. IEEE, 56, 1197-1204.
- Stanford, J. L., M. A. Lind and G. S. Takle, 1971: Electromagnetic noise studies of severe convective storms in Iowa: The 1970 storm season. J. Atmos. Sci., 28, 436-448.
- Taylor, W. L., 1971: Review of electromagnetic radiation data from severe storms in Oklahoma during April 1970. NOAA Tech. Memo. ERL WPL-6, Boulder, Wave Propagation Lab., 80 pp.
- _____, 1972: Atmospherics and severe storms. Chapter 17, Remote Sensing of the Troposphere, V. E. Derr, Editor, Washington, D.C., U.S. Government Printing Office.
- _____, 1973a: Evaluation of an electromagnetic tornado-detection technique. Preprints, Eighth Conference on Severe Local Storms, Boston, Amer. Meteor. Soc., 165-168.
- _____, 1973b: Electromagnetic radiation from severe storms in Oklahoma during April 29-30, 1970. J. Geophys. Res., 78, 8761-8777.
- _____, 1974: Radio-frequency electrical activity associated with severe storms in Oklahoma during April 29-30, 1970. Papers on Oklahoma Thunderstorms, April 29-30, 1970, S. L. Barnes, Editor. NOAA Tech. Memo. ERL NSSL-69, Norman, Nat. Severe Storms Lab., 195-213.

Chapter 10

DIRECTIONAL MEASUREMENTS OF VERY LOW FREQUENCY (VLF) SFERICS IN THE UNION CITY TORNADIC STORM

Rodger A. Brown

*National Severe Storms Laboratory
Norman, Oklahoma 73069*

and

Herbert G. Hughes

*Naval Electronics Laboratory Center
San Diego, California 92152*

The Naval Electronics Laboratory Center made directional sferics measurements in the Union City, Oklahoma tornadic storm. These data verify the very interesting findings of two earlier directional sferics studies. Whereas sferics activity in tornado-producing storms is known to peak near tornado time, all these studies show conclusively that sferics do not originate in the tornado itself but rather do originate throughout the parent thunderstorm.

10.1 Introduction

Tornadoes long have been a source of fascination for both scientist and layman. In addition to the incredible destruction that a tornado can cause, the parent storm frequently displays intense electrical activity. Noting the apparent relationship between tornadoes and electrical activity, in 1947 Jones began a pioneering study of atmospherics (sferics) associated with tornadic storms. His published results (Jones, 1951; Jones and Hess, 1952; Jones, 1958, 1965), employing 150 kHz measurements, led to the concept that high sferics rates are associated with the tornado funnel. Other omnidirectional studies at a variety of frequencies convey the same impression (e.g., Kohl, 1962; Silberg, 1965; Stanford *et al.*, 1971; Lind *et al.*, 1972; Trost and Nomikos, 1975). Omnidirectional measurements do not isolate the portion of a storm from which extremely high sferics rates emanate--the tornado typically is assumed to be the source.

Similar assumptions have been used to postulate exotic theories that link electrical activity with the formation and maintenance of tornadoes. These theories can be divided into two general categories: those based on electrodynamic motion and those based on thermodynamics caused by electrical heating.

10. VLF Sferics Measurements

Electrodynamic models (e.g., Rathbun, 1960; Vonnegut, 1960; Rossow, 1966) generally assume a particular distribution of charged particles that is perturbed in such a way as to initiate a cyclonic circulation. As the charged particles rotate, surrounding air is accelerated into a tornado vortex. Wilkins (1964) examined some of these models and concludes that "any model showing promise of forming a vortex by electrodynamic action is so improbable in nature as to be unworthy of serious consideration".

Thermodynamic models (e.g., Vonnegut, 1960; Brook, 1967¹; Colgate, 1967) assume that a vertical channel of air is heated by repeated lightning discharges or by a continuous arc or glow discharge. These models have been proposed to explain hypothesized sonic wind speeds in tornadoes. However, most reliable wind speed estimates made during the past 20 years (summarized by Davies-Jones and Kessler, 1974) have maximum values only one-third the speed of sound. Using more realistic wind speeds, Wilkins (1964) deduced that repeated lightning strokes must continue in the same channel for several minutes in order to generate the same amount of buoyancy that is readily available from latent heat release. Based on field observations near 18 tornadic storms, Davies-Jones and Golden (1975) report a pronounced lack of lightning activity in the immediate vicinity of tornado genesis regions. Directional sferics measurements appear to hold the most promise for further examination of thermodynamic hypotheses.

In this chapter, we discuss directional sferics measurements made in the Union City tornadic storm and compare them with directional measurements made in other tornadic storms. Location and movement of the Union City storm allows unambiguous differentiation of tornado sferics from those originating within the main body of the storm.

10.2 EQUIPMENT

During the month of May 1973, the Naval Electronics Laboratory Center (NELC) conducted radio propagation measurements at 1 to 50 kHz in the very low frequency (VLF) region between three widely separated locations (Oklahoma, California and Hawaii). The measurements were of naturally occurring electromagnetic emissions (sferics) generated by lightning flashes (Hughes and Gallenberger, 1974). The Oklahoma station (in Norman about 6 km SSE of NSSL) was used to locate and identify the types of sferics sources propagating to the remote stations.

The NELC sferics receiver is a high-speed digital system capable of recording several thousand impulses per minute. A detailed description of the system is presented by Gallenberger (1972). Basically the system--through a minicomputer controlled process--records on magnetic tape the digitized analog voltages of the VLF vertical electric and horizontal magnetic field components of a received atmospheric, its direction of arrival (DOA) and time of arrival

¹Zrnich (1976) has shown that the magnetometer perturbation that Brook (1967) attributed to the presence of a nearby tornado actually was due to a global magnetospheric disturbance.

to the nearest $10 \mu\text{s}$ of universal time. DOA selectivity is provided such that only sferics arriving from a preselected azimuthal value are recorded. System gain is controlled through logic circuitry and a programmable amplifier whose gain is automatically set to accept peak voltage of the triggering waveform. After a preselected time the amplifier switches to maximum gain. This allows recording of the low amplitude skywaves that follow the precursory high-amplitude ground wave from nearby flashes. The VLF sensors include a one-meter whip antenna and, for DOA information, a set of electrostatically shielded loop antennae. Frequency response of the vertical whip antenna is flat between -3 dB points of 1 kHz and 50 kHz . Digitizing of signals in each channel is accomplished via 8-bit analog-to-digital converters. Sampling rate and number of samples for each waveform are independently variable and are set by teletype input to the computer. Digital values are stored in computer memory until a specified number of waveforms have been accumulated; these are then output as one record to 9-track magnetic tape in a format suitable for subsequent computer processing.

10.3 DATA ANALYSIS

At VLF, strong sferics are produced by the return stroke of a cloud-to-ground discharge. Much weaker signals are generated by K processes (small rapid electric field charges) occurring both in ground and intracloud flashes, and still weaker sferics are produced during the leader phase of the discharge to earth (Malan, 1958).

On 24 May 1973, the sferics receiver began data collection on the Union City storm at about 1450 CST, shortly after NSSL meteorologists decided that the storm had distinct tornado-producing potential. The storm was about 75 km west-northwest of, and moving generally toward, the receiver at approximately 10 m s^{-1} .

During the recording period, the system was programmed to record all impulses having an electric field intensity greater than 1.6 V m^{-1} . As storms approach the sferics receiver, the sferics magnitude increases (for a given discharge rate) and therefore the number of impulses exceeding the threshold level increases. Computer processing allows the data to be analyzed using a selected azimuth-time window. In this study, sferics counts measured in a five-degree azimuthal sector over a three-minute period were chosen for analysis. (There is an unknown azimuthal uncertainty caused by the presence of nearby buildings, telephone wires, etc.)

The number of sferics events recorded between 1450 and 1630 are presented in Fig. 10.1. To aid sferics data interpretation, an azimuth-time plot of maximum low-level radar reflectivity was prepared (Fig. 10.2). An important feature is the long thin shaded region that indicates the location of the tornado vortex at the southwest edge of the radar echo. Prior to tornado touchdown at 1538, the region represents the tornadic vortex signature aloft, which had been detectable on the NSSL Doppler radar for well over half an hour (see Donaldson, Chapter 7; Brown and Lemon, Chapter 15); after 1538 it represents both the tornado on the ground and the signature above cloud base. The width of the shaded region indicates the north-northeast tilt of the tornado vortex with height.

10. VLF Sferics Measurements

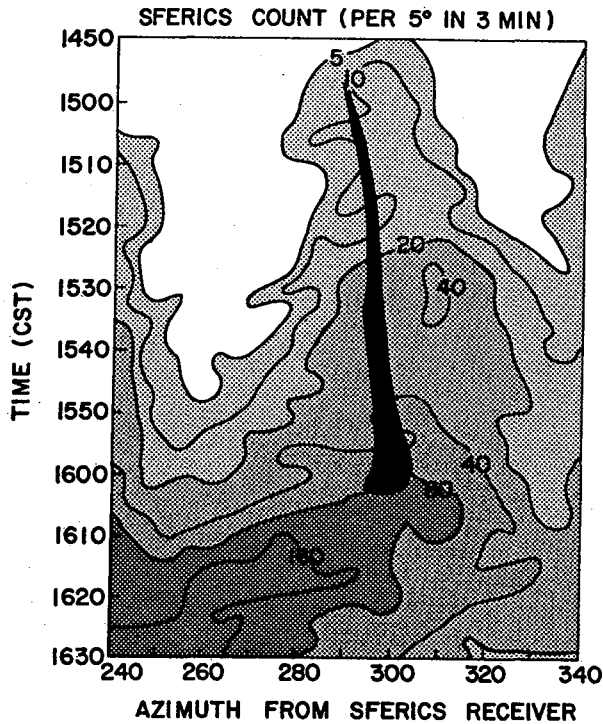


Fig. 10.1 Azimuth-time plot of the total number of sferics events received per five-degree azimuth sector in a three-minute period. Long, thin dark region is the horizontal projection of the tilted tornado and Doppler velocity tornadic vortex signature aloft.

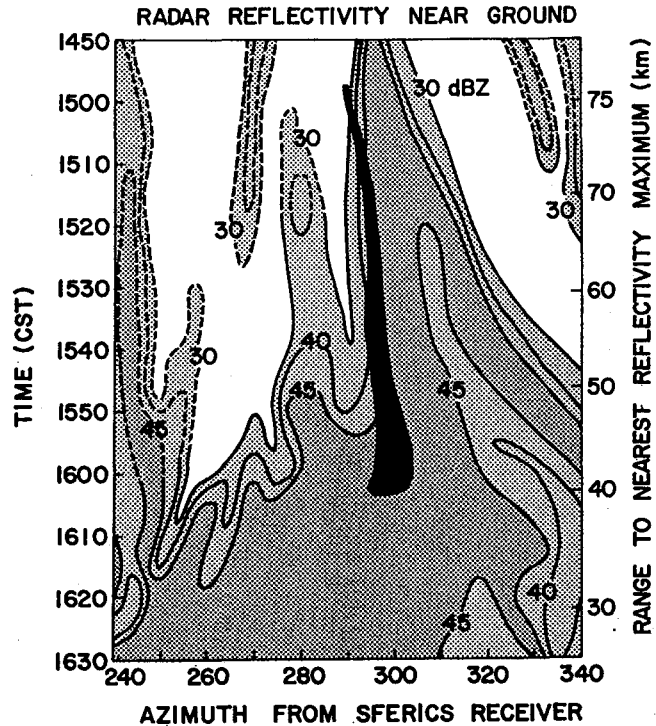


Fig. 10.2 Maximum radar reflectivity factor near the ground as a function of azimuth and time. Echoes greater than 100 km from the receiver have dashed contours. Long, thin dark region is the horizontal projection of the tilted tornado and Doppler velocity tornadic vortex signature aloft. Range to nearest radar echo core within the overall azimuth sector (as a function of time) is indicated along right side.

A very interesting picture emerges--the peak count, as a function of time, coincides with peak radar reflectivity. Since the radar echoes have greater areal extent aloft to the south of the Union City storm (see Burgess and Lemon, Chapter 5), sferics activity extends to the left of the low-level reflectivity contours. In the azimuth sector containing the Union City storm (generally 280° to 340°), sferics activity peaks just after tornado demise, then decreases. At the same time, new storm development to the south passed within 20 to 40 km west and southwest of the receiver, producing high sferics counts due in part to the proximity of electrical discharges.

No apparent correlation exists between the sferics and the location of the tornado vortex either before or after touchdown (1538). Likewise, tornado dissipation at 1604--along with the disappearing tornadic vortex signature aloft--had no effect on the sferics activity. At all times the tornado stayed near the edge of both radar echo and peak sferics region.

These findings are consistent with those of the only two other directional sferics studies known for tornado-producing storms (Scouten et al., 1972; Taylor, 1973). Scouten et al. analyzed some of Jones' directional 150 kHz measurements in the 1955 Blackwell, Oklahoma tornadic storm: one sample 40 min prior to touchdown and the other while the tornado was on the ground. They found that high sferics count rates do not originate from an isolated portion of the storm, but from the storm as a whole. In fact, tornado touchdown did not produce any significant changes in the sferics rate. Taylor recorded the arrival direction of sferics from the 1970 Oklahoma City tornadic storms using a wide-band unit with a frequency response between 2 and 600 kHz. He found that while the sferics rate increased near the time of the two reported tornadoes, the directional measurements clearly indicated that sferics activity peaked in the center of the respective storm masses (radar echoes), with no significant activity at the respective tornado azimuths. Nontornadic severe storms likewise have sferics events distributed throughout the storm (e.g., Taylor, 1973; Kinzer, 1974).

Based on these directional sferics studies, one may reasonably conclude that the tornado is not the source for enhanced sferics activity at the time of the tornado. Apparently tornado-producing storms undergo an electrical life cycle such that lightning occurrence reaches a peak near tornado time. Concurrently (as Lemon and Burgess documented in Chapter 8), tornado-producing storms undergo a thermodynamical life cycle that peaks at the time of tornado production, then quickly subsides. This correspondence of events agrees with the speculations of Scouten et al. and Taylor that the buildup of high sferics count rates is related to vigorous convective activity peaking in the storm at about the time of tornado occurrence.

10.4 CONCLUSIONS

Directional sferics measurements in the Union City tornadic storm substantiate recent findings of Scouten et al. (1972) and Taylor (1973) that sferics activity peaking at the time of a tornado is not associated with the tornado but is associated with the parent thunderstorm. The preferred location of tornadoes along the southwest flank of storms makes it possible to distinguish between sferics generated along the tornado azimuth and those originating within the parent storm. It appears that as storm dynamics build up to tornado production, electrical discharges in the storm simultaneously build to a peak.

This rather consistent simultaneity led researchers using omnidirectional sferics detectors to understandably, but erroneously, conclude that tornadoes are the source of intense electrical activity. Theorists, in turn, have used the erroneous information to propose exotic electrical processes for tornado formation and maintenance.

10.5 ACKNOWLEDGMENTS

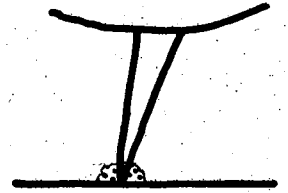
We appreciate the constructive comments of William Taylor (Wave Propagation Laboratory) and Dr. E. T. Pierce (NSSL).

10. VLF Sferics Measurements

10.6 REFERENCES

- Brook, M., 1967: Electric currents accompanying tornado activity. Science, 157, 1434-1436.
- Brown, R. A., and L. R. Lemon, 1976: Evolution of the Doppler radar tornadic vortex signature in the Union City storm. Chapter 15, The Union City, Oklahoma Tornado of 24 May 1973, R. A. Brown, Editor. NOAA Tech. Memo. ERL NSSL-80, Norman, Nat. Severe Storms Lab., 167-175.
- Burgess, D. W., and L. R. Lemon, 1976: Union City storm history. Chapter 5, The Union City, Oklahoma Tornado of 24 May 1973, R. A. Brown, Editor. NOAA Tech. Memo. ERL NSSL-80, Norman, Nat. Severe Storms Lab., 35-51.
- Colgate, S.A., 1967: Tornadoes: Mechanism and control. Science, 157, 1431-1434.
- Davies-Jones, R., and E. Kessler, 1974: Tornadoes. In Weather and Climate Modification, W. N. Hess, Editor, New York, John Wiley and Sons, 552-595.
- _____ and J. H. Golden, 1975: On the relation of electrical activity to tornadoes. J. Geophys. Res., 80, 1614-1616.
- Donaldson, R. J., Jr., 1976: Observations of the Union City tornadic storm by plan shear indicator. Chapter 7, The Union City, Oklahoma Tornado of 24 May 1973, R. A. Brown, Editor. NOAA Tech. Memo. ERL NSSL-80, Norman, Nat. Severe Storms Lab., 67-83.
- Gallenberger, R. J., 1972: A high-speed digital recording system for VLF and ELF sferic waveforms. Naval Electronics Laboratory Center, Interim Report No. 208-1.
- Hughes, H. G., and R. J. Gallenberger, 1974: Propagation of extremely low-frequency (ELF) atmospherics over a mixed day-night path. J. Atmos. and Terr. Physics, 36, 1643-1661.
- Jones, H. L., 1951: A sferic method of tornado identification and tracking. Bull., Amer. Meteor. Soc., 32, 380-385.
- _____, 1958: The identification of lightning discharges by sferic characteristics. In Recent Advances in Atmospheric Electricity, L. G. Smith, Editor, New York, Pergamon Press, 543-556.
- _____, 1965: The tornado pulse generator. Weatherwise, 18, 78-79, 85.
- _____ and P. N. Hess, 1952: Identification of tornadoes by observation of waveform atmospherics. Proc., I.R.E., 40, 1049-1052.
- Kinzer, G. D., 1974: Cloud-to-ground lightning versus radar reflectivity in Oklahoma thunderstorms. J. Atmos. Sci., 31, 787-799.
- Kohl, D. A., 1962: Sferics amplitude distribution jump identification of a tornado event. Mon. Wea. Rev., 90, 451-456.

- Lemon, L. R., and D. W. Burgess, 1976: Tornadic storm airflow and morphology derived from single Doppler radar measurements. Chapter 8, The Union City, Oklahoma Tornado of 24 May 1973, R. A. Brown, Editor. NOAA Tech. Memo. ERL NSSL-80, Norman, Nat. Severe Storms Lab., 85-106.
- Lind, M. A., J. S. Hartman, E. S. Takle, and J. L. Stanford, 1972: Radio noise studies of several severe weather events in Iowa in 1971. J. Atmos. Sci., 29, 1220-1223.
- Malan, D. J., 1958: Radiation from lightning discharges and its relation to the discharge process. In Recent Advances in Atmospheric Electricity, L. G. Smith, Editor, New York, Pergamon Press, 557-563.
- Rathbun, E. R., 1960: An electromagnetic basis for the initiation of a tornado. J. Meteor., 17, 371-373.
- Rossow, V. J., 1966: On the origin of circulation for tornado formation. Proc., Twelfth Conf. on Radar Meteor., Boston, Amer. Meteor. Soc., 183-189.
- Scouten, D. C., D. T. Stephenson and W. G. Biggs, 1972: A spheric rate azimuth-profile of the 1955 Blackwell, Oklahoma, tornado. J. Atmos. Sci., 29, 929-936.
- Silberg, P. A., 1965: Passive electrical measurements from three Oklahoma tornadoes. Proc., I.E.E.E., 53, 1197-1204.
- Stanford, J. L., M. A. Lind and G. S. Takle, 1971: Electromagnetic noise studies of severe convective storms in Iowa: The 1970 storm season. J. Atmos. Sci., 28, 436-448.
- Taylor, W. L., 1973: Electromagnetic radiation from severe storms in Oklahoma during April 29-30, 1970. J. Geophys. Res., 78, 8761-8777.
- Trost, T. F., and C. E. Nomikos, 1975: VHF radio emissions associated with tornadoes. J. Geophys. Res., 80, 4117-4118.
- Vonnegut, B., 1960: Electrical theory of tornadoes. J. Geophys. Res., 65, 203-212.
- Wilkins, E. M., 1964: The role of electrical phenomena associated with tornadoes. J. Geophys. Res., 69, 2435-2447.
- Zrnica, D. S., 1976: Magnetometer data acquired during nearby tornado occurrences. J. Geophys. Res., 81, 5410-5412.



PART IV: THE TORNADO

11. HISTORY OF THE UNION CITY TORNADO
12. COMPARISON OF UNION CITY TORNADO LIFE CYCLE WITH FLORIDA KEYS WATERSPOUT LIFE CYCLE
13. INTERPRETATION OF SURFACE MARKS AND DEBRIS PATTERNS FROM THE UNION CITY TORNADO
14. AIRFLOW CHARACTERISTICS AROUND THE UNION CITY TORNADO
15. EVOLUTION OF THE DOPPLER RADAR TORNADIC VORTEX SIGNATURE IN THE UNION CITY STORM

Chapter 11

HISTORY OF THE UNION CITY TORNADO

Daniel Purcell

*National Severe Storms Laboratory
Norman, Oklahoma 73069*

A major tornado struck the small farming community of Union City, Oklahoma on 24 May 1973. It was on the ground for 26 minutes and attained a maximum width (at cloud base) of nearly 600 meters. Even though the funnel narrowed toward the ground, the width of the damage path consistently equalled funnel width at cloud base. The tornado life cycle consisted of four distinct parts: organizing stage (visible funnel intermittently touching ground with continuous damage path), mature stage (tornado at largest size), shrinking stage (entire funnel decreasing to thin column) and decaying stage (fragmented, contorted funnel). Even in its final stages, the tornado retained its destructive intensity.

11.1 Introduction

The embryo of the Union City tornadic storm was first detectable by radar in west-central Oklahoma, shortly after 1400 CST on 24 May 1973 (Burgess and Lemon, Chapter 5). As the storm grew, it developed characteristics (isolated, explosive growth) that attracted the attention of the NSSL tornado intercept team. The team was positioned about 40 km west of the storm at 1440 when the decision was made to intercept the storm and photograph whatever tornado might appear (see Golden, Appendix A).

As the intercept team moved east-southeastward to get to the storm's south side, the formation of a wall cloud with its characteristic lowered cloud base (defined by Fujita, 1960) was observed shortly after 1500. After the wall cloud began to rotate slowly, some short-lived funnel-like protrusions formed beneath it (Fig. 11.1). The bottom edge of the wall cloud went through many rapid changes in form as moist air was drawn up through the wall cloud base into the storm's rotating updraft. At 1538, a short smooth funnel appeared beneath the wall cloud.

Overall tornado damage track (1538 to 1604) and associated characteristic funnel shapes are depicted in Fig. 11.2. Damage extent at each farmstead location along the damage path is presented in Table 11.1. The F-scale column in the table refers to a descriptive scale devised by Fujita (1971) for classifying tornadoes according to the damage they caused; the scale typically runs from F 0 (damage to chimneys and TV antennas; twigs broken off trees) to F 5 (frame houses destroyed with little or no debris remaining on foundations; automobile-sized missiles generated).

11. Tornado History



Fig. 11.1 Developing wall cloud, looking east at 1515. NSSL tornado intercept team members in foreground (l. to r.): Purcell, Golden, Vleek and Morgan. Photo courtesy of Robert Gannon.

The following sections discuss the tornado and damage path in more detail. Tornado life cycle is divided into four distinct stages: organizing, mature, shrinking and decaying.

11.2 ORGANIZING STAGE

Initiation of surface damage 9.7 km west of Union City coincided with funnel formation (Fig. 11.3). At the time of formation the funnel was determined by photogrammetry to be 175 m wide at cloud base and it extended only a third of the way to the ground. The first hint of anything unusual at Farmstead A was swirling dust, leaves and trash that approached from the west and momentarily engulfed the farmhouse. From a distance, this debris cloud was observed to remain on the ground beneath the funnel as the tornado headed east at a speed of 8 m s^{-1} .

During most of the first 10 min of its lifetime, the visible condensation funnel remained aloft, extending to the ground only twice for periods of less than 15 s. The lower two-thirds of the funnel appeared and disappeared in a ghostlike manner. However, the tornado produced a continuous damage path as it passed over five farmsteads (A through E in Fig. 11.2). These farmsteads sustained moderate damage; several wooden sheds were destroyed along with two silos (Table 11.1). None of the farm homes in this area received structural damage (for example, see Fig. 11.4).

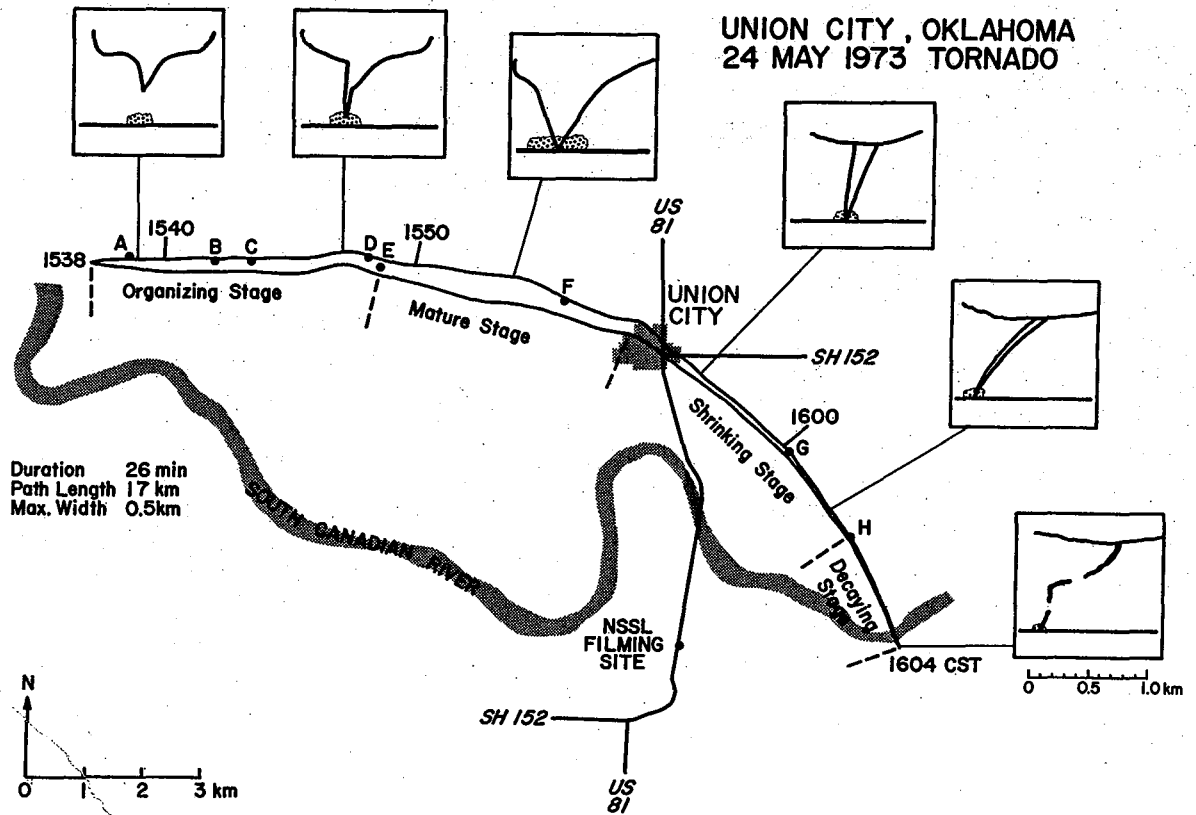


Fig. 11.2 Damage path of the Union City tornado with sketches of the funnel and associated debris cloud as seen from the south. Letters A through H indicate damaged farmsteads (details in Table 11.1).

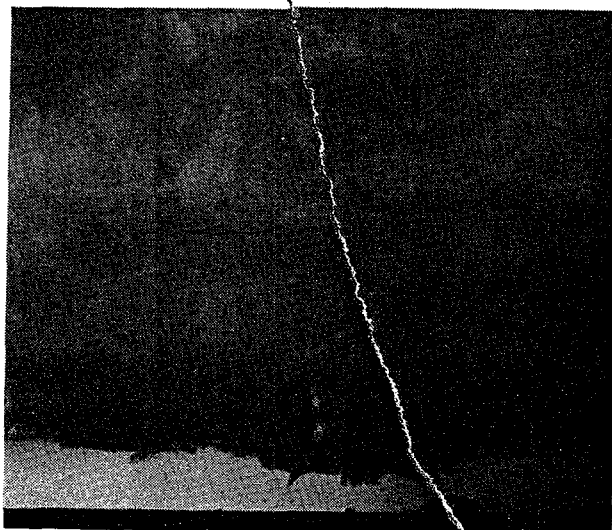


Fig. 11.3 Condensation funnel at 1541 near beginning of Union City tornado organizing stage. Looking toward west-northwest. Photo courtesy of Steve Tegtmeier.

11. Tornado History

TABLE 11.1 Damage to Farmsteads Near Union City

	<u>Time</u>	<u>Farmstead</u>	<u>F-Scale</u>	<u>Damage Extent</u>
A	1539	Aust	1	Corral blown over; telephone poles knocked down.
B	1541	Bollinger	2	One silo blown over, another damaged; farm building and barn destroyed; standing trees denuded.
C	1542	Dawson	2	Two barns destroyed; garage damaged.
D	1547	Acres	2	Trees blown over but not denuded.
E	1548	Pappes	2	Tool shed and barn destroyed.
F	1555	Sanders	5	Carport carried intact to north, rest of house gone, foundation clean; barn destroyed; standing trees denuded; flatbed truck rolled over; car torn apart with only frame remaining nearby (Fig. 13.5).
G	1600	Bosler	4	Twisted second story of farmhouse came to rest on collapsed first story; hay barn, machinery barn, garage and other outbuildings gone; standing trees denuded, others blown over but not denuded; car rolled over; farm machinery damaged or destroyed (Fig. 13.9).
H	1602	Ninman	5	Small frame house gone with foundation clean; nearby barn undamaged except for some sheet metal roofing torn off; car and pickup truck flipped over.

Condensation funnel width and damage path width increased at a relatively slow rate during the tornado's organizing stage. Both damage path width at the ground and funnel width at 550 m height averaged 200 m.

During this stage of the tornado's life cycle the wall cloud was well-defined (Fig. 11.5). Its sides were nearly vertical making it quite distinct from the surrounding cloud base. Photogrammetric measurements indicate that wall cloud width was approximately 1100 m and its base was 600 m above the ground.



Fig. 11.4 Aerial photograph (toward south) of damage at Farmstead C. Tornado was in its organizing stage at this time. NSSL photo.

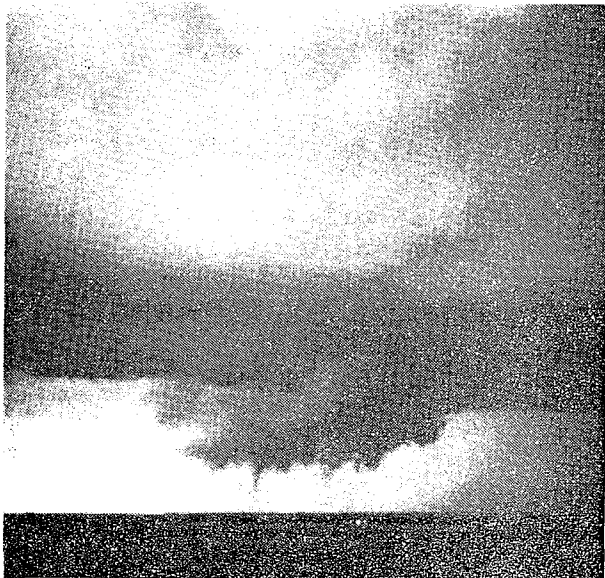


Fig. 11.5 Union City tornado at 1545 near end of organizing stage. Note well-defined wall cloud. Looking toward west-northwest. Photo courtesy of Steve Tegtmeier.

11. Tornado History

11.3 MATURE STAGE

The condensation funnel remained on the ground beginning at 1548 (Fig. 11.6). During this period the funnel began to widen rapidly as it continued east-southeast over open countryside at a speed of 9 m s^{-1} . Associated tree damage indicated a concurrent broadening of the damage path.

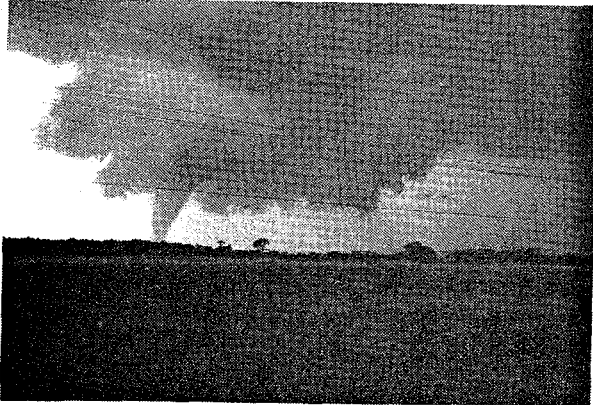


Fig. 11.6 Union City tornado funnel making contact with ground at beginning of mature stage (1548). Looking northwest from NSSL filming site. Photo courtesy of Robert Gannon.



Maximum tornado size was attained at 1552:30 with funnel width of 590 m at cloud base and 155 m at 150 m above ground. The tornado's shape was that of a broad, truncated, inverted cone--a characteristic of the mature stage (Fig. 11.7). Note that the wall cloud had become indistinct by this time. Damage path width also reached its overall maximum of 500 m here. In the same area, just west of Farmstead F, wheat in an open field was swirled in odd patterns (see Davies-Jones *et al.*, Chapter 13).

A barn and two-story farmhouse at F were the only buildings hit by the tornado during its mature stage. Both were completely destroyed with only the bare foundation of the house remaining. An eyewitness reported that the house as a whole was lifted 5 to 10 m before it disintegrated. Beyond Farmstead F, funnel width as well as damage width began to decrease slowly as the tornado continued east-southeast toward Union City.

11.4 SHRINKING STAGE

The tornado hit the northwest edge of Union City at 1556:30 and began its shrinking stage. A large bend developed in the middle of the funnel at this point (Fig. 11.8), as the tornado turned sharply to the southeast.

Fig. 11.7 Union City tornado at 1554 during its mature stage. Looking toward northwest. Photo courtesy of Steve Tegtmeier.

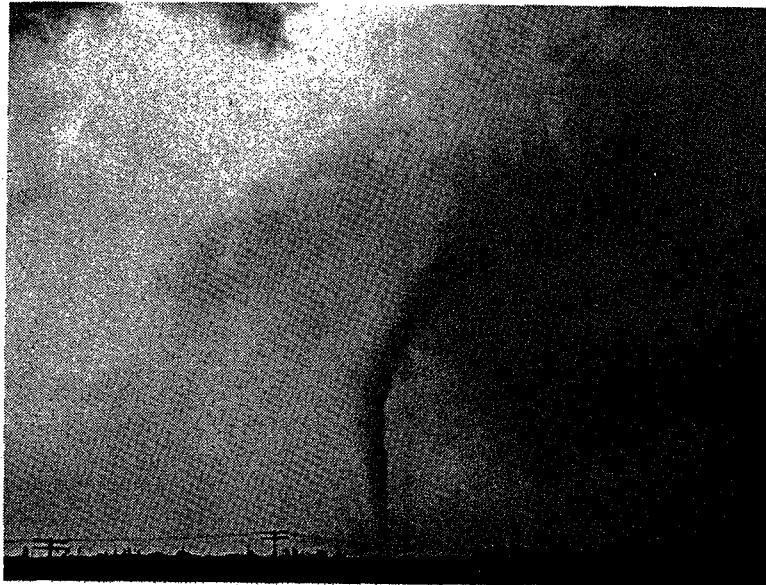


Fig. 11.8 Tornado at beginning of shrinking stage (1556:30) as it was entering northwest edge of Union City. View toward north-northwest from NSSL filming site. NSSL photo.

As the tornado passed through the middle of town, it shrank rapidly. Whereas the upper part of the funnel was 290 m wide at the northwest edge of town, it measured only 60 m in width at the same height 3.5 min later. The damage path likewise narrowed from 220 m to 160 m. Many people who took shelter in town insisted that there were two separate tornadoes. They thought the tornado they saw approaching town before they took shelter was entirely different from the one they saw heading away from town when they came out.

Destruction was complete along the center of the damage path (Fig. 11.9) with the exception of one house that had half its walls left standing. Maximum F-scale damage was between F 4 and F 5. In all, about 20 homes and 18 mobile homes were destroyed. Another 20 homes suffered major damage and 23 received minor damage. Several commercial buildings and a couple of churches were heavily damaged (NOAA, 1973).

The tornado shrank more slowly as it headed southeast from Union City and tilted strongly to the east-northeast with height (Fig. 11.10). Its translational velocity had increased to 15 m s^{-1} by this time--a speed it maintained for the remainder of its lifetime.

As the vortex passed through wheat fields southeast of town, its damage path gradually narrowed to a width of 100 m at point G. The family at Farmstead H saw the tornado hit Farmstead G where the house and several barns were destroyed. When they realized that the funnel was curving toward them, they tried to outrun it in their car. The tornado overtook them and rolled the car over, causing minor injuries. Crawling out of the car, they found that their home nearby had disappeared--only a bare concrete slab remained.

11. Tornado History



Fig. 11.9 Aerial view (toward southeast) of damage path through Union City from northwest of town. Photo courtesy of Oklahoma Publishing Company.

11.5 DECAYING STAGE

After striking Farmstead H at 1602, the tornado entered its decaying stage. At a height of 350 m, funnel diameter now was only 40 m. The bottom third of the condensation funnel temporarily evaporated after hitting the farm, although the vortex maintained contact with the ground. At the same time, it began bending rapidly into a serpentine shape (Fig. 11.11). The lower part of the condensation funnel reformed briefly before the tornado dissipated over the South Canadian River at 1604 (Fig. 11.12).

11.6 SUMMARY

The entire lifetime of the Union City tornado spanned 26 minutes: longest stage was the organizing stage (10 min) followed by the mature (8.5



Fig. 11.10 Tornado in its shrinking stage (1600) southeast of Union City near Farmstead G. Looking toward north-northeast from NSSL filming site. NSSL photo.



Fig. 11.11 Union City tornado at 1603 during decaying stage. Looking toward east-northeast from NSSL filming site. Photo courtesy of Robert Gannon.

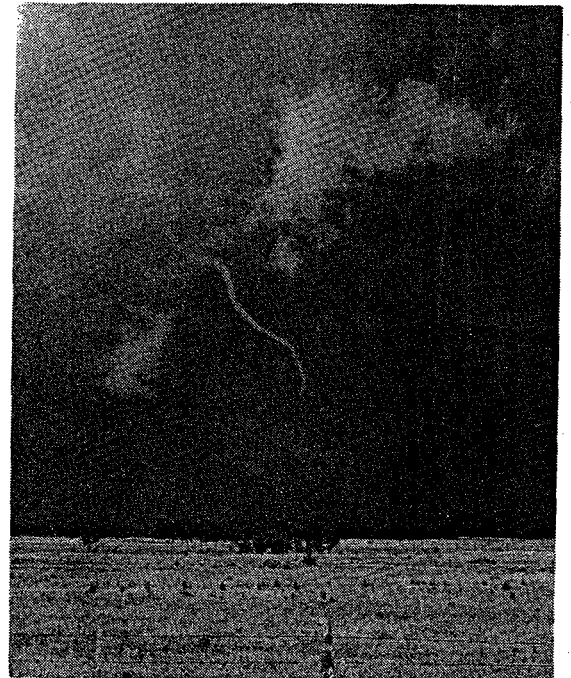


Fig. 11.12 Union City tornado at point of final decay (1604) over South Canadian River. Looking east from NSSL filming site. Photo courtesy of Robert Gannon.

11. Tornado History

min), shrinking (5.5 min) and decaying stages (2 min). These stages were marked by significant differences in funnel width, funnel shape, damage path width and damage characteristics.

During the organizing stage, overall funnel size increased only slightly (Fig. 11.13). Even though the visible tornado funnel touched ground intermittently, a continuous dust cloud and damage track was evident. During this stage, as well as in the later stages, damage path width bears a remarkable resemblance to funnel width at 550 m (Fig. 11.14).

When the visible funnel finally remained on the ground (mature stage), both funnel cloud and damage path width rapidly increased, peaking at about the same time. At the beginning of the shrinking stage, the tornado underwent significant changes in addition to becoming narrower: it tilted more toward the east-northeast with height, a bend developed in the middle of the funnel and its translational speed nearly doubled. In the last stage of decay, the funnel had a contorted and fragmented rope-like structure. When it was all over, the people of Union City and Canadian County knew that they had been visited by one of the most intense tornadoes anywhere during 1973.

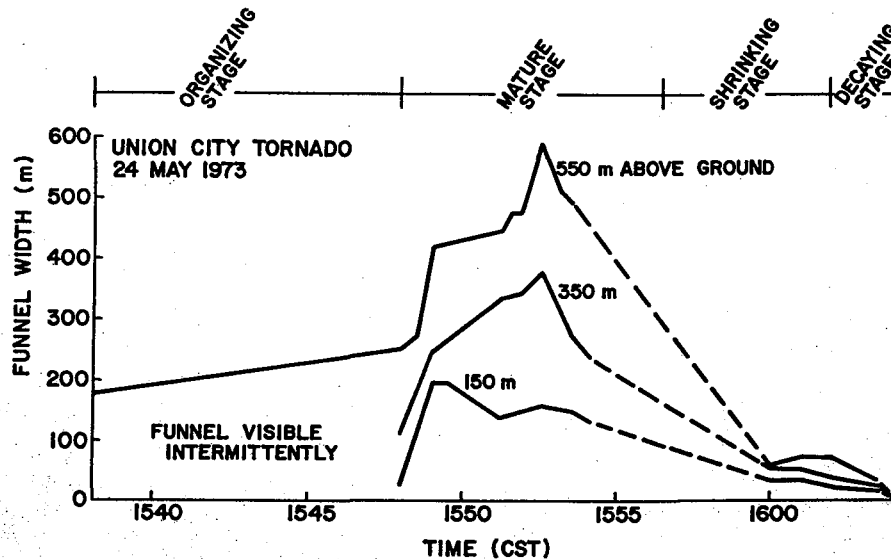


Fig. 11.13 Photogrammetric funnel widths at three heights above ground. Measurement errors are estimated to be less than ± 5 percent. Dashed lines indicate missing data.

11.7 ACKNOWLEDGMENTS

The author thanks Rodger Brown for his help preparing the manuscript. Many thanks go to Don Burgess, Jerry Reutlinger, Larry Hennington and Charles Vlcek for their help in gathering field data during the weeks following the tornado. I also thank Steve Tegtmeier, the Oklahoma Publishing Company and Robert Gannon of Popular Science, for the photographs presented in this chapter. I appreciate the cooperation of the many residents of Union City and the surrounding area who provided NSSL with their photographs of the tornado. Together, the photographs contributed to an overall understanding of structural changes that took place in the tornado funnel and its associated wall cloud.

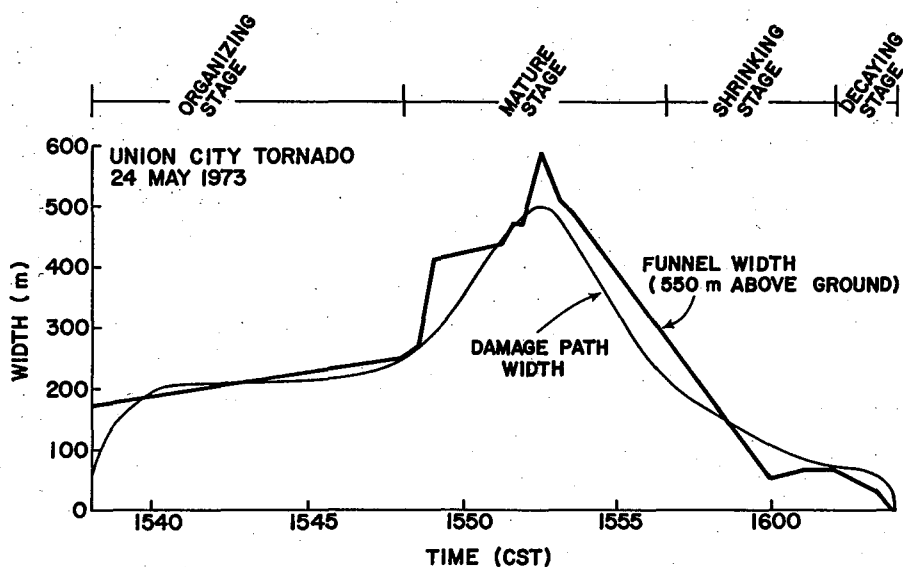


Fig. 11.14 Funnel width near cloud base compared with surface damage path width.

11.8 REFERENCES

- Burgess, D. W., and L. R. Lemon, 1976: Union City storm history. Chapter 5, The Union City, Oklahoma Tornado of 24 May 1973, R. A. Brown, Editor. NOAA Tech. Memo. ERL NSSL-80, Norman, Nat. Severe Storms Lab., 35-51.
- Davies-Jones, R. P., D. W. Burgess, L. R. Lemon and D. Purcell, 1976: Interpretation of surface marks and debris patterns from the Union City tornado. Chapter 13, The Union City, Oklahoma Tornado of 24 May 1973, R. A. Brown, Editor. NOAA Tech. Memo. ERL NSSL-80, Norman, Nat. Severe Storms Lab., 141-156.
- Fujita, T. T., 1960: A detailed analysis of the Fargo tornadoes of June 20, 1957. Research Paper No. 42, Washington, D.C., U.S. Weather Bureau, 67 pp.
- _____, 1971: Proposed characterization of tornadoes and hurricanes by area and intensity. Satellite and Mesometeor. Res. Proj., Research Paper No. 91, Dept. of Geophys. Sci., Univ. of Chicago, 42 pp.
- Golden, J. H., 1976: Tornado intercept strategy and morphological observations. Appendix A, The Union City, Oklahoma Tornado of 24 May 1973, R. A. Brown, Editor. NOAA Tech. Memo. ERL NSSL-80, Nat. Severe Storms Lab., 185-189.
- NOAA, 1973: Storm Data, Asheville, Environmental Data Service, 15 (5), 16.

Chapter 12

COMPARISON OF UNION CITY TORNADO LIFE CYCLE WITH FLORIDA KEYS WATERSPOUT LIFE CYCLE

Joseph H. Golden¹

*National Severe Storms Laboratory
Norman, Oklahoma 73069*

The life cycle of the Union City tornado is found to resemble, in many respects, the typical life cycle of the Florida Keys waterspout. Both commence with surface evidence of vortex existence before a visible funnel cloud has descended a significant distance toward the surface. Approaching the mature stage, the tornado and waterspout exhibit spiral inflow characteristics with a distinct boundary between warm, moist air and cool, dry air. The cooler air mass from a nearby precipitation area apparently cuts off flow of warm, moist air into the circulation, leading to vortex decay. The visible funnel becomes thin and increasingly tilted and distorted as it dissipates. Major differences between the tornado and waterspout appear to be vortex and parent cloud scales and, to a lesser extent, vortex lifetimes and intensities.

12.1 Introduction

Golden (1973, 1974a, 1974b) has shown that Florida Keys' waterspouts undergo a characteristic life cycle consisting of five discrete but overlapping stages: (1) the dark spot, a prominent light-colored disc on the sea surface surrounded by a dark patch, diffuse on its outer edges, which represents a complete vortex column from cloudbase to sea surface; (2) the spiral pattern, the primary growth phase of the waterspout, characterized by alternating dark- and light-colored surface bands around the dark spot; (3) the spray ring (incipient spray vortex), concentrated around the dark spot, with a lengthening funnel above; (4) the mature waterspout (spray vortex), the stage of maximum overall organization and intensity; and (5) the decay stage, when waterspout dissipation (often abrupt) is initiated by cool downdrafts from a nearby developing rainshower.

It has been hypothesized on the basis of detailed waterspout observations in the Lower Florida Keys (Golden, 1974a, c) and Tornado Intercept Project results in Oklahoma (Golden and Morgan, 1972) that the two vortices are qualitatively similar, but differ in certain quantitative aspects. Primary

¹ Present affiliation: NOAA, Environmental Research Laboratories, Office of Programs, Boulder, Colorado 80302.

12. Tornado - Waterspout Comparison

differences between waterspouts and tornadoes elucidated by the Union City study are funnel size, three-dimensional structure of the synoptic and sub-synoptic environments (see Vlcek, Chapter 2; Brandes, Chapter 3; and Golden, 1974 a,c for details), parent cloud size and organization, and, to a lesser extent, differences in vortex intensity and translational speeds. Scale considerations are implicitly manifest in the vortex differences listed above in that the forcing functions which concentrate vorticity are larger and operate over larger space and time scales for the tornado. Many waterspout parent clouds and the Union City cloud system exhibit organized rotation on the subcloud scale well before waterspout/tornado formation.

12.2 ORGANIZING STAGE

The first stage of the Union City tornado life-cycle began at 1538 CST, and may be termed the "organizing stage", analogous to the combined dark spot and spiral pattern stages of waterspouts. A wide but short, tapered funnel cloud was observed descending rapidly from the rotating "wall cloud". When the funnel had descended to a pencil-point about one-third of the way downward from cloud base, a large dust whirl could be clearly seen over open fields below the slightly tilted funnel. (Similarly, Golden (1974a,b) has demonstrated that the dark spot is associated with a closed circulation on the sea surface.) During the period 1538 to 1545, the funnel cloud touched the ground momentarily, and then withdrew rapidly upward into the rotating wall cloud, repeating the process several times.

The second stage of the waterspout life cycle, the spiral pattern stage, represents the primary growth phase of the vortex. Similarly, about 1545 a larger, blunt funnel began its earthward descent 5 km to the west of Union City. As the lower tip of the funnel reached the ground, an outer shell of condensate formed temporarily around the funnel mid-section. The double-walled funnel resembled in structure and development sequence a large double-walled waterspout studied by Golden. However, the double-walled tornado funnel evolved further, within a few minutes, to one larger-diameter funnel. (It appears likely that the tornado funnel's double-walled structure was the result of rapid, irregular vortex intensification and inhomogeneities in the surrounding low-level air's moisture content.)

12.3 MATURE STAGE

The second stage of the Union City tornado, the "mature stage", lasted from about 1548 to 1556. During this period, the rotating wall cloud became better organized with stronger rotation apparent around its edge. A 'feeder band' of low-hanging fracto-cumulus clouds could be seen spiraling into the upper portion of the tornado funnel from the northeast. By the end of the mature stage, the tornado funnel evolved to a large, slightly-tapered cylinder with a large debris cloud at its base. A composite-schematic plan view of the tornado and associated cloud structures and mean subcloud flow field is given in Fig. 12.1. The subcloud flow field has been inferred from eyewitness and surface mesonet observations and photogrammetric cloud-tag motions. For comparative purposes, Fig. 12.2 shows the boundary layer vector wind field

around the spiral pattern of a large mature waterspout. We note the strong resemblance, apart from scale, between the pre-existent dark 'shear-band' from which the spiral pattern evolved and the flanking cloud line in Fig. 12.1 which spirals into the rotating wall cloud. Both the flanking line and waterspout shear-band appear to be the demarcation of gust-fronts from nearby precipitation, and both signify pronounced low-level wind discontinuities with large cyclonic shear (vorticity). In Fig. 12.1, the portion of the flanking line closest to the wall cloud and tornado appeared to accelerate northeastward more rapidly than the remainder of the line, as it was intruded in the rear by an enlarging tongue of drier air. Note also the similar geometry in shower locations relative to the major circulation centers in Figs. 12.1 and 12.2. Limited aircraft measurements over waterspout spiral patterns suggest that cool, drier air is present in the anticyclonically-turning outflow to the north of the shear-band in Fig. 12.2. Likewise, observations from the NSSL intercept vehicle and University of Oklahoma students at other locations in Fig. 12.1 indicate the presence of cool, drier air in the clear intrusion to the west of the flanking line axis and very warm, moist air to the east. The primary high-intensity precipitation core in Fig. 12.1 was located to the northeast of the tornado during this stage, and new precipitation developed southward from the core and in southern portions of the flanking line later.

At about 1552, some 3 km west of town, the tornado reach its maximum overall size and apparent intensity. During the tornado's mature stage, strong rising motions (in cloud tags) appeared to be concentrated along the 'feeder-band' of clouds streaming into the tornado's circulation from the northeast (Fig. 12.1). There are also definite indications on the NSSL films of descending, evaporating cloud tags in the southeast quadrant of the peripheral cloud circulation around the tornado funnel. This apparent descent may be partly due to the large northeastward tilt of the funnel near cloudbase during the mature stage.

12.4 SHRINKING STAGE

As the tornado moved into the northwestern portion of Union City, the funnel diameter decreased rapidly at all altitudes, the easterly tilt component increased and the tornado turned toward the southeast at greatly increased speed. This sequence of events defines the onset of the tornado's "shrinking stage". Even though the funnel diameters and damage swath width were considerably smaller southeast of town, the funnel remained in contact with the ground, practically destroying everything in its path (see Purcell, Chapter 11).

12.5 DECAYING STAGE

As the tornado continued its southeastward movement, the heavy precipitation core to the northeast (Fig. 12.1) spread southward. At 1602, the tornado began its "decaying stage" as warm, moist inflow was cut off by rain-cooled air from a precipitation boundary about one kilometer to the northeast. As

12. Tornado - Waterspout Comparisons

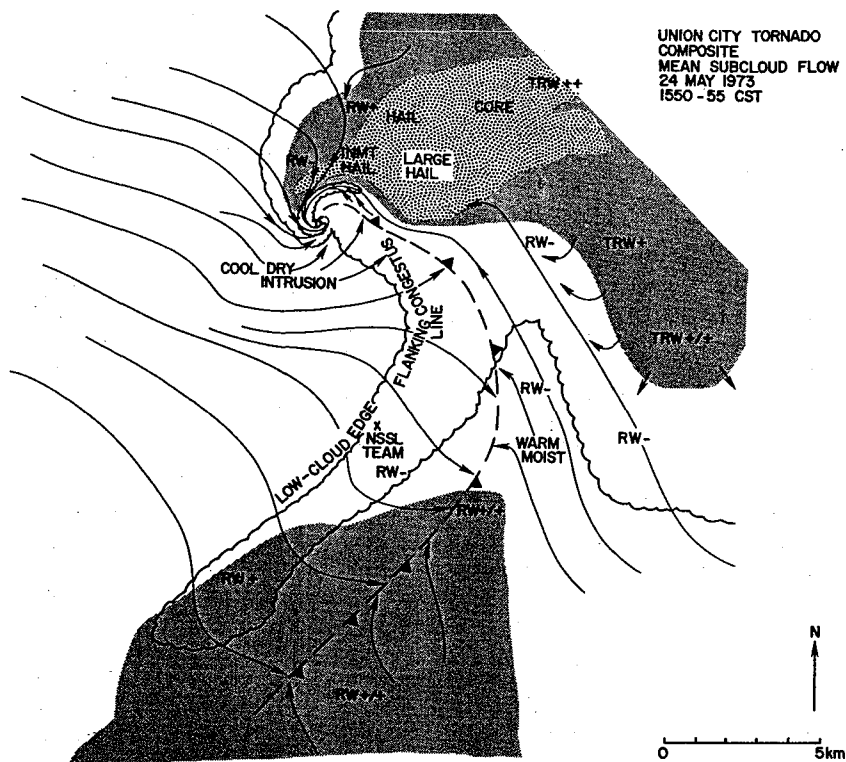


Fig. 12.1 Schematic plan view of composited mean subcloud mesoscale flow around Union City tornado (at circulation center) during mature stage. Surface gust-front location is dashed, major low-level cloud boundaries, precipitation types and intensities are indicated. Regions of heavier precipitation are shaded. Note flanking line cloud base relative to surface gust-front, streamflow, and tornado.

with decaying waterspouts, the visible funnel continued to shrink, increased its tilt rapidly from the local vertical and became very contorted. At 1604, the ephemeral rope-like vortex quickly disappeared as it moved over the north bank of the North Canadian River about 3.5 km east of the NSSL intercept team. The combined shrinking and decaying stages resemble in remarkable detail the morphological changes for the decay stage of waterspouts.

12.6 SUMMARY

In summary, the Union City tornado has afforded the first complete description of a tornado life cycle by a team of trained meteorologists who witnessed it, and it appears in many respects to resemble the waterspout life cycle. Major differences appear to be vortex and parent cloud scales and, less important, vortex lifetimes and intensities. The primary mechanism responsible for the decay of both types of vortices appears to be the formation and slow movement into the vortex circulations of density-surge

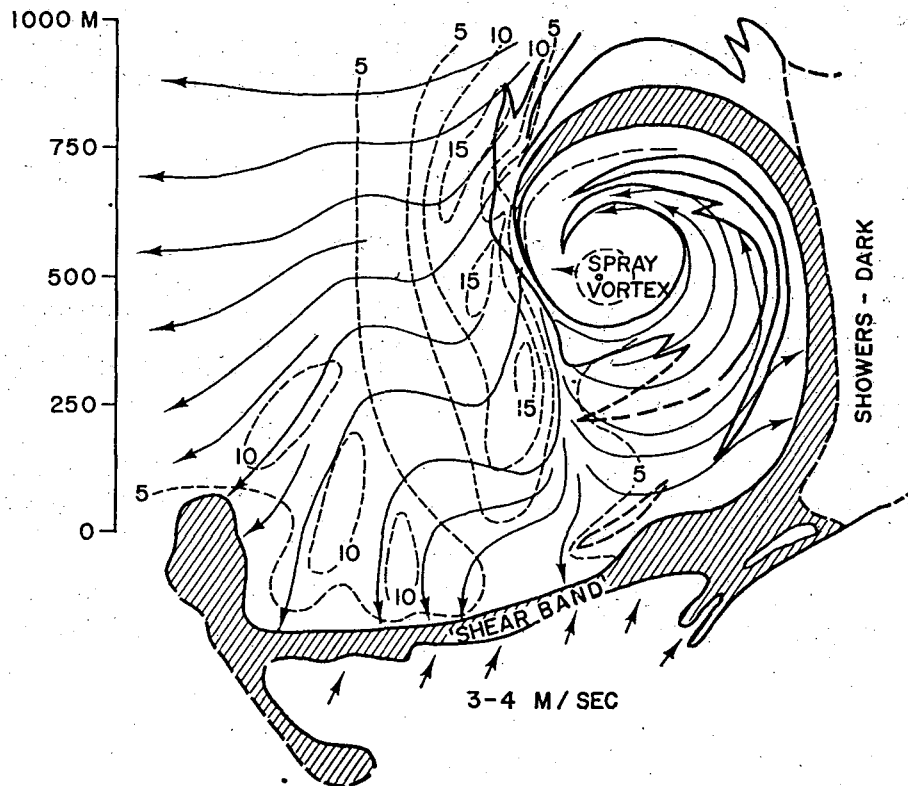


Fig. 12.2 Streamlines (solid) and isotachs (dashed) of boundary layer flow on spiral scale around cyclonic, mature waterspout of 10 September 1969. Isotachs are in $m s^{-1}$. The boundary layer circulation is assumed to be steady as the spray vortex advances; streaklines approximate relative streamlines, after Golden (1974 c).

lines (Charba and Sasaki, 1971) from nearby precipitation areas.* An important analogous intermediate scale of vortical circulation and organization of air mass properties has been documented for each vortex (Figs. 12.1 and 12.2).

12.7 ACKNOWLEDGMENTS

We extend our appreciation to NASA's L.B.J. Space Center, Houston, for lending us the two 16 mm cameras and for making enhanced copies of the original footage. We thank the other members of the 1973 NSSL Tornado Intercept Project, Dr. Bruce Morgan of Notre Dame University, Dr. Gary Achtemeier,

*This hypothesis is consistent with visual observations by the NSSL and University of Oklahoma intercept teams and with radar echo evolution (see Fig. 12.1); the density-surge line could be effective in disrupting vortex flow fields and cutting off inflow.

12. Tornado - Waterspout Comparisons

Charles Vlcek, and Dan Purcell for their contributions to success. Dr. Robert Davies-Jones provided useful comments on this manuscript. This work was partially supported by the Nuclear Regulatory Commission under Interagency Agreement AT(49-25)-1004.

12.8 REFERENCES

- Brandes, E. A., 1976: Subsynoptic-scale meteorological features and associated convective activity on 24 May 1973. Chapter 3, The Union City, Oklahoma Tornado of 24 May, 1973, R. A. Brown, Editor. NOAA Tech. Memo. ERL NSSL-80, Norman, Nat. Severe Storms Lab., 19-25.
- Charba, J., and Y. Sasaki, 1971: Gravity current model applied to analysis of quall-line gust-front. Proceedings, Seventh Conference on Severe Local Storms, Boston, Amer. Meteor. Soc., 277-283.
- Golden, J. H., 1973: The life cycle of the Florida Keys waterspout as the result of five interacting scales of motion. Ph.D. Dissertation, Tallahassee, Florida State University, 371 pp.
- _____, 1974a: Life cycle of Florida Keys' waterspouts. Nat. Severe Storms Lab., NOAA Tech. Memo. ERL NSSL-70, 147 pp.
- _____, 1974b: On the life cycle of Florida Keys' waterspouts, I. J. Appl. Meteor., 13, 676-692.
- _____, 1974c: Scale-interaction implications for the waterspout life cycle, II. J. Appl. Meteor., 13, 693-709.
- _____, and B. J. Morgan, 1972: The NSSL/Notre Dame Tornado Intercept program, Spring, 1972. Bull., Amer. Meteor. Soc., 53, 1178-1179.
- Purcell, D., 1976: History of the Union City tornado. Chapter 11, The Union City, Oklahoma Tornado of 24 May 1973, R. A. Brown, Editor. NOAA Tech. Memo. ERL NSSL-80, Norman, Nat. Severe Storms Lab., 123-133.
- Vlcek, C. L., 1976: General synoptic situation. Chapter 2, The Union City, Oklahoma Tornado of 24 May 1973, R. A. Brown, Editor. NOAA Tech. Memo. ERL NSSL-80, Norman, Nat. Severe Storms Lab., 11-17.

Chapter 13

INTERPRETATION OF SURFACE MARKS AND DEBRIS PATTERNS FROM THE UNION CITY TORNADO

Robert P. Davies-Jones, Donald W. Burgess,
Leslie R. Lemon¹ and Daniel Purcell

*National Severe Storms Laboratory
Norman, Oklahoma 73069*

Changes in tornado structure were accompanied by corresponding changes in damage intensity and debris configuration. Initially, damage was light over a 200 m wide path but the vortical nature of the winds was clearly evident. During the mature stage, damage was severe and still showed signs of circulation. Intriguing and mysterious microscale patterns were observed in wheat. In the shrinking and decaying stages, heavy damage occurred over a 150 m wide path and there was evidence of strong radial inflow in the lowest meter above the surface. Generally, debris was thrown ahead of the vortex, with heavy objects coming to rest on the right forward side. Signs of circulation were no longer apparent in the debris configuration. Flow relative to the moving vortex appeared asymmetrical with strongest winds on the right side of the funnel.

13.1 Introduction

Fujita, Bradbury, and Black (1967) first classified tornado-produced marks or debris patterns on the ground. They divided the marks into six categories:

- (a) Captive-debris marks--consisting of small debris captured by loose wires. Debris also is collected by fences and buildings which withstand the tornado. The side on which the debris impacts reveals wind direction.
- (b) Scratch marks on fields--produced by sharp-edged objects dragged by strong winds. These marks are extremely rare, most objects roll or become airborne in tornadic winds.
- (c) Bounce marks--made by heavy objects rolling and bouncing downwind.

¹Present affiliation: National Severe Storms Forecast Center, Techniques Development Unit, Federal Building, Kansas City, Missouri 64106.

13. Debris Pattern Interpretation

- (d) Drift marks--short lines of wind-driven debris oriented in the direction of the strong wind which caused the final drifting of the debris. These patterns reflect the final effects of high winds upon the debris distribution.
- (e) Debris marks--referring to the configuration of debris from known origins. Lines of debris distribution emanating from a given source approximate streaklines rather than streamlines.
- (f) Cycloidal suction marks--consisting of short light pieces of debris such as corn stubble laid in cycloidal rows about 15 cm high and 2 m wide. They are indicative of local "suction spots" of convergence rotating around the axis of the vortex system. The suction spots are thought to be multiple vortices in a single convergence area (Fujita, 1971; Ward, 1972). Strong radial inflow very near the surface carries small pieces of debris into the bases of these vortices. As each vortex translates in a cycloidal path, it deposits debris on the ground. This explanation clearly requires that the radial flow component be greater than the tangential wind next to the surface and that the debris never be sucked up high enough to encounter the strong swirling winds above this surface layer (otherwise, such high organization would not be observed). Relatively few tornadoes make suction marks.

During the Union City damage survey we observed all these marks except suction marks and in addition, identified three other patterns, namely;

- (g) Wheat bundled together in circular clumps 0.5 - 2 m in diameter. In each bundle the wheat was twisted together cyclonically as if by a small scale cyclonic whirlwind. These swirls were found in the convergence-divergence patterns described below but were also distributed haphazardly in other parts of the path.

- (h) Patterns of convergence and adjacent divergence in the wheat in rows of characteristic length of 6-12 m (Fig. 13.1). In some areas as many as a dozen convergence-divergence rows were found together before the pattern broke down. Each row was approximately 1 m wide. In the convergence rows the wheat was twisted together in cyclonic bundles as described in (g). The divergence was strong enough to reveal bare ground in the center of the divergence rows. The rows did not appear to be oriented in any systematic manner relative to the tornado's motion.

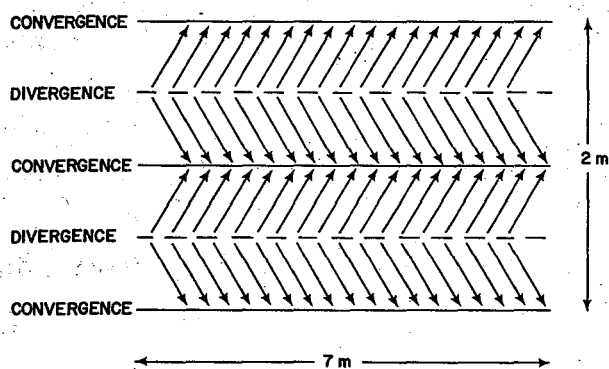


Fig. 13.1 Convergence-divergence pattern in the wheat.

- (i) A quasi-rectilinear deposition line (Fig. 13.2) similar in origin to the cycloidal suction marks but caused by a single rather than multiple vortex system. The width of the deposition line averaged 0.6 m. The line consisted of soil, mud balls about 1 to 2 cm in diameter, and small debris (such as straws, wood splinters, small sticks and wheat) generally less than 0.3 m in length and precisely aligned parallel to the line. Across a plowed field the deposition line looked like a narrow dirt road as the soil had partly filled in the furrows. Suction marks also have this same appearance on occasion (Fujita *et al.*, 1972).



Fig. 13.2 The composition of the deposition line southeast of Union City. Deposition line runs from left to right and is delineated by furrows filled up with mud balls. Individual mud balls and pieces of stubble are visible in the foreground.

The depth of the line varied according to composition. When wheat made up a large portion of the deposited material a 30 cm depth was typically observed while in areas where soil was the main deposit the depth ranged between 5 and 20 cm. At one point the deposition line was sinusoidal with a small amplitude. The mud balls are believed to have been generated by wind scouring over clay soil still moist from a previous day's rain. This idea is based on observations that in several places the ground bore scour marks and exposed objects were covered by a thin layer (1 mm) of soil (Fig. 13.3).

A broader area (30-50 m wide) on either side of the deposition line showed a debris pattern (flattened wheat, small pieces of straw, wood splinters aligned along curved lines as shown in Fig. 13.4), suggesting strong radial inflow into a moving vortex. A similar inflow configuration was observed by Staats and Turrentine (1956).



Fig. 13.3 Mud-covered acetylene tank found in this position south-east of Union City. Ground in vicinity is scoured by mud.

13. Debris Pattern Interpretation

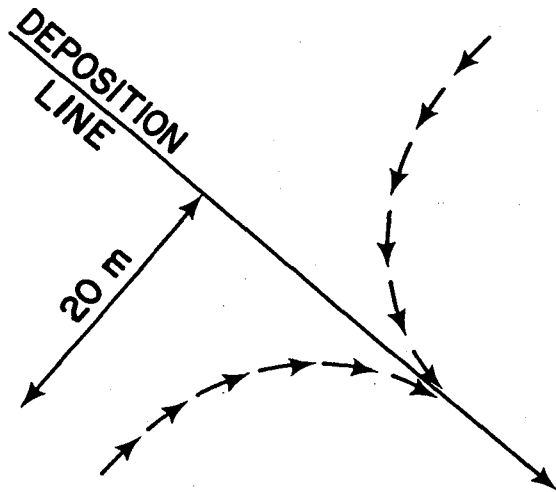


Fig. 13.4 Debris orientation pattern either side of the deposition line.

In addition to analyses of all the preceding debris patterns, we can make inferences about the tornadic flow field from directions in which wheat and grass were matted down and in which trees, fence posts, and telephone poles fell or leaned. The final positions of fence posts and telephone poles may not be always representative of the tornado wind as they were connected by wire initially. Partially damaged houses also reveal wind direction. The heaviest damage usually occurs on the windward side (Eagleman and Muirhead, 1971). Also, windward walls tend to fall inwards whereas the other three walls experience outward forces.

13.2 INTERPRETATION OF DEBRIS PATTERNS FROM UNION CITY TORNADO

In this section we interpret information reported by the damage survey crews (both ground and aerial) and deduce some features of the vortex flow in the first few meters above the ground. Since characteristics of the surface damage pattern changed with the visible structure of the funnel, the description is divided into four parts, each covering a different stage of the tornado's life cycle (for more detailed description of life cycle see Purcell, Chapter 11 and Moller *et al.* 1974).

13.2.1 Organizing Stage

Damage began 10 km west of Union City and 2 km north¹ in the form of broken tree limbs. For the next 5 km the tornado (which was moving east at an estimated 9 m s^{-1}) was in the 'organizing stage' of its life cycle since the condensation funnel was a narrow cone which reached the ground only intermittently. However, a debris cloud near the ground was observed continuously throughout this period. Surrounding the upper portion of the funnel was a turbulent rotating wall cloud (in fact, the wall cloud pre-existed the funnel by 30 min). This stage apparently represented a concentration of pre-existing low level mesoscale vorticity into the funnel scale; the vortex was intensifying but in an unsteady manner as evidenced by two observed funnel retractions.

¹Distances from Union City are precisely from the intersection of Highways 81 and 152 (see Fig. 11.2 for map).

The damage pattern confirmed the above picture of the flow. The terrain around Union City is flat farmland and there were few buildings or trees outside town for the tornado to blow down. However, the debris patterns showed definite signs of circulation. For example, on the north side of the damage path, debris from a chicken house and a tool shed were found to the west and a large tree was blown over to the west. On the south side similar evidence was found for westerly winds. The width of the damage path during this stage was about 400 m. Barns, sheds and a silo were blown away, telephone poles were downed but two houses 30 m and 60 m from the apparent center of damage were unharmed except for scars from flying debris so that the damage must be classified as light during this period.

13.2.2 Mature Stage

The next stage was the mature stage, characterized by a very broad condensation funnel in the form of an inverted cone truncated by the surface. The rotating wall cloud still surrounded the upper funnel. The tornado was moving east-southeast during this period of its life. The damage path widened to 500 m and the vortex became immensely destructive. Apparently, the transition from organizing to mature stage was similar to the processes occurring in a numerical experiment described by Leslie (1971). Cyclostrophic balance became established at consecutively lower levels and as the vortex started interacting with the ground, accelerated amplification took place because of restrictions on the inflow (which is confined to the lower boundary layer) and the associated surface pressure fall.

The intensification of the vortex was evident from the total destruction to the Sanders' farm 2 km west of town and to many structures in Union City. All that remained of the Sanders' house (one-story frame construction) was the concrete foundation and debris was widely scattered (Fig. 13.5). The carport was found over 75 m north. A large roof section impacted from a northerly direction, about 300 m west of the house and shattered, leaving a long NNW-SSE arc of small debris. The engine from a car originally parked by the house ended up 300 m south. The car's frame was found just east of the house and other parts such as the horn and grill about 0.8 km east along the center of the damage path. Several cattle were killed in the field south of the house, one by a 5x10 cm board driven through its hips. The Catholic recreation hall on the western edge of town was irreparably damaged with total collapse of its steel frame (Fig. 13.6). One steel I-beam was found 150 m north in a cemetery. Some mobile home frames were also wind driven 50 m northwest into the cemetery. Three other trailer frames were wrapped around the east sides of trees and telephone poles (Fig. 13.7).

Tree falls and debris marks showed pronounced signs of circulation with an appreciable amount of debris landing upstream (relative to tornado translation). For example, in the field immediately west of town many boards (presumably originating from town) were discovered driven into the ground from the NW, N or NE.

The wheat in this portion of the tornado path was badly damaged (some stalks were cropped about half way up) and arrayed in a chaotic pattern. However, the two organized patterns described in Section 13.1 (g) and (h)

13. Debris Pattern Interpretation

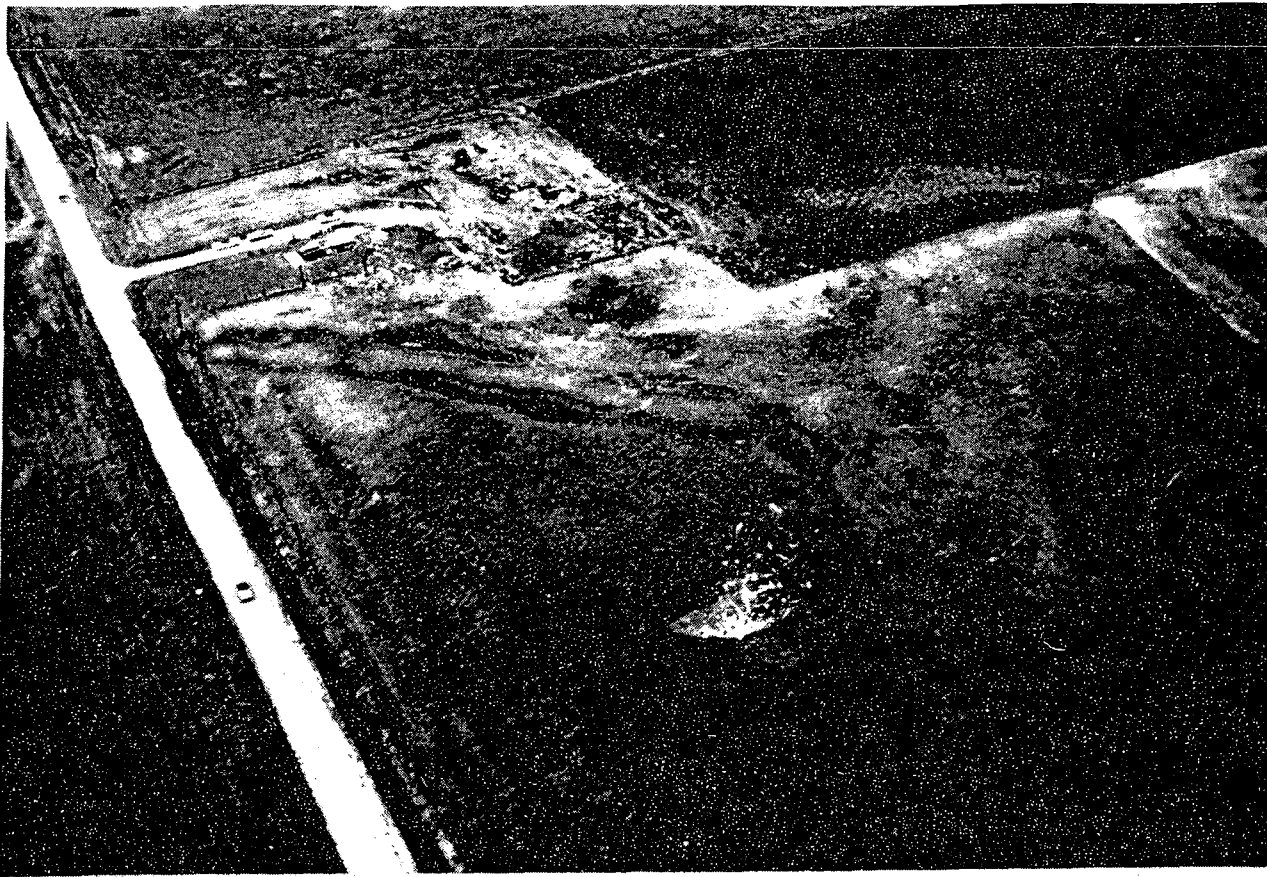


Fig. 13.5 Aerial photograph (toward south-southwest) of the debris from the Sanders' house. Carport roof is light area in lower center.

stood out. The convergence-divergence rows (h) were observed between 3.2 and 2.7 km west of town, and also about 1.0 km west. The swirled wheat bundles (g) were seen in these rows, and were also distributed randomly outside of the rows in this same general area of the damage path. The origin of these wheat patterns is a mystery. We can only speculate that they arise from boundary layer instabilities. The convergence-divergence rows may be visualizations of shallow horizontal roll vortices generated by a local Ekman-type instability.

Mrs. Sanders noted some small dust vortices in the debris cloud as the tornado approached her house. Miniature whirlwinds were also observed moving around the base of the 1957 Kansas City tornado by one observer (Bigler, 1957), and are visible in a movie of the 26 May 1973 Wichita, Kansas tornado (Gerber, personal communication).

The direction of wheat fall in the field east of Sanders' house revealed signs of low level convergence for 40 m each side of the damage center line.



Fig. 13.6 Aerial photograph (toward southeast) of the western side of Union City. The Catholic recreation hall is in the foreground. Photo courtesy of Oklahoma Publishing Company.



Fig. 13.7 Trailer frame bent around broken-off telephone pole.

13. Debris Pattern Interpretation

13.2.3 Shrinking Stage

As the tornado was passing through Union City the funnel narrowed rapidly, and began accelerating to about 15 m s^{-1} , tilting increasingly toward the northeast with height, and veering toward the southeast. In addition, the wall cloud became much smaller and eventually disappeared. The narrower funnel and smaller wall cloud were indications of decreasing circulation, presumably caused by weakening of the parent updraft and by the immediate environment becoming less rich in cyclonic vorticity.

The width of the damage path narrowed to less than 200 m on the east side of town but within this swath property losses were high (Fig. 13.8). Sharp gradients in damage severity were observed on both sides of the damage path.

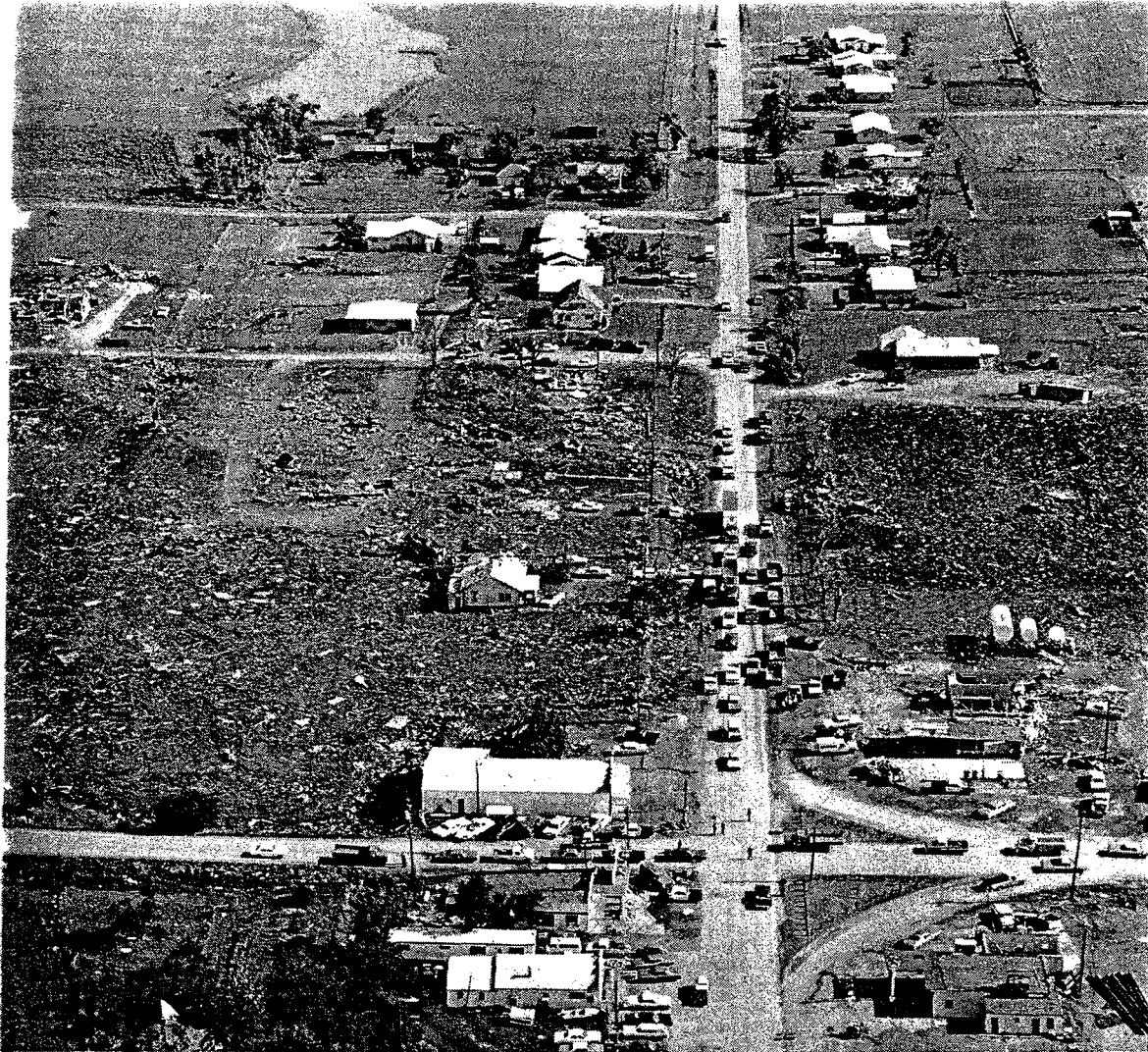


Fig. 13.8 Aerial photograph (toward north) of eastern side of Union City. Intersection of U.S. Highway 81 and State Highway 152 in foreground. Photo courtesy of Oklahoma Publishing Company.

Along the center line of the tornado track the walls of only one house in town withstood the winds. Trees along this line tended to be defoliated but not uprooted whereas on either side trees were uprooted but the leaves were not stripped off.

Evidence for strong radial inflow in the lowest meter was found at the intersection of highways 81 and 152. The tornado passed to the left (east) of this intersection and buildings were damaged on their north and west walls, consistent with mainly tangential winds. However, 1 m high reflector posts at the intersection were smudged with mud on their southwest sides only, implying mainly radial flow into the vortex in the lowest meter. The deposition line and attendant inflow pattern in the fallen wheat described in (i) above are further evidence for such radial flow. They were observed in the fields immediately southeast of town.

The existence of the deposition line suggests that there is a point of strong surface convergence in the vortex core. For a symmetric vortex such a point would exist only if the vortex were of the one-cell variety (Rott, 1958) with updraft along the axis. However, Golden (1974) has observed that waterspouts are two-celled vortices (Sullivan, 1959) with central downdrafts, that they are usually asymmetrical and that at times there is a point of strong convergence located at the edge of the core in the right front quadrant of the vortex. Thus, an asymmetric two-celled vortex could also give rise to a deposition line.

Radial inflow next to the ground is expected according to boundary layer theory. Outside the boundary layer the radial forces are in cyclostrophic balance (inward radial pressure gradient force is balanced by centrifugal force). In the boundary layer, tangential velocity is frictionally retarded, hence the centrifugal force is reduced. However, pressure is nearly constant across the boundary layer except very close to the vortex core. The reduction in centrifugal force thus results in a net inward force which creates inward radial flow along the surface. Experimental laboratory measurements by Ying and Chang (1970) and calculations by Kuo (1971) indicate that the tangential and radial velocities are comparable in magnitude in the boundary layer. However, sophisticated theoretical work matching a laminar boundary layer to a potential vortex by Burggraf *et al.* (1971) showed that for a lower surface of finite radius, the boundary layer in fact has a double structure with an inner layer next to the surface in which the flow is primarily radial and an outer layer of predominantly inviscid nature in which the flow recovers to the external potential vortex. The boundary layer erupts upward very close to the axis.

On both sides of the downed wheat that comprised the inflow pattern were swaths of undamaged wheat running parallel to the deposition line at 20 m distance. Outside of these swaths the wheat was flattened along strips 15 m wide about 100 m from the deposition line. The chaotic manner in which the wheat was laid down suggested that a strong downward flow might have been responsible.

During this stage, the debris from known sources were strewn primarily in cones between south and east. This was most clearly evident from the debris marks (see Section 13.1 (e)) emanating from the Bosler house (2.1 km E, 1.6 km

13. Debris Pattern Interpretation

S of Union City) (Fig. 13.9) and the Ninman house (3.2 km E, 2.9 km S). Heavy wooden and metallic objects and large pieces of roofing were found only on the right side of the southeasterly pointing deposition line. Large debris on the left side were light projectiles such as sheet metal. A movie loop of the tornado at the time it hit Ninman's farm revealed that debris orbiting around the back of the funnel were ejected far ahead of the tornado on the right side--same effect in the 1957 Dallas tornado has been noted by Hoecker (1960). In addition, numerous missiles were generated on the right side. Thus, both the damage and movie observations imply that there was an isotach maximum (hence more damaging winds) on the right side of the funnel. This maximum is due only in part to the translation of the vortex. Asymmetries in the flow relative to the vortex with maximum winds on the right would explain why debris in orbit around the vortex would be centrifuged out on the right side and land ahead of the vortex. The vertical velocities due to the tornado's northeast tilt - upward on the back side, downward on the front side - were also favorable for debris fallout ahead of the tornado. The resulting debris distribution showed little signs of circulation and, in other circumstances, could have been mistaken for straight line wind damage. In fact, damage with no signs of circulation along narrow paths less than 1 km wide, often attributed to plow winds (Huschke, 1959), are probably caused by tornadoes.



Fig. 13.9 Aerial photograph (toward north-northeast) of Bosler's farm showing debris strewn out in cone between south and east. Line of changing albedo in wheat field (upper left) delineates deposition line.

Reynolds (1957), Hall and Brewer (1959), Prosser (1965) and Browning and Donaldson (1965) described other tornadoes which showed no obvious evidence of rotary winds in their damage patterns at times.

There were very few signs of circulation in the damage. Although the damaging winds were predominantly northwesterly, some bales of hay, sheet metal and branches were found NW of their original location at the Bosler's farm. Also, along a fence line 0.8 km SE of town cyclonic rotation was evident from the directions in which fence posts and telephone poles were leaning.

An empty 7600 liter gasoline storage tank (Fig. 13.10) originally supported with others on a pedestal 0.1 km northeast of the intersection of Highways 151 and 82 was discovered badly crumpled 0.8 km SE. It was about 1.5 m in diameter, 3 m long and made of 6 mm steel. Bounce marks on the ground showed that the tank was airborne for 400 m then bounced to its final position. A 60-70 kg steel instrument container and an acetylene tank (Fig. 13.2) were found 1.9 km E, 1.3 km S and 0.8 km E, 0.5 km S of Union City, respectively. Their points of origin were unknown.

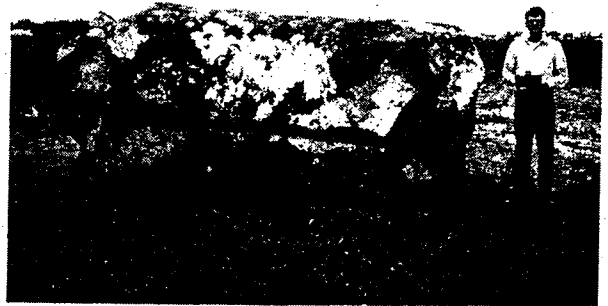


Fig. 13.10 7600 liter gasoline storage tank moved 0.8 km by the tornado.

13.2.4 Decaying Stage

The decaying stage began as the tornado passed the Ninman farm. The tornado's death throes appeared similar to those of waterspouts (Golden, Chapter 12). The vortex became very rope-like, contorted and unsteady before becoming invisible. By this time the mesoscale circulation had become very weak. Until within 1 min of the vortex's demise, a debris cloud (present continuously) indicated the vortex was still in strong contact with the ground.

The Ninman farm was the last structure hit by the tornado. The house, completely swept away, demonstrated that even rope-like tornadoes can be locally destructive. The debris was strewn in a cone along the direction of motion as described in the previous subsection.

13.3 PERIPHERAL DAMAGE

Two areas of Union City were damaged even though they lay completely outside the main damage swath about 400 m from the center of the tornado track. The areas were 400 m W of the intersection of US 81 and SH 152 where three trailers (Fig. 13.11) were damaged and 800 m E of the intersection where three structures were damaged from the southeast. This pattern was consistent

13. Debris Pattern Interpretation

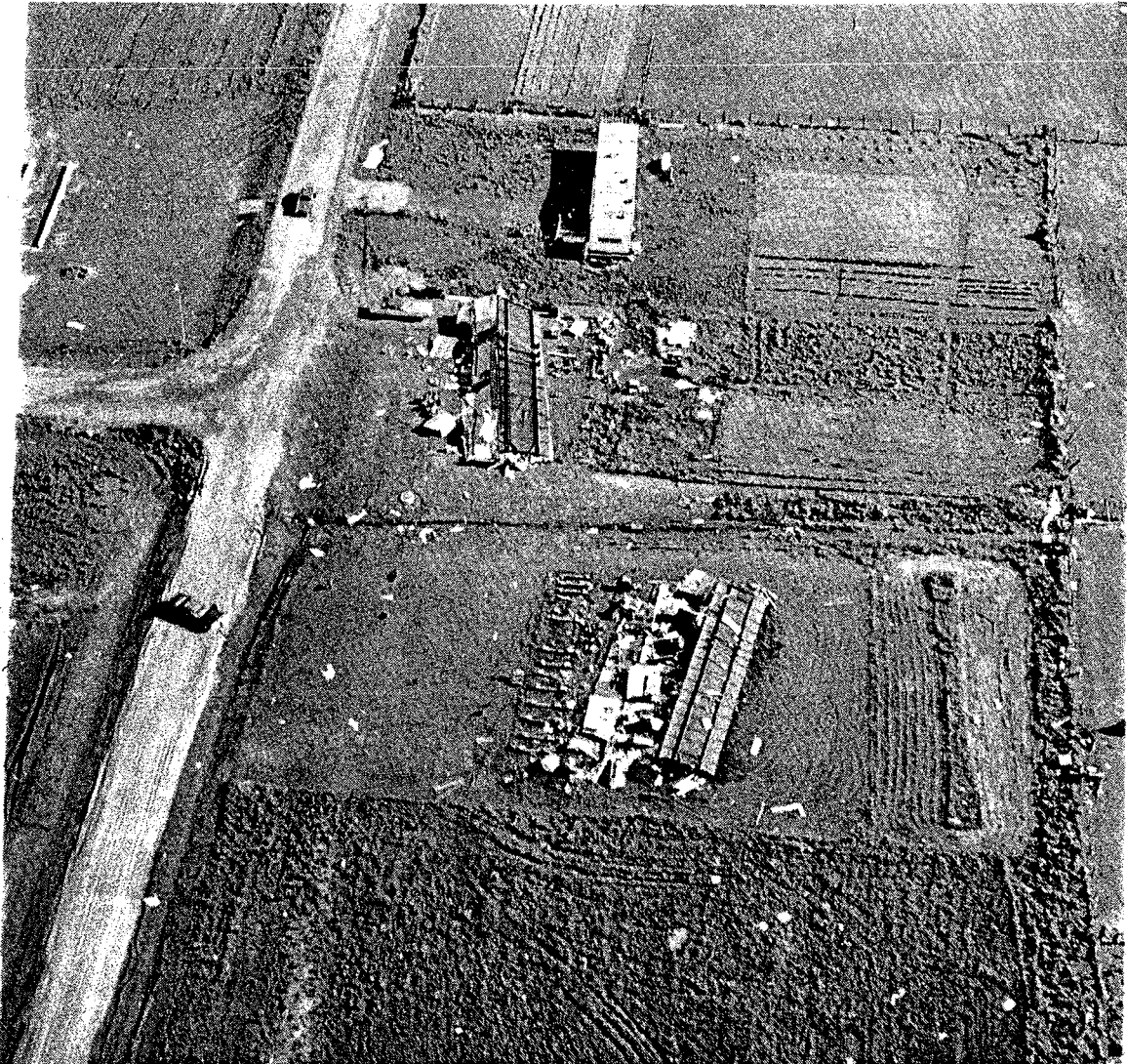


Fig. 13.11 Aerial photograph (toward north) of damaged trailers outside main damage path. Photo courtesy of Oklahoma Publishing Company.

with a secondary vortex rotating around the main tornado at a radius of 400 m. This satellite vortex was not intense enough to have its own condensation funnel--otherwise, it would have been observed by the NSSL intercept team.

13.4 LIST OF MISSILES

Heavy missiles generated by the tornado are listed in Table 13.1 for the interest of engineers working on designs of tornado-proof structures.

TABLE 13.1 *Crudely Estimated Diameter (D), Length (L), and Weight (W) of Heavy Missiles Generated by the Tornado. Units are MKS.*

MISSILE	D	L	W	REMARKS
7600 liter gas storage tank	1.5	3	700	Made of 6 mm steel. Airborne 400 m, then bounced 400 m.
Acetylene storage tank	0.4	1.5	65	
Steel container	1	1.2	60	
Steel I-beams		10	225	Carried 150 m.
Steel trailer frames		15	900	Width 4 m. Carried 50 m.
Cars and pickup trucks		5	1800	Width 2 m.
Car engine		1.2	250	Width 0.6 m. Carried 300 m.
House roofs		10		
Telephone pole sections	0.36	3	100	

13.5 SCORCHING

Scorching and dehydration of vegetation, reported along some tornado tracks (Vonnegut, 1960; Silberg, 1966), was not observed anywhere along the path. Such burning has been associated with intense electrical activity near the funnel; however, no such activity was seen by the NSSL observers any time during the tornado's life cycle.

13.6 CONCLUSIONS

We have shown that the damage caused by the Union City tornado varied in form and intensity during its life cycle. These changes accompanied corresponding changes in morphology. The organizing stage was characterized by a large wall cloud, a debris cloud, and a condensation funnel which was only intermittently in contact with the ground. Damage, light over a path 400 m wide, clearly indicated the vortical nature of the winds. The mature stage was similar, but the condensation funnel was wide and continuously on the ground and damage was severe. Intriguing microscale patterns were seen in the wheat. In the shrinking and decaying stages, the tornado funnel speeded up, became narrow and increasingly tilted. The wall cloud was much smaller. Heavy damage occurred over a 200 m wide path. Evidence was found for strong

13. Debris Pattern Interpretation

radial inflow in the lowest meter above the surface. Generally, debris was thrown ahead of the vortex with heavy objects coming to rest on the right forward side. Signs of circulation were no longer obvious in the debris. We surmise that there was a pronounced isotach maximum on the right side of the vortex during the last two stages.

13.7 ACKNOWLEDGMENTS

Discussions with Dr. Joe Golden helped clarify some deductions about the flow near the tornado. This paper would not have been possible without the observations and interviews conducted by other members of the damage survey crews: Dr. Ron Alberty, Rodger Brown, Charles Clark, J. T. Dooley, Dr. Richard Doviak, Dr. Joe Golden, Dr. Peter Ray, Charles Vlcek, Ken Wilk and David Zittel of NSSL; Charles Doswell, John McGinley, Alan Moeller, Dr. Gene Walker and Randy Zipser of University of Oklahoma; Ralph Donaldson, Air Force Cambridge Research Labs; Robert Gannon, Popular Science; Dr. Bruce Morgan, University of Notre Dame. We are grateful to the Oklahoma Publishing Company for use of their excellent aerial photographs of the damage in Union City. This work was supported partially by the Nuclear Regulatory Commission under Interagency Agreement AT(49-25)-1004.

13.8 REFERENCES

- Bigler, S. G., 1957: Tornado damage surveys. Final Report on Contract Cwb-9116, Department of Oceanography and Meteorology, The Agricultural and Mechanical College of Texas, 85 pp.
- Browning, K. A., and R. J. Donaldson, 1965: Surface weather associated with the severe storms. Chapter 7, A Family Outbreak of Severe Local Storms - A Comprehensive Study of the Storms in Oklahoma on 26 May 1963, K. A. Browning, Editor. Air Force Cambridge Research Labs., Special Reports, No. 32, 346 pp.
- Burggraf, O., K. Stewartson and R. Belcher, 1971: Boundary layer induced by a potential vortex. Phys. Fluids, 14, 1821-1833.
- Eagleman, J., and V. U. Muirhead, 1971: Observed damage from tornadoes and safest location in houses. Preprints, Seventh Conference on Severe Local Storms, Boston, Amer. Meteor. Soc., 171-177.
- Fujita, T. T., 1971: Proposed mechanism of suction spots accompanied by tornadoes. Preprints, Seventh Conf. on Severe Local Storms, Boston, Amer. Meteor. Soc., 208-213.
- _____, D. L. Bradbury and P. G. Black, 1967: Estimation of tornado wind speeds from characteristic ground marks. University of Chicago, SMRP Research Paper 69, 19 pp.

- _____, K. Watanabe, K. Tsuchiya and M. Shimada, 1972: Typhoon-associated tornadoes in Japan and new evidence of suction vortices in a tornado near Tokyo. J. Meteor. Soc. Japan, 50, 431-453.
- Golden, J. H., 1974: On the life cycle of Florida Keys waterspouts, I. J. Appl. Meteor., 13, 676-692.
- _____, 1976: Comparison of Union City tornado life cycle with Florida Keys waterspout life cycle. Chapter 12, The Union City, Oklahoma Tornado of 24 May 1973, R. A. Brown, Editor. NOAA Tech. Memo. ERL NSSL-80, Norman, Nat. Severe Storms Lab., 135-140.
- Hall, R., and R. D. Brewer, 1959: A sequence of tornado damage patterns. Monthly Weather Review, 87, 207-216.
- Hoecker, W. H., Jr., 1960: Wind speed and air flow patterns in the Dallas tornado of April 2, 1957. Monthly Weather Review, 88, 167-180.
- Huschke, R. E., 1959: Glossary of Meteorology. Boston, American Meteorological Society, 638 pp.
- Kuo, H. L., 1971: Axisymmetric flows in the boundary layer of a maintained vortex. J. Atmos. Sci., 28, 20-41.
- Leslie, L. M., 1971: The development of concentrated vortices: A numerical study. J. Fluid Mech., 48, 1-21.
- Moller, A., C. Doswell, J. McGinley, S. Tegtmeier and R. Zipser, 1974: Field observations of the Union City tornado in Oklahoma. Weatherwise, 27, 68-77.
- Prosser, N. E., 1965: Aerial photographs of a tornado path in Nebraska, May 5, 1964. Monthly Weather Review, 92, 593-598.
- Purcell, D., 1976: History of the Union City tornado. Chapter 11, The Union City, Oklahoma Tornado of 24 May 1973, R. A. Brown, Editor. NOAA Tech. Memo. ERL NSSL-80, Norman, Nat. Severe Storms Lab., 123-133.
- Reynolds, G. W., 1957: A common wind damage pattern in relation to the classical tornado. Bull. Amer. Meteor. Soc., 38, 1-5.
- Rott, N., 1958: On the viscous core of a line vortex. Zeit. f. Angew. Math. u. Physik, 96, 543-553.
- Silberg, P. A., 1966: Dehydration and burning produced by the tornado. J. Atmos. Sci., 23, 202-205.
- Staats, W. F., and M. Turrentine, 1956: Some observations and radar pictures of the Blackwell and Udall tornadoes of May 25, 1955. Bull. Amer. Meteor. Soc., 37, 495-505.

13. *Debris Pattern Interpretation*

- Sullivan, R. D., 1959: A two-cell vortex solution of the Navier-Stokes equation. J. Aero Space Sci., 26, 767-768
- Vonnegut, B., 1960: Electrical theory of tornadoes. J. Geophys. Res., 65, 203-212.
- Ward, N. B., 1972: The exploration of certain features of tornado dynamics using a laboratory model. J. Atmos. Sci., 29, 1194-1204.
- Ying, S. J. and C. C. Chang, 1970: Exploratory model study of tornado-like vortex dynamics. J. Atmos. Sci., 27, 3-14.

Chapter 14

AIRFLOW CHARACTERISTICS AROUND THE UNION CITY TORNADO

Joseph H. Golden¹ and Daniel Purcell

*National Severe Storms Laboratory
Norman, Oklahoma 73069*

The NSSL tornado intercept team intercepted and photographed an intense tornado that struck Union City, Oklahoma on 24 May 1973. The life cycle of the tornado was photographically documented. Photogrammetric data have permitted velocities to be measured from debris and cloud tag motions. When the tornado was at its peak size and intensity, maximum measured horizontal velocities in the debris cloud were 60 to 80 m s⁻¹ at 90 m elevation and radius of 200 to 250 m. At the same time, cloud tags rotating around the upper periphery of the tornado funnel had horizontal velocities as strong as 30 to 45 m s⁻¹ at radii of 400 to 700 m from the tornado's axis. A few representative calculations of upward velocities yield 13 to 30 m s⁻¹ in the debris cloud below 100 m elevation, and 10 to 15 m s⁻¹ in a "feeder" band of cloud tags which spiralled into the tornado near cloud base from the northeast. During the tornado's decaying stage, tangential velocities of particles orbiting the funnel ranged from 40 to 65 m s⁻¹, at radii generally between 25 and 50 m. Throughout the tornado's lifetime, its apparent flow structure was strongly asymmetric in both rotational and vertical flow components.

14.1 Introduction

The most intensely concentrated atmospheric vortex, the tornado, has received increasing attention in the research community during the last two decades. More sophisticated laboratory vortex models have been developed (Ying and Chang, 1970; Ward, 1972), but some of the underlying assumptions and boundary restrictions remain questionable in light of limited tornado observations. Physically realistic numerical vortex models (Gutman, 1957; Kuo, 1966, 1971; and Leslie, 1971) produce very diverse flow patterns in the radial-vertical plane.

Most of our current knowledge of tornado structure has been derived from piecemeal reconstruction and analysis of eyewitness accounts and photographs of tornadoes (e.g., Dinwiddie, 1959; Beebe, 1960; Fujita, 1960; Williams,

¹Present affiliation: NOAA, Environmental Research Laboratories, Office of Programs, Boulder, Colorado 80302.

14. *Airflow Around Tornado*

1960). There remains much disagreement over the three-dimensional flow structure of a tornado, particularly maximum horizontal windspeeds and the vertical motions within and surrounding the core. Several attempts have been made to estimate the maximum tangential windspeeds and their distribution near funnels by applying the cyclostrophic wind equation to still tornado photographs (Fujita, 1960; Glaser, 1960; Dergarbedian and Fendell, 1970). This approach also has employed the hydrostatic approximation, the validity of which at low levels in tornadoes is open to question. Tornadoes have passed within a mile or two of conventional anemometers, and the instruments recorded gusts of 45 to 70 m s⁻¹ (Fujita et al. 1970; Barnes, 1974). Another indirect method of estimating tornado windspeeds near the ground has been assessments of structural damage caused by tornadoes (Segner, 1960). Mehta et al. (1971) performed a careful engineering analysis of many buildings damaged by the huge Lubbock, Texas tornado on 11 May 1970. Their best estimate of the highest wind velocity generated near the ground by the storm was 90 m s⁻¹, but most of the damage was caused by winds in the range 35 to 55 m s⁻¹. Aerial surveys of tornado damage have revealed characteristic ground marks, sometimes in the form of multiple cycloidal swaths (Van Tassel, 1955). Fujita et al. (1967) hypothesized that the cycloidal marks are produced by one or more vortices rotating around the periphery of the tornado core. Using the shape and spacing of the cycloidal marks and inferred values of the ratio of the tornado's tangential to translational speeds, Fujita (1967) found maximum windspeeds of almost 90 m s⁻¹ for one of the Palm Sunday, 1965 tornadoes. Similar calculations on cycloidal swaths in the Lubbock tornado damage led Fujita (1970) to conclude that rotational speeds in that tornado were between 65 and 130 m s⁻¹.

Probably the most reliable estimates of rotational and vertical motion fields in tornadoes have been derived from photogrammetric analyses of eyewitness motion pictures. The most definitive photogrammetric studies are those by Fujita (1960) on the Fargo, North Dakota tornadoes of 20 June 1957 and Hoecker (1960a, b) on the Dallas, Texas tornado on 2 April of the same year. Both efforts utilized scaling of the motion pictures from known camera characteristics and site surveys to synthesize air tracer motions near the tornado. Fujita (1960) tracked cloud tags in rotation around the bottom of a suspended funnel and edge of the parent wall cloud at Fargo, and thereby derived both tangential and vertical windspeeds. No eyewitness film data were available for the tornado's lower debris cloud at Fargo. Hoecker (1960 a,b) synthesized his photogrammetric tracking of cloud tags, dust parcels and solid debris around the Dallas tornado funnel to obtain radial-vertical profiles of tangential and vertical windspeeds. A comprehensive review of previous observational and theoretical tornado research is given by Kessler (1970) and Davies-Jones and Kessler (1974). Lilly (1965) has noted that further progress in both the analytic-numerical and laboratory modelling of tornadic vortices is hindered by the lack of observational data.

14.2 DATA SOURCES AND ANALYSIS TECHNIQUES

The primary data source for this paper is high-resolution, 16 mm color motion picture footage taken of the Union City tornado from the tornado intercept vehicle located 5 km south of Union City. Two Skylab movie cameras,

on loan from the National Aeronautics and Space Administration (NASA), were run at 24 frames per second. We started filming the tornado funnel as it descended to the ground for the second time at 1545 CST 8.5 km northwest of our position. As the tornado approached the western outskirts of Union City at 1556, both NASA cameras ran out of film. A Super-8 zoom movie camera was utilized to record the tornado as it continued southeast of Union City.

In addition, a fairly complete sequence of regular, wide-angle and telephoto still photographs were taken of the tornado throughout its life-cycle from the intercept vehicle. Well-documented photographic and meteorological observations were taken by two University of Oklahoma student teams, viewing the tornado from nearly opposite directions (Moller et al., 1974). Finally, many valuable eyewitness still photographs and three movies were taken of the tornado from all directions, encompassing most of its life cycle. The excellent surface visibility, immense size of the funnel and tornado warnings issued by the National Weather Service all contributed to enhanced public awareness and observations of this storm.

The photographic sites were carefully marked and subsequently surveyed with a transit and rod. Landmarks clearly visible in the foreground of the film sequences were located in vertical and horizontal angular measure with respect to camera location and principal axis of the lens. Scales of features in the movie frames were derived by trigonometrically combining the angular measurements with known radial distances to the tornado's surface damage track and landmarks. Landmarks such as telephone poles and large trees were most useful in the scaling procedure. Overall scaling errors are estimated to be less than ± 2 percent.

Analysis of the Union City film data was divided into two parts: (a) scaling and (b) tracking of air tracers around the tornado at various elevations. Closed movie loops of 200 frames each (at constant focal length) were made from NASA enhanced copies of the original 16 mm and Super-8 (enlarged to 16 mm) tornado footage. After scaling characteristic tornado features on each movie loop, aggregates of debris near the tornado's base or cloud tags in peripheral rotation about its upper portion were tracked on a simple grid. In some clear-cut cases, the outline of a tracer element was followed and recorded at regular frame intervals. In all cases, an effort was made to retrack the same tracer element (debris aggregate or cloud tag) several times for consistency; the resulting mean velocity value was accepted only if all tracking estimates were within 10 percent of the mean.

An overall scaled drawing of the Union City tornado which illustrates features tracked on the film loops is given in Fig. 14.1. Note the rotation of cloud elements around the upper periphery of the funnel; the leading edge of the brightest portions of cloud streamers at different radii and elevations have been traced at regular frame intervals. Protrusions on the funnel wall and low-level cloud pendants on the funnel were observed to be moving upward at times. A schematic, scaled debris cloud is also indicated in the figure with typical orbital trajectories of debris elements. The first debris and upper-peripheral cloud tag tracking on the film was performed during a two-minute interval (1554-1556) when the tornado was about 2 km west of Union City. It is apparent from various photographs taken during this period that the rotating debris cloud is asymmetric with respect to the tornado's center. Surface damage analyses in this area indicate that the debris particles are

14. Airflow Around Tornado

composed primarily of dust and small bits of vegetation (see Purcell, Chapter 11 and Davies-Jones et al., Chapter 13). There were no manmade dwellings in the tornado path during the primary film sequences used in debris tracking. In this regard, we would expect that trajectories derived from the tracking of these aggregates of small debris particles should be more representative of actual air motion than larger pieces of building material. On the other hand, keeping in mind the relatively homogeneous size distribution of debris, we could not follow discrete debris elements for one or more revolutions around the tornado. The pattern of low-level windflow and tangential windspeed analysis given later were derived by the repetitive tracking of darker aggregates in the debris cloud. These aggregates had irregular shapes, as depicted in Fig. 14.1, with largest dimension about 10 to 30 m. In general, it was not possible to distinguish debris aggregates on the near edge of the debris annulus from those in the rear. Separation and radial location was possible in some cases by carefully noting the slowing down and radius of curvature of debris aggregates as their orbits became parallel to the line of sight.

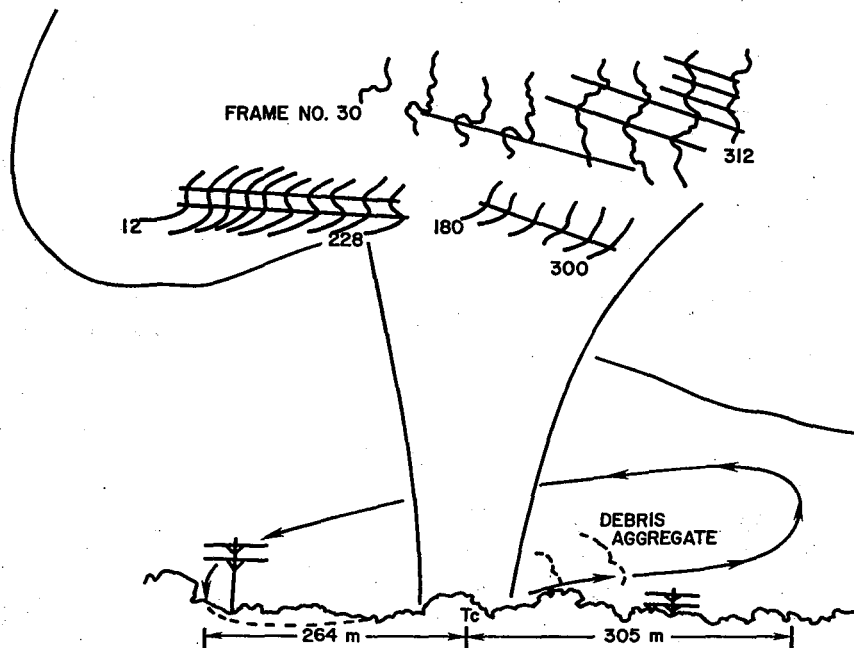


Fig. 14.1 Schematic outline of Union City tornado funnel and upper wall cloud from single movie frame showing features tracked photogrammetrically on movie loops. Sequential outline of cloud tags and streamers in wall cloud and typical trajectory and displacement of debris aggregate are superimposed. Note asymmetric structure of debris cloud with respect to funnel axis.

14.3 PHOTOGAMMETRIC VELOCITY FIELDS

14.3.1 Mature Stage

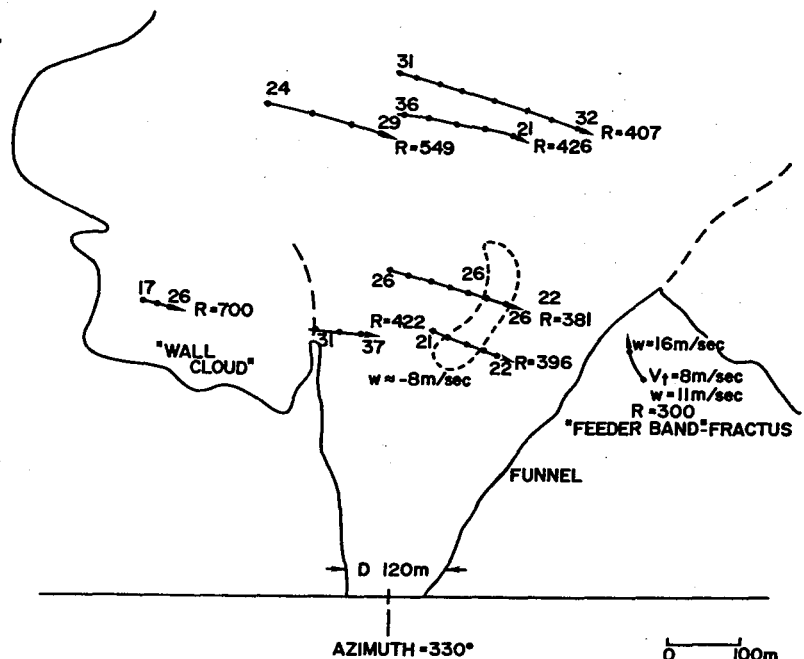
At the final NSSL intercept vehicle stopping point, the lowest 55 to 80 m of the tornado's debris cloud circulation was obscured by an elevated railroad track and shrubbery in the foreground (see Fig. 14.1). Moreover, debris circulating around the left side of the tornado funnel was illuminated by bright sunlight. Poor photographic contrast in this region obviated the

possibility of tracking debris aggregates there. Thus, the bulk of our debris velocity data was obtained to the right of the funnel wall, at elevations from 75 to 145 m. Since the debris aggregates have a variable optical depth in the debris cloud, our derived velocities represent means through a horizontal depth estimated to be of the order of 50 m.

Between 1552 and 1554, photogrammetric measurements at an estimated radius of 200 m indicate tangential velocities of 50 to 80 m s⁻¹ at heights of between 60 and 120 m above the ground; maximum velocities occurred at a height of 90 m. Vertical velocity components in the same height interval range from about 13 to 30 m s⁻¹. Measurements imply that as the small debris particles are picked up off the ground on the south side of the tornado, they accelerate (with the wind) upward and outward before orbiting the east side of the tornado. Comparative measurements have been obtained by Fujita (1960) who tracked cloud pendants around the base of the Fargo tornado funnel (height of approximately 100 m). He found tangential velocities between 40 and 48 m s⁻¹ for radii ranging from 30 to 110 m.

A composite, scaled outline of the tornado funnel with cloud-tag motion vectors superimposed is given in Fig. 14.2. Some of these cloud motions were derived from the successive cloud-tag positions traced on Fig. 14.1. Approximate radius from the funnel center has been noted for each major cloud streamer. Since the cloud-tag speeds are those actually measured in the image plane, only those near the tilted center line of the funnel represent true velocities. Visual observations from the NSSL intercept vehicle of peripheral cloud rotation about the upper southeast quadrant of the funnel indicated that cloud elements were sinking and evaporating. This downward motion, confirmed in Fig. 14.2, is in excess of 8 m s⁻¹ halfway up the funnel, near its closest edge. Maximum values of cloud-tag tangential velocities (along each trajectory near the tilted center line) range from 30 to 40 m s⁻¹ at a radius of approximately 400 m.

Fig. 14.2 Scaled outline of tornado funnel with cloud-tag trajectories superimposed. Cloud-tag velocities (m s⁻¹) and radii (m) are indicated along each trajectory. Since cloud-tag speeds are those actually measured in the image plane, only those near the tilted funnel center line represent the true velocities. Note pronounced sinking motion, as large as -8 m s⁻¹ (dashed region), on SE side of funnel and rising motion into base of "feeder band" of clouds spiralling into upper funnel from NE.



14. Airflow Around Tornado

14.3.2 Shrinking Stage

Fig. 14.3 illustrates changes in tornado structure when the funnel was about 4 km NE of the camera site. Note that there is no well-defined 'wall cloud' and precipitation is evident in the near-background to the funnel. Most important, there were cloud streamers which rotated around the upper periphery of the funnel.

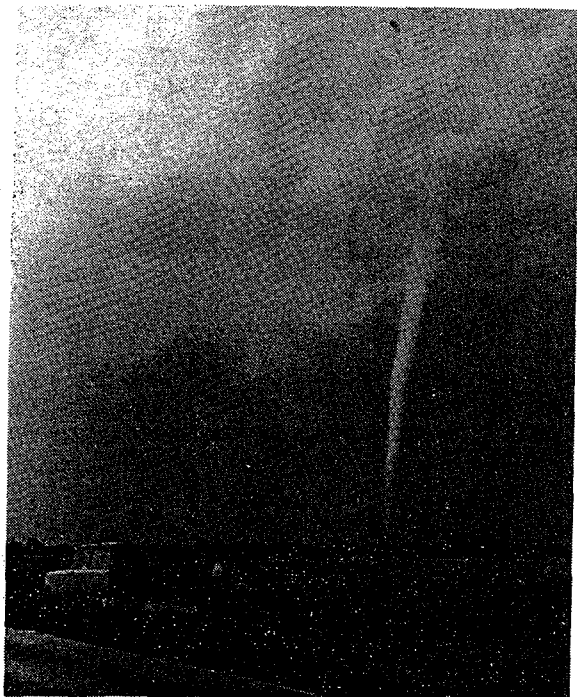


Fig. 14.3 Union City tornado during shrinking stage. NSSL intercept team and vehicle in foreground. Photo courtesy of Robert Gannon.

radius from 25 to 50 m. In general, the tangential velocities of particles orbiting the funnel ranged from 40 to 60 m s^{-1} . Maximum velocities occurred at heights between 50 and 80 m. Most debris tended to sink as it orbited ahead of the vortex.

Using the funnel's upper section for scaling and orientation, cloud-tag velocities of 35 to 45 m s^{-1} were derived for mean rotation radii of 100 m (1600-1601 CST). There are definite indications that cloud tags evaporated as they descended around the right side of the tilted funnel, as was apparent when the tornado was much larger west of Union City.

14.3.3 Decaying Stage

As the tornado continued toward the southeast, it entered the decaying stage just as the tornado destroyed the Ninman house (see Purcell, Chapter 11). At that point, the tornado was about 3 km ENE of the NSSL intercept vehicle location. Large amounts of debris from the house could be followed in orbits at several elevations around the tornado for several successive frames on the film (1602-1603 CST). It was not possible to determine radii for all debris particles tracked, but those which could be followed in revolution around the right side of the funnel ranged in

14.4 CONCLUSIONS

Photogrammetrically derived horizontal wind speeds indicate that after devastating Union City, the tornado decreased in both size and, to a lesser extent, intensity. Using representative maximum rotational windspeeds and estimated true radii, we find that the tornado's debris-cloud circulations decreased from 6.0×10^4 to $1.6 \times 10^4 \text{ m}^2 \text{ s}^{-1}$ between the mature and decaying stages. These values are both of the same order of magnitude as the circulation

computed from Hoecker's (1960a) data for the Dallas tornado. Wind speeds should be taken as conservative estimates of both the expected maxima and tangential components at larger radii. Somewhat higher tangential velocities may be found within the funnel wall, or below the apparent horizon. Correspondingly, a representative value of circulation in the upper, peripheral cloud tags when the tornado was southeast of Union City is $2.8 \times 10^4 \text{ m}^2 \text{ s}^{-1}$. This is about one-fourth of the cloud tag circulation computed when the tornado was west of Union City.

Finally, the tornado's structure, inferred from debris and cloud-tag trajectories, appears strongly asymmetric in both rotational and vertical flow components. Rotational flow asymmetries may have been due in part to the tornado's differing translation speeds before and after striking Union City. Vertical motion asymmetries can be related in part to the three-dimensional vortex tilt, but they may have a changing dynamical cause as well. The maximum rotational velocities in the tornado's debris cloud west of Union City are of comparable magnitude to Hoecker's (1960a) for the Dallas tornado; however, the Union City funnel was much broader, wind speeds higher over a larger radial distance outward and maxima occurred at higher elevations above the ground.

14.5 ACKNOWLEDGMENTS

We extend our appreciation to NASA's L.B.J. Space Center, Houston, for lending us the two 16 mm cameras and for making enhanced copies of the original footage. We thank the other members of the 1973 NSSL Tornado Intercept Project, Dr. Bruce Morgan of Notre Dame University, Dr. Gary Achtemeier and Charles Vlcek for their contributions to success. Gordon Gerber assisted with the photogrammetric measurements. Dr. Robert Davies-Jones provided useful comments on this manuscript. This work was supported partially by the Nuclear Regulatory Commission under Interagency Agreement AT(49-25)-1004.

14.6 REFERENCES

- Barnes, S. L., 1974: Papers on Oklahoma thunderstorms, April 29-30, 1970. NOAA Tech. Memo. ERL NSSL-69, Norman, National Severe Storms Laboratory, 233 pp.
- Beebe, R. G., 1960: The life cycle of the Dallas tornado. Research Paper No. 41, The Dallas Tornadoes of April 2, 1957, Washington, D.C., U.S. Weather Bureau, 3-9.
- Davies-Jones, R. P., and E. Kessler, 1974: Tornadoes. Chapter 16 in Weather and Climate Modification, W. N. Hess, Editor, New York, John Wiley and Sons, 552-595.
- _____, D. W. Burgess, L. R. Lemon and D. Purcell, 1976: Interpretation of surface marks and debris patterns from the Union City tornado. Chapter 13, The Union City, Oklahoma Tornado of 24 May 1973, R. A. Brown, Editor. NOAA Tech. Memo. ERL NSSL-80, Norman, Nat. Severe Storms Lab., 141-156.

14. *Airflow Around Tornado*

- Dergarbedian, P., and F. Fendell, 1970: Estimation of maximum wind speeds in tornadoes. Tellus, 22, 511-515.
- Dinwiddie, F. B., 1959: Waterspout-tornado structure and behavior at Nags Head, N.C., August 12, 1952. Mon. Wea. Rev., 87, 239-250.
- Fujita, T., 1960: A detailed analysis of the Fargo tornadoes of June 20, 1957. Research Paper No. 42, Washington, D.C., U.S. Weather Bureau, 67 pp.
- _____, 1967: Estimated wind speeds of the Palm Sunday tornadoes. SMRP Research Paper No. 53, The University of Chicago, Dept. of Geophys. Sci., 25 pp.
- _____, 1970: The Lubbock tornadoes: A study of suction spots. Weatherwise, 23, 161-173.
- _____, D. L. Bradbury and P. G. Black, 1967: Estimation of tornado wind speeds from characteristic ground marks. SMRP Research Paper No. 69, Univ. of Chicago, Dept. of Geophys. Sci., 19 pp.
- _____, _____ and C. F. Van Thullenar, 1970: Palm Sunday tornadoes of April 11, 1965. Mon. Wea. Rev., 98, 29-69.
- Glaser, A. H., 1960: An observational deduction of the structure of a tornado vortex. Cumulus Dynamics, C. E. Anderson, Editor, Oxford, Pergamon Press, pp. 157-166.
- Gutman, L. N., 1957: Theoretical model of a waterspout. Bull. Acad. Sci. USSR (Geophys. Ser.), New York, Pergamon Press translation, 1, 87-103.
- Hoecker, W. H., 1960a: Wind speed and air flow patterns in the Dallas tornado of April 2, 1957. Mon. Wea. Rev., 88, 167-180.
- _____, 1960b: The dimensional and rotational characteristics of the tornadoes and their parent cloud system. Research Paper No. 41, The Dallas Tornadoes of April 2, 1957, Washington, D.C., U. S. Weather Bureau, 53-112.
- Kessler, E., 1970: Tornadoes. Bull. Amer. Meteor. Soc., 51, 926-936.
- Kuo, H. L., 1966: On the dynamics of convective atmospheric vortices. J. Atmos. Sci., 23, 25-42.
- _____, 1971: Axisymmetric flows in the boundary layer of a maintained vortex. J. Atmos. Sci., 28, 20-41.
- Leslie, L. M., 1971: The development of concentrated vortices: A numerical study. J. Fluid Mech., 48, 1-21.
- Lilly, D. K., 1965: Experimental generation of convectively driven vortices. Geofisica Internacional, 5, 43-48.
- Mehta, K. C., J. R. McDonald, J. E. Minor and J. A. Sanger, 1971: Response of structural systems to the Lubbock storm. Storm Res. Report 3, Institute for Disaster Research, Texas Tech University.

- Moller, A., C. Doswell, J. McGinley, S. Tegtmeier and R. Zipser, 1974: Field observations of the Union City tornado in Oklahoma. Weatherwise, 27, 68-77.
- Purcell, D., 1976: History of the Union City tornado. Chapter 11, The Union City, Oklahoma Tornado of 24 May 1973, R. A. Brown, Editor. NOAA Tech. Memo. ERL NSSL-80, Norman, Nat. Severe Storms Lab., 123-133.
- Segner, E. P., 1960: Estimates of minimum wind forces causing structural damage. Research Paper No. 41, The Dallas Tornadoes of April 2, 1957, Washington, D.C., U. S. Weather Bureau, 169-175.
- Van Tassel, E. L., 1955: The North Platte Valley tornado outbreak of June 27, 1955. Mon. Wea. Rev., 83, 255-264.
- Ward, N. B., 1972: The exploration of certain features of tornado dynamics using a laboratory model. J. Atmos. Sci., 29, 1194-1204.
- Williams, D. T., 1960: On the role of a subsidence inversion. Research Paper No. 41, The Dallas Tornadoes of April 2, 1957, Washington, D.C., U. S. Weather Bureau.
- Ying, S. J., and C. C. Chang, 1970: Exploratory model study of tornado-like vortex dynamics. J. Atmos. Sci., 27, 3-14.

Chapter 15

EVOLUTION OF THE DOPPLER RADAR TORNADIC VORTEX SIGNATURE IN THE UNION CITY STORM

Rodger A. Brown and Leslie R. Lemon¹

*National Severe Storms Laboratory
Norman, Oklahoma 73069*

Doppler velocity measurements in the Union City storm have revealed--for the first time--a unique tornadic vortex signature (TVS) associated with a tornado. This signature--approximately one beamwidth across--documents the spatial and temporal evolution of the Union City tornado. The TVS originates at storm midlevels, descends to the ground with the tornado, becomes most intense when the tornado is largest and finally disappears at all heights when the tornado dissipates.

15.1 INTRODUCTION

The promise of Doppler radar has been tornado detection and determination of tornadic wind speeds (e.g., Atlas, 1963). Various investigators have used Doppler velocity spectra of within-storm motions to deduce the presence of tornadoes (e.g., Smith and Holmes, 1961; Kraus, 1973; Zrnic *et al.*, 1976). A continuous-wave Doppler radar used by Smith and Holmes measured velocities up to 92 m s^{-1} in the developing funnel of a major tornado that struck El Dorado, Kansas on 10 June 1958. For pulsed Doppler radars that have low pulse repetition frequencies, Zrnic *et al.* (1976) proposed a technique for estimating peak tangential velocities from the folded Doppler velocity spectra; folding refers to the situation where velocities greater than the radar's velocity-measuring capability are aliased back into the measurable interval, thus greatly complicating spectrum interpretation. (See Brown, Appendix E, for more information about spectrum folding.)

In this chapter, we discuss a new way to detect tornadoes and estimate peak velocities without the use of Doppler velocity spectra. We take advantage of the mean of the Doppler velocity spectrum; the mean can be computed in real-time--using a covariance estimator (e.g., Sirmans and Bumgarner, 1975), for example--without requiring knowledge of spectral characteristics. Up to the time of the NSSL Doppler velocity measurements in the Union City, Oklahoma tornadic storm of 24 May 1973, it had not been expected that the presence of a tornado could be detected in a field of mean Doppler velocity values. However, data collected on that day did reveal a distinct tornadic vortex signature

¹Present affiliation: National Severe Storms Forecast Center, Techniques Development Unit, Federal Building, Kansas City, Missouri 64106.

15. Tornadoic Vortex Signature

(TVS).² We compare the measurements with simulations and then, after establishing the nature of the TVS, proceed to describe the temporal and spatial behavior of the tornadoic vortex within the storm.

15.2 VORTICES MEASURED BY DOPPLER RADAR

The single Doppler velocity signature of a vortex is a function of vortex size relative to radar beam size. At one extreme, mesoscale vortices--having dimensions considerably greater than the beamwidth--produce a unique signature when mean Doppler velocity values are plotted as a function of range and azimuth (e.g., Donaldson, 1970; Lemon and Burgess, Chapter 8).

At the other extreme, a tornado vortex within a radar beam is expected to produce a broad velocity spectrum with a mean of zero (e.g., Atlas, 1963; Lhermitte, 1964). However, when the radar beam is not centered on the vortex, it is difficult to accurately predict the spectra and mean Doppler velocity fields. Fortunately, Zrnic recently developed a model that simulates a Doppler radar looking at a Rankine combined vortex (see Zrnic and Doviak, 1975). The radar and vortex characteristics are sufficiently flexible that the model can be used to simulate Doppler velocity measurements in vortices ranging from very small tornadoes to large mesocyclones. The model also allows the reflectivity profile across the vortex to be varied; a uniform profile is used for the simulations presented in this paper.

The Zrnic model aids understanding of data from a finite Doppler radar beam scanning across a vortex. In a Rankine combined vortex (heavy curve in

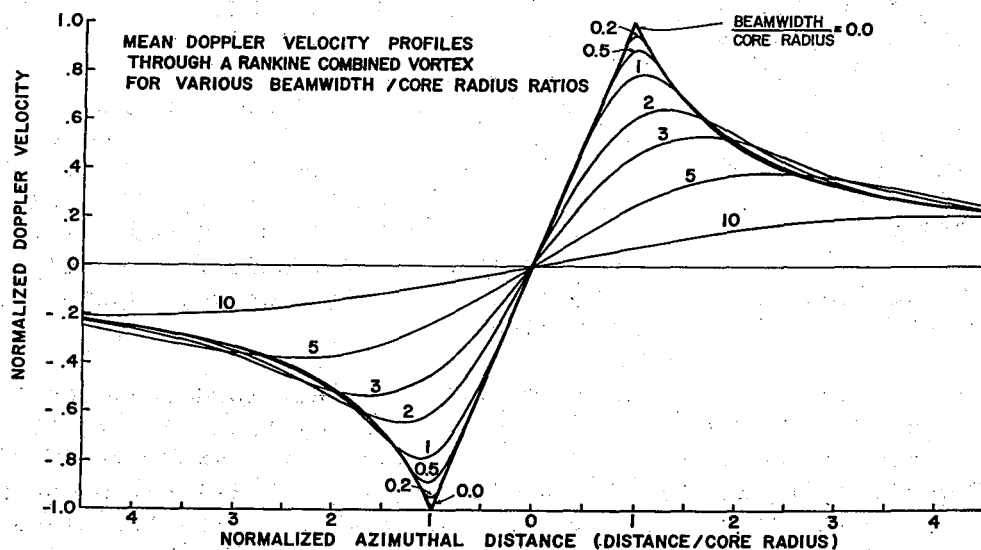


Fig. 15.1 Theoretical change of mean Doppler velocity azimuthal profile through a Rankine combined vortex (heavy curve labeled 0.0) as the beamwidth becomes progressively larger relative to the vortex core radius. Velocities and distances are normalized relative to peak vortex tangential velocity and core radius of peak velocity, respectively.

²This signature had been referred to by the interim descriptive name of "gate-to-gate shear" by Burgess et al. (1975 a,b) and Lemon et al. (1975).

Fig. 15.1), the tangential velocity increases linearly until the maximum velocity at the outer edge of the "core" is reached then decreases inversely proportional to radius. Various sized vortices generated by the model can be normalized by dividing all velocities by the maximum core velocity and by dividing all lengths by the core radius.

As indicated in Fig. 15.1, when the radar half-power beamwidth is a small fraction of the vortex core radius (beamwidth/core radius ratios much less than one), Doppler velocity measurements reproduce the mesoscale vortex very well. However, when the beam becomes significantly wider than the core radius, and the vortex center is encompassed by the beam, some portion of both the positive and negative vortex peaks will be within the beam and they will tend to cancel each other. Therefore, one would not expect the mean Doppler velocity value to maximize until the beam edge has just cleared the vortex center. For example, when the beamwidth is three times the core radius, the peak is approximately 1.5 core radii or one-half beamwidth from the center. Likewise, for beamwidths 5 and 10 times greater than the core radius, the peaks are at approximately 2.5 and 5 core radii, respectively. Also, the wider the beam, the greater the smoothing of the true tangential velocity profile and consequently the smaller the magnitude of the peak Doppler velocities. Detectability decreases with range as the beam becomes larger relative to the vortex.

Since the Doppler velocity profiles appear to peak at a radius of about one-half beamwidth, the curves in Fig. 15.1 were replotted relative to beamwidth. The resulting curves (Fig. 15.2) vividly portray what we call the tornadic vortex signature (TVS). The peak-to-peak diameter is not significantly affected by the size of the within-beam tornado. However, signature amplitude, which is affected, plays an important role in TVS detectability. The TVS can not be resolved unless the peak-to-peak Doppler velocity shear is appreciably greater than the background cyclonic shear produced by the parent mesocyclone.

Several other practical limitations must be considered when attempting to identify tornadic vortex signatures from mean Doppler velocity measurements. First of all, when data are collected at discrete azimuthal increments, peak values may not be sampled when the sampling interval is greater than one beamwidth. Secondly, Zrnic and Doviak (1976) have shown that a radar antenna rotating rapidly relative to the sampling time has an effectively broadened beamwidth. Thus, for a given peak tangential velocity and tornado size, the amplitude of the TVS will decrease as the antenna rotation rate increases.

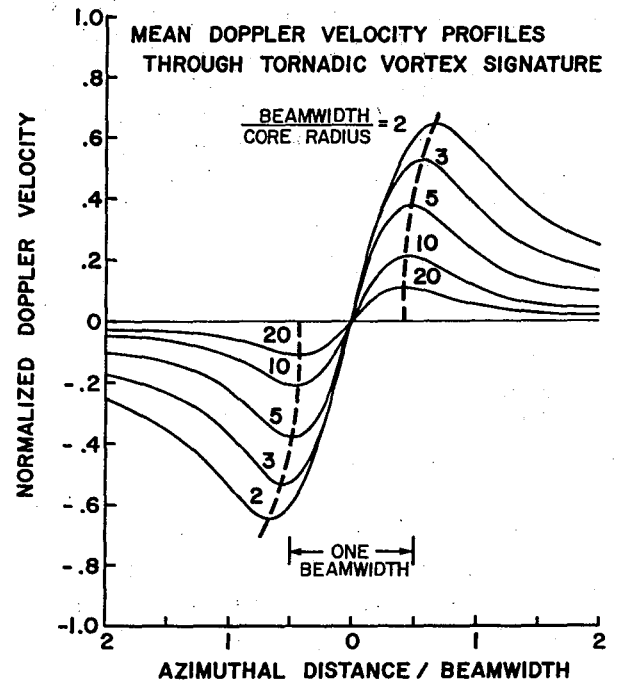


Fig. 15.2 Theoretical change in size and magnitude of tornadic vortex signature as radar beamwidth changes relative to core radius of peak tangential velocity in tornado.

15. Tornadoic Vortex Signature

15.3 SIGNATURE OF THE UNION CITY TORNADO

The NSSL 10-cm pulsed Doppler radar has a 0.8 deg half-power (one way) beamwidth and 0.15 km pulse length. Using this radar, data were collected in the Union City storm primarily with an azimuthal sampling interval of 1.0 deg or 1.25 beamwidths; it has been fortuitous for TVS detection that data rarely are collected at intervals greater than 1.0 deg.

Discovery of the TVS was facilitated by its anomalous character relative to the surrounding mean Doppler velocity field (Figs. 15.3 and 15.4). At 0° elevation, the TVS coincides very closely with the surface damage path. As an example, the shaded TVS at 1545 in Fig. 15.3--with a Doppler velocity gradient from -30 to +23 m s⁻¹ in less than 1 km--is positioned on the tornado azimuth (black circle) and within a few hundred meters in range. The range uncertainty is a consequence of the sampling volumes being four pulse lengths (0.6 km) apart.

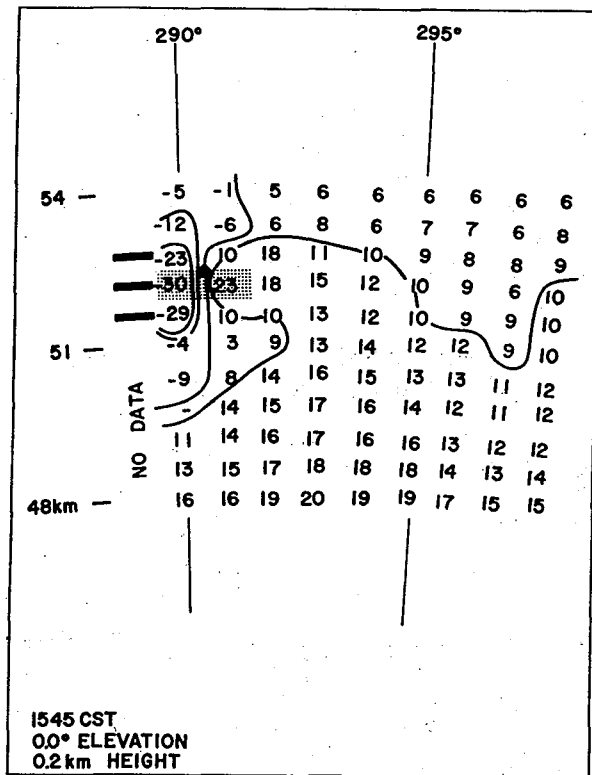


Fig. 15.3 Tornadoic vortex signature near ground (stippled) within field of single Doppler mean velocities (m s⁻¹). Velocities are relative to TVS motion (10.0 m s⁻¹ from 283°). Velocities away from radar are positive, toward radar are negative. Dark dot indicates surface tornado position. Dark rectangles show relative sampling volume (range gates) size. Azimuths and ranges are from the NSSL Doppler radar in Norman.

Above cloud base, the TVS can not be directly related to the tornado position because the latter is unknown. However, as illustrated at a height of 3.5 km in Fig. 15.4, the signature has vertical continuity--revealing significant tornado vertical extent.

An azimuthal Doppler velocity profile through the TVS at 3.5 km is very similar to the theoretical simulation (Fig. 15.5). The data points were positioned by plotting them on an overlay and manually adjusting the overlay for best overall fit to sets of curves having different peak TVS velocities. The best fit (Fig. 15.5) was for a TVS having peak velocities of 45 m s⁻¹.

A basic TVS feature is revealed in Fig. 15.5--namely, the signature remains essentially invariant for a wide range of tornado sizes and peak tangential velocities. Thus, the fitting of mean Doppler velocity measurements to theoretical curves can not be used by itself to determine either the size or peak velocity of the vortex that produces a TVS. However, if core size could be determined independently, the peak tangential velocity then could be estimated. For

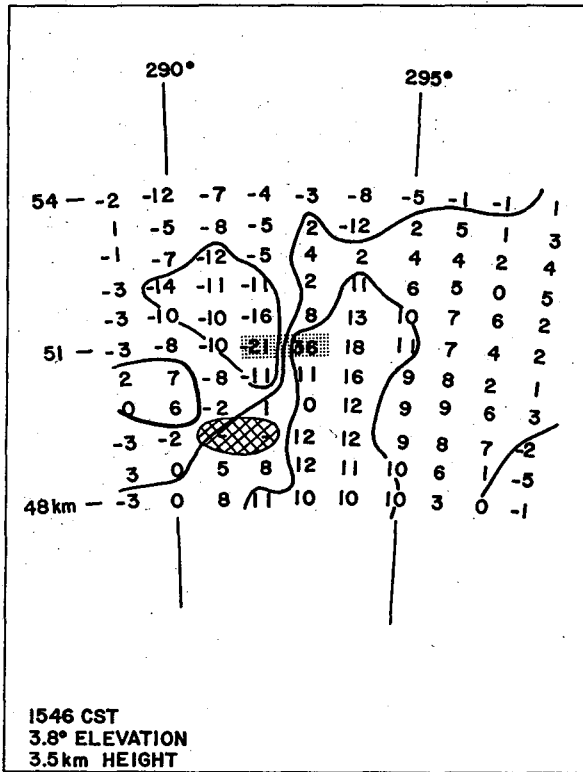


Fig. 15.4 Tornadic vortex signature (stippled) at height of 3.5 km. Weak reflectivity data void region is hatched. Rest of figure same as Fig. 15.3.

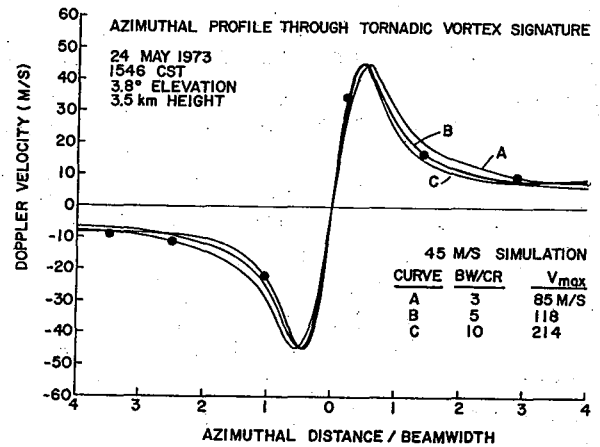


Fig. 15.5 Theoretical Doppler velocity profile through tornadic vortex signature of Fig. 15.4. The three curves (from Fig. 15.2) represent various tornado peak tangential velocities (V_{max}) chosen to produce a peak TVS value of 45 m s^{-1} . Dots are observed Doppler velocity values adjusted for best overall fit.

example, if core radius at 1546 is assumed to equal the visual tornado radius below cloud base (about 120 m), the ratio of beamwidth to core radius would be about 6. The corresponding peak tangential velocity would be about 135 m s^{-1} . The highest photogrammetric velocity in the outer edges of the surface debris cloud was an expectedly lower value of 80 m s^{-1} (see Golden and Purcell, Chapter 14).

15.4 EVOLUTION OF THE UNION CITY TVS

The NSSL Doppler radar in Norman was first trained on the Union City storm at 1446. For the first half hour, tilt sequence data collection alternated between the real-time scalar mean velocity processor (SMVP--described by Sirmans and Doviak, 1973) and the Air Force Cambridge Research Laboratories' Plan Shear Indicator (PSI--described by Armstrong and Donaldson, 1969); PSI measurements are discussed by Donaldson in Chapter 7. Unfortunately it was not understood at the time that biases in the scalar mean velocity processor renders this mode of data processing useless for severe storm applications,

15. Tornadoic Vortex Signature

where Doppler velocities exceed $\pm 20 \text{ m s}^{-1}$. Thus, none of the SMVP data collected could be used with confidence.

At 1515, alternating tilt sequences between time-series and PSI data collection commenced. (Time-series data permit the mean and variance of velocities within the radar beam to be computed later on the NSSL computer.) The first tilt sequence of time-series data at one-degree azimuthal intervals revealed the presence of a TVS from about 2.5 km to a height of over 6 km (end of data). The TVS was not at the center of the parent mesocyclone, but it moved to the center with time (see Lemon and Burgess, Chapter 8).

A time-height profile of the maximum Doppler velocity value for each TVS pair (Fig. 15.6) reveals that the TVS originates aloft in the storm and descends to the ground at about the same time that the first damage occurs. The signature is strongest at all observed heights when the tornado below cloud base is the widest (funnel diameter near cloud base is given by black area at bottom of figure). TVS magnitude decreases markedly at all heights during the tornado's shrinking and decaying stages.

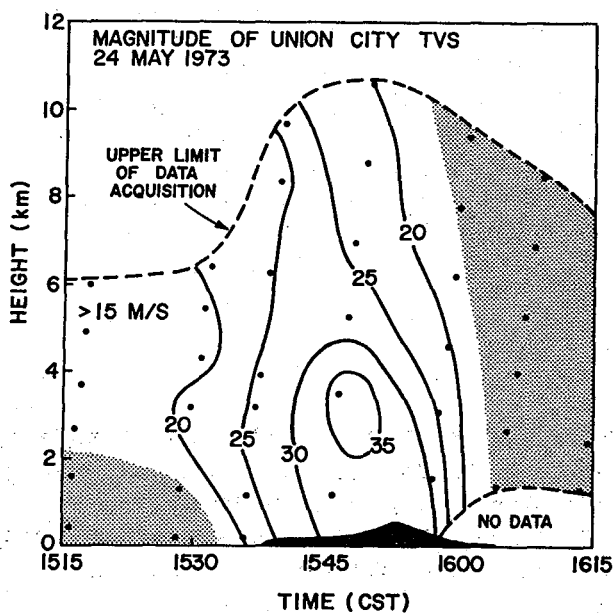


Fig. 15.6 Time-height profile of the magnitude of the maximum Doppler velocity value for each TVS pair (adjusted for TVS motion). Dots indicate data points and dashed lines represent the limits of data collection. In the lightly shaded regions, velocity shear was below the TVS detectability level. The black region at bottom center is the diameter (using ordinate scale) of the tornado funnel near cloud base.

As discussed earlier, TVS magnitude is directly proportional to both vortex size and peak tangential velocity. It is impossible to know - whether changes in TVS magnitude are due to size changes, velocity changes, or both. For the case of the Union City TVS, one might speculate that the signature magnitude was primarily influenced by vortex size because its magnitude and the observed tornado diameter varied together, while damage intensity remained unchanged. One also might speculate that the magnitude decrease above 4 to 5 km is due to vortex expansion with accompanying tangential velocity decrease (conserving angular momentum).

A horizontal projection of the TVS data points (Fig. 15.7) reveals that the signature consistently tilts towards the north-northeast at an average angle of 25 deg from the vertical. Relative to the direction of storm motion, TVS tilt is to the left, consistent with the observed tilt of the tornado funnel below cloud base (see Purcell, Chapter 11).

Plan Shear Indicator measurements--interspersed between the SMVP or time-series measurements--reveal

the same general evolution of the TVS (Donaldson, Chapter 7). The PSI, with its continuous display in azimuth (in contrast with discrete azimuthal sampling discussed in this chapter), is extremely well suited for displaying the complete tornadic vortex signature. Most pronounced on the indicator scope are azimuthal shears larger than $1 \times 10^{-2} \text{ s}^{-1}$. At the time of the first PSI indications of a vortex (1457), the peak-to-peak diameter was several times greater than a TVS--indicating a mesoscale circulation. By 1522, the vortex was characteristic of a TVS. The data vividly illustrate the descent of the TVS prior to 1538 and its disappearance after 1604.

15.5 SUMMARY

The presence of a tornadic vortex within a radar sampling volume results in a unique signature that had not been anticipated. The peak values of the signature occur about one beamwidth apart, regardless of tornado size or strength. However, the magnitude of the signature decreases as tornado size (relative to beamwidth) and/or peak tangential velocity decreases. Detectability of a TVS depends upon the Doppler velocity shear between signature peaks being significantly stronger than the surrounding shear. Based on this first study, it is premature to specify the azimuthal shear required for the classification of a TVS.

The TVS is a qualitative signature. However, the signature can produce quantitative tangential velocities when the tornado's core radius can be determined reliably.

Detection of a TVS in the Union City storm led to the first substantiated information about tornadic vortex behavior above cloud base. The tornadic vortex signature originated at storm midlevels. It took at least 25 min for the signature to work its way to the ground. During this time, the signature magnitude increased at all detectable heights and continued to increase until the tornado reached its maximum observed size. As the tornado progressed through its shrinking and decaying stages, the signature magnitude and vertical extent gradually decreased (measurements from the surface to over 10 km height). The TVS was no longer detectable at any height after the tornado dissipated.

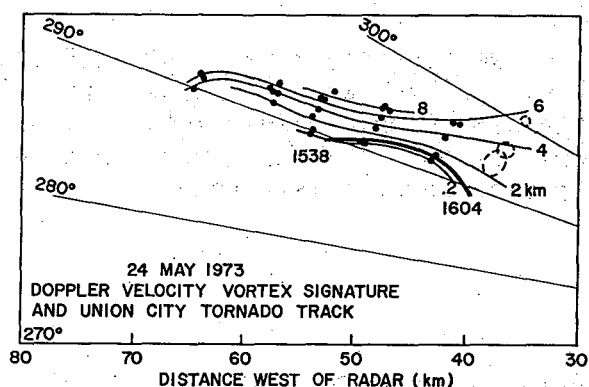


Fig. 15.7 Plan view of all TVS observations (dark dots). Each dot represents the surface projection of an elevated TVS position and groups of dots (adjusted to a reference time) indicate individual tilt sequences. The left-most dots represent a reference time of 1515 and the progression is 1515, 1528, 1536, 1545, 1556 and 1604. Broader regions of lesser shear (dashed circles at 1604) appear after tornado and TVS dissipation. Thin solid lines are contours of TVS height above the surface and thick solid line is the tornado track.

15. *Tornadic Vortex Signature*

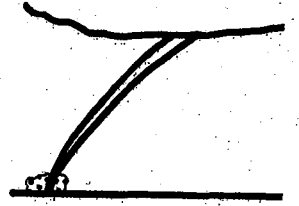
15.6 ACKNOWLEDGMENTS

We appreciate many informative discussions with Don Burgess and Dr. Dusan Zrnica. Also, we are indebted to Dale Sirmans and Glen Anderson for developing the NSSL Doppler radar into a viable research tool and for assisting with data collection. This work was supported partially by the Federal Aviation Administration under Interagency Agreement FA72 WAI-265.

15.7 REFERENCES

- Armstrong, G. M., and R. J. Donaldson, Jr., 1969: Plan shear indicator for real-time Doppler radar identification of hazardous storm winds. J. Appl. Meteor., 8, 376-383.
- Atlas, D., 1963: Radar analysis of severe storms. Meteor. Monographs, 5 (27), 177-220.
- Brown, R. A., 1976: Single Doppler radar data acquisition and analysis. Appendix E, The Union City, Oklahoma Tornado of 24 May 1973, R. A. Brown, Editor. NOAA Tech. Memo. ERL NSSL-80, Norman, Nat. Severe Storms Lab., 215-228.
- Burgess, D. W., L. R. Lemon and R. A. Brown, 1975 a: Evolution of a tornado signature and parent circulation as revealed by single Doppler radar. Preprints, Sixteenth Radar Meteor. Conf., Boston, Amer. Meteor. Soc., 99-106.
- _____, _____ and _____, 1975 b: Tornado characteristics revealed by Doppler radar. Geophys. Res. Letters, 2, 183-184.
- Donaldson, R. J., Jr., 1970: Vortex signature recognition by a Doppler radar. J. Appl. Meteor., 9, 661-670.
- _____, 1976: Observations of the Union City tornadic storm by Plan Shear Indicator. Chapter 7, The Union City, Oklahoma Tornado of 24 May 1973, R. A. Brown, Editor. NOAA Tech. Memo. ERL NSSL-80, Norman, Nat. Severe Storms Lab., 67-83.
- Golden, J. H., and D. Purcell, 1976: Airflow characteristics around the Union City tornado. Chapter 14, The Union City, Oklahoma Tornado of 24 May 1973, R. A. Brown, Editor. NOAA Tech. Memo. ERL NSSL-80, Norman, Nat. Severe Storms Lab., 157-165.
- Kraus, M. J., 1973: Doppler radar observations of the Brookline, Massachusetts tornado of 9 August 1972. Bull. Amer. Meteor. Soc., 54, 519-524.
- Lemon, L. R., and D. W. Burgess, 1976: Tornadic storm airflow and morphology derived from single Doppler radar measurements. Chapter 8, The Union City, Oklahoma Tornado of 24 May 1973, R. A. Brown, Editor. NOAA Tech. Memo. ERL NSSL-80, Norman, Nat. Severe Storms Lab., 85-106.

- _____, _____ and R. A. Brown, 1975: Tornado production and storm sustenance. Preprints, Ninth Conf. on Severe Local Storms, Boston, Amer. Meteor. Soc., 100-104.
- Lhermitte, R. M., 1964: Doppler radars as severe storm sensors. Bull. Amer. Meteor. Soc., 45, 587-596.
- Purcell, D., 1976: History of the Union City tornado. Chapter 11, The Union City, Oklahoma Tornado of 24 May 1973, R. A. Brown, Editor. NOAA Tech. Memo. ERL NSSL-80, Norman, Nat. Severe Storms Lab., 123-133.
- Sirmans, D., and R. J. Doviak, 1973: Pulsed-Doppler velocity isotach displays of storm winds in real time. J. Appl. Meteor., 12, 694-697.
- _____ and B. Bumgarner, 1975: Numerical comparison of five mean frequency estimators. J. Appl. Meteor., 14, 991-1003.
- Smith, R. L., and D. W. Holmes, 1961: Use of Doppler radar in meteorological observations. Mon. Wea. Rev., 89, 1-7.
- Zrnic, D. S., and R. J. Doviak, 1975: Velocity spectra of vortices scanned with a pulse-Doppler radar. J. Appl. Meteor., 14, 1531-1539.
- _____ and _____, 1976: Effective antenna pattern of scanning radars. IEEE Transactions on Aerospace and Electronic Systems, AES-12, 551-555.
- _____, _____, D. Burgess and D. Sirmans, 1976: Tornado characteristics revealed by a pulse-Doppler radar. Preprints, Seventeenth Conf. on Radar Meteor., Boston, Amer. Meteor. Soc., 110-117.



PART V: EPILOGUE

16. UNION CITY TORNADO AND BEYOND

CHAPTER 16

UNION CITY TORNADO AND BEYOND

Ronnie L. Alberty and Rodger A. Brown

*National Severe Storms Laboratory
Norman, Oklahoma 73069*

The Union City study, a milestone for the National Severe Storms Laboratory (NSSL), provides a clearer understanding of severe storm kinematics and tornado evolution. During the report preparation period, equipment improvements--especially with the dual-Doppler radar system--have resulted in more efficient data collection procedures. Over the past several years, a high correlation between tornado occurrences and Doppler mesocyclone and tornadic vortex signatures has been documented. As a consequence, a joint tornado warning experiment with other federal agencies is planned for Spring 1977. Doppler radar systems continue to reveal unprecedented details of internal severe storm circulations. Research meteorologists now need today's technology applied to sampling and recording of all meteorological parameters in the near environment of these storms. An initial improvement would be to digitally record data from our surface and upper air mesonetworks.

16.1 Introduction

In preceding pages the reader has available detailed documentation of physical interpretations and perceptions developed as a result of carefully executed observational and analytical efforts. Such studies are a vital part of NSSL efforts to continually prod the frontiers of meteorological knowledge as applied to perhaps the most transitory and violent of nature's atmospheric manifestations, the severe thunderstorm. Chapters 2 through 4 outline the meteorological setting in which the Union City storm developed; Chapters 5 through 10 discuss various aspects of the storm, including embedded circulations and electrical properties; while Chapters 11 through 15 discuss characteristics and implied properties of the resulting large and very intense tornado.

NSSL offers visiting scientists a nearly unique opportunity to actively participate with the highly competent Laboratory staff in a carefully conceived attack on severe storms. Such cross-fertilization of expertise provides for both cooperative and complementary studies (examples are Chapters 6, 7, 9, and 10) and allows a more comprehensive approach to severe storm research than is possible through separate independent efforts.

16.2 SIGNIFICANT FINDINGS

Advancement of severe storm knowledge presented in this report has been due primarily to the availability of a pulsed Doppler radar. Most important is the discovery of a unique tornadic vortex signature (TVS) in the field of mean Doppler velocity values (Chapter 15). The presence of such a signature has made it possible to document the three-dimensional evolution of the tornadic vortex in the Union City and subsequent storms. Basically, the TVS originates at storm midlevels and works its way both upward and downward, reaching cloud base at about the same time that a visible funnel appears. The TVS completely disappears with tornado decay.

Single Doppler velocity measurements also provided insight about larger-scale flow fields within the storm. Doppler data collection began as the developing Union City storm split into right-moving and left-moving (relative to mean wind) portions (Chapter 5). The right-moving storm included a region of mesoscale cyclonic circulation, within which the TVS and tornado developed (Chapters 7 and 8). Storm dissipation apparently was related to tornado production (Appendix F). The left-moving storm did not exhibit any pronounced rotation but an anticyclonic vortex appeared briefly at midlevels (Chapter 6). Though not entirely conclusive, it appears that deviate storm motion is due primarily to propagative effects and secondarily, perhaps, to rotational forces.

Directional sferics measurements from the Union City storm complex provide additional evidence to discount the theory that tornadoes are caused by electrical activity and consequently become the source region for sferics activity. These data clearly indicate that sferics emanate from the entire storm and that sferics activity is unaffected by the development, maturation and decay of the tornado (Chapter 10). The directional, as well as nondirectional (Chapter 9), measurements indicate that sferics activity peaked just after tornado dissipation.

The importance of mobile tornado intercept teams was demonstrated on 24 May 1973 (Appendix A). Three separate teams of meteorologists converged on the Union City storm, guided by portentous visual characteristics that were augmented by radar observations. Their documentation of the tornado's position in time and space established the significance of the TVS. In addition, the NSSL team obtained movies that revealed tangential velocities as great as 80 m s^{-1} and vertical velocities up to 30 m s^{-1} in the surface debris cloud (Chapter 14).

Tornado characteristics varied during the different stages of development (Chapters 11 through 13). During the organizing stage, there was continuous surface damage even though the visible funnel only briefly extended to the ground. As the tornado matured, it attained a maximum cloud-base diameter of nearly 600 m; at the same time, surface damage path width was 500 m. In the later stages, even though the funnel became narrower and eventually contorted, the tornado retained its destructive intensity. Throughout its lifetime, tornado width at cloud base closely paralleled surface damage width. In all, over a 26 min period, the tornado produced a damage track 17 km long.

Some hints of why the Union City storm formed ahead of an advancing cold front/squall line have emerged from this study (Chapters 2 through 4). A low-level inversion concentrated morning heating into a fairly shallow layer of moist air. During the day, southerly winds advected a deeper moist layer into central and western Oklahoma. Ahead of the front was a surface confluence zone between southwesterly and southeasterly winds. The first echo of the Union City storm formed near the zone at about the same time that a minor upper-air trough passed overhead. Apparently, the presence of surface confluence and abundant low-level moisture, coupled with strong vertical instability and wind shear, provided a favorable environment in which strong convection could be triggered by upper-air trough passage.

16.3 RAMIFICATIONS OF THIS STUDY

Ongoing research since the Union City storm (e.g., Burgess *et al.*, 1975; Davies-Jones *et al.*, 1976; Nelson, 1976; Ray *et al.*, 1976; Brandes, 1977) has benefited from knowledge of severe storm characteristics reported in this volume. Perhaps the most exciting possibility for future operational application is detection of the parent mesocyclone and the tornadic vortex signature which provides the basis for earlier and more exact definitions of those storms having very high tornado potential (Brown and Lemon, 1976; Burgess, 1976). This discovery has led to a cooperative effort--beginning in Spring 1977--involving the National Weather Service, Air Weather Service, Air Force Geophysics Laboratory, Federal Aviation Administration and NSSL to more fully evaluate the operational warning potential of Doppler radar.

The Norman Doppler radar has undergone many improvements since 1973, as has the newer Doppler radar that was activated at Cimarron Airport in 1974. These improvements facilitate data acquisition and processing, provide for multiple Doppler probing of selected storms, allow selection of an increased unambiguous velocity interval, and provide data of increased reliability. Further refinement of the Doppler radar systems hopefully will continue to address reliability and data quality.

Other improvements in supporting data sources are now needed. While Doppler radars can provide unprecedented details of internal thunderstorm flow fields, the requirement for mapping internal thermodynamics and all aspects of external flows has not been adequately satisfied. Some very recent successes in mapping flow fields in the absence of hydrometeors and radar-reflective chaff shows potential of revealing prestorm circulations on spatial and temporal scales previously unattainable throughout the near-surface layer. Unfortunately, inherent range limitations may preclude areal coverage sufficient to reveal mesoscale forcing mechanics. Additionally, no remote sensing technique is presently visible that will allow simultaneous mapping of environmental flows and the adjacent thunderstorm echo. Most meteorologists agree that physical understanding of the severe storm environment, the interaction of internal and external storm flows, and energetics of the entire system are ultimately required to effectively address the thunderstorm prediction problem.

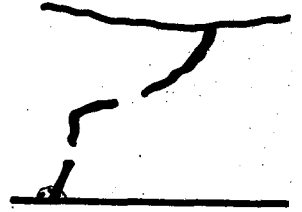
16. *Union City Tornado and Beyond*

Meteorological research at NSSL can be further improved through available modern techniques to acquire and process data. Analog information from the surface station network is currently extremely difficult to prepare for analysis and, as a result, seldom is utilized in other than individualized case studies. A similar restriction applies to rawinsonde data. We urge implementation of state of the art technology to acquire, process and display observational information in optimum fashion for meteorological interpretation.

Research scope at NSSL is being carefully expanded. A rejuvenated effort in severe storm electrification is on the very near horizon, modeling studies now are receiving new attention and the scientific expertise of the staff is growing steadily. Cooperative studies both among staff scientists and with experts outside the Laboratory are being nurtured to expand the capabilities required to further unravel the complicated physical processes attendant to thunderstorms. This study of the Union City tornadic storm has helped to put some of these processes into a more understandable framework.

16.4 REFERENCES

- Brandes, E. A., 1977: Flow in severe thunderstorms observed by dual-Doppler radar. Mon. Wea. Rev., 105.
- Brown, R. A., and L. R. Lemon, 1976: Single Doppler radar vortex recognition: Part II - Tornadic vortex signatures. Preprints, Seventeenth Conf. on Radar Meteor., Boston, Amer. Meteor. Soc., 104-109.
- Burgess, D. W., 1976: Single Doppler radar vortex recognition: Part I - Mesocyclone signatures. Preprints, Seventeenth Conf. on Radar Meteor., Boston, Amer. Meteor. Soc., 97-103.
- _____, L. R. Lemon and R. A. Brown, 1975: Tornado characteristics revealed by Doppler radar. Geophys. Res. Lett., 2, 183-184.
- Davies-Jones, R. P., D. W. Burgess and L. R. Lemon, 1976: An atypical tornado-producing cumulonimbus. Weather, 31, 336-347.
- Nelson, S. P., 1976: Characteristics of multicell and supercell hailstorms in Oklahoma. Preprints, Second WMO Sci. Conf. on Weather Modification, Geneva, World Meteor. Organ., 335-340.
- Ray, P. S., C. E. Hane, R. P. Davies-Jones and R. L. Alberty, 1976: Tornado-parent storm relationship deduced from a dual-Doppler radar analysis. Geophys. Res. Lett., 3, 721-723.



APPENDICES

- A. TORNADO INTERCEPT STRATEGY AND MORPHOLOGICAL OBSERVATIONS
- B. HOURLY SURFACE WEATHER MAPS AND ANALYZED FIELDS OF METEOROLOGICAL VARIABLES: 24 MAY 1973
- C. RAWINSONDE OBSERVATIONS ON 24 MAY 1973
- D. NSSL DOPPLER AND WSR-57 RADAR CHARACTERISTICS
- E. SINGLE DOPPLER RADAR DATA ACQUISITION AND ANALYSIS
- F. TORNADIC STORM EVOLUTION: VORTEX VALVE HYPOTHESIS

Appendix A

TORNADO INTERCEPT STRATEGY AND MORPHOLOGICAL OBSERVATIONS

Joseph H. Golden¹

*National Severe Storms Laboratory
Norman, Oklahoma 73069*

Early in the afternoon of 24 May 1973, the NSSL tornado intercept team headed west toward a developing squall line in western Oklahoma. After passing near a region of growing cumulus congestus clouds, it became apparent (with the help of radar observations) that the congestus area was developing into an isolated storm ahead of the squall line--a favorable location for tornadic storm formation. The team then turned around and started moving toward the southeast in order to catch up with the storm, while maintaining a safe position to its south. Just as the anticipated tornado was touching down, the camera crew was in position 5 km south of Union City.

As noted by Vlcek (Chapter 2) and Brandes (Chapter 3), a cold front was moving into northwestern Oklahoma late in the morning of 24 May 1973. Shortly after noon, a scattered line of thunderstorms developed rapidly along the front in western and north central Oklahoma. At about 1300 CST, the National Severe Storms Forecast Center issued a tornado watch for much of northern and central Oklahoma, valid from 1330 to 1930 CST. A decision already had been made for the National Severe Storms Laboratory (NSSL) tornado intercept vehicle and crew (Golden, Morgan, Achtemeier, Vlcek and Purcell, plus Popular Science reporter, Robert Gannon) to depart at 1300, and have as its initial intercept goal the southernmost developing thunderstorm along the front.

Heading north on Interstate 35 (see map, Fig. A.1), the largest visible storms at this time (1315) were NNE, NW and W in order of decreasing size. We were anticipating that new cell development would continue to occur on the southern end of the line, in the region W or WSW of NSSL. The cell NNE was immense (top over 15 km AGL) and had a definite protruding cumulus top. At about the same time, a funnel pendant from that cell was reported by the public.

¹ Present affiliation: NOAA, Environmental Research Laboratories, Office of Programs, Boulder, Colorado 80302.

A. Tornado Intercept Strategy

NSSL INTERCEPT TEAM
24 MAY 1973

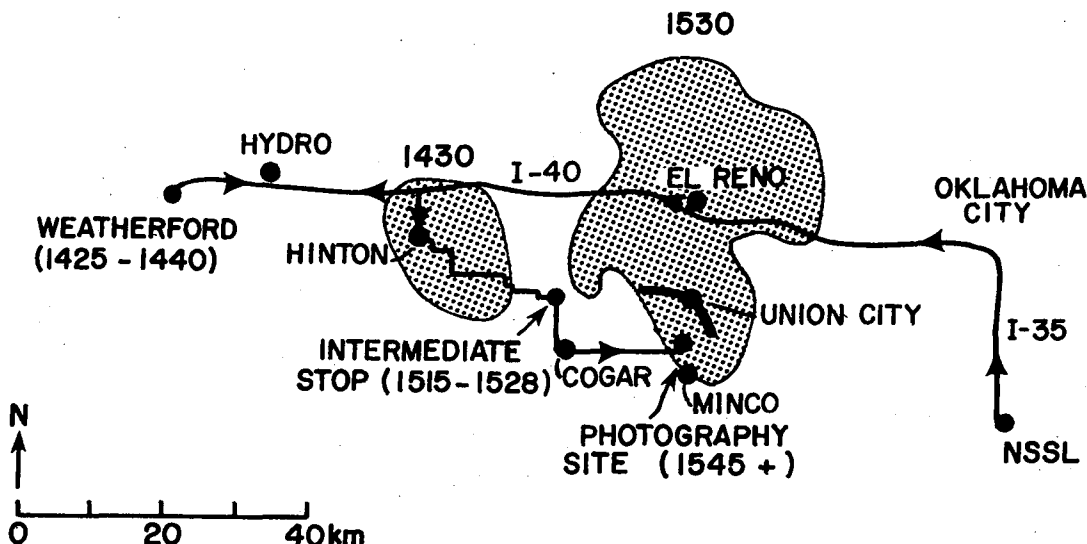


Fig. A.1 Map of NSSL intercept vehicle route relative to Union City storm (two radar echo outlines) and relative to Union City tornado damage path (dark curved path).

As the intercept vehicle moved westward from Oklahoma City on I-40, the cluster of cumulus congestus NW began to build rapidly. We could also perceive a broad band of cumulus humilis extending N-NW-W-SW. The vehicle passed under the eastern border of these cumuli a few kilometers west of El Reno. Continuing westward toward the increasing line of thunderstorms, we passed about 5 km north of a small, developing cluster of cumulus congestus when we were near the Hydro exit. Little or no precipitation was evident from the congestus cluster then (roughly 1420), but it had darkening cloud bases. (It should be noted that this congestus cluster was the embryonic Union City storm.) Moreover, there were broken smaller cumuli north and south of the Hydro exit with many narrow cloud towers rising rapidly, pinching off slightly in the middle and shearing noticeably toward the east-northeast.

The vehicle intercepted new cloud developments at the leading edge of the squall line about 1425 in Weatherford. It was dark with anvil cloud above to the west (we were told via radio-telephone that NSSL radar showed a large cell in the line 90 km to our southwest). In addition, cumulonimbi were building NW-NNE and SW of Weatherford. We set up the 16 mm camera for vertically-pointing time-lapse, with rapidly rising cumulus congestus cloud towers and nearly overcast middle cloud conditions both north and south of our position. Low-level fractocumulus was moving from the WSW, while cumulus cloud turrets were being strongly sheared by northwesterly flow aloft. The surface wind was from the WSW at about 5 m s^{-1} . We could see a rapidly developing cirrus anvil in the large congestus cluster to the east.

The most crucial decision in the tornado intercept strategy of 24 May 1973 had to be made at Weatherford. The storm intercept coordinator at NSSL indicated that there were two severe cells within our reach in the squall line, which was nearly over us at the time (1435), one cell north and another southwest. A third option was to head east on I-40. The cluster of cumulus congestus which we had passed to the north some fifteen minutes earlier had explosively developed into an isolated, severe storm which was continuing to increase in intensity as it passed just south of the Hinton exit on I-40. Based on previous experience among ourselves and the OU student chase groups, we decided that the severe, developing isolated cell to the east of Weatherford would be the best storm for intercept attempt. The decision was based on the fact that isolated supercell storms forming and moving out ahead of a squall line in Oklahoma have often been observed to spawn a tornado. The decision was facilitated because of the extreme difficulty in surface vehicle navigation and visibility restrictions encountered previously in squall line interceptions. Even though one of the primary objectives of the Tornado Intercept Project is to obtain detailed scientific photography of tornadoes and their parent storm structures, those squall lines with embedded hook echoes should in general be intercepted and followed only with great caution and only when there are no isolated severe storms available. This rule is based on both scientific data acquisition and safety considerations.

The NSSL tornado intercept vehicle headed east from Weatherford at 1440. As we were approaching the backside of the storm from about 5 to 10 km west of the Hinton exit at 1500, we could see that it was very extensive in north-south dimensions and in vertical extent. A multitude of hard, sharply-defined cumulus caps extended upward on the rear flank of the storm, where they merged with streamers of thick, anvil cirrus from the squall line to the west. Several dark cumulus bases could be seen ahead of us to the east, being drawn into the rear flanks of the storm from the WNW. We could see that the dark precipitation core extended from 080° through 110°, relative to our position. This was confirmed from the NSSL WSR-57 radar, which indicated a large echo core about 25 km east of our position straddling the interstate highway. Finally, we noted one of the telltale signs of a potentially-tornadic thunderstorm--a flanking line of small cumulus congestus clouds merging into the main body of the storm from the southwest. The storm had the additional distinction of several cloud towers which merged as a solid mass with thick anvil cirrus overhead to the ESE.

In order to avoid the heavy rain and large hail being reported at the time by the public and indicated by NSSL radar ahead of the vehicle on Interstate 40, we turned south and then followed the zig-zag highway southeast through Hinton. This decision also was based on strategy rules set up beforehand. One of the most important rules for successful tornado interception has been to position the vehicle on the south or southeast flanks of a potentially-tornadic thunderstorm. This relative position has to be maintained while moving with the storm on the ground and allows the best visibility and contrast with a light background for photography.

Shortly after 1500, we could see ahead of us (ESE) the development of a dark, lowering cloud base just southwest of the main precipitation core. This dark cloudbase which at first was somewhat ragged began to exhibit slow cyclonic rotation about its edges, and gradually lowered in a shallow bowl-like

A. Tornado Intercept Strategy

shape from the higher, flat bases (1 km AGL) in the flanking cumulus line. The upper rim of the left side of this dark, slowly rotating "wall cloud" merged with the heavy precipitation veil over 8 km to our northeast. Several large condensate elements formed in situ within a hundred meters above the ground and rose very rapidly in a helical fashion into the wall cloud above. There were no funnel clouds or funnel-scale rotations discernible in these condensate elements at this time. When the intercept vehicle was about midway between Hinton and Cogar at 1515 (see Fig. A.1), we stopped on a curve in the road and took 16 mm movies of two large, apparently truncated funnel clouds located side-by-side and pendant from the wall cloud. These two 'funnel protrusions' had lifetimes of 5 to 7 min and were located at about 085° and 100°. Both funnels had weak cyclonic rotation evident in cloud tags with strong rising motion apparent on each funnel edge. Three or four cloud-to-ground lightning discharges apparently came down through one of the funnel protrusions. Observations made of the same lightning discharges by Mr. Steve Tegtmeier, on the opposite side of the flanking side, confirm our impression that the lightning bolts did emanate from the protrusion. Frequent cloud-to-ground lightning was also observed from the precipitation core immediately to the northeast of the wall cloud and funnels. The rain area extended from about 020 to 070°, darkest at about 040°, but was not as dark as it was earlier from the west on the Interstate. Cumulus clouds from the storm extended overhead at this point and were rapidly being drawn into the storm from the west.

We were increasingly convinced that a tornado would form. At about 1520, the funnel protrusions became tilted slightly away from the heavy rain area to the north and their smooth edges started to fragment. We noticed that it was completely clear behind the funnels and to the E-SE-SSE, ahead of the major flanking cumulus congestus line. Lightning in the precipitation core became most frequent at this time, to the northeast, and the surface wind was strong and gusty from the west-northwest. We continued to be impressed by the developing cyclonic rotation in the wall cloud and by the rapidly-rising cumulus fractus beneath the southern portion of the wall cloud. The NSSL intercept vehicle left the first stopping area at 1528 and continued south. Before reaching Cogar we observed that the wall cloud appeared to be lowering and becoming more pronounced. At this time (near 1530), the wall cloud was centered about due east of our position.

Continuing southward, the intercept vehicle turned east at Cogar. As we were approaching Minco, a definite funnel, very large in diameter near the top, started to descend from the southwestern edge of the wall cloud. As the intercept vehicle reached the highway between Minco and Union City, the funnel had tapered down to a pencil point near the bottom and was more than two-thirds extended to the ground. Even though the visible funnel was not touching the surface at this time, a definite large dust whirl could be seen on the ground. As we turned north toward Union City, the funnel appeared to retract upwards after its initial 1 to 2 min of existence. Then, within another minute or two, the halfway-extended funnel appeared to become much larger in diameter and began to descend in an irregular manner to the ground. At 1545, just before the large Union City tornado funnel descended earthward for the final time, the NSSL intercept vehicle stopped at a point 5 km south of Union City and began photographic data acquisition that continued until tornado demise at 1604.

REFERENCES

- Brandes, E. A., 1976: Subsynoptic-scale meteorological features and associated convective activity on 24 May 1973. Chapter 3, The Union City, Oklahoma Tornado of 24 May 1973, R. A. Brown, Editor. NOAA Tech. Memo. ERL NSSL-80, Norman, Nat. Severe Storms Lab., 19-25.
- Vlcek, C. L., 1976: General synoptic situation. Chapter 2, The Union City, Oklahoma Tornado of 24 May 1973, R. A. Brown, Editor. NOAA Tech. Memo. ERL NSSL-80, Norman, Nat. Severe Storms Lab., 11-17.

Appendix B

HOURLY SURFACE WEATHER MAPS AND ANALYZED FIELDS OF METEOROLOGICAL VARIABLES: 24 MAY 1973

Edward A. Brandes

*National Severe Storms Laboratory
Norman, Oklahoma 73069*

Regional surface maps drawn by computer have been prepared with a modified version of the analysis scheme developed by Barnes (1973). Observations were interpolated to grid points (25 km spacing) with a Gaussian spatial weight function. Two passes are made through the observations. The first pass uses the observations themselves while differences (corrections) between the first analysis and the input observations are used in the second pass to generate a field of corrections for adjusting the first analysis.

The weight (W_i) each observation or correction (G_i) receives at a particular grid point is given by

$$W_i = \exp(-r^2/EP) \quad (\text{B.1})$$

where r is the distance between the observation site and the grid point and EP is a constant. The analyzed grid point value (P) is determined from

$$P = \frac{\sum_{i=1}^n W_i G_i}{\sum_{i=1}^n W_i} \quad (\text{B.2})$$

The observations and analyzed data fields are presented in Figs. B.1 through B.5. All input weather observations (National Weather Service stations supplemented with NSSL α mesonetwork stations) are plotted in observed (English) units. Streamlines for a subsection of the analysis grid and composite low-level weather echoes from NSSL (denoted by a +), Amarillo (AMA), Wichita (ICT), and Fort Worth (GSW) radars are overlaid. Analyzed fields in metric units are also displayed (for only a subgrid). Dimensions and multiplicative factors are given in Table B.1.

The persistent moisture maximum (dew-point temperature, moisture convergence, wet-bulb potential temperature) found in southwestern Oklahoma is due to Fort Sill (FSI) measurements, which may have some local bias.

B. Subsynoptic Analyses

SURFACE MAP TIME 1300 CST DATE 052473

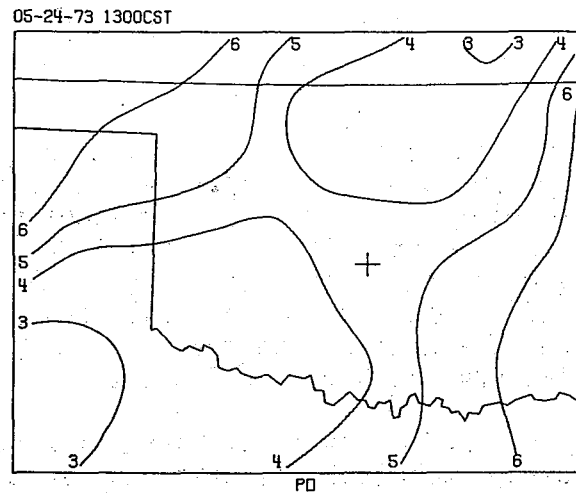
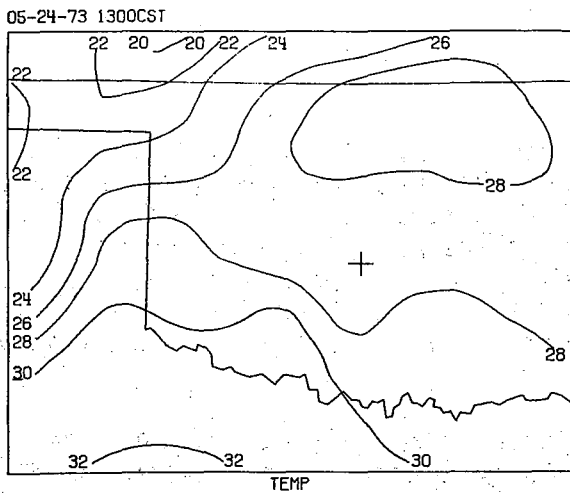
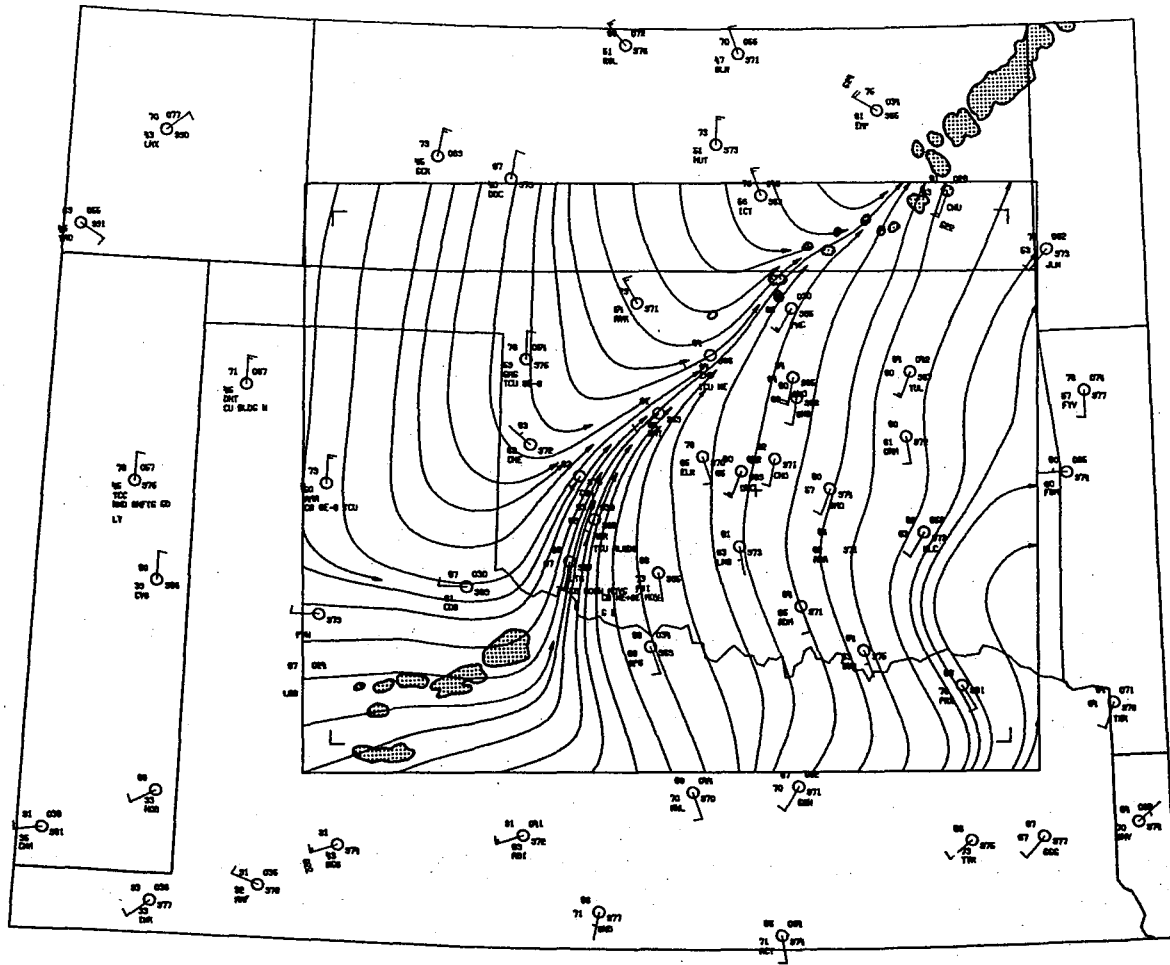
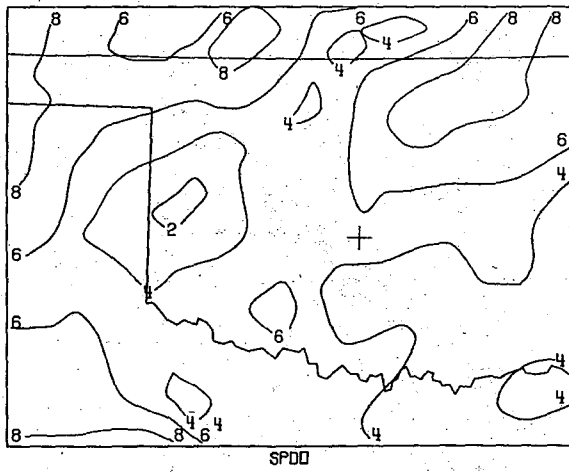
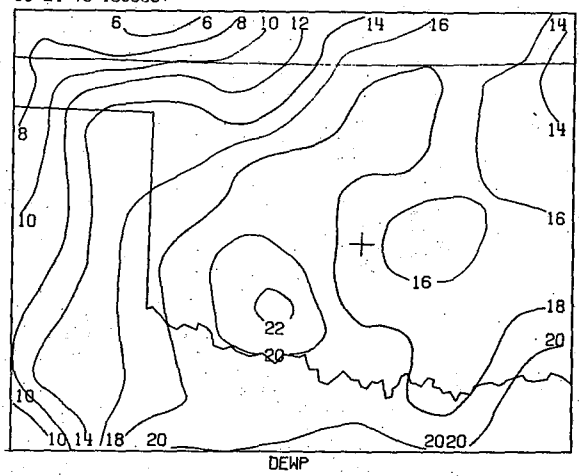


Fig. B.1 Surface observations (English units) and analyzed data fields (metric units) at 1300 CST on 24 May 1973; shaded areas are composite low-level radar echoes from NSSL (+), Amarillo, Wichita and Ft. Worth radars. Analyzed fields include temperature, pressure anomaly (from 1000 mb), wind speed, dew-point temperature, wet-bulb potential temperature, moisture convergence, divergence and vorticity.

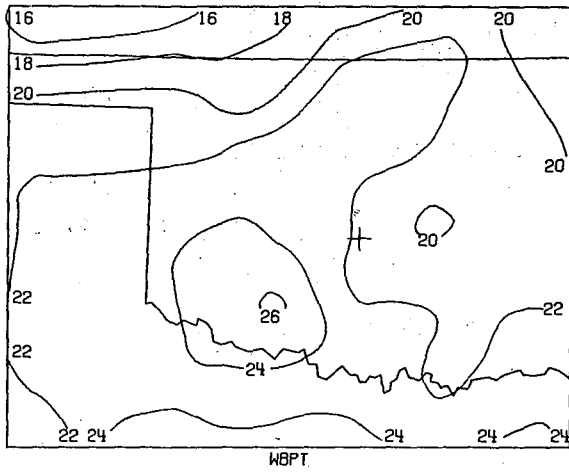
05-24-73 1300CST



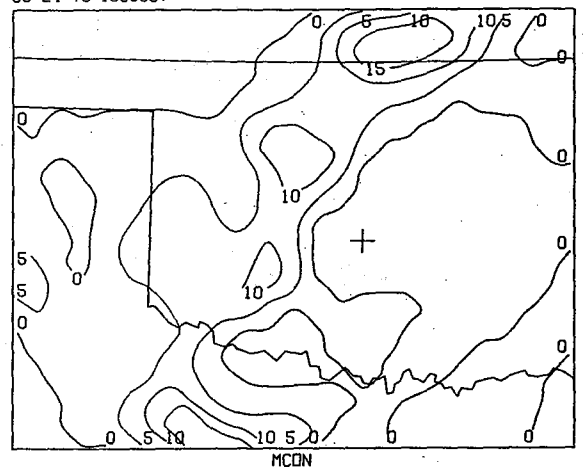
05-24-73 1300CST



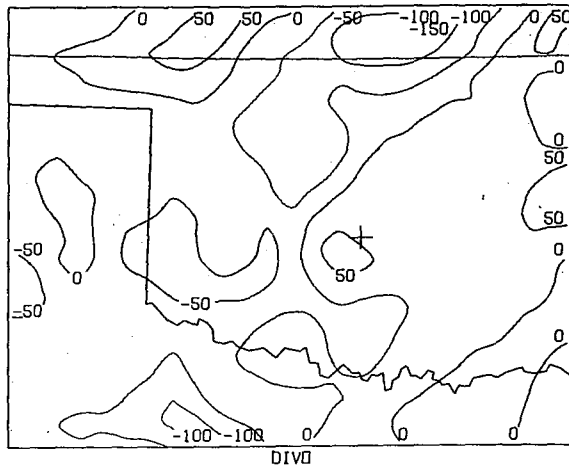
05-24-73 1300CST



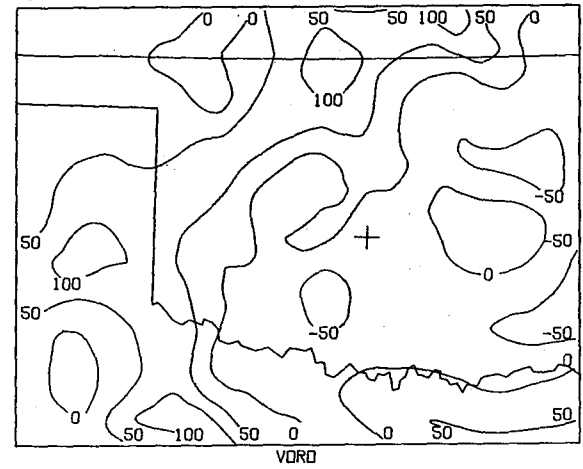
05-24-73 1300CST



05-24-73 1300CST



05-24-73 1300CST



B. Subsynoptic Analyses

SURFACE MAP TIME 1400 CST DATE 052473

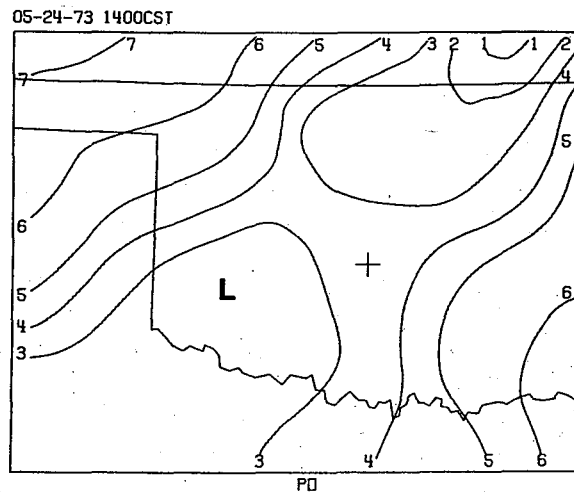
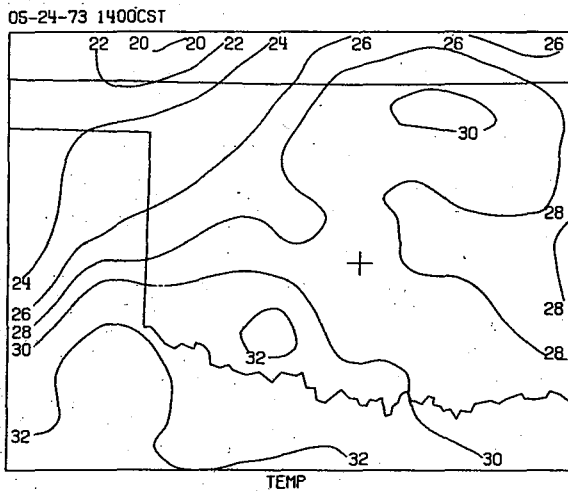
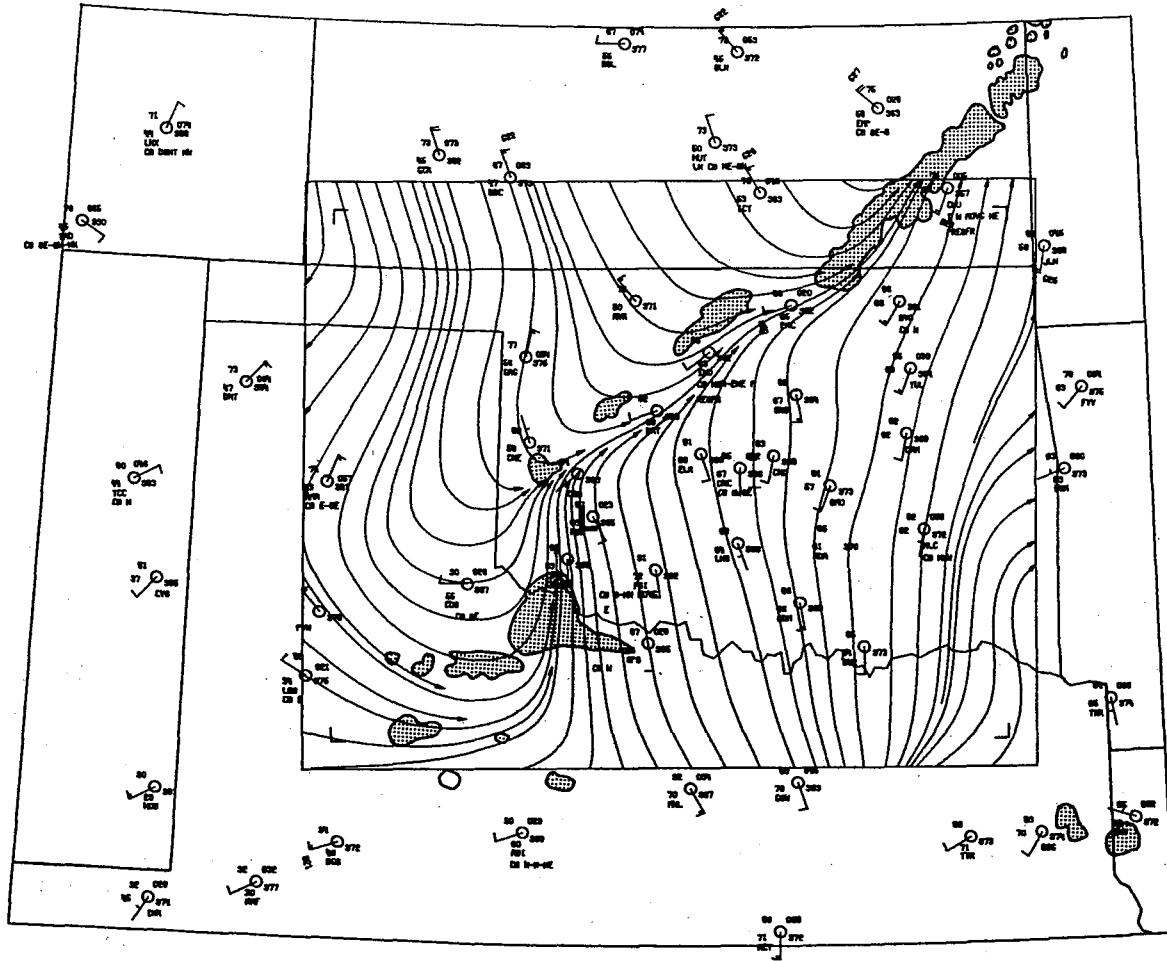
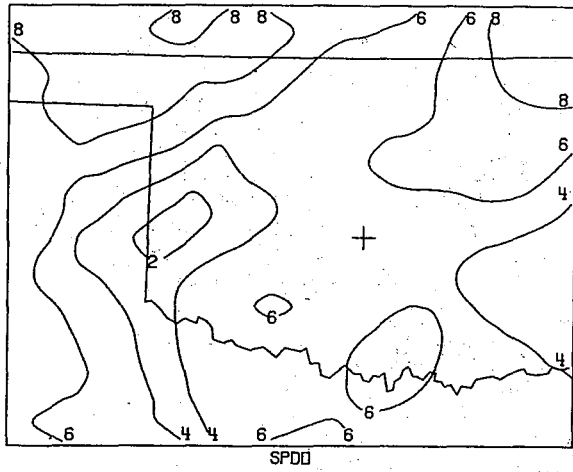
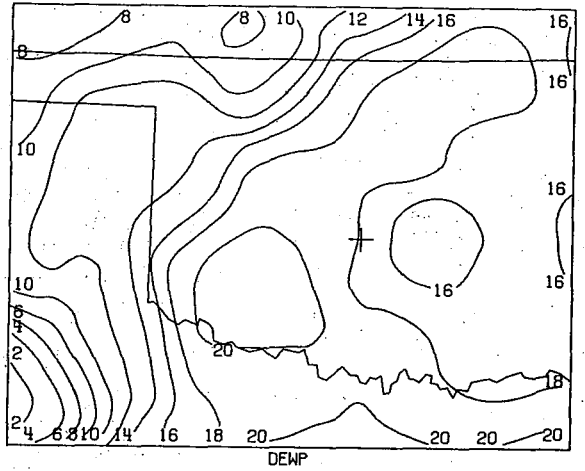


Fig. B.2 Same as Fig. B.1, except at 1400 CST.

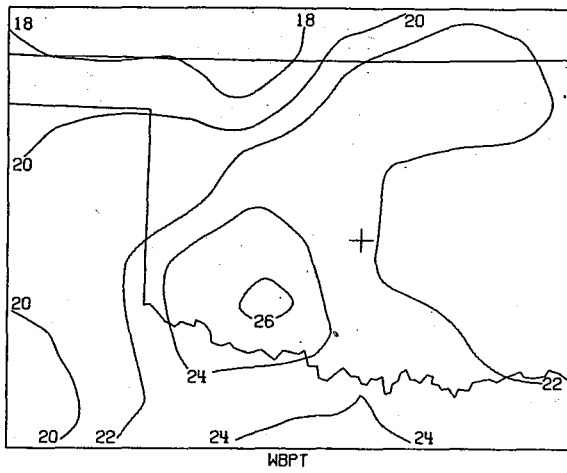
05-24-73 1400CST



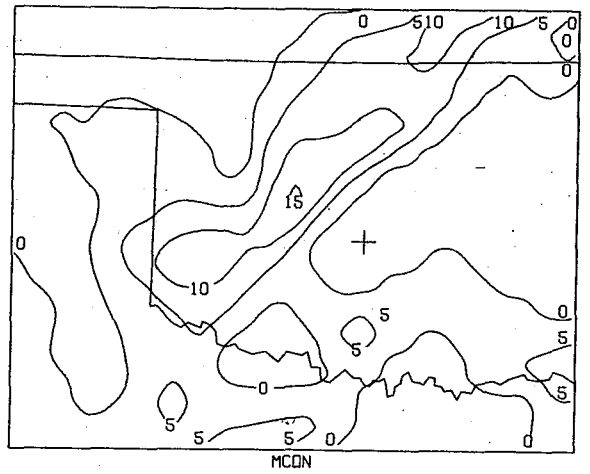
05-24-73 1400CST



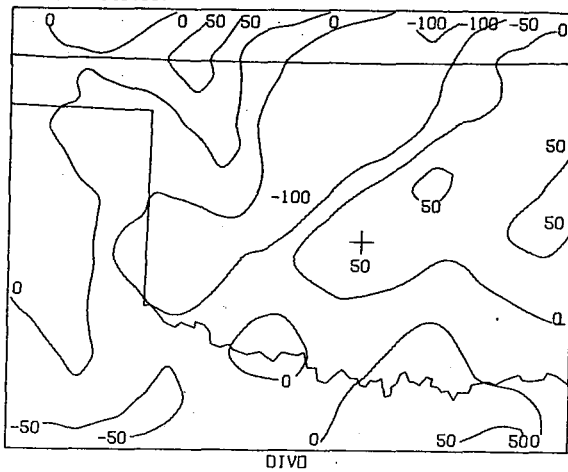
05-24-73 1400CST



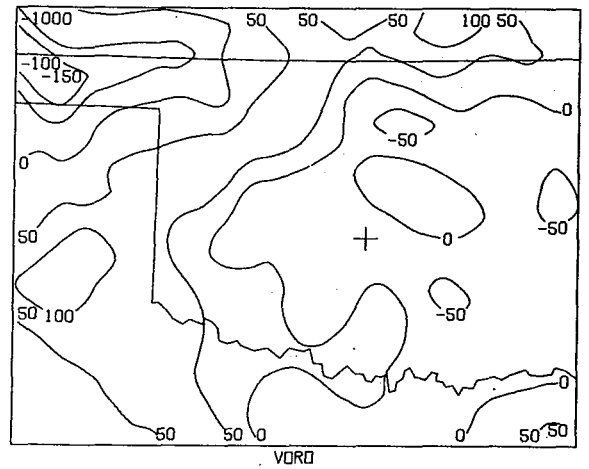
05-24-73 1400CST



05-24-73 1400CST

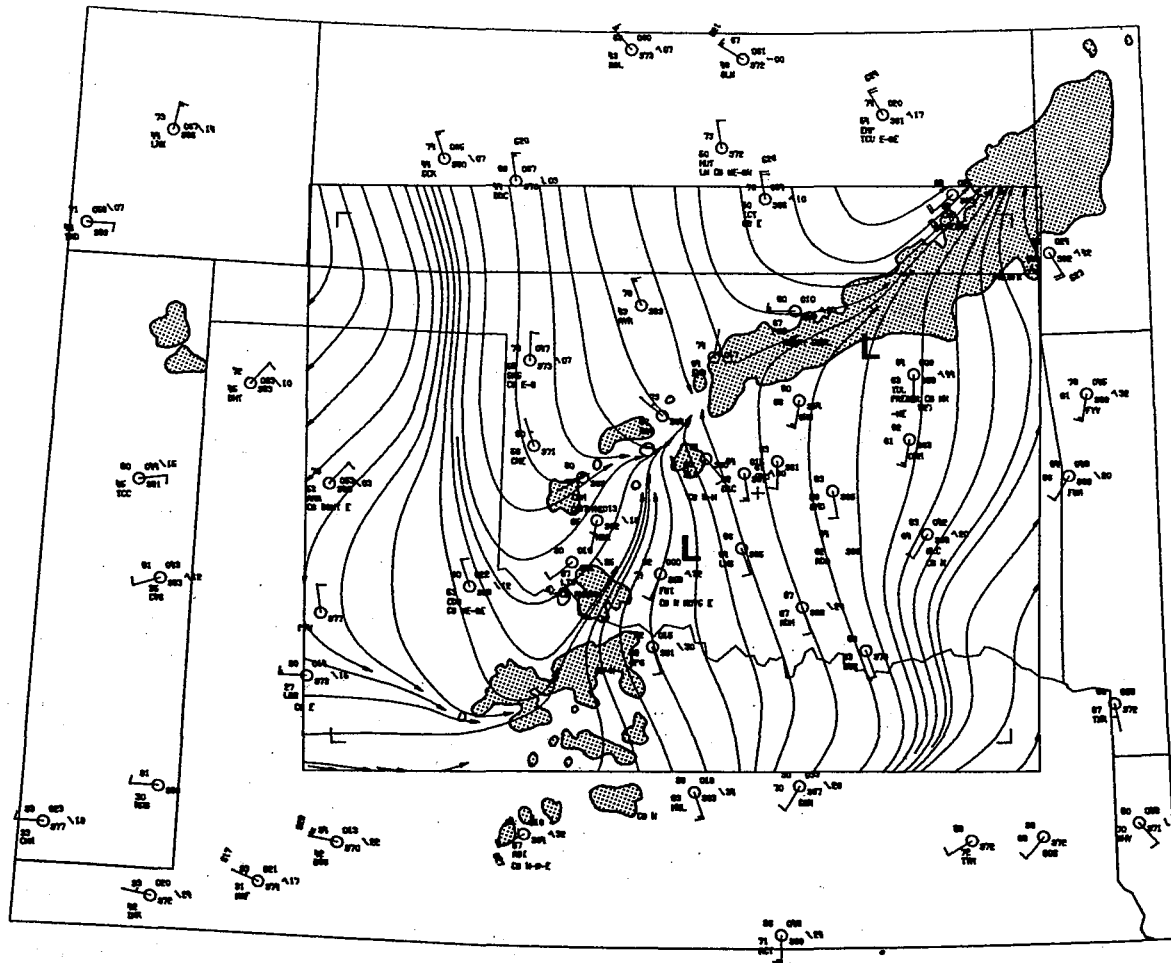


05-24-73 1400CST

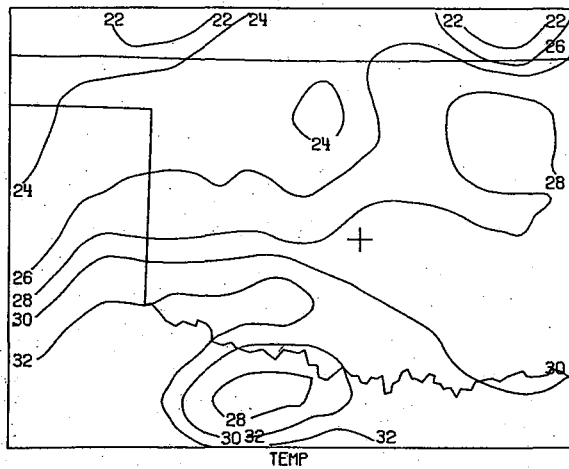


B. Subsynoptic Analyses

SURFACE MAP TIME 1500 CST DATE 052473



05-24-73 1500CST



05-24-73 1500CST

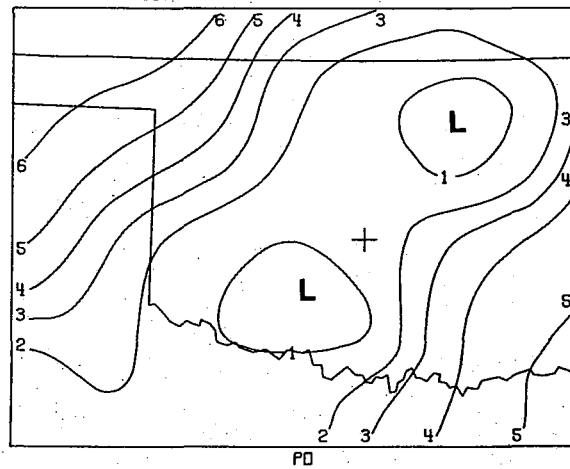
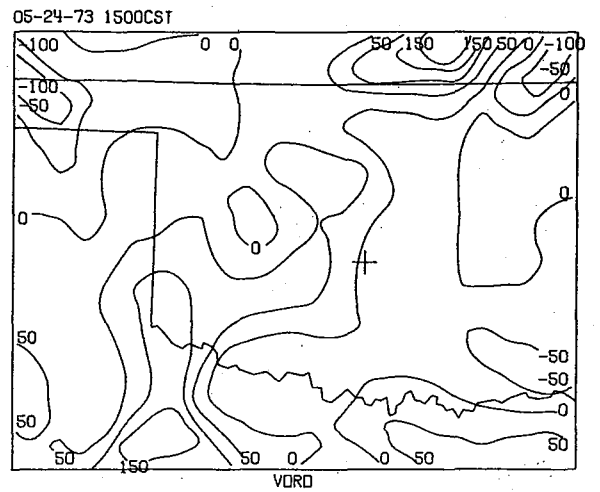
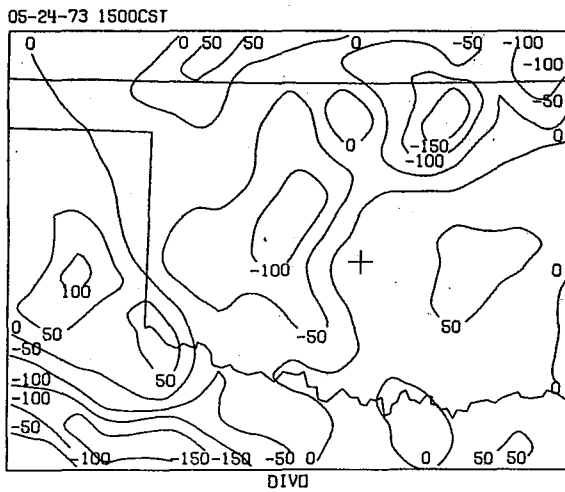
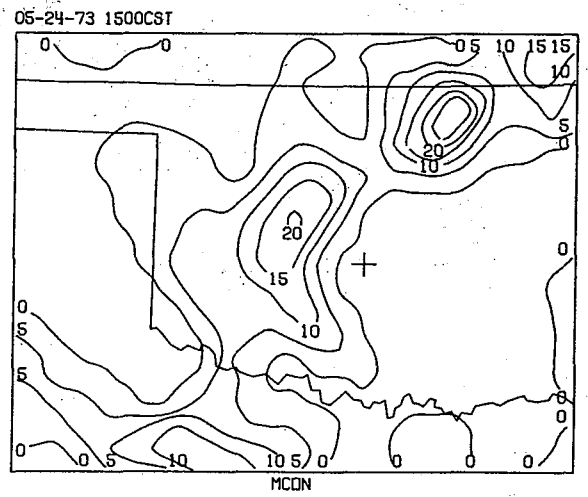
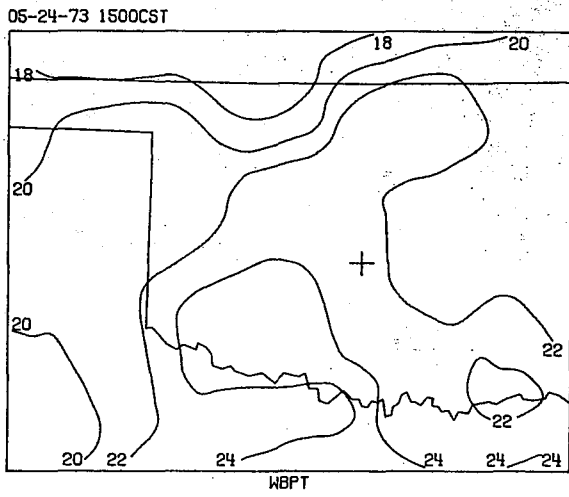
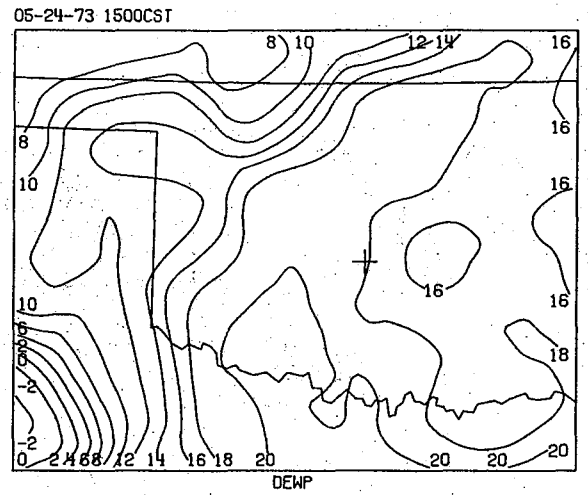
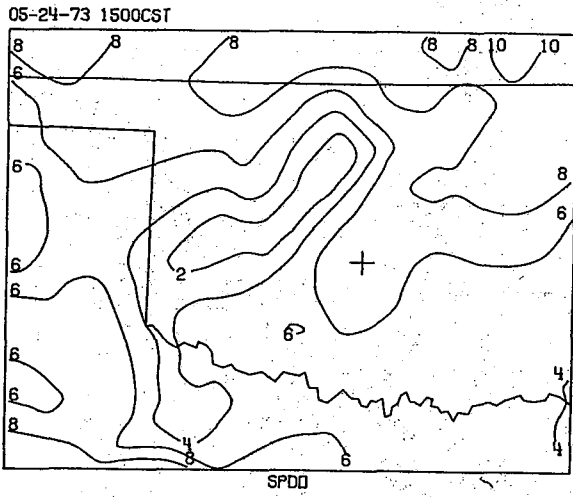
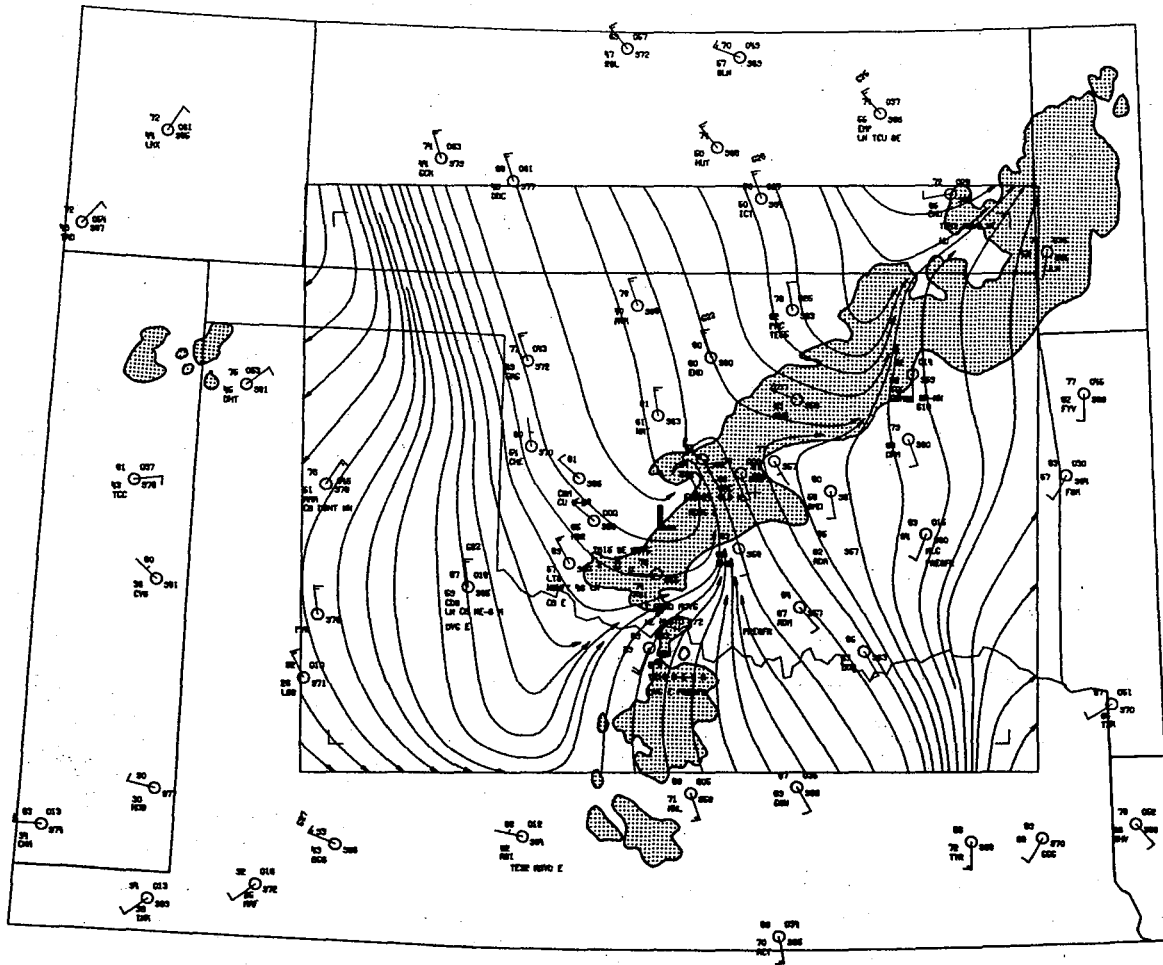


Fig. B.3 Same as Fig. B.1, except at 1500 CST.

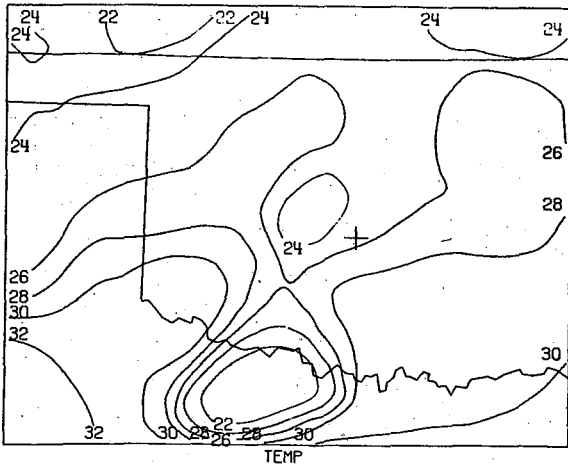


B. Subsynchronous Analyses

SURFACE MAP TIME 1600 CST DATE 052473

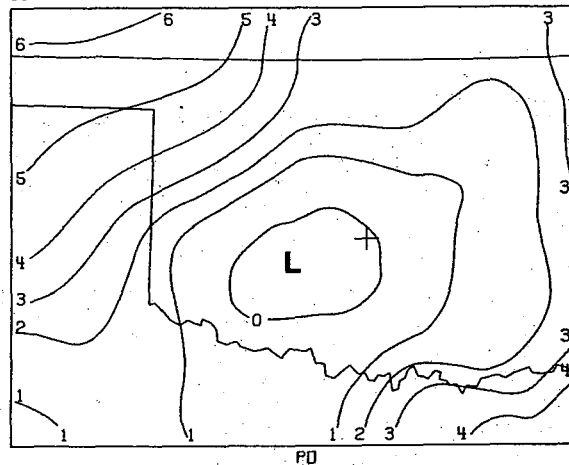


05-24-73 1600CST



TEMP

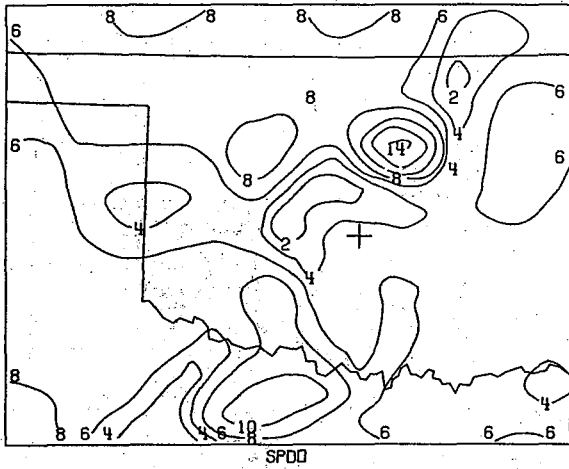
05-24-73 1600CST



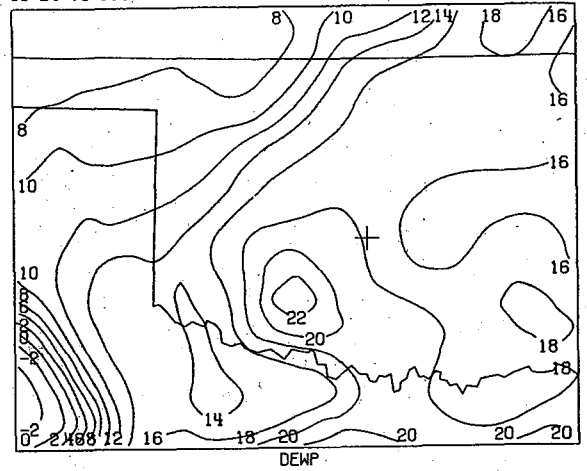
PD

Fig. B.4 Same as Fig. B.1, except at 1600 CST.

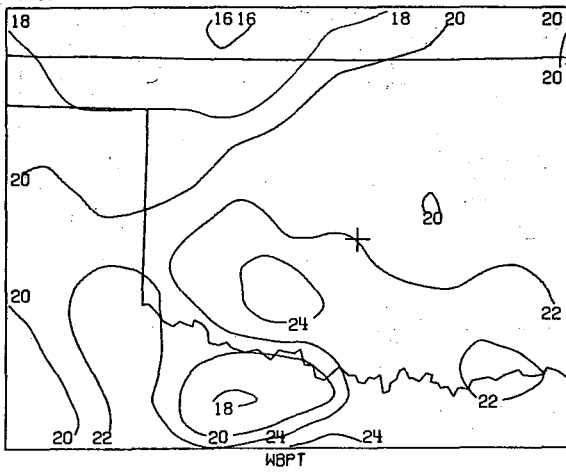
05-24-73 1600CST



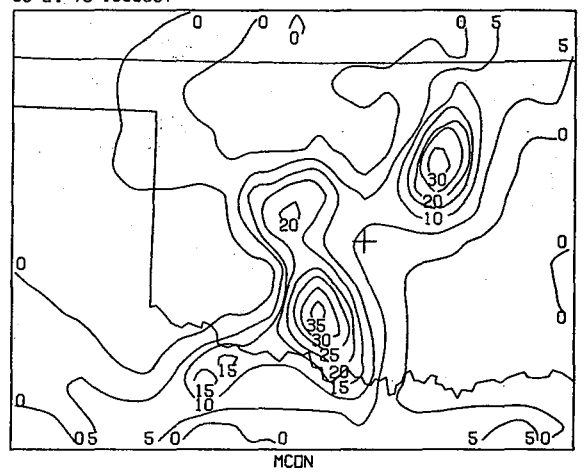
05-24-73 1600CST



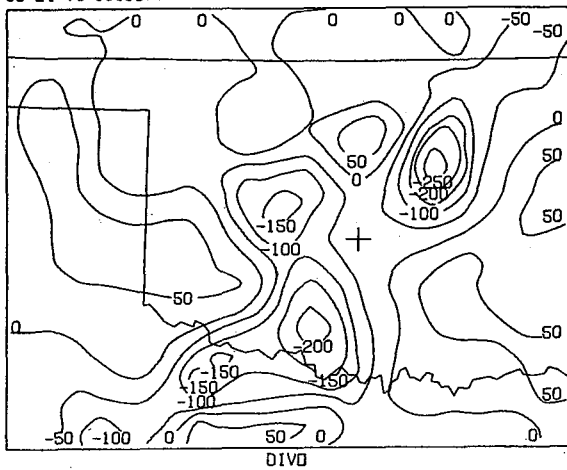
05-24-73 1600CST



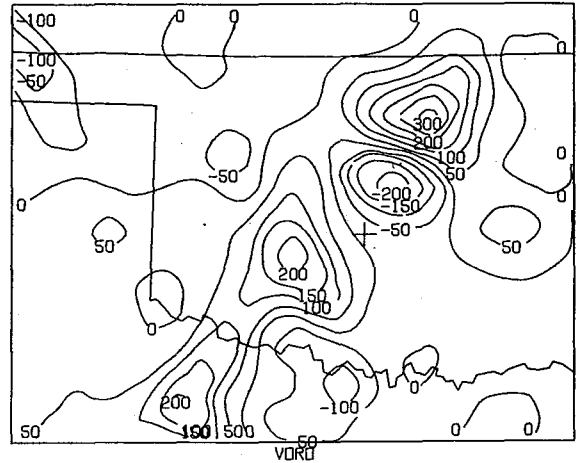
05-24-73 1600CST



05-24-73 1600CST

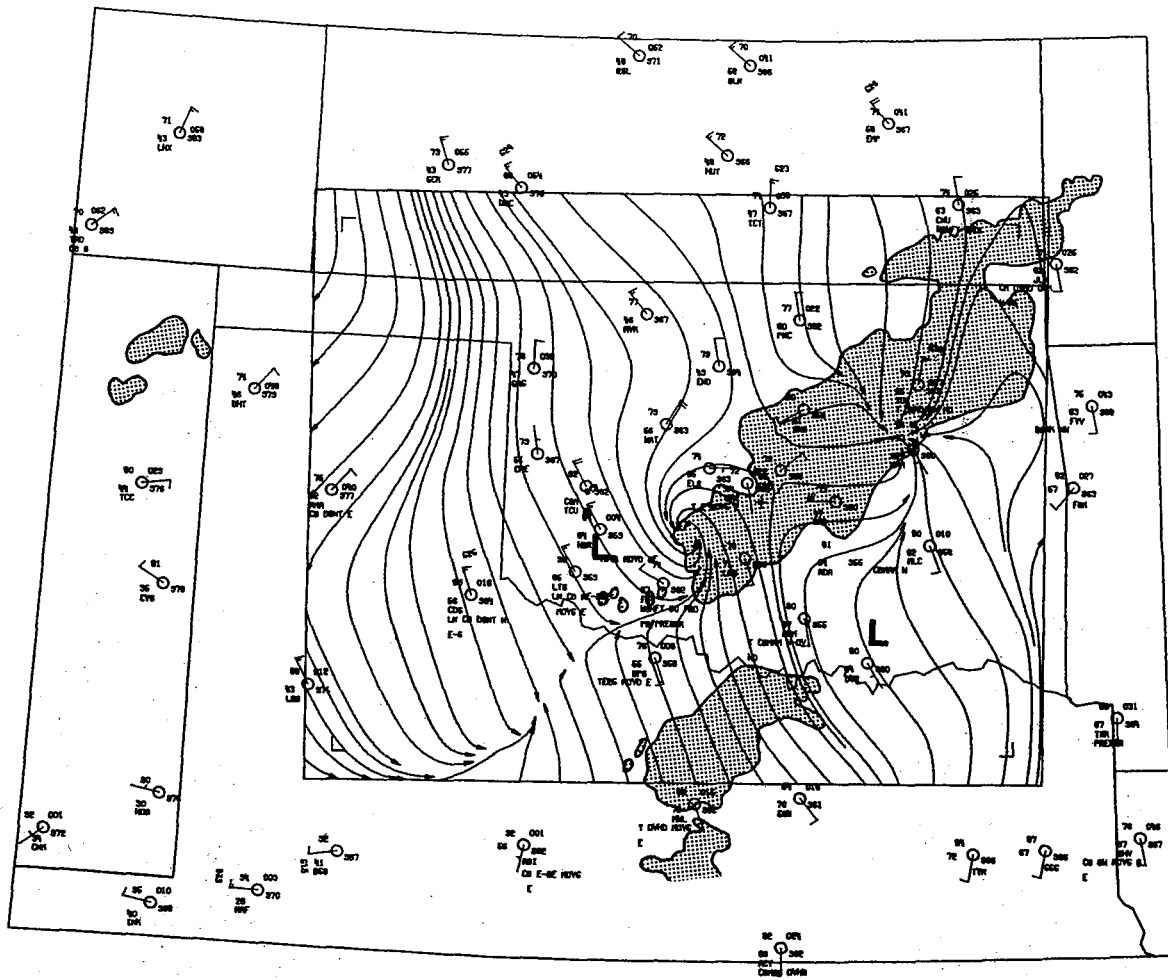


05-24-73 1600CST

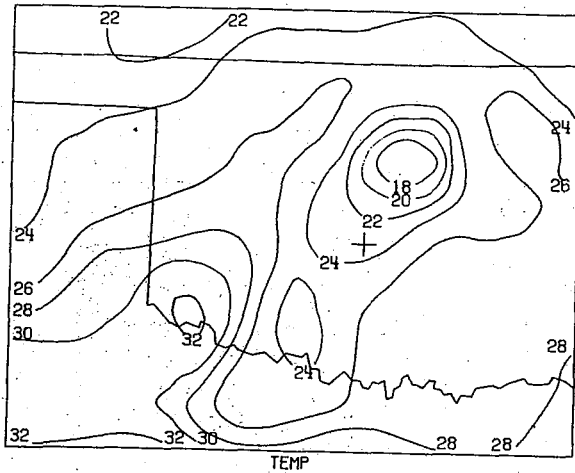


B. Subsynoptic Analyses

SURFACE MAP TIME 1700 CST DATE 052473



05-24-73 1700CST



05-24-73 1700CST

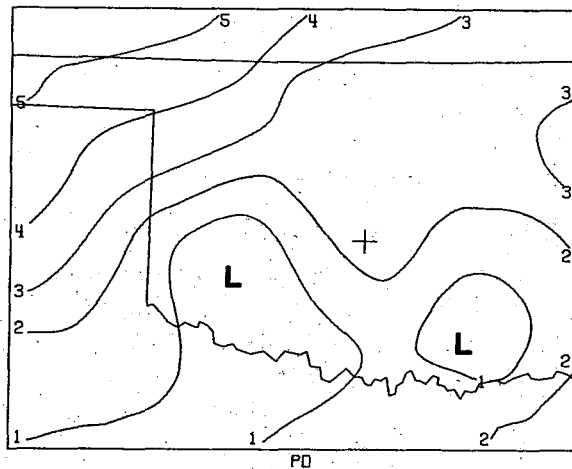
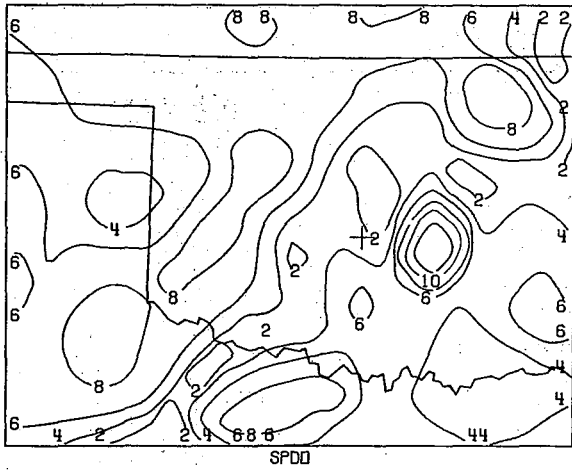
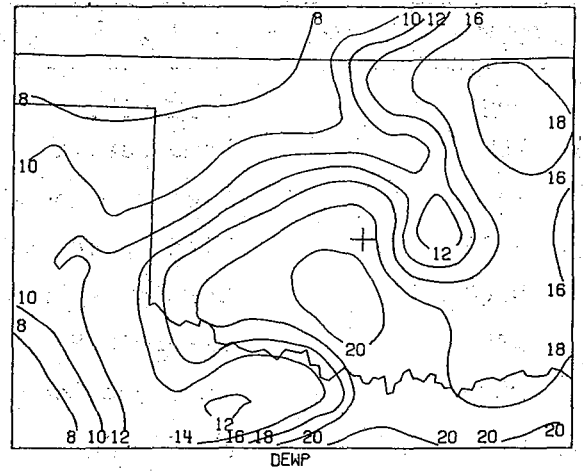


Fig. B.5 Same as Fig. B.1, except at 1700 CST.

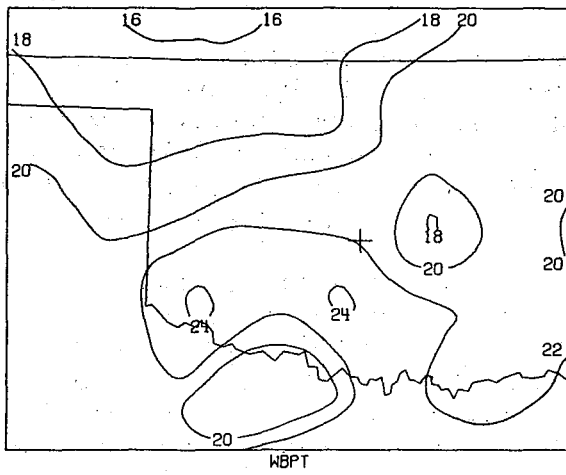
05-24-73 1700CST



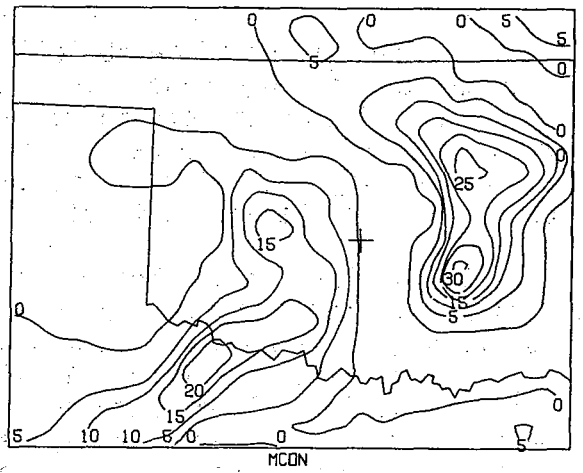
05-24-73 1700CST



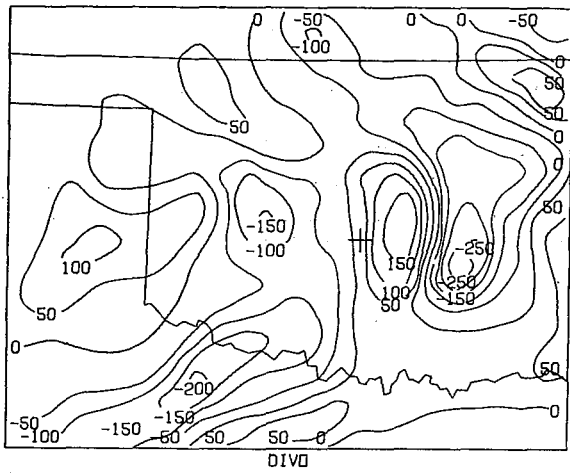
05-24-73 1700CST



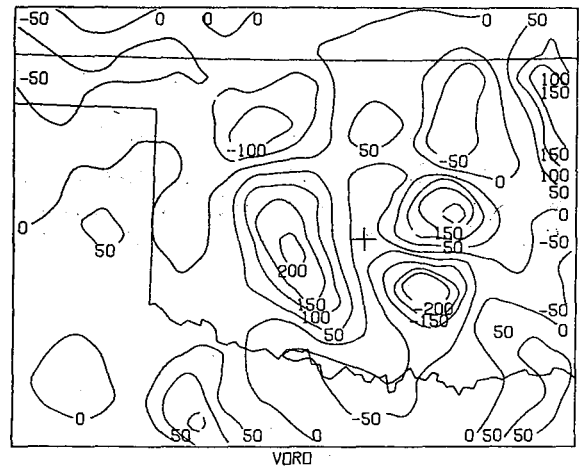
05-24-73 1700CST



05-24-73 1700CST



05-24-73 1700CST



B. *Subsynoptic Analyses*

TABLE B.1 *Key to Analyzed Meteorological Fields*

<u>CODE</u>	<u>PARAMETER</u>	<u>DIMENSIONS</u>
TEMP	Temperature	°C
PO	Pressure Anomaly (from 1000 mb)	mb
SPDO	Wind Speed	m s ⁻¹
DEWP	Dew-Point Temperature	°C
WBPT	Wet-Bulb Potential Temperature	°C
MCON	Moisture Convergence	10 ⁻⁴ g kg ⁻¹ s ⁻¹
DIVO	Divergence	10 ⁻⁶ s ⁻¹
VORO	Vorticity	10 ⁻⁶ s ⁻¹

The usefulness of an objective surface analysis program cannot be ascertained with one case study. Nevertheless, the following observations are made. All thundershowers formed and for the most part were contained within wind and moisture convergent areas. Although a large maximum was located in the Union City area at the time the tornado was on the ground, there was less continuity in the vorticity field than other meteorological fields.

It is clear that care must be used when interpreting meteorological fields computed with observations influenced by convection. Exclusion or suppression of such observations may help to define "undisturbed" meteorological fields. The objective analysis scheme tended to place fronts or other discontinuities halfway between observation sites rather than close to a particular site. Consequently, features may appear to "jump" in sparse data areas. In such cases, the plotting of remarks such as FROPA 1453 (frontal passage at 1453) can be a valuable aid to the user when evaluating the product.

ACKNOWLEDGMENTS

The author is indebted to Guy Lappie, Lester Showell and Gerald Wardius for setting up and maintaining the NSSL α mesonet stations used in this analysis. James Henderson developed the computer plotting program and Dr. Gary Achtemeier wrote the streamline and contour line algorithms.

REFERENCES

Barnes, S. L., 1973: Mesoscale objective map analysis using weighted time series observations. NOAA Tech. Memo. ERL NSSL-62, Norman, National Severe Storms Laboratory, 60 pp. (Available from National Technical Information Service, Springfield, Virginia 22151, No. COM-73-10781.)

Appendix C

RAWINSONDE OBSERVATIONS ON 24 MAY 1973

Edward A. Brandes

*National Severe Storms Laboratory
Norman, Oklahoma 73069*

Special rawinsonde observations for Fort Sill (FSI), Tinker Air Force Base (TIK), and NSSL (NRO) are presented. Data are displayed as computer-drawn Stüve diagrams. Wind vectors extend in the direction from which the wind blows and vector lengths are proportional to the observed speed (scale at lower right). Balloon ascent rates are assumed constant and height data (scale at right, km above sea level) are plotted versus time (circles), hence fluctuations in ascent rates indicate changes in environmental vertical velocity.

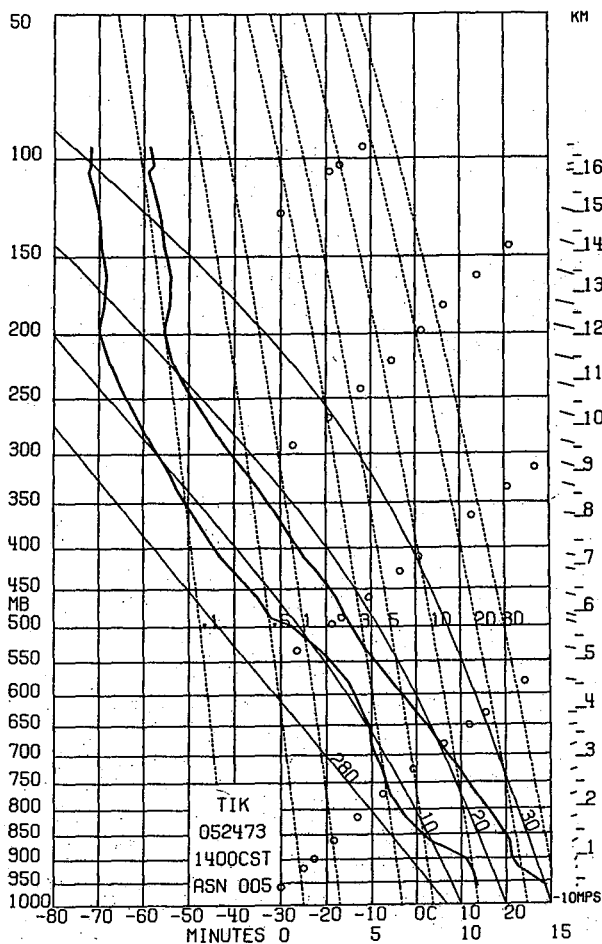
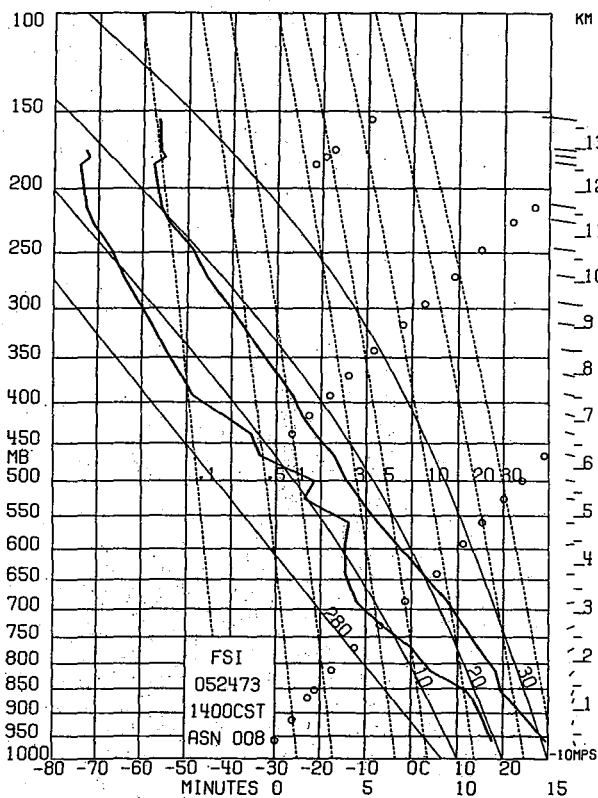


Fig. C.1 Rawinsonde released from Fort Sill, Oklahoma at 1400 CST on 24 May 1973.

Fig. C.2 Rawinsonde released from Tinker Air Force Base, Oklahoma at 1400 CST on 24 May 1973.

C. Rawinsonde Observations

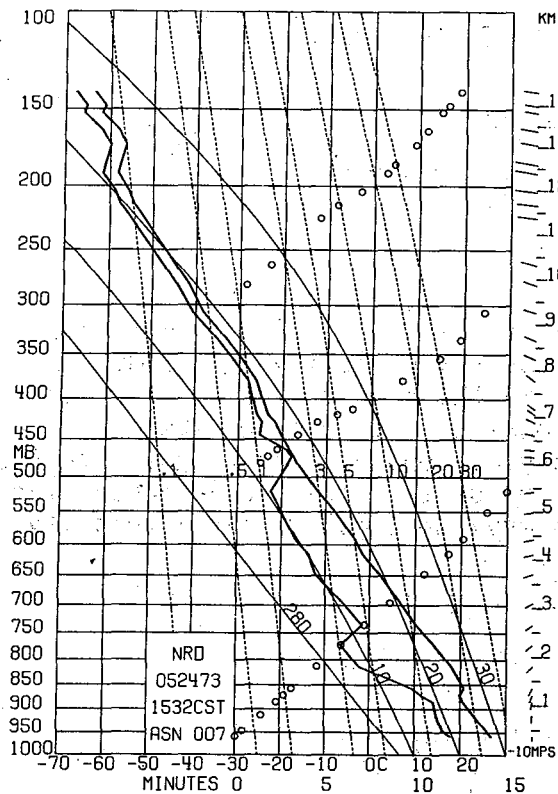


Fig. C.3 Rawinsonde released from NSSL, Norman, Oklahoma at 1532 CST on 24 May 1973.

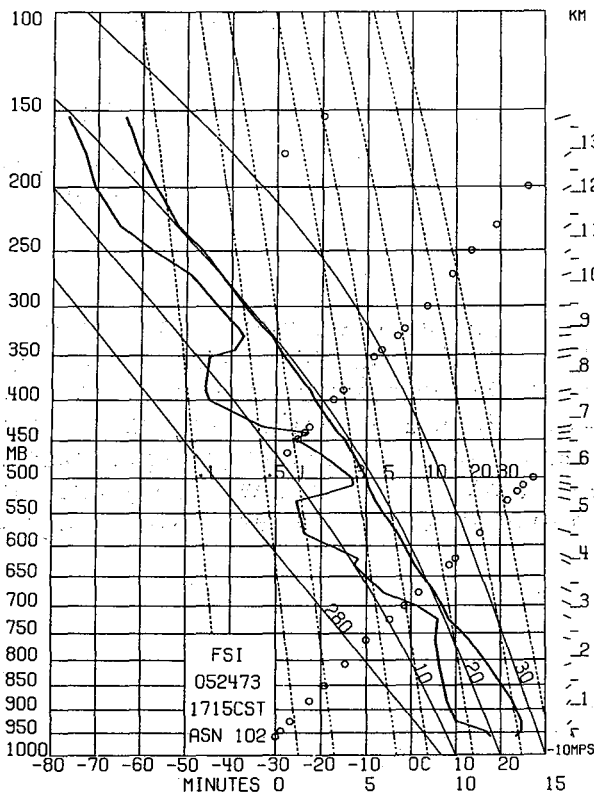


Fig. C.5 Rawinsonde released from Fort Sill, Oklahoma at 1715 CST on 24 May 1973.

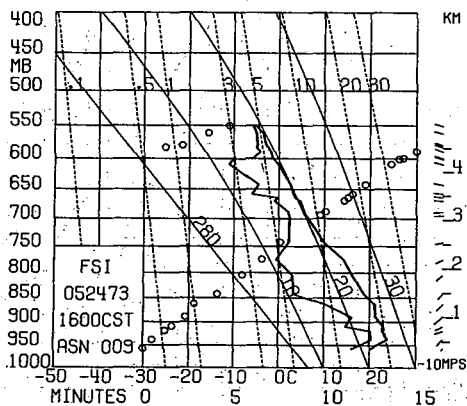


Fig. C.4 Rawinsonde released from Fort Sill, Oklahoma at 1600 CST on 24 May 1973.

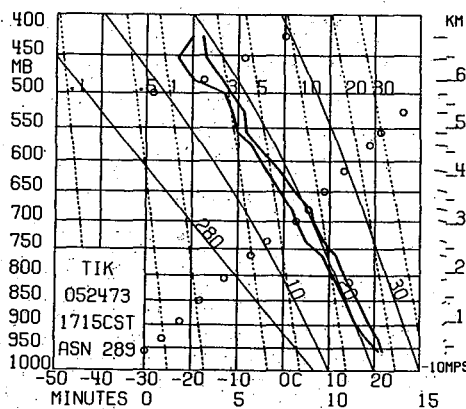


Fig. C.6 Rawinsonde released from Tinker Air Force Base, Oklahoma at 1715 CST on 24 May 1973.

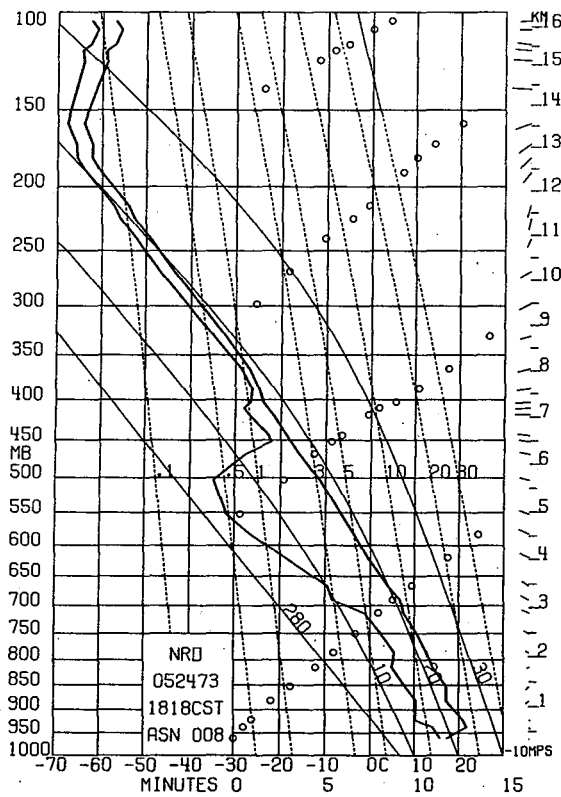


Fig. C.7 Rawinsonde released from NSSL, Norman, Oklahoma at 1818 CST on 24 May 1973.

ACKNOWLEDGMENTS

The special rawinsondes released by Fort Sill, Tinker Air Force Base and National Severe Storms Laboratory personnel are most appreciated. NSSL releases were handled by Robert Ketchum, Lester Showell and Gerald Wardius. Robert Ketchum established release procedures and performed the tedious task of reducing and thoroughly checking the data. James Henderson wrote the computer program for plotting the data.

Appendix D

NSSL DOPPLER AND WSR-57 RADAR CHARACTERISTICS

Dale Sirmans

*National Severe Storms Laboratory
Norman, Oklahoma 73069*

The NSSL Doppler radar and WSR-57 surveillance radar, both located at NSSL, have been central to the study of the Union City tornado and its parent storm. These 10-cm wavelength systems have comparable transmitter peak power and receiver performance, but the Doppler radar provides velocity estimates and much finer spatial resolution.

D.1 DOPPLER RADAR PARAMETERS

In 1971, NSSL put into operation the first 10-cm wavelength Doppler radar developed for severe storm studies. The radar's pencil beam (0.8° wide) and 150 m pulse length is well-suited for probing details of thunderstorm flow fields. Output of real time processors (mean velocity and intensity) and complex video (for spectrum analysis) are recorded on digital magnetic tape.

During the Spring 1973, the radar operated in one of two basic modes. One was the conventional or normal mode with a pulse repetition time (PRT) of 768 μ s and included capability of recording the digital complex video as well as radar intensity (Sirmans and Doviak, 1973a) and mean velocity by scalar phase change (Sirmans, 1973; Sirmans and Doviak, 1973b). Detailed characteristics of this mode are listed in Table D.1.

In the other mode, the radar PRT was slaved to the Air Force Cambridge Research Laboratories' coherent memory filter (Groginsky, 1965; Armstrong and Donaldson, 1969; Donaldson, Chapter 7). Although the real time estimates were available for analog display, no digital recording was possible. When slaved to the coherent memory filter and plan shear indicator (PSI), the radar pulse repetition frequency (PRF) and acquisition parameters were dictated by PSI characteristics given in Table D.2.

A hardware malfunction worthy of note in the 24 May 1973 data set is the failure of the digital intensity integrator caused by the 4 bit of the output word always being active. The failure was detected early in data acquisition and the system automatic gain control (AGC), which utilizes the integrator output, was switched off. Almost all data analyzed were taken in this fashion. AGC loss resulted in a decrease in effective dynamic range of the Doppler receiver chain to about 40 dB for undistorted spectral density estimates. Also, loss of the digital intensity estimate required the reflectivity to be calculated from the digital time series root mean square (RMS) amplitude (Zrnica, 1974).

D. NSSL Radar Characteristics

TABLE D.1 *Norman Doppler Radar System Characteristics During 1973*

Antenna

Diameter	9.15 m
Half-Power Beamwidth	0.81°
Gain	46.8 dB
Polarization	Vertical

Transmitter

Wavelength (f=2.85 GHz)	10.52 cm
Peak Power	500 kW
Pulsewidth	1 μs
Pulse Repetition Time (PRF=1302 Hz)	768 μs

Receiver

Transfer Function	Doppler - linear Intensity - logarithmic
Dynamic Range	60 dB
Bandwidth	4 MHz
Min. Detectable Signal (SNR=1)	-98 dBm

Doppler Time Series Data Acquisition

No. of Simultaneous Range Gates (1 Block)	16
Max. No. of Range Gate Blocks Along Radial	8
Range Gate Spacing	150, 300, 600, 1200 m
Complex Video Digital Word Length	10 bits (binary)
No. of Time Samples	2 ⁿ ; n = 2, 3, 4, 5...10 n = 6 (usually)

Intensity Data Acquisition

Averaging Weighting Function (Time Only)	Linear
No. of Range Gates	200
Range Gate Spacing	150, 300 m
No. of Samples in Estimate (Every Fourth Radar Pulse)	64
Recorded Word Length	6 bits (binary)
Estimate Standard Deviation	-1 dB

Real Time Velocity Data Acquisition (Scalar Phase Change)

No. of Range Gates	200
Range Gate Spacing	150, 300 m
No. of Samples in Estimate	256
Recorded Word Length	6 bits (signed binary)
Estimate Standard Deviation	-1 m s ⁻¹

General Features

Maximum Unambiguous Range	115 km
Maximum Unambiguous Velocity	±34 m s ⁻¹
Data Recording Interval:	
Azimuth	0.5, 1, 2°
Elevation	0.5, 1, 2°
Time	1, 5... s
Antenna Rotation Rate - Commensurate with Spatial Sampling and Data Acquisition Time	2° s ⁻¹ (usually)

TABLE D.2 Norman Doppler Radar Characteristics* in PSI Mode During 1973

System PRF	917 Hz
Receiver Bandwidth (PSI)	640 kHz
Gate Spacing (PSI gates)	5.7 μ s
Unambiguous Velocity	± 24 m s ⁻¹
Unambiguous Range	160 km
Antenna Rotation Rate	12° s ⁻¹

*Only those radar system characteristics which are different from Table D.1 are given.

Practically all quantitative analysis is performed on velocity estimates made from the time series data (complex video) by either fast Fourier transform (FFT) or the covariance technique known as pulse pair processing (PPP). Performance of these estimators are examined in detail by Berger and Groginsky (1973) and Sirmans and Bumgarner (1975). Comparisons of the two techniques for estimating mean velocity are shown in Figs. D.1 and D.2.

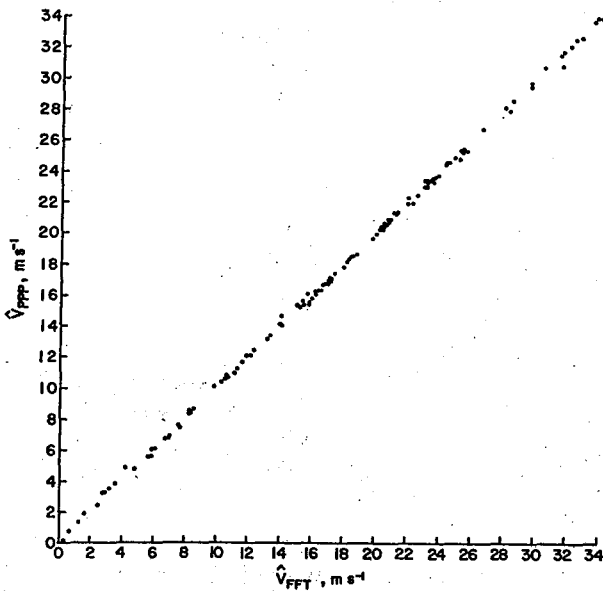


Fig. D.1 Regression of mean Doppler velocity estimate (\hat{V}) by covariance (PPP) versus estimate by fast Fourier transform (FFT). Estimates calculated from 64 sample time-series data having FFT spectrum widths between 0.5 and 4.3 m s⁻¹ and signal-to-noise ratios between 15 and 35 dB. Data were collected on 30 May 1973.

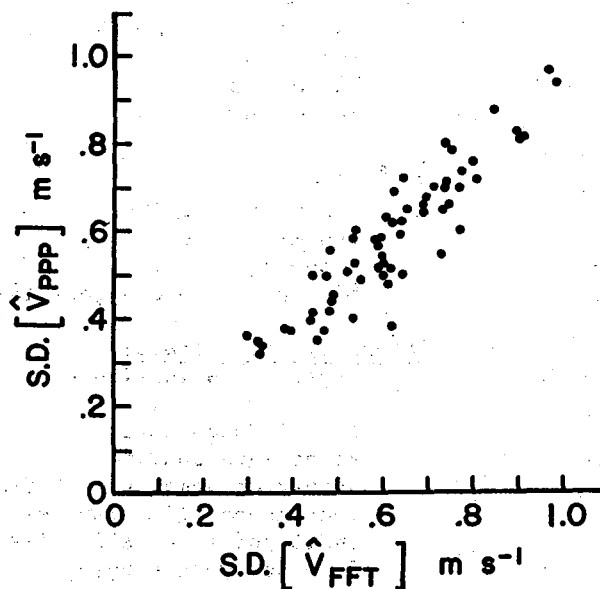


Fig. D.2 Standard deviation (S.D.) of mean Doppler velocity estimates using 64 sample time-series data. Standard deviation calculated from 15 mean velocity estimates having FFT spectrum widths between 1.0 and 3.6 m s⁻¹ and signal-to-noise ratios between 15 and 25 dB. Data were collected on 30 May 1973.

D. NSSL Radar Characteristics

Most of the intensity estimates were inferred from the RMS amplitude of the complex video. The standard deviation of these estimates are dependent on Doppler spectrum width with a value of about 1.5 dB for a spectrum width of 3 m s^{-1} .

D.2 WSR-57 RADAR PARAMETERS

The NSSL WSR-57 surveillance radar is a slightly modified version of the type used by the National Weather Service. It is equipped with a mean intensity processor and associated digital recorder. Radar system characteristics are listed in Table D.3.

TABLE D.3 NSSL WSR-57 Radar Characteristics During 1973

<u>Antenna</u>	
Diameter	3.66 m
Half-Power Beamwidth	2.2°
Gain	38.2 dB
Polarization	Horizontal
<u>Transmitter</u>	
Wavelength ($f=2.834 \text{ GHz}$)	10.58 cm
Peak Power	305 kW
Pulsewidth	4 μs
Pulse Repetition Time (PRF = 162.75 Hz)	6.144 ms
<u>Receiver</u>	
Transfer Function	Logarithmic
Dynamic Range	70 dB
Bandwidth	0.75 MHz
Min. Detectable Signal (SNR=1)	-100 dBm
<u>Intensity Data Acquisition</u>	
Averaging Weighting Function	Time = exponential Range = linear
No. of Range Gates	200
Range Gate Spacing	1 km
Number of Samples in Estimate	65
Independent Time Samples	31
Independent Range Samples	2.1
Recorded Word Length	6 bits (binary)
<u>General Features</u>	
Maximum Unambiguous Range	910 km
Data Recording Interval	
Azimuth	2°
Elevation	Selectable in 1° steps
Antenna Rotation Rate	18° s^{-1}

The standard deviation of the intensity estimate (both theoretical and measured) is 0.7 dB. Theory of the signal processing can be found in Sirmans and Doviak (1973a) and a detailed examination of the WSR-57 radar performance can be found in Sirmans (1974).

D.3 ACKNOWLEDGMENTS

The radar data represents the work of many NSSL personnel and in particular the effort of Walter Watts, Glen Anderson, and Jesse Jennings.

D.4 REFERENCES

- Armstrong, G. M., and R. J. Donaldson, Jr., 1969: Plan shear indicator for real-time Doppler radar identification of hazardous storm winds. J. Appl. Meteor., 8, 376-383.
- Berger, T., and H. L. Groginsky, 1973: Estimation of the spectral moments of pulse trains. Presented at Int. Conf. on Inform. Theory, Tel Aviv, Israel.
- Donaldson, R. J., Jr., 1976: Observations of the Union City tornadic storm by plan shear indicator. Chapter 7, The Union City, Oklahoma Tornado of 24 May 1973, R. A. Brown, Editor. NOAA Tech. Memo. ERL NSSL-80, Norman, Nat. Severe Storms Lab., 67-83.
- Groginsky, H. L., 1965: The coherent memory filter. Electron. Prog. (Raytheon), 9 (3).
- Sirmans, D., 1973: Real time estimates of mean velocity by averaging quantized phase displacements of Doppler radar echoes. 1973 SWIEEEO Record of Tech. Reports, 25th Annual Southwestern IEEE Conf. & Exhibition, New York, Inst. Electrical and Electronic Eng., 71-72 (IEEE Catalog No. 73CH0719-5 SWIEEEO).
- _____, 1974: Statistics of the intensity estimate with the WSR-57 digital integrator. Unpublished NSSL Memo.
- _____ and R. J. Doviak, 1973a: Meteorological radar signal intensity estimation. NOAA Tech. Memo. ERL NSSL-64, Norman, Nat. Severe Storms Lab., 84 pp.
- _____ and _____, 1973b: Pulsed Doppler velocity isotach displays of storm winds in real time. J. Appl. Meteor., 12, 694-697.
- _____ and B. Bumgarner, 1975: Numerical comparison of five mean frequency estimators. J. Appl. Meteor., 14, 991-1003.
- Zrnic, D. S., 1974: Determination of the true RMS value of a Gaussian process from the clipped data. Unpublished NSSL Memo.

Appendix E

SINGLE DOPPLER RADAR DATA ACQUISITION AND ANALYSIS

Rodger A. Brown

*National Severe Storms Laboratory
Norman, Oklahoma 73069*

Due to desired temporal and spatial data resolution in severe storms, Doppler radar measurements are restricted to limited regions of space. Preparation of these recorded data for analysis involve two major steps. First, an archive data tape is prepared where hardware and recording problems have been corrected. Second, the meteorologist prepares a user tape that contains data tailored to analysis and research specifications. Once data are in proper form, they can be interpolated to grid points for further analysis and interpretation. A data sample, from the Union City tornadic storm, illustrates how an interpolation scheme modifies the extreme values and gradients within the data field.

E.1 INTRODUCTION

The purpose of this Appendix is to outline the data collection, editing and analysis procedures employed at NSSL during 1973 and especially for the Union City tornadic storm on 24 May 1973. To clarify the reasons for some of these procedures, we start with a discussion of pulsed Doppler radar general characteristics.

E.2 GENERAL DOPPLER RADAR CHARACTERISTICS

A Doppler radar transmits a coherent signal and detects the phase difference between transmitted and received radar signals. The time rate of phase change ($d\phi/dt$) is related to the radial component of target motion relative to the radar by the Doppler radar equation (Battan, 1973):

$$\frac{1}{2\pi} \frac{d\phi}{dt} = f_d = -2 V/\lambda , \quad (E.1)$$

where f_d is Doppler frequency shift, V is Doppler velocity (by convention, velocities toward the radar are negative, those away are positive), and λ is radar wavelength. Thus as a Doppler radar scans a storm it measures the radial components of all targets within the radar sample volume weighted by their respective reflectivity values; the net result is a spectrum of Doppler velocity values.

E. Doppler Acquisition and Analysis

A pulsed Doppler radar is a time sampled data system and thus is subject to sampling criteria. It can be shown (e.g., Battan, 1973) that the maximum unambiguous range (r_{\max}) and maximum unambiguous Doppler velocity (V_{\max}) measured by a Doppler radar are governed by the relationships:

$$r_{\max} = c/(2 \text{ PRF}) , \quad (\text{E.2})$$

$$V_{\max} = \pm \lambda(\text{PRF})/4 , \quad (\text{E.3})$$

where c is radio wave propagation speed ($3 \times 10^8 \text{ m s}^{-1}$) and PRF is the pulse repetition frequency of the transmitter.

A basic limitation of pulsed Doppler radars becomes apparent when Eqs. (E.2) and (E.3) are combined:

$$V_{\max} \cdot r_{\max} = \lambda c/8 . \quad (\text{E.4})$$

The larger the desired maximum unambiguous range, the smaller will be the unambiguous velocity interval, and vice versa (Fig. E.1). Therefore, a compromise must result. Investigators using 3.2-cm wavelength Doppler radars typically choose a maximum range of about 75 km and maximum velocity of about $\pm 16 \text{ m s}^{-1}$ --indicated by the dot in Fig. E.1 (e.g., Lhermitte, 1970; Lhermitte, 1974).

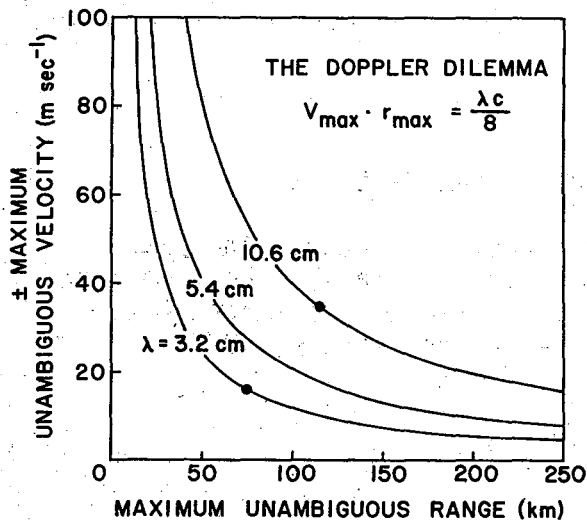


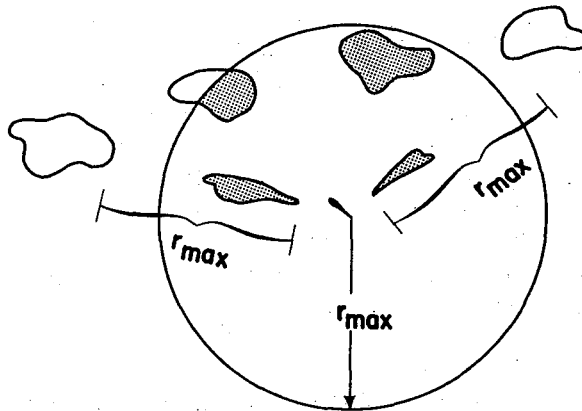
Fig. E.1 Relationship between maximum unambiguous range and maximum unambiguous Doppler velocity as a function of radar wavelength (λ). Dots indicate typical trade-offs between range and velocity.

For the study of severe storms in Oklahoma, however, much larger unambiguous velocities and ranges are required. One must then use as long a wavelength as is practical, considering beamwidth and antenna size limitations. At 10-cm wavelengths, the compromise chosen for the NSSL Doppler radar was a maximum range of 115 km and maximum velocity of $\pm 34 \text{ m s}^{-1}$ (Sirmans, Appendix D). Another advantage of operating at this longer wavelength is reduced signal attenuation by heavy precipitation areas in severe storms.

The maximum unambiguous range is the maximum distance (radial) at which a transmitted pulse can be reflected and return to the radar before the next pulse is transmitted. When a radar echo is located beyond the maximum unambiguous range, the signal

returns from that area after the next pulse is transmitted--consequently, range is determined relative to the second pulse. Thus, the echo appears on the PPI scope at a range equal to the true range minus r_{max} (Fig. E.2). Since the angular width of the echo area remains unchanged, the echo usually appears elongated along the radial.

While maximum unambiguous range affects the apparent range of a radar echo, the maximum unambiguous velocity affects the measured Doppler velocity values. If the true radial velocity exceeds the maximum unambiguous velocity limits of $\pm V_{max}$, the radar measures an erroneous "folded" velocity value within the $\pm V_{max}$ velocity limits that is offset from the true value by a multiple of $2 V_{max}$ (Fig. E.3). For example, a 3-cm Doppler radar having a maximum unambiguous velocity of $\pm 16 \text{ m s}^{-1}$ measures a true spectrum mean velocity of $+20 \text{ m s}^{-1}$ as -12 m s^{-1} ($20 - 32 \text{ m s}^{-1}$); in fact, true velocities of $+52, +20, -12, -44 \text{ m s}^{-1}$, etc., all produce a measured mean Doppler velocity of -12 m s^{-1} . On the other hand, a 10-cm radar with $\pm 35 \text{ m s}^{-1}$ unambiguous velocity measures the true 20 m s^{-1} velocity correctly; in this case, mean velocities would have to be as extreme as $+90$ or -50 m s^{-1} (20 ± 70) before a folded mean velocity of 20 m s^{-1} would be measured.



DOPPLER RADAR RANGE AMBIGUITY

Fig. E.2 Schematic radar scope presentation of range ambiguity involving a WSW-ENE line of four radar echoes. Shaded echoes are those that actually would be detected by a Doppler radar with limited unambiguous range (r_{max}).

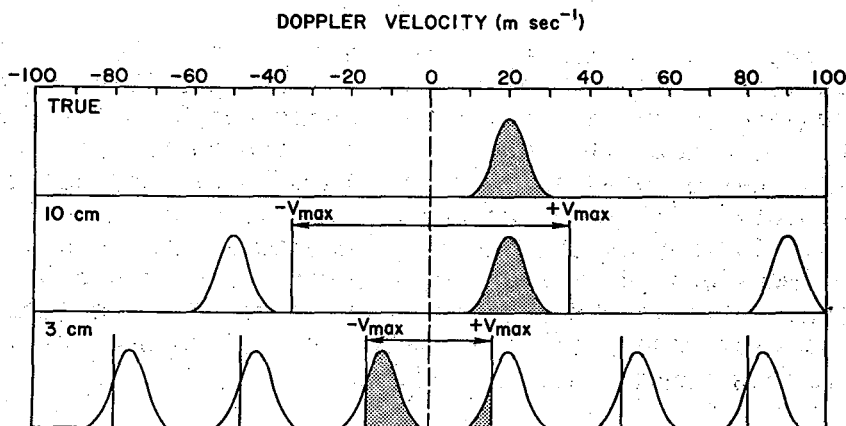


Fig. E.3 Hypothetical Doppler velocity spectra illustrating the velocity folding problem at 3 and 10 cm wavelengths.

E.3 DATA ACQUISITION PROCEDURES

The NSSL WSR-57 surveillance radar plays an important role in conjunction with Doppler radar investigations of severe storms. It provides a continuous history of storm evolution (recorded on film and digital tape) and aids in selection of individual storms for limited azimuthal sector scanning by Doppler radar. With an unambiguous maximum range of 910 km, the WSR-57 radar is used to resolve Doppler range ambiguities that may not be as apparent as those in Fig. E.2. When the surveillance radar indicates that two echoes are at the same azimuth and separated in range by r_{\max} , no data are collected unless the more distant echo is significantly weaker. When a nonoverlapping storm of interest is beyond the maximum unambiguous range, a flag is set (on the digital tape) to indicate that r_{\max} should be added to all range values during computer processing.

The mass of data required for Doppler velocity processing and the four-dimensional density of data required for meteorological analysis dictate that data collection be restricted to a limited region of space. In 1973, all Doppler velocity measurements were in the form of time-series data, that is, the in-phase and quadrature components of the radar complex video signal were recorded for a finite number of pulses. Typically the time-series record consisted of 64 consecutive pulses from the same point in space. For the radar characteristics tabulated by Sirmans (Appendix D), a mean Doppler velocity value computed from 64 samples has a standard error of approximately 1 m s^{-1} ; the standard error of the mean velocity estimate decreases proportionately as the square root of the number of samples increases.

Time-series data are recorded simultaneously at 16 discrete range locations. About 0.07 s are required for the sampling and recording of 64 pulses from one block of 16 range gates. A number of 16-gate blocks with gates separated by 0.6 km, for example, are needed to cover the range interval (30 to 40 km) of a severe thunderstorm. Thus, the radar antenna must rotate slowly enough for the returned signal to be sampled and recorded before the next desired data azimuth is reached. For azimuthal data spacing of 1 deg (1 km increment at range of 60 km), typical rotation rates are 2 to 4 deg s^{-1} .

At these rates, approximately 4 to 6 min are required to complete a tilt sequence up through a storm. Sometimes it is not possible to record a complete tilt sequence on one digital tape (maximum of 3000 16-gate blocks). When this happens, a new tilt sequence is started on the next tape because the several minutes that elapsed during tape change would produce too large a time gap in the completed tilt sequence and would double the time interval between tilt sequences. In many cases, one must compromise the acquisition parameters (e.g., three-dimensional data spacing, azimuthal sector width, Doppler velocity resolution, etc.) in order to record measurements from the entire storm on the same computer tape. (This situation has since been relieved by use of more efficient data acquisition procedures.)

E.4 DATA PREPARATION PROCEDURES

Time-series data recorded at the radar site are transformed into frequency data that are directly proportional to Doppler velocities. From these data and other measurements an archive tape is generated. Archive tapes provide the basic data source for meteorological analyses. However, before performing analyses, the user frequently edits the data by using a signal-to-noise ratio (SNR) threshold, unfolding folded velocities and eliminating obviously erroneous values.

E.4.a Archive Tape Preparation

Preparation of NSSL Doppler radar archive tapes is the responsibility of the Computation and Data Processing (CDP) Group. The most time-consuming part of the task is to diagnose and correct correctable hardware and recording errors. These errors can occur in the time-series data, integrated reflectivity and "housekeeping" information (that is, range, azimuth, elevation, time, etc.). As a matter of policy, no missing data or bad data are replaced by interpolated values on the archive tape.

A routine aspect of the task is transforming time-series measurements from the time domain to the frequency domain through the use of a fast Fourier transform (FFT) process (Sirmans and Bumgarner, 1975). This procedure results in a Doppler velocity spectrum from which the spectrum mean and standard deviation can be computed. However, before these parameters are computed, several things must be done. First, a threshold (15 dB below the spectrum peak for strong signals) must be specified to eliminate noise and the ever-present secondary mirror image (relative to zero Doppler velocity) of the primary velocity spectrum. Second, a check must be made for partially folded spectra (like shaded 3-cm spectrum in Fig. E.3); the side containing the spectral peak is assumed to be correct (wrong choice for Fig. E.3 example) and the smaller portion is unfolded to its proper relative position before the mean and standard deviation are computed. (For the 3-cm spectrum example, the mean spectrum velocity would be identified as being folded during preparation of the user data tape.)

During 1973 (continuing through mid-1975), equipment problems caused a strong spectrum mirror image to occur in specific range gates. For Doppler velocity magnitudes greater than 17 m s^{-1} , the image was slightly stronger than the true spectrum; the computer program chose the image to be correct and discarded the other half of the spectrum. The resulting mean Doppler velocity was of nearly proper magnitude but wrong sign.

When one is not interested in seeing the Doppler velocity spectrum, a pulse-pair processor (PPP) computer algorithm can be used to compute the vector mean and standard deviation directly from the time-series data (Sirmans and Bumgarner, 1975). The PPP procedure has two distinct advantages over the FFT process: signal can be extracted at lower signal-to-noise ratios and the mean is computed directly (without spectrum manipulations) when the spectrum is partially folded.

E. Doppler Acquisition and Analysis

In addition to housekeeping information that identifies data location in four dimensions, the archive tape contains range-normalized reflectivity (from hardwired integrator), Doppler velocity mean and standard deviation computed from time-series data using either the FFT or PPP algorithm and, in 1973 only, a hardwired scalar mean velocity processor that proved to be inappropriate for severe storm applications. Since the reflectivity integrator failed on 24 May 1973, reflectivity data had to be computed from the time-series data; unfortunately the signal was saturated at higher reflectivities and, thus, reflectivity values have an upper limit of 45 to 50 dBZ (Sirmans, Appendix D).

E.4.b User Tape Preparation

When pursuing one's own research objectives, a meteorologist may use specialized analysis techniques that require data in a unique format; thus, more than one type of user tape may be produced. Typically the user tape is a condensed version of the archive tape with data having weak returned power deleted (because velocity measurements are unreliable when the ratio of signal to noise is small) and with mean Doppler velocity values corrected for folding.

To aid the analyst in determining data quality and information content, B-scan printer outputs (range versus azimuth display of data at each elevation from the archive tape) are requested from CDP. By comparing signal-to-noise ratio values with the region where mean Doppler velocity values become noisy, a SNR threshold is established. On the user tape, all data are flagged as missing when the SNR is below the threshold value (typically 15 dB).

Inspection of the B-scan print-out reveals the location of gates with mean velocity image problems. On the user tape, mean Doppler velocity values at these gate locations either are flagged as missing or are corrected.

With SNR thresholds, image gates, and any obviously erroneous mean Doppler velocity values taken care of, the correction of folded mean velocities can commence. A unique characteristic of velocity folding is the abrupt change in velocity (such as from $+34$ to -34 m s^{-1} for the Norman Doppler radar). The unfolding technique we employ computes the velocity difference between adjacent range gates along each radial from the radar. With range gates positioned 600 m apart, the radial difference (due to velocity folding) frequently is less than 68 m s^{-1} . Therefore one must establish a threshold value that is greater than naturally occurring radial velocity differences but less than differences observed with velocity folding. Typical threshold values are 45 to 50 m s^{-1} between adjacent gate positions.

Final preparation of the user tape includes a data print-out incorporating all modifications for confirming that the data set is error-free. With confidence in the corrected data tape, the user proceeds with data analysis.

E.5 DATA INTERPOLATION TECHNIQUE

Radar data--collected at uniform range, azimuth and elevation increments--are not uniformly distributed in space and, more importantly, are not distributed in horizontal or vertical planes that the meteorologist prefers. Therefore, data are interpolated to planar surfaces before meteorological analysis and interpretation proceed.

There are a number of interpolation techniques available, ranging from a simple procedure using the value of the closest data point for the grid point value to more sophisticated procedures designed to bring out particular wavelengths in the data (e.g., Cressman, 1959; Barnes, 1973) or that use a weighting function based on the autocorrelation of the data field (e.g., Eddy, 1967). Considering the fact that radar data density decreases with range, an approach has been devised for Union City data analysis that uses the same number of data points for interpolating grid point values, regardless of grid point range from the radar. The variable radius of influence--which is the maximum distance a data point can be away from a grid point and still influence the interpolated grid point value--consequently is based on the average three-dimensional data separation; for every 10-km range interval a different influence radius is used.

E.5.a Three-Dimensional Weighting Function

A weighting function (W) of the following form--originally proposed by Cressman (1959)--is used for the computation of grid point values:

$$W = \frac{R_0^2 - R^2}{R_0^2 + R^2} \geq 0, \quad (E.5)$$

where R_0 is radius of influence and R is distance from grid point to data point. When a data point coincides with the grid point ($R=0$), a weight of 1.0 is given to that data value (Fig. E.4). As the distance between grid point and data point increases, the value of the weighting function decreases until at $R = R_0$ the weight is zero. No data points at distances greater than R_0 contribute to the grid point value.

Choice of the Cressman weighting function was based primarily on its computational simplicity. Also the decision to use it as a spherical instead of ellipsoidal weighting function was based on simplicity. Although not an optimum weighting function, it is adequate for objective analysis of single Doppler radar data.

Even though a fairly large number of data points may occur within the sphere of influence, slightly less than one-fifth of them have a weight greater than 0.5 (Fig. E.4). In fact half of the data points have a weight of 0.23 or less. Therefore, the interpolated grid point value will be highly influenced by relatively few nearby data values, with the lesser influence of more distant values serving to smooth or filter out small-scale meteorological noise.

E. Doppler Acquisition and Analysis

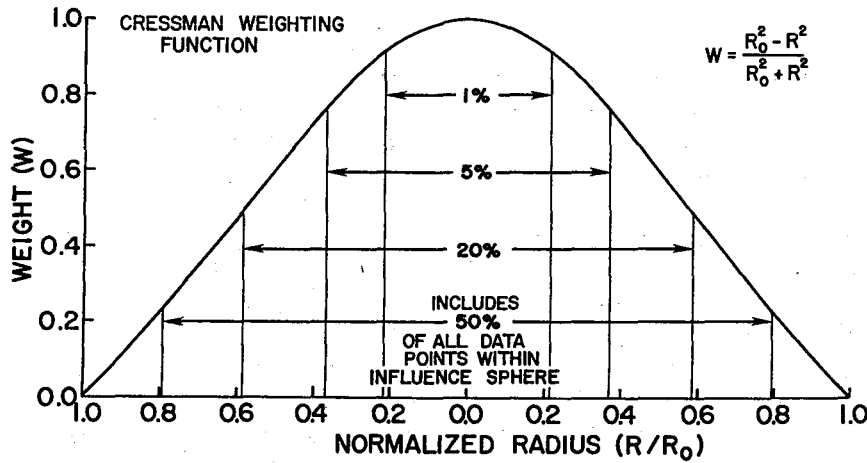


Fig. E.4 Data point weighting values as a function of normalized distance from grid point. Percentages of all data points (within influence sphere) which lie within various normalized distances of the grid point are indicated.

E.5.b Computation of Weighted Mean Value

This technique uses the method of least squares to determine the interpolated grid point value. For each of the N data points within the sphere of influence, let ϵ_n be the difference between the interpolated grid point value (\hat{V}) and the n th data point value (V_n):

$$\epsilon_n = (\hat{V} - V_n) \quad (E.6)$$

Summing the weighted squares of differences,

$$S = \sum_{n=1}^N W_n \epsilon_n^2 = \sum_{n=1}^N W_n (\hat{V} - V_n)^2 \quad (E.7)$$

We want to choose \hat{V} such that the weighted variance, S , is minimized. Thus, differentiating S with respect to \hat{V} and setting the result equal to zero, we obtain the normal equation,

$$\sum_{n=1}^N W_n (\hat{V} - V_n) = 0 \quad (E.8)$$

The summation can be expanded into

$$\hat{V} \sum_{n=1}^N W_n = \sum_{n=1}^N W_n V_n \quad (E.9)$$

where \hat{V} is a constant relative to the summation. Rearranging terms, we have the expression for computing the weighted mean value

$$\hat{V} = \frac{\sum_{n=1}^N W_n V_n}{\sum_{n=1}^N W_n} \quad , \quad (E.10)$$

where the W_n are determined from Eq. (E.5).

The above development, following Draper and Smith (1966), shows that the expression commonly used to compute the weighted mean grid point value is a weighted least-squares fit to all data point values within the sphere of influence centered on the grid point.

Since a storm typically moves several kilometers during the time required to collect a three-dimensional data set, it is necessary to spatially adjust each data point to the location it would have had at a specified reference time. This spatial adjustment is accomplished by using the speed and direction of a characteristic storm feature (e.g.; reflectivity centroid, bounded weak echo region, tornadic vortex signature, parent circulation center). The adjusted data then are interpolated to grid point locations on arbitrarily-oriented vertical or horizontal cross-sections through the storm. A set of such cross-sections constitutes a three-dimensional grid array of a particular radar parameter (reflectivity, mean Doppler velocity, standard deviation of the Doppler velocity spectrum).

Actual employment of Eq. (E.10) is not on a grid point by grid point basis but rather data point by data point. For each data value read from the user data tape, the grid point subset within the influence radius is determined. The properly weighted data value then is accumulated at each grid point position; the weight value itself also is accumulated at the same time. After all data points have been read, the summed weighted value at each grid point is divided by the corresponding sum of weights.

Since a particular radar echo will not occupy the entire grid array, care must be taken such that data are not extrapolated to grid points outside the echo area. Two independent checks are made to prevent data extrapolation; if (a) the number of data points within the influence sphere is less than a specified percentage of the maximum number possible or (b) the accumulated weights are less than a specified value, then a flag is set to indicate that the grid point is too far away from data points to have a representative weighted mean value computed.

E.5.c Effect of Influence Radius

Any interpolation scheme produces a smoothed analyzed field. The amount of smoothing typically can be controlled by the user. Interpolation leads to

E. Doppler Acquisition and Analysis

several noticeable changes in the analyzed fields relative to the raw data values; namely, smaller scale "noise" is suppressed and extreme data values and gradients of large scale features are reduced in magnitude.

Elimination of small scale noise can be expressed as a reduction of over-all variance in the data field. Doviak *et al.* (1976) derived the following expression for computing variance reduction for a spherical Cressman weighting function:

$$\text{Variance Reduction} = 1 - 0.418(R_0/\bar{D})^{-3/2}, \quad (\text{E.11})$$

where R_0/\bar{D} is the ratio of the influence radius to the three-dimensional average data spacing (\bar{D}). Derivation of Eq. (E.11) is based on the assumption that data points are uniformly distributed within the influence sphere; this assumption is not strictly satisfied in general. The equation is approximate for R_0/\bar{D} values less than 1.5.

Choice of an appropriate influence radius depends, in part, upon the scale of phenomena being investigated. To illustrate effects of the influence radius, Doppler velocity and reflectivity data from the 1545 CST tilt sequence on 24 May 1973 were objectively analyzed at a height of 3.0 km. In the sub-region selected for display, average three-dimensional data spacing ranged from approximately 1.0 to 1.4 km (Fig. E.5).

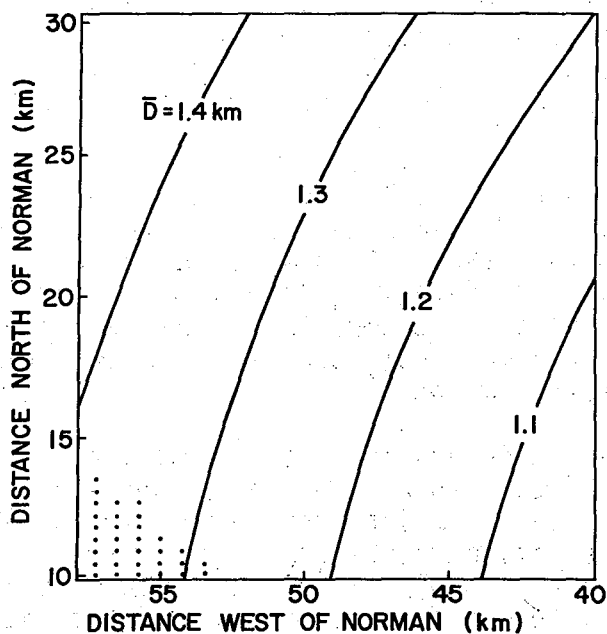


Fig. E.5 Average three-dimensional data spacing (\bar{D}) for the fields presented in Figs. E.6 and E.7. Grid point spacing (dictated by print-out) indicated in lower left corner.

There is a pronounced interpolation influence on small scale features of the Doppler velocity field (Fig. E.6). The data field collected at 3.8 deg elevation (Fig. E.6a)--primary source of data affecting the 3.0 km objective analysis--contains the tornadic vortex signature (48 km west, 20 km north) discussed by Brown and Lemon (Chapter 15). Extreme values of -21 and $+36 \text{ m s}^{-1}$ occur at adjacent data points about 0.9 km apart. With an average three-dimensional data spacing of 1.2 km in that area, the use of a 1.2 km influence radius ($R_0/\bar{D} = 1.0$) completely masks the signature because both extreme values lie within the influence radius of all grid points in the immediate vicinity (Fig. E.6b). Note that larger scale features are retained relatively unchanged except for decreased gradients. As the radius of influence

increases (Fig. E.6c and d), the field becomes progressively flatter with only the prevailing larger scale features remaining.

The corresponding radar reflectivity field (Fig. E.7) exhibits similar features. In general, the most significant change is between the subjective analysis and the first objective analysis ($R_0/\bar{D} = 1$); this fact is reflected in a theoretical variance reduction of 58%. With an increase of R_0 to twice \bar{D} , 85% of the variance in the original data field has been smoothed out.

Cressman (1959), Barnes (1973) and others have used the method of successive corrections to recover smaller scale features lost during the first analysis pass through the data. On successive passes, the difference between the original data value and the previously analyzed value (interpolated back to the data position) is interpolated to the grid location and added to the previous value. One (Barnes) or more (Cressman) passes are required to bring out details in the original data. This approach has not been used here because small-scale features such as the tornadic vortex signature should not appear in the larger-scale analyses.

Stephens and Stitt (1970) have investigated optimum influence radii for the successive corrections approach. They find that the optimum radius is primarily dependent upon average data spacing. For a given data spacing, the radius increases as the data noise level increases. Also, for the same average data spacing, nonuniform spacing (indicating some areas with larger distances between data points) requires a larger influence radius than uniformly distributed data. Under average conditions, the optimum radius of influence for first pass should be between 1.0 and 1.5 times the average data spacing; this radius size seems reasonable relative to Figs. E.6 and E.7.

E.6 SUMMARY

The acquisition and analysis of Doppler velocity data is more complicated than that for conventional radar reflectivity data. During data collection, trade-offs among the acquisition parameters (overall azimuthal sector width, data density, Doppler velocity resolution, etc.) must be considered in order to fit one tilt sequence of time-series data on a single data tape.

Prior to data analysis, the user must have sufficient knowledge of general Doppler radar characteristics to be on the look-out for superimposed range-folded echoes, areas of velocity folding, presence of image gates, Doppler velocity values that are too noisy to use (resulting from low signal-to-noise ratios), etc. As is the situation with all types of meteorological data, the user must be aware of instrument idiosyncracies and must be familiar with data quality before attempting data analysis.

Since Doppler radar data must be interpolated to a set of horizontal or vertical cross-sections to facilitate data interpretation, the user also must be very familiar with the interpolation scheme. Otherwise, one might develop an erroneous theory because the ramifications of using a particular analysis procedure were not understood.

E. Doppler Acquisition and Analysis

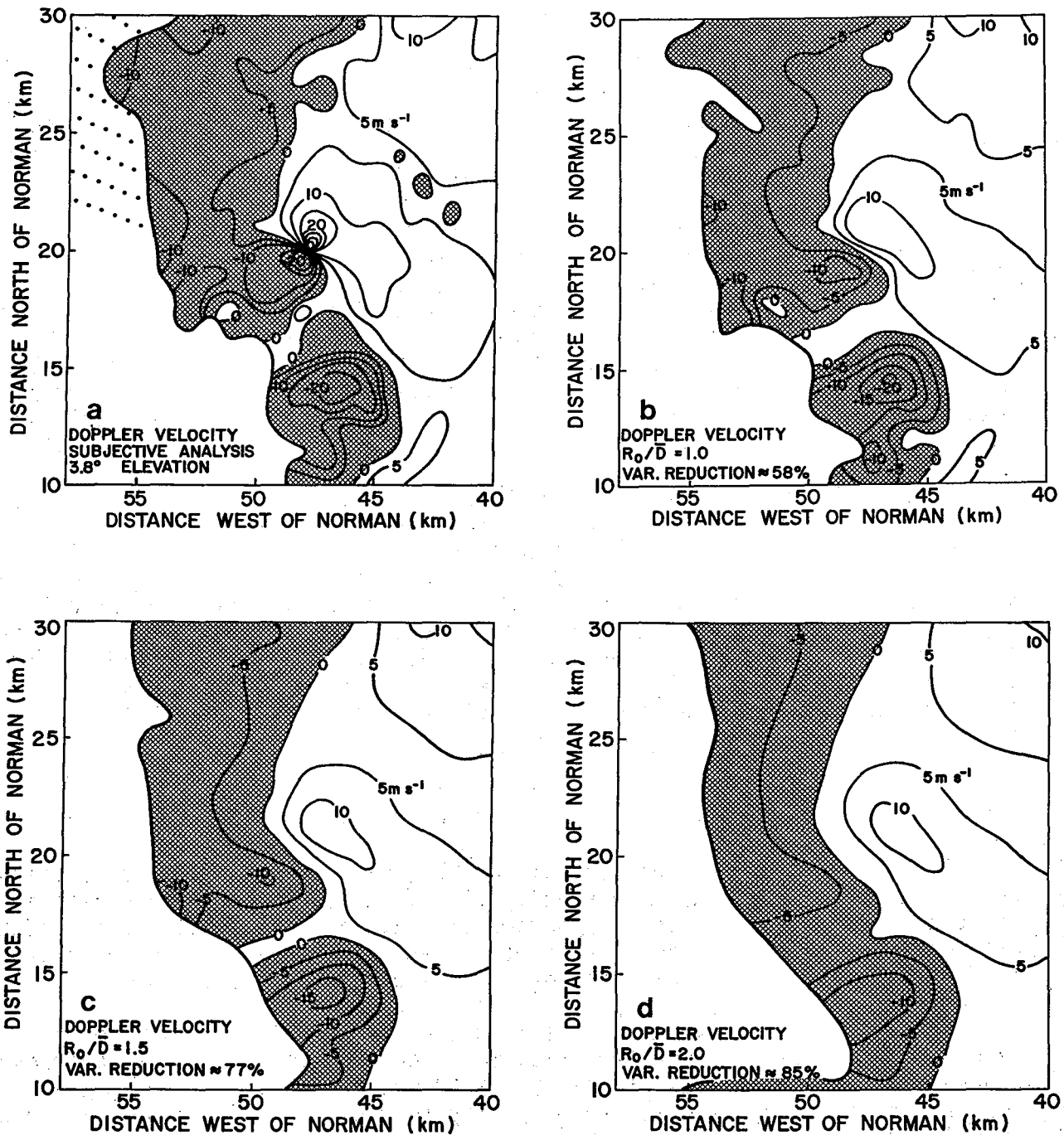


Fig. E.6 (a) Subjective analysis of Norman Doppler velocity field measured at 3.8 deg elevation angle. Data point spacing indicated in upper left corner. (b) Objective analysis of Doppler velocity field at 3.0 km height for $R_0/\bar{D} = 1.0$. Typically between 6 and 9 data points within influence sphere. (c) Objective analysis for $R_0/\bar{D} = 1.5$. Typically between 16 and 22 data points within influence sphere. (d) Objective analysis for $R_0/\bar{D} = 2.0$. Typically between 35 and 50 data points within influence sphere.

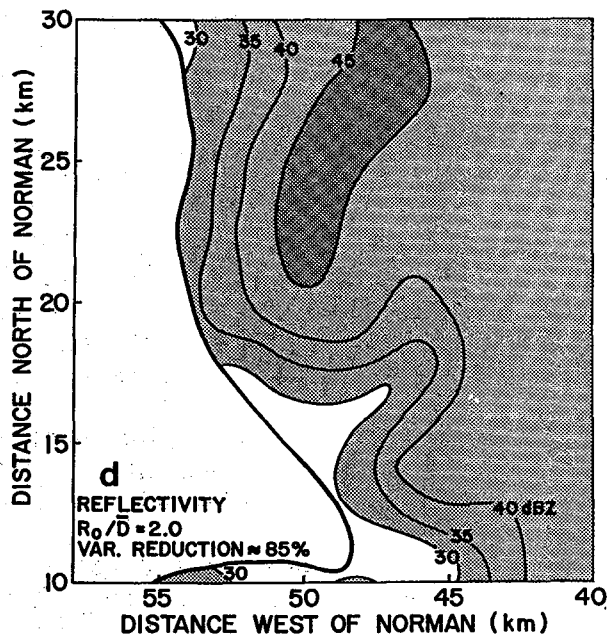
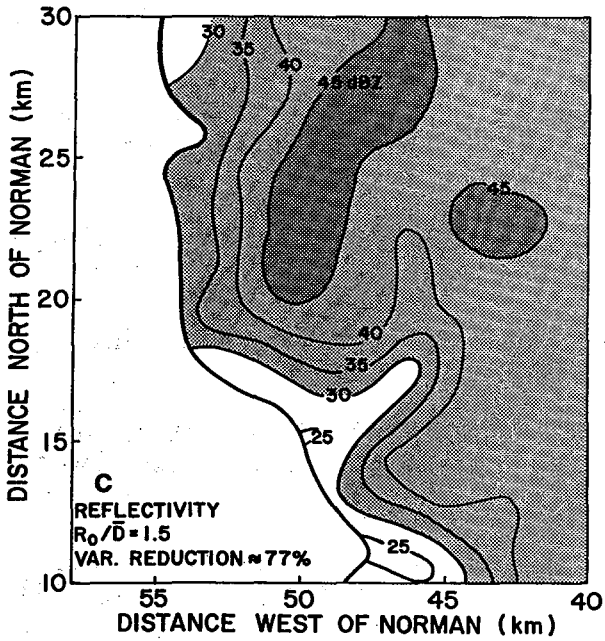
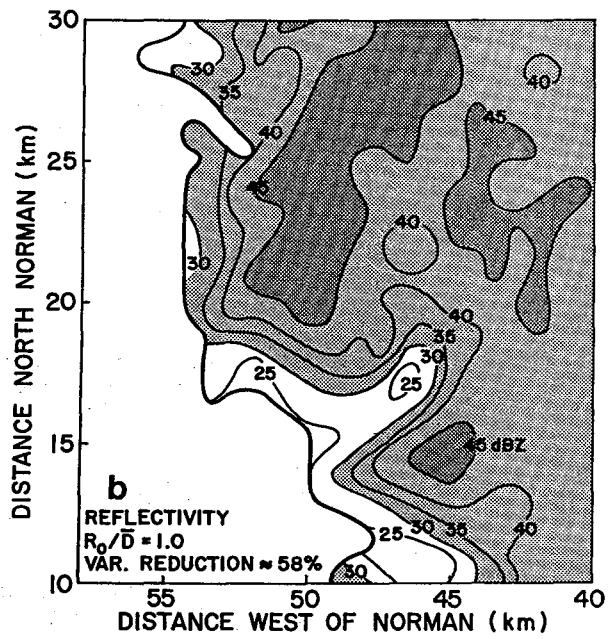
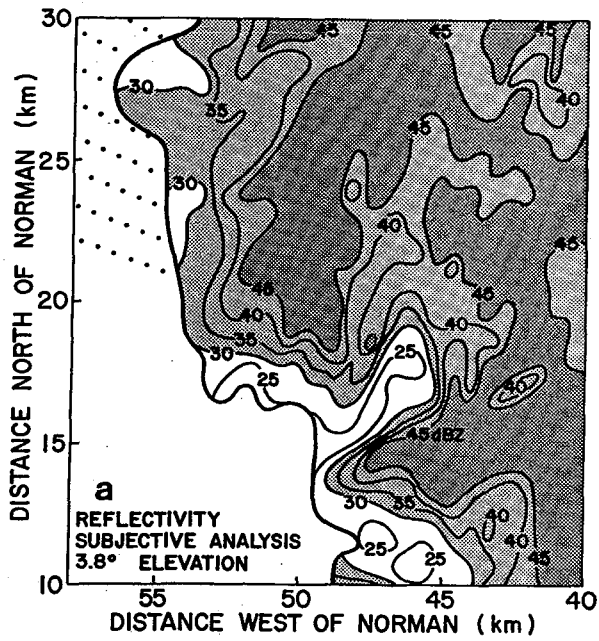


Fig. E.7 Same as Fig. E.6, except that fields are Norman Doppler radar reflectivity.

E.7 ACKNOWLEDGMENTS

Messrs. Bill Bumgarner, Don Burgess and Dale Sirmans have improved the quality of this appendix through informative general discussions and their clarifying comments concerning the text. This work was supported partially by the Federal Aviation Administration under Interagency Agreement FA72 WAI-265.

E.8 REFERENCES

- Barnes, S. L., 1973: Mesoscale objective map analysis using weighted time-series observations. NOAA Tech. Memo. ERL NSSL-62, Norman, Nat. Severe Storms Lab., 60 pp.
- Battan, L. J., 1973: Radar Observation of the Atmosphere. Chicago, Univ. of Chicago Press, 324 pp.
- Brown, R. A., and L. R. Lemon, 1976: Evolution of the Doppler radar tornadic vortex signature in the Union City storm. Chapter 15, The Union City, Oklahoma Tornado of 24 May 1973, R. A. Brown, Editor. NOAA Tech. Memo. ERL NSSL-80, Norman, Nat. Severe Storms Lab., 167-175.
- Cressman, G. P., 1959: An operational objective analysis scheme. Mon. Wea. Rev., 87, 367-374.
- Doviak, R. J., P. S. Ray, R. G. Strauch and L. J. Miller, 1976: Error estimation in wind fields derived from dual-Doppler radar measurement. J. Appl. Meteor., 15, 868-878.
- Draper, N. R., and H. Smith, 1966: Applied Regression Analysis, New York, John Wiley and Sons, 407 pp.
- Eddy, A., 1967: The statistical objective analysis of scalar data fields. J. Appl. Meteor., 6, 597-609.
- Lhermitte, R. M., 1970: Dual-Doppler radar observation of convective storm circulation. Preprints, Fourteenth Radar Meteor. Conf., Boston, Amer. Meteor. Soc., 139-144.
- _____, 1974: Dual Doppler radar study of south Florida convective storms. Preprints, Conf. on Cloud Physics, Boston, Amer. Meteor. Soc., 328-332.
- Sirmans, D., 1976: NSSL Doppler and WSR-57 radar characteristics. Appendix D, The Union City, Oklahoma Tornado of 24 May 1973, R. A. Brown, Editor. NOAA Tech. Memo. ERL NSSL-80, Norman, Nat. Severe Storms Lab., 209-213.
- _____, and B. Bumgarner, 1975: Numerical comparison of five mean frequency estimators. J. Appl. Meteor., 14, 991-1003.
- Stephens, J. J., and J. M. Stitt, 1970: Optimum influence radii for interpolation with the method of successive corrections. Mon. Wea. Rev., 98, 680-687.

Appendix F

TORNADIC STORM EVOLUTION: VORTEX VALVE HYPOTHESIS

Leslie R. Lemon¹

*National Severe Storms Laboratory
Norman, Oklahoma 73069*

In the Union City and other tornadic storms, weakening of the supercell updraft and collapse of storm top coincide with peak core circulation and tornado strength. The "vortex valve" phenomenon is invoked to explain this. Thus, as the energy represented by the mesocyclone pressure deficit is expended to produce swirl (tangential velocity), less energy remains to drive the vertical motion.

During the past two decades, kinematic properties of severe storms have been deduced from conventional radar reflectivity measurements. Updrafts have been inferred from the presence of sustained echo overhang (weak echo region--WER) and bounded weak echo region (BWER) or vault (Browning and Ludlum, 1960, 1962; Browning, 1964; Chisholm and Renick, 1972). These inferences have been supported extensively by aircraft measurements, chaff and balloon releases (Hart and Cooper, 1968; Marwitz *et al.* 1969; Chisholm, 1970; Marwitz and Berry, 1971; Marwitz *et al.* 1972). Maxima in updraft intensity, storm top, echo intensity and reflectivity gradients have been noted during the organized stages of echo overhang (Marwitz, 1972a). Organized updrafts have also been noted by the presence of lowered rain-free cloud base due to "scud", lens-shaped, or pedestal clouds (Auer *et al.*, 1970). Marwitz (1972b) observed that as updrafts within a WER weakened the WER filled with echo and developed downward (overhang and WER collapse). Lemon and Burgess (Chapter 8) used the results of these studies to conclude that--as overhang and storm top collapsed, storm reflectivities weakened and cloud base lifted--the Union City storm supercell updraft correspondingly weakened and eventually ceased.

Severe thunderstorm updrafts, unlike stratiform lifting, are confined flows venting low-level unstable air masses through "holes" in typically strong inversions (e.g., Miller, 1972). Ward (1968), using laboratory simulations, concluded that moderate rotation in a localized thunderstorm updraft decreased entrainment aloft, increased surface convergence and enhanced mass flow. However, large rotation rates inhibit effects of buoyancy (or vertical mass flow) as shown by Ward (1967) and Sasaki *et al.* (1968). The fluidic vortex valve (invented by Thoma, 1928, and described in Lewellen, 1971) makes use of decreased mass flow caused by vortex development in a confined fluid flow. Mass flow through an exhaust is reduced by a vortex because much of the

¹Present affiliation: National Severe Storms Forecast Center, Techniques Development Unit, Federal Building, Kansas City, Missouri 64106.

F. Vortex Valve Hypothesis

pressure head available to drive the flow is diverted into the swirl motion (Lewellen, 1971). For each of several flow types (e.g., steady, inviscid, potential flow) Lewellen determined that swirl and mass flow were approximately inversely proportional.

For the Union City storm, core circulation tangential velocities increased (Fig. F.1) as storm top, BWER B and echo overhang collapsed (Fig. F.2). Plan Shear Indicator Doppler data (Donaldson, Chapter 7) coupled with digital Doppler data suggest that BWER A collapse and 1 km storm top lowering also took place while core circulation tangential velocities increased (1457 to 1515). These data imply that increasing swirl can reduce significantly the updraft mass flow and velocity. The associated surface mesolow provides a finite amount of potential energy to drive both vertical motion and core circulation tangential velocities. As increasing amounts of available pressure head are used to generate increasing tangential flow, progressively less is available to drive air vertically. When updraft strength decreases, water loading effects begin to dominate more as precipitation is allowed to descend in the updraft maxima and develop at lower levels (Kessler, 1969). Additional mass flow reduction may be due either to decreased updraft diameter (evidenced by core circulation diameter reduction) or to cut-off of low-level inflow air by the gust front occlusion process discussed by Burgess and Lemon (Chapter 5) and Brandes (1976).

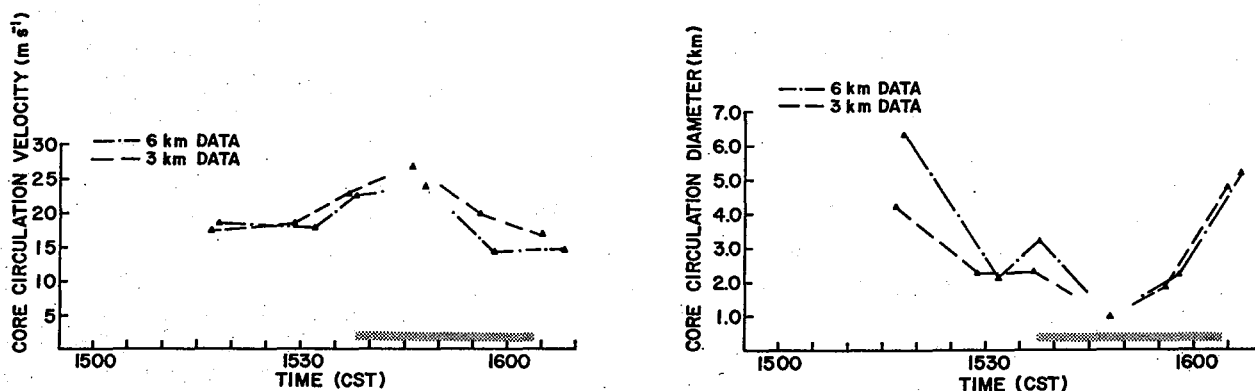


Fig. F.1 Core circulation tangential velocity and diameter at two heights above ground as a function of time. Velocity and diameter values obtained at about 1547 are from the TVS gates and are therefore considerable under and over estimates, respectively. Tornado duration on the ground indicated by stippled bar. From Lemon and Burgess (Chapter 8).

Increase in downdraft (as theorized by Fujita, 1973) also occurs because of enlarged precipitation descent associated with overhang and BWER collapse. Core circulation tangential velocity or swirl decreased (vortex valve choking decreased) after 1550 in the Union City storm and thus increased updraft velocities, or mass flow, again were favored. However, by then the residual updraft region was dominated by large amounts of descending precipitation.

While the vortex valve is an appealing analogy, an important unanswered question remains. What is the critical or threshold tangential velocity beyond which rotation becomes detrimental rather than beneficial to the updraft? Ward's (1967) data clearly show a critical rotation rate beyond which the mass flux decreases with increasing swirl. In these experiments the flow through an exhaust is forced by a fan and enhanced by the variable addition of heat to the rotating buoyant column. The critical rotation rate increased as the buoyancy of the rotating column increased (for a fixed fan speed--corresponding to low level atmospheric forcing). In the atmosphere the critical core circulation rotation rate is probably variable and a function of surface forcing, initial (before rotation) updraft strength or buoyancy and updraft diameter. The critical laboratory determined rotation values, however, are not directly applicable to the atmosphere (just as laboratory flow experiments using molecular viscosity and Reynolds numbers are not.)

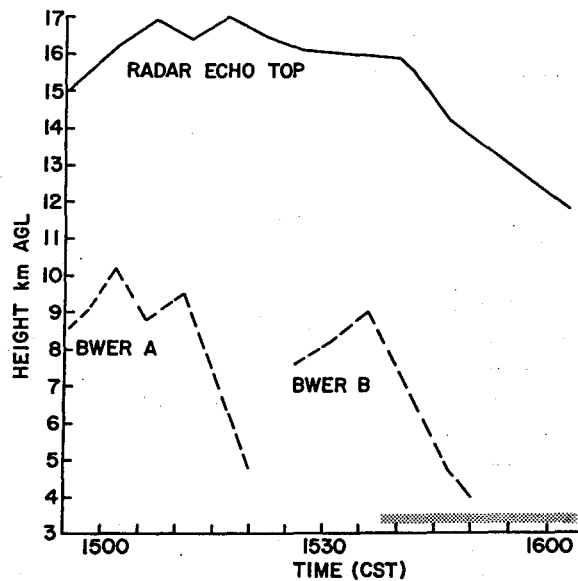


Fig. F.2 Graph of Union City storm top and maximum height of bounded weak echo regions A and B as a function of time. Tornado duration on the ground indicated by stippled bar. From Lemon and Burgess (Chapter 8).

In summary, the vortex valve effect may have an important influence on the following observed steps in the Union City storm evolution (Lemon and Burgess, Chapter 8):

1. The storm updraft increases rapidly and develops an overhang and bounded weak echo region (BWER).
2. BWER and core circulation are coincident at mid levels where both are detectable. Separation of radar detected echo mass into left and right moving thunderstorms begins.
3. The Doppler radar tornadic vortex signature (TVS) is first detected in mid levels.
4. Swirl in the core circulation increases as circulation diameter decreases. BWER and circulation separate as BWER begins collapse.
5. Echo overhang and storm top begin collapse.
6. Tornado and TVS reach the surface.

F. *Vortex Valve Hypothesis*

7. Upper limit of circulation lowers and is replaced by divergence.
8. Reorganization begins with new updraft development on the forward storm flank.
9. Supercell updraft, tornado and TVS dissipate.
10. Newly organized moderate thunderstorm persists without supercell characteristics.

While the vortex valve effect appears applicable to the Union City storm, a quasi-steady balance between core circulation and updraft is possible. When balance is achieved, rare long-lasting, long-track tornadoes can occur. Rarity of long-track quasi-continuous tornadic damage is perhaps due to the storm "self destruct" vortex valve mechanism.

REFERENCES

- Auer, A. H., Jr., D. L. Veal and J. D. Marwitz, 1970: The identification of organized cloud base updrafts. J. Rech. Atmos., 6, 1-6.
- Brandes, E. A., 1976: Gust front evolution in severe thunderstorms: Preliminary investigation. Preprints, Seventh Conf. on Aerospace and Aeron. Meteor. and Symposium on Remote Sensing from Satellites, Boston, Amer. Meteor. Soc., 56-61.
- Browning, K. A., 1964: Airflow and precipitation trajectories within severe local storms which travel to the right of the winds. J. Atmos. Sci., 4, 634-639.
- _____ and F. H. Ludlam, 1960: Radar analysis of a hailstorm. Tech. Note No. 5, Contract AF61 (052)-254, Dept. of Meteorology, Imperial College, London, 109 pp.
- _____ and _____, 1962: Airflow in convective storms. Quart. J. Roy. Meteor. Soc., 88, 117-135.
- Burgess, D. W., and L. R. Lemon, 1976: Union City storm history. Chapter 5, The Union City, Oklahoma Tornado of 24 May 1973, R. A. Brown, Editor. NOAA Tech Memo. ERL NSSL-80, Norman, Nat. Severe Storms Lab., 35-51.
- Chisholm, A. J., 1970: Alberta hailstorms: A radar study and model. Ph.D. Thesis, Dept of Meteorology, McGill Univ., Montreal, 237 pp.
- _____ and J. H. Renick, 1972: The kinematics of multicell and supercell Alberta hailstorms. Research Council of Alberta, Hail Studies Report 72-2, 24-31.

- Donaldson, R. J., Jr., 1976: Observations of the Union City tornadic storm by plan shear indicator. Chapter 7, The Union City, Oklahoma Tornado of 24 May 1973, R. A. Brown, Editor. NOAA Tech. Memo. ERL NSSL-80, Norman, Nat. Severe Storms Lab., 67-83.
- Fujita, T. T., 1973: Proposed mechanism of tornado formation from rotating thunderstorm. Preprints, Eighth Conf. on Severe Local Storms, Boston, Amer. Meteor. Soc., 191-196.
- Hart, H. E., and L. W. Cooper, 1968: Thunderstorm airflow studies using radar transponders and super-pressure balloons. Preprints, Thirteenth Weather Radar Conf., Boston, Amer. Meteor. Soc., 196-201.
- Kessler, E., 1969: On the distribution and continuity of water substance in atmospheric circulation. Meteor. Monogr., 10 (32), 84 pp.
- Lemon, L. R., and D. W. Burgess, 1976: Tornadic storm airflow and morphology derived from single Doppler radar measurements. Chapter 8, The Union City, Oklahoma Tornado of 24 May 1973, R. A. Brown, Editor. NOAA Tech. Memo. ERL NSSL-80, Norman, Nat. Severe Storms Lab., 85-106.
- Lewellen, W. S., 1971: A review of confined vortex flows. Report NASA CR-1772, National Aeron. and Space Administration.
- Marwitz, J. D., 1972a: The structure and motion of severe hailstorms, Part II: Multi-cell storms. J. Appl. Meteor., 11, 180-188.
- _____, 1972b: The structure and motion of severe hailstorms, Part III: Severely sheared storms. J. Appl. Meteor., 11, 189-201.
- _____, and E. X. Berry, 1971: The airflow within the weak echo region of an Alberta hailstorm. J. Appl. Meteor., 10, 487-492.
- _____, A. H. Auer, Jr., and D. L. Veal, 1972: Locating the organized updraft on severe thunderstorms. J. Appl. Meteor., 11, 236-238.
- _____, A. J. Chisholm and A. H. Auer, Jr., 1969: The kinematics of severe thunderstorm sheared in the direction of motion. Preprints, Sixth Conf. on Severe Local Storms, Boston, Amer. Meteor. Soc., 310-313.
- Miller, R. C., 1972: Notes on analysis and severe storm forecasting procedures of the Air Force Global Weather Central. Air Weather Service Tech. Report 200 (Rev), 188 pp.
- Sasaki, Y., E. W. Friday, Jr. and E. M. Wilkins, 1968: Behavior of convective elements in a rotating medium. Univ. of Okla., Atmos. Res. Lab. Report ARL-1524-5 (NSF GP-5161), 117 pp.
- Thoma, D., 1928: Fluid lines, U. S. Patent 1,839,616.
- Ward, N. B., 1967: An effect of rotation on a buoyant convective column. Preprints, Fifth Conf. on Severe Local Storms, Boston, Amer. Meteor. Soc., 368-373.

OTHER PAPERS PERTAINING TO THE UNION CITY TORNADIC STORM

- Achtemeier, G. L., 1975: Doppler velocity and reflectivity morphology of a severe left-moving split thunderstorm. Preprints, Sixteenth Radar Meteor. Conf., Boston, Amer. Meteor. Soc., 93-98.
- Brown, R. A., and L. R. Lemon, 1976: Single Doppler radar vortex recognition: Part II - Tornadic vortex signatures. Preprints, Seventeenth Conf. on Radar Meteor., Boston, Amer. Meteor. Soc., 104-109.
- Burgess, D. W., L. R. Lemon and R. A. Brown, 1975a: Tornado characteristics revealed by Doppler radar. Geophys. Res. Letters, 2, 183-184.
- _____, _____ and _____, 1975b: Evolution of a tornado signature and parent circulation as revealed by single Doppler radar. Preprints, Sixteenth Radar Meteor. Conf., Boston, Amer. Meteor. Soc., 99-106.
- Donaldson, R. J., Jr., 1975. History of a tornado vortex traced by plan shear indicator. Preprints, Sixteenth Radar Meteor. Conf., Boston, Amer. Meteor. Soc., 80-82.
- Golden, J. H., and D. Purcell, 1974: Photogrammetric velocity and morphological analysis of the Union City, Oklahoma tornado, May 24, 1973. Presented at Fall Meeting, Amer. Geophys. Union. Abstract in EOS, 56, 1130.
- _____ and R. P. Davies-Jones, 1975; Photogrammetric windspeed analysis and damage interpretation of the Union City, Oklahoma tornado, May 24, 1973. Proceedings, Second U. S. Nat. Conf. on Wind Eng. Res., Washington, Wind Eng. Res. Council, National Science Foundation, II-2-1 - II-2-4.
- Lemon, L. R., D. W. Burgess and R. A. Brown, 1975: Tornado production and storm sustenance. Preprints, Ninth Conf. on Severe Local Storms, Boston, Amer. Meteor. Soc., 100-104.
- Moller, A., C. Doswell, J. McGinley, S. Tegtmeier and R. Zipser, 1974: Field observations of the Union City tornado in Oklahoma. Weatherwise, 27, 68-77.
- Zrnic, D. S., and R. J. Doviak, 1975: Velocity spectra of vortices scanned with a pulse-Doppler radar. J. Appl. Meteor., 14, 1531-1539.
- _____, _____, D. Burgess and D. Sirmans, 1976: Tornado characteristics revealed by a pulse-Doppler radar. Preprints, Seventeenth Conf. on Radar Meteor., Boston, Amer. Meteor. Soc., 110-117.

NATIONAL SEVERE STORMS LABORATORY

The NSSL Technical Memorandum, beginning with No. 28, continue the sequence established by the U. S. Weather Bureau National Severe Storms Project, Kansas City, Missouri. Numbers 1-22 were designated NSSL Reports. Numbers 23-27 were NSSL Reports, and 24-27 appeared as subseries of Weather Bureau Technical Notes. These reports are available from the National Technical Information Service, Operations Division, Springfield, Virginia 22151, for \$3.00 and a microfiche version for \$0.95. NTIS numbers are given below in parentheses.

- No. 1 National Severe Storms Project Objectives and Basic Design. Staff, NSSL. March 1961. (PB-168207)
- No. 2 The Development of Aircraft Investigations of Squall Lines from 1956-1960. B. B. Goddard. (PB-168208)
- No. 3 Instability Lines and Their Environments as Shown by Aircraft Soundings and Quasi-Horizontal Traverses. D. T. Williams. February 1962. (PB-168209)
- No. 4 On the Mechanics of the Tornado. J. R. Fulks. February 1962. (PB-168210)
- No. 5 A Summary of Field Operations and Data Collection by the National Severe Storms Project in Spring 1961. J. T. Lee. March 1962. (PB-165095)
- No. 6 Index to the NSSL Surface Network. T. Fujita. April 1962. (PB-168212)
- No. 7 The Vertical Structure of Three Dry Lines as Revealed by Aircraft Traverses. E. L. McGuire. April 1962. (PB-168213)
- No. 8 Radar Observations of a Tornado Thunderstorm in Vertical Section. Ralph J. Donaldson, Jr. April 1962. (PB-174859)
- No. 9 Dynamics of Severe Convective Storms. Chester W. Newton. July 1962. (PB-163319)
- No. 10 Some Measured Characteristics of Severe Storms Turbulence. Roy Steiner and Richard H. Rhyne. July 1962. (N62-16401)
- No. 11 A Study of the Kinematic Properties of Certain Small-Scale Systems. D. T. Williams. October 1962. (PB-168216)
- No. 12 Analysis of the Severe Weather Factor in Automatic Control of Air Route Traffic. W. Boynton Beckwith. December 1962. (PB-168217)
- No. 13 500-Kc./Sec. Sferics Studies in Severe Storms. Douglas A. Kohl and John E. Miller. April 1963. (PB-168218)
- No. 14 Field Operations of the National Severe Storms Project in Spring 1962. L. D. Sanders. May 1963. (PB-168219)
- No. 15 Penetrations of Thunderstorms by an Aircraft Flying at Supersonic Speeds. G. P. Roys. Radar Photographs and Gust Loads in Three Storms of 1961 Rough Rider. Paul W. J. Schumacher. May 1963. (PB-168220)
- No. 16 Analysis of Selected Aircraft Data from NSSL Operations, 1962. T. Fujita. May 1963. (PB-168221)
- No. 17 Analysis of Methods for Small-Scale Surface Network Data. D. T. Williams. August 1963. (PB-168222)
- No. 18 The Thunderstorm Wake of May 4, 1961. D. T. Williams. August 1963. (PB-168223)
- No. 19 Measurements by Aircraft of Condensed Water in Great Plains Thunderstorms. George P. Roys and Edwin Kessler. July 1966. (PB-173048)
- No. 20 Field Operations of the National Severe Storms Project in Spring 1963. J. T. Lee, L. D. Sanders, and D. T. Williams. January 1964. (PB-168224)
- No. 21 On the Motion and Predictability of Convective Systems as Related to the Upper Winds in a Case of Small Turning of Wind with Height. James C. Fankhauser. January 1964. (PB-168225)
- No. 22 Movement and Development Patterns of Convective Storms and Forecasting the Probability of Storm Passage at a Given Location. Chester W. Newton and James C. Fankhauser. January 1964. (PB-168226)
- No. 23 Purposes and Programs of the National Severe Storms Laboratory, Norman, Oklahoma. Edwin Kessler. December 1964. (PB-166675)

- No. 24 Papers on Weather Radar, Atmospheric Turbulence, Sferics, and Data Processing. August 1965. (AD-621586)
- No. 25 A Comparison of Kinematically Computed Precipitation with Observed Convective Rainfall. James C. Fankhauser. September 1965. (PB-168445)
- No. 26 Probing Air Motion by Doppler Analysis of Radar Clear Air Returns. Roger M. Lhermitte. May 1966. (PB-170636)
- No. 27 Statistical Properties of Radar Echo Patterns and the Radar Echo Process. Larry Armijo. May 1966. The Role of the Kutta-Joukowski Force in Cloud Systems with Circulation. J. L. Goldman. May 1966. (PB-170756)
- No. 28 Movement and Predictability of Radar Echoes. James Warren Wilson. November 1966. (PB-173972)
- No. 29 Notes on Thunderstorm Motions, Heights, and Circulations. T. W. Harrold, W. T. Roach, and Kenneth E. Wilk. November 1966. (AD-644899)
- No. 30 Turbulence in Clear Air Near Thunderstorms. Anne Burns, Terence W. Harrold, Jack Burnham, and Clifford S. Spavins. December 1966. (PB-173992)
- No. 31 Study of a Left-Moving Thunderstorm of 23 April 1964. George R. Hammond. April 1967. (PB-174681)
- No. 32 Thunderstorm Circulations and Turbulence from Aircraft and Radar Data. James C. Fankhauser and J. T. Lee. April 1967. (PB-174860)
- No. 33 On the Continuity of Water Substance. Edwin Kessler. April 1967. (PB-175840)
- No. 34 Note on the Probing Balloon Motion by Doppler Radar. Roger M. Lhermitte. July 1967. (PB-175930)
- No. 35 A Theory for the Determination of Wind and Precipitation Velocities with Doppler Radars. Larry Armijo. August 1967. (PB-176376)
- No. 36 A Preliminary Evaluation of the F-100 Rough Rider Turbulence Measurement System. U. O. Lappe. October 1967. (PB-177037)
- No. 37 Preliminary Quantitative Analysis of Airborne Weather Radar. Lester P. Merritt. December 1967. (PB-177188)
- No. 38 On the Source of Thunderstorm Rotation. Stanley L. Barnes. March 1968. (PB-178990)
- No. 39 Thunderstorm - Environment Interactions Revealed by Chaff Trajectories in the Mid-Troposphere. James C. Fankhauser. June 1968. (PB-179659)
- No. 40 Objective Detection and Correction of Errors in Radiosonde Data. Rex L. Inman. June 1968. (PB-180284)
- No. 41 Structure and Movement of the Severe Thunderstorms of 3 April 1964 as Revealed from Radar and Surface Mesonet Data Analysis. Jess Charba and Yoshikazu Sasaki. October 1968. (PB-183310)
- No. 42 A Rainfall Rate Sensor. Brian E. Morgan. November 1968. (PB-183979)
- No. 43 Detection and Presentation of Severe Thunderstorms by Airborne and Ground-Based Radars: A Comparative Study. Kenneth E. Wilk, John K. Carter, and J. T. Dooley. February 1969. (PB-183572)
- No. 44 A Study of a Severe Local Storm of 16 April 1967. George Thomas Haglund. May 1969. (PB-184970)
- No. 45 On the Relationship Between Horizontal Moisture Convergence and Convective Cloud Formation. Horace R. Hudson. March 1970. (PB-191720)
- No. 46 Severe Thunderstorm Radar Echo Motion and Related Weather Events Hazardous to Aviation Operations. Peter A. Barclay and Kenneth E. Wilk. June 1970. (PB-192498)
- No. 47 Evaluation of Roughness Lengths at the NSSL-WKY Meteorological Tower. Leslie D. Sanders and Allen H. Weber. August 1970. (PB-194587)
- No. 48 Behavior of Winds in the Lowest 1500 ft in Central Oklahoma: June 1966-May 1967. Kenneth C. Crawford and Horace R. Hudson. August 1970.
- No. 49 Tornado Incidence Maps. Arnold Court. August 1970. (COM-71-00019)
- No. 50 The Meteorologically Instrumented WKY-TV Tower Facility. John K. Carter. September 1970. (COM-71-00108)

- No. 51 Papers on Operational Objective Analysis Schemes at the National Severe Storms Forecast Center. Rex L. Inman. November 1970. (COM-71-00136)
- No. 52 The Exploration of Certain Features of Tornado Dynamics Using a Laboratory Model. Neil B. Ward. November 1970. (COM-71-00139)
- No. 53 Rawinsonde Observation and Processing Techniques at the National Severe Storms Laboratory. Stanley L. Barnes, James H. Henderson, and Robert J. Ketchum. April 1971. (COM-71-00707)
- No. 54 Model of Precipitation and Vertical Air Currents. Edwin Kessler and William C. Bumgarner. June 1971. (COM-71-00911)
- No. 55 The NSSL Surface Network and Observations of Hazardous Wind Gusts. Operations Staff. June 1971. (COM-71-00910)
- No. 56 Pilot Chaff Project at the National Severe Storms Laboratory. Edward A. Jessup. November 1971. (COM-72-10106)
- No. 57 Numerical Simulation of Convective Vortices. Robert P. Davies-Jones and Glenn T. Vickers. November 1971. (COM-72-10269).
- No. 58 The Thermal Structure of the Lowest Half Kilometer in Central Oklahoma: December 9, 1966-May 31, 1967. R. Craig Goff and Horace R. Hudson. July 1972. (COM-72-11281)
- No. 59 Cloud-to-Ground Lightning Versus Radar Reflectivity in Oklahoma Thunderstorms. Gilbert D. Kinzer. September 1972. (COM-73-10050)
- No. 60 Simulated Real Time Displays of Velocity Fields by Doppler Radar. L. D. Hennington and G. B. Walker. November 1972. (COM-73-10515)
- No. 61 Gravity Current Model Applied to Analysis of Squall-Line Gust Front. Jess Charba. November 1972. (COM-73-10410)
- No. 62 Mesoscale Objective Map Analysis Using Weighted Time-Series Observations. Stanley L. Barnes. March 1973. (COM-73-10781)
- No. 63 Observations of Severe Storms on 26 and 28 April 1971. Charles L. Vlack. April 1973. (COM-73-11200)
- No. 64 Meteorological Radar Signal Intensity Estimation. Dale Sirmans and R. J. Doviak. September 1973. (COM-73-11923/2AS)
- No. 65 Radiosonde Altitude Measurement Using Double Radiotheodolite Techniques. Stephan P. Nelson. September 1973. (COM-73-11934/9AS)
- No. 66 The Motion and Morphology of the Dryline. Joseph T. Schaefer. September 1973. (COM-74-10043)
- No. 67 Radar Rainfall Pattern Optimizing Technique. Edward A. Brandes. March 1974.
- No. 68 The NSSL/WKY-TV Tower Data Collection Program: April-July 1972. R. Craig Goff and W. David Zittel. May 1974.
- No. 69 Papers on Oklahoma Thunderstorms, April 29-30, 1970. Stanley L. Barnes, Editor. May 1974.
- No. 70 Life Cycle of Florida Key's Waterspouts. Joseph H. Golden. June 1974.
- No. 71 Interaction of Two Convective Scales Within a Severe Thunderstorm: A Case Study and Thunderstorm Wake Vortex Structure and Aerodynamic Origin. Leslie R. Lemon. June 1974.
- No. 72 Updraft Properties Deduced from Rawinsoundings. Robert P. Davies-Jones and James H. Henderson. October 1974.
- No. 73 Severe Rainstorm at Enid, Oklahoma - October 10, 1973. L. P. Merritt, K. E. Wilk, and M. L. Weible. November 1974.
- No. 74 Mesonet Array: Its Effect on Thunderstorm Flow Resolution. Stanley L. Barnes. October 1974.
- No. 75 Thunderstorm-Outflow Kinematics and Dynamics. R. Craig Goff. December 1975.
- No. 76 An Analysis of Weather Spectra Variance in a Tornadic Storm. Philippe Waldteufel. May 1976.
- No. 77 Normalized Indices of Destruction and Deaths by Tornadoes. Edwin Kessler and J. T. Lee. June 1976.

No. 78 Objectives and Accomplishments of the NSSL 1975 Spring Program. K. Wilk, K. Gray, C. Clark,
D. Sirmans, J. T. Dooley, J. Carter, and W. Bumgarner. July 1976.